Investigation of Triose Phosphate Isomerase dysfunction and Redox Stress in a *Drosophila Melanogaster* model of Neurodegenerative Disease

Ælfwin Stone

Acknowledgements

This thesis would not be here if not for the help of a huge number of people. Firstly, I would like to thank the BBSRC for funding this project, and the university of Nottingham for hosting my PhD.

The help of my supervisor Assistant prof. Joern Steinert was invaluable throughout this work, for guidance through the literature, experiment planning, optimisation and writing my thesis, I could not have done it without you. Contributions from research technician Maria Haig towards the optimisation and data collection for Western blotting and immunohistochemistry, the general facilitation of lab work, as well as being a huge moral support for me in labs was also essential for me to put this thesis together, I owe you a huge thanks for everything.

Support from Vladyslava Yarosh, Megan de Lange, and Jen Cale from the Steinert lab group is greatly appreciated. Through the last four years you all helped kept me sane (ish).

Big thanks to undergraduate medical students; Caitlin McDonnell, Isabel Hawthorn, Kevin Farrell, Larua Pereira Rocha, Mok-Min Jung, Renee Patil, and undergraduate neuroscience student Sophie Wenje for the larval crawling, and learning and memory data collection. I would also like to thank Sophie Wenje for collecting the bulk of the adult fly climbing data.

The help of Zuzanna Kula and Dr Carlo Breda from De Monfort University in the collection of the circadian rhythm data is also greatly appreciated.

The help of the SLIM team was invaluable for the confocal imaging and electron microscopy, particular thanks go to Ian Ward and Denise Mclean for all their help with these protocols.

I would also like to thank Zsuzsa Marcus for her help with fly food preparation and stock maintenance, as well as her incredibly useful advice on *Drosophila* use and care, my flies were much happier for it.

My internal examiner Associate Prof. Paul Smith was a great help throughout this work, with prudent feedback on end of year reports and readily given insightful suggestions when experiments were not going to plan.

The writing up of my thesis has not been as smooth a path as I would have planned, but it is here now because of the last minute incredibly generous support I received from Associate prof Tracy Farr, and Associate prof Angus Brown. Both of whom have provided support when needed throughout the four

years and in the final stage of writing up my thesis. An extra thanks to Angus who stepped up as my secondary supervisor in the last month of my PhD.

Along with support from individuals at my own university I need to thank the people outside university, without whose help I would not have finished this work. My family and friends were huge sources of support throughout the last four years. In particular my dad (Prof.) Peter, who constantly reminded me that everyone hates their PhD sometimes, helped me to maintain a sense of perspective throughout this work, and gave regular advice on how to navigate academia. My sister Mo, mum Genevieve, and my brothers Wilf and Berni, who always listened to me venting when things were not going as planned, and who provided comic relief and a step into nonsense when I needed a break. My friends Holly, Malik, Anj, Milind, Izzy among others, also helped a huge amount by listening to rants and giving me much needed breaks from concentration, thanks to you all.

Declaration

Learning and memory data was collected by undergraduate medical and neuroscience students under my, and my supervisor Joern Steinert's, supervision.

Circadian rhythm data was collected and analysed by Zuzanna Kula and Dr Carlo Breda from De Monfort University.

Western blot data was collected by research technician Maria Haig, Maria and I planned and optimised these experiments together.

COVID 19 impact statement

COVID-19 heavily impacted my first two years of studies, I started my PhD in September 2020. All in person work for the first year was significantly reduced with only a couple of training opportunities available in person. As a new student coming from an undergraduate in a different specialty, this reduction in introductory training and collaborative learning was a huge handicap moving forwards. When I managed to start lab work properly in my second year experiments still took dramatically longer than expected due to delays in orders both externally and internally, and months of delays for required technical support. For example, the instalment of the air table for electrophysiology work was planned in my first year but not set up until Christmas in my second year. This was particularly relevant for me as I had joined a new lab group in a lab room that had been previously unoccupied for multiple years, so required setting up nearly from scratch including basics such as setting up a fume hood, fridges, freezers, and bench space for experimental use. As a lab we also needed to set up various experimental protocols for use in the lab, which was more time consuming than it would have been as many researchers that could normally have helped were working from home due to COVID.

Publications

Triose-phosphate isomerase deficiency is associated with a dysregulation of synaptic vesicle recycling in *Drosophila melanogaster*, Front. Synaptic Neurosci., Vol 15, 2023, Ælfwin Stone, Oliver Cujic, Angel Rowlett, Sophia Aderhold, Emma Savage, Bruce Graham, Joern Steinert.

Medium-Chain Fatty Acids Rescue Motor Function and Neuromuscular Junction Degeneration in a *Drosophila* Model of Amyotrophic Lateral Sclerosis, Cells, Vol 12 Issue 17, 2023, Ella Dunn, Joern R Steinert, Aelfwin Stone, Virender Sahota, Robin S B Williams, Stuart Snowden, Hrvoje Augustin

Plum modulates Myoglianin and regulates synaptic function in *D. melanogaster*, Open Biology, Vol 13 Issue 9, 2023, Virender K. Sahota, Aelfwin Stone, Nathaniel S. Woodling, Jereme G. Spiers, Joern R. Steinert, Linda Partridge, and Hrvoje Augustin

Poster presentations

Triose-phosphate isomerase (TPI) dysfunction alters synaptic vesicle release mechanisms and reduces life span, Europhysiology 2022, Ælfwin Stone, Joern Steinert

Triose-phosphate isomerase (TPI) dysfunction alters synaptic vesicle release mechanisms and reduces life span, BNA 2023, Ælfwin Stone, Joern Steinert

Triose-phosphate isomerase (TPI) dysfunction alters synaptic vesicle release mechanisms and reduces life span, Physiology in Focus 2024, Ælfwin Stone, Joern Steinert

Oral presentations

Suppressed Triose-phosphate isomerase (TPI) activity affects synaptic vesicle release mechanisms and reduces *Drosophila* life span, Physiology 2023, Ælfwin Stone, Joern Steinert

Triose Phosphate Isomerase and redox stress in a *Drosophila* model of neurodegeneration, Physiology in Focus 2024 - Neurophysiology SIG Meeting, Ælfwin Stone, Joern Steinert

Triose Phosphate Isomerase dysfunction and redox stress in a *Drosophila* model of neurodegeneration, London fly meeting 2024, Ælfwin Stone, Joern Steinert

PIP reflection

During my PhD I was required to complete a three month placement outside the topic of my PhD. My PIP placement was based at the University of Newcastle within the NuBrain consortium, a group aimed to improving the public understanding and policy decisions around brain health and nutrition. My role was to support with the admin, social media, and public outreach aspects of the project. NuBrain was divided into various work packages. Previous work packages had been more research focused, the work package I was involved with focused on informing the public and policy makers of the results found in earlier packages, concluding in January 2023. NuBrain broadly aimed to improve the understanding and availability of information regarding the link between brain health and food culture, both for the general public, and for the policy makers. During my PIP I attended executive meetings, and had the opportunity to work with academics, researchers, and some policy makers at the top of their fields. I also was able to spend time with members of the public and gained a better comprehension of how to convey scientific principals to a wide and varied audience. Throughout the project I helped to create leaflets on brain health and the link to food, and food culture, targeted specifically to the public or to policy makers. I was an integral part of organising outreach meetings with members of the public and guest academic speakers. These meetings included talks, food, and activities to get participants thinking about brain health and diet. I also headed up the social media pages for NuBrain, creating engaging posts that linked to various trusted information sources, both to inform about the activity of the consortium and more generally about food and diets for better brain health. This work required a lot of organisation, especially as involvement in the consortium was a secondary role for most participants, so effective communication and scheduling was essential. I had to learn how to effectively use social media from a professional account, and engage the public with scientific studies. The variety and quantity of smaller jobs that I was responsible for throughout the project created a different manner of working than I had been previously used to, requiring a higher level of flexibility and creative scheduling. I think the experience of my PIP project expanded my professional skillset, many of these skills I have since transferred to my own research, particularly when scheduling work with multiple participants who all have busy timetables and other responsibilities. Doing this project gave me experience of working in an office setting with computer based work, which I will now try and avoid as the basis for my future work. It also gave me experience working in public outreach in various forms, which has improved my knowledge of public understanding of science and health, and helped my

communication skills when explaining complicated concepts to diverse audiences, often with no scientific background. My PIP project was a fantastic opportunity to experience how research bleeds out into society at large, and the role scientists have to take to get new discoveries to be effectively represented in policy and culture.

Abstract

Neurodegenerative diseases have been extensively associated with increased redox stress, often this is linked to aberrant production of reactive species such as advanced glycation end products (AGEs). AGEs, and smaller reactive species like nitric oxide (NO), have been shown to increase redox stress, promoting protein and DNA modification, often via post translational modifications such as 3-Nitrotyrosination. Triose phosphate isomerase (TPI) is one protein that has been shown to undergo such modifications. TPI is an important, but non-essential, glycolytic enzyme whose main role is in the conversion of dihydroxyacetone phosphate (DHAP) to glyceraldyhyde-3-phosphate (G3P). This is an important conversion as it controls levels of methylglyoxal (MGO) which when increased significantly has also been directly linked to increased redox stress, protein modification, and DNA modification via AGE production. Thus, TPI dysfunction has been reported to lead to increased redox stress, enhancing glycation signalling, neuroinflammation, and neurodegeneration, and to be sensitive to redox stress itself, containing multiple sites for 3-nitrotyrosination. The resulting physiological mechanisms of TPI dysfunction are not yet well understood. TPI dysfunction has in turn been linked to various neurodegenerative disorders, including Alzheimer's disease. Glyoxalase (Glo) is another key enzyme which provides an innate protective mechanism against MGO build up. This work aims to use *Drosophila melanogaster* to identify impacts of altered TPI on neuronal physiology linking aberrant TPI function and redox stress to synaptic deficits at the glutamatergic *Drosophila* neuromuscular junction (NMJ). A *Drosophila* mutant expressing reduced Glo activity is also reported to further investigate this metabolic pathway, and subsequent connection to neurodegeneration. Electrophysiology and immunohistochemistry, among other techniques, are utilised to investigate this pathology.

This work suggests that the phenotype arising from dysfunctional TPI is in part due to altered vesicle dynamics, possibly in vesicle pool organisation of the presynaptic neuron or endo/exocytosis, thus expanding our knowledge of the resultant mechanisms of TPI dysfunction. The data presented here implies that there are various mechanisms of dysfunction, likely to be via exacerbated redox stress, and compensatory mechanisms, suggested to be primarily via altered vesicle dynamics, leading to distinct pathologies with different mutations of the TPI protein. Impaired TPI and Glo activity are suggested to enhance protein glycation, redox stress, and post translational modifications, implying a possible route of pathology and presenting a potential target for therapies.

Summary of thesis

As described in the abstract, this thesis investigates pathology stemming from the glycolytic metabolic pathway through impaired triose phosphate isomerase (TPI) function, and the observed connection to neurodegeneration and synaptic dysfunction. The main role of TPI is in the interconversion between dihydroxyacetone phosphate (DHAP) and glyceraldehyde-3-phosphate (G3P). Increased DHAP levels lead to increased methylglyoxal (MGO), which in turn lead to increased levels of advanced glycation end products (AGEs), which have been extensively linked to increased redox stress, protein modification, and DNA modification. An innate protective pathway via glyoxalase (Glo) removes excess MGO however this is not sufficient to compensate for TPI dysfunction. Impaired TPI function has been associated with multiple neurodegenerative disorders, both directly in diseases like TPI deficiency, and indirectly in diseases like Alzheimer's disease.

Drosophila mutants containing a dysfunctional TPI protein have reduced lifespans and increased neurodegeneration (Gnerer et al. 2006). However, an energetic deficit was not found in these models, with ATP levels unaffected compared to control lines (Celotto et al. 2006b). Various mechanisms have been suggested as the cause of dysfunction in such models, such as increased clearance of the mutated TPI proteins via molecular chaperones (Hrizo and Palladino 2010), or altered synaptic activity including altered vesicle dynamics (Roland et al. 2016; Stone et al. 2023). Mutants containing reduced Glo expression have been reported to exhibit pathologies reminiscent of type 2 diabetes with increased insulin resistance and increased tendency to develop obesity in a *Drosophila* model (Moraru et al. 2018).

Four *Drosophila* melanogaster disease models will be discussed here, three mutant lines expressing dysfunctional triose phosphate isomerase (TPI), M80T, wstd^{1}, and I170V, and one Glo 1 knock out line Glo(KO). The control lines w^{1118} and Canton.S will be reported alongside the relevant mutant lines. Lines are chosen from published papers and obtained from respective groups. Comparisons between mutant lines and controls were based on the genetic information available in published work (Celotto et al. 2006a; Celotto et al. 2006b; Gnerer et al. 2006; Seigle et al. 2008; Roland et al. 2014). This PhD does not go into the details of the genetic mutations as this was not the expertise of our lab; instead the genetic details from the previously published work has been trusted. Key protein targets and mechanisms involved in synaptic neurodegeneration, specifically redox damage, will be identified, and the subsequent impact on calcium mediated glutamatergic transmission at the

Drosophila neuromuscular junction (NMJ) will be investigated. The primary technique used is electrophysiology, to investigate the synaptic activity of neuromuscular junctions, supported by immunohistochemistry, Western blotting, and fluorometric assays to quantify protein expression, and various behavioural techniques to assess full animal physiology.

Electrophysiological recordings were taken from muscle 6/7 in segments A2/3 of third instar larvae; evoked and spontaneous excitatory junctional currents and potentials (e/sEJCs and e/sEJPs) were recorded, alongside 10-60 Hz train stimulations and recovery protocols. These recordings allow detailed investigation of synaptic activity in excitatory glutamatergic neuromuscular junctions (NMJs), which were found to be altered in mutant *Drosophila* lines.

TPI levels *in vivo* were assessed by Western blot to investigate protein clearance, which was found to be increased in I170V mutants and reduced in $wstd^{1}$ and M80T mutant lines. Immunohistochemistry (IHC) was run to investigate the morphology of NMJs staining for horseradish peroxidase (HRP) as a measure of neuronal area, and bruchpilot (BRP) as a measure of active zones. This was found to be minimally altered in some TPI mutant lines. IHC was also run to quantify redox stress *in vivo*, staining for AGEs and caspase as measures of redox stress and cell death respectively. Redox stress was further quantified by fluorometric assays to measure superoxide dismutase (SOD) activity and lipid peroxidation. Redox stress and cell death found to be altered in the TPI mutant lines. Whole animal physiology was also investigated in mutant lines via longevity, circadian rhythm, motor activity, and olfactory memory assays: significant changes in whole animal physiology were reported for all mutant lines.

Contents

Figures

Tables

Abbreviations

3NT:	3- Nitrotyrosination
ACh(R):	Acetylcholine (receptor)
AGEs:	Advance glycation end products
APOE:	Apolipoprotein E
APP:	Amyloid precursor protein
ATP:	Adenosine triphosphate
BHT:	Butylated hydroxytoluene
Brp:	Bruchpilot
DHAP:	Dihydroxyacetone phosphate
eEJP/C:	Evoked excitatory junction potential/current
G3P:	Glyceraldehyde-3-phosphate
Glo:	Glyoxalase
HL3:	Haemolymph like solution
HRP:	Horse radish peroxidase
(i/e/n) NOS:	(Inducible/endothelial/neuronal) nitric oxide synthase
MDA:	Malondialdehyde
MGO:	Methylglyoxal
NGS(-T):	Normal goat serum in 1XPBS-T
NMJ:	Neuromuscular junction
NO:	Nitric oxide
PFA:	Paraformaldehyde
PI:	Preference index
PTM:	Post translational modification
RNS:	Reactive nitrogen species
ROS:	Reactive oxygen species
sEJP/C:	Spontaneous excitatory junction potential/current
SOD:	Superoxide dismutase
TBA:	Thiobarbituric acid
TEVC:	Two electrode voltage clamp
TPI:	Triose phosphate isomerase

Chapter 1: Introduction

1.1: Neurodegenerative disease

Neurodegenerative disease (ND) is an escalating problem with *Human* lifespans increasing globally. In 2023 there were 55 million people suffering some form of dementia worldwide according to the World Health Organisation, and a predicted 10 million new cases annually (WHO 2023). In the UK in 2019 dementia cost £34.7 billion pounds, this figure is expected to rise to £45.4 billion for the anticipated >1.6 million cases by 2040, 40 % of this coming from the taxpayer (Care Policy and Evaluation Centre 2019; Office for Health Improvement and Disparities 2022). Most of this cost comes from daily patient care so treating the symptoms of dementia, and so reducing the extent of care required is imperative to reduce this. ND disease is a disproportionately large problem in low and middle income countries which contain over 60 % of worldwide dementia cases (WHO 2023). Improving quality of life for patients and stalling the progress of ND diseases is important to address this problem on a global level. To be able to reduce the impact of ND disorders, a better understanding of the detailed mechanisms involved in the pathologies is required.

One contributary factor to ageing related and genetic ND conditions is a dysfunctional protein Triose phosphate isomerase (TPI), an important but not essential glycolytic enzyme. The mechanism of pathology stemming from dysfunctional TPI is not yet well understood and is the primary focus of this thesis. Genetic mutation of the TPI gene causes the condition TPI deficiency, an aggressive disorder strongly associated with neurodegeneration among other phenotypes (Olah et al. 2002; Orosz et al. 2006; Orosz et al. 2009; NIH Medline plus 2014; Ganetzky 2015; GARD 2023). TPI dysfunction is also linked to the pathology of ageing related diseases such as Alzheimer's disease (Orosz et al. 2006; Tajes et al. 2013). Post translational modification of TPI has been linked to normal aging, ND disease, and other aging related diseases including cancer (Orosz et al. 2006; Tajes et al. 2013; Picón-Pagès et al. 2019; Enriquez-Flores et al. 2020; Enriquez-Flores et al. 2023). Both cell lines and animals containing dysfunctional TPI have been used to model ND in the literature (Celotto et al. 2006b; Gnerer et al. 2006; Seigle et al. 2008; Guix et al. 2009; Stone et al. 2023; Orosz et al. 2006; Tajes et al. 2013; Picón-Pagès et al. 2019; Enriquez-Flores et al. 2020; Enriquez-Flores et al. 2023). Understanding the mechanism resulting

from this protein dysfunction therefore would be incredibly beneficial for the treatment and management of ND diseases.

Alzheimer's disease is the most common form of dementia (60-80 %) (Goedert and Spillantini 2006), which exists either as the sporadic or familial form, with late onset sporadic dementia accounting for the majority of cases (Piaceri et al. 2013). Due to the prevalence of Alzheimer's disease it is a good example of a common ageing related ND disorder that has been reported to exhibit dysfunctional TPI (Orosz et al. 2006; Tajes et al. 2013). In early stages of Alzheimer's disease amyloid-β (Aβ42) proteins aggregate to form Aβ plaques, this can begin 20-30 years before symptoms appear (Goedert and Spillantini 2006). In healthy neurons any free Aβ proteins are normally removed from the brain via blood flow. Free Aβ proteins arise in neuronal tissue from the breakdown of amyloid precursor protein (APP) via α, β, and γ secretases, APP is present in all neuronal cell membranes, and is thought to promote healthy growth and repair, where a disruption in these functions has been suggested to be one cause of Alzheimer's disease (Wentzell et al. 2012). In healthy function α-secretase acts on APP first, followed by γ-secretase, cleaving APP into three soluble segments, which can be further broken down by proteasomes. In Alzheimer's disease however, β-secretase cuts APP first instead of α-secretase, but γ-secretase still acts second, which leads to a smaller first fragment and larger second fragment (Aβ protein) which is not soluble and so aggregates just outside the neuronal cell. These plaques cause an immune response, leading to inflammation and damage to the surrounding tissue. This mechanically impacts neurons leading to brain atrophy and cell death resulting in compromised synaptic functions (Akiyama et al. 2000; Goedert and Spillantini 2006; Pini et al. 2016).

Another important protein implicated early in Alzheimer's disease pathology is tau. Tau proteins are normally localised to axons, and in neuronal tissue they maintain and stabilise microtubules, which supply nutrients to neuronal cells. When hyper-phosphorylated these tau proteins aggregate and destabilise the microtubule walls, forming tangles inside neuronal cells and interrupting nutrient supply, eventually forming neurofibrillary tangles. (Guix et al. 2009) This process can begin up to 15 years before clinical Alzheimer's disease symptoms appear (Goedert and Spillantini 2006; Guo et al. 2024). It is at this initial stage that has recently been suggested that blood plasma profiles can allow predictions of disease onset (Guo et al. 2024). Tau fibrillation has been linked to post translational modification (PTM) of TPI, in an Amyloid-dependent mechanism (Guix et al. 2009).

Both tangles and plaques mechanically interrupt cell function, inducing an immune response, and neuro-inflammation as the disease progresses. Not only

does this mechanical disruption lead to inflammatory and immune responses which are linked to increased redox stress (Akiyama et al. 2000), it also has been suggested to directly increase redox stress, Aβ plaques for example have been reported to generate reactive oxygen species (Liu et al. 2017). This leads to oxidative damage *via* reactive oxygen species (ROS) and reactive nitrogen species (RNS), i.e. nitrergic stress via by nitric oxide (NO). Aβ oligomers or fibrils form as the disease progresses creating pore like structures in the brain and impacting various neuronal functions such as glutamate receptor activity (Danysz and Parsons 2012). Amyloid angiopathy (amyloid plagues forming around blood vessels in the brain) is another problem in Alzheimer's disease, weakening the capillary walls, increasing risk of haemorrhage and impairing oxygen and nutrient flow (Goedert and Spillantini 2006). Brain atrophy or shrinkage is a later symptom of Alzheimer's disease as more neuronal cells die, gyri (ridges of brain) get narrower, while sulci (crevices in the brain) and ventricles (nutrient storage) get larger (Pini et al. 2016).

Alzheimer's disease begins in the hippocampus and cortex, manifested in early symptoms affecting memory and cognition. The progression of the disease is generally thought to move outwards with the formation of Aβ plaques, and inwards with the formation of neurofibrillary tangles. The majority of Alzheimer's disease cases are not of genetic origin, with a minority where the dysfunction generally stems from mutation in three genes; APP, Presenilin 1, and Presenilin 2 (PS1, PS2 – affecting γ-secretase) (Karch et al. 2014; Fernandez-Funez et al. 2015). One of the key exacerbators of Alzheimer's disease pathology is redox stress, leading to posttranslational modifications such as 3-nitrotyrosination. One of the proteins affected by this kind of post translational modification (PTM) in Alzheimer's disease is TPI, which when inactive, can lead to an increase in advanced glycation end products (AGE), altered synaptic function, and reduced efficiency of glycolysis among other phenotypes, this has been shown in humans, cell lines, and *Drosophila* models (Orosz et al. 2006; Tajes et al. 2013; Picón-Pagès et al. 2019)

Multiple genetic factors have been linked to Alzheimer's disease such as the APOE (Apolipoprotein E) e4 allele, suggested to increase the risk of Alzheimer's disease, making it a possible therapeutic target (Piaceri et al. 2013; Karch et al. 2014). In normal function APOE is a pleiotropic glycoprotein that mediates cholesterol production, is involved in neuronal growth and repair, and neuronal immune response. APOE breaks down β amyloid but the e4 allele is less effective than other endogenous alleles, and has been linked to late onset, sporadic Alzheimer's disease. Mutations in Presenilin 1 and 2, subunits of γ secretase, have been linked to early onset familial Alzheimer's disease. They are thought to change the position γ secretase cuts APP and affect the efficacy of

the produced subunits to clump into tangles (Piaceri et al. 2013; Karch et al. 2014). Trisomy 21 (Down syndrome) has also been linked to familial Alzheimer's disease, Trisomy 21 is an extra copy of chromosome 21 which contains the gene for APP, so individuals with this gene are likely to express higher amounts of APP and are often diagnosed with Alzheimer's disease as early as 40 (Karch et al. 2014).

Many factors impact the development of diseases such as Alzheimer's disease, and many associated potential therapeutic targets have been identified to slow progression. For example, acetylcholine receptor (AChR) density is reduced in Alzheimer's, and some therapies currently in use aim to reduce the breakdown of ACh, compensating for the reduced number of receptors (Kihara and Shimohama 2004). Treatments like this however only target symptoms of the disease rather than the cause, limiting their medical potential.

Preventative measures are therefore more promising with the current knowledge of disease initiation and progression. Targeting the primary cause of disease and the start of the cascade mechanism would minimise the damage done by the cascade. This could be approached by mediating lifestyle risk factors or by pharmaceutical targeting of early proteins in the cascade. Lifestyle has always been an important determining factor for risk of developing Alzheimer's disease. Exercise has been shown to reduce risk of Alzheimer's disease (Rosa et al. 2020), the gut microbiome has been linked to exacerbated neurodegeneration in Alzheimer's disease via increased oxidative stress from ROS and inflammatory immune responses (Akiyama et al. 2000; Wu et al. 2017). An imbalance in the gut microbiome in a *Drosophila* model of Alzheimer's disease was shown to worsen the pathology, via increasing levels of haemocytes (immune cells) in the brain, shown by immunostaining. This was suggested as a possible therapeutic or preventative route of treatment via targeting of the gut microbiome (Wu et al. 2017).

A less common neurodegenerative disease is TPI deficiency. TPI deficiency is a genetic recessive degenerative neuromuscular disorder stemming from a dysfunctional TPI, causing reduced function of the enzyme. It is the only glycolytic enzyme deficiency characterised by neurodegeneration. TPI deficiency is extremely rare with only approximately 40 cases having been reported in the literature by 2014 (Celotto et al. 2006b; NIH Medline plus 2014), and only 100 reported cases worldwide (Harris et al. 2020). TPI deficiency is caused by various autosomal recessive mutations in the TPI1 gene (Celotto et al. 2006b), the most common variant being p.Glu105Asp (Harris et al. 2020), and it will frequently lead to mortality in children (GARD 2023). As TPI deficiency is caused by a genetic mutation of the TPI gene, it is the best comparative *Human* disease for animal or cell models of ND that endogenously express

dysfunctional TPI. Although inferences can be made from such models about the impact of dysfunctional TPI on ageing related diseases like Alzheimer's, the mechanisms of pathology are likely to differ when the enzyme dysfunction develops later in life. Therefore comparison to a genetic disease like TPI deficiency, despite its rarity, alongside the later onset diseases like Alzheimer's is prudent.

As previously mentioned, TPI is an important but not essential glycolytic enzyme, its main role is in the interconversion of Dihydroxyacetone phosphate (DHAP) and glyceraldehyde 3 phosphate (G3P) (Orosz et al. 2006; NIH Medline plus 2014; Ganetzky 2015; GARD 2023). This step in the glycolysis cascade increases the efficiency of glycolysis and minimises the production of methylglyoxal (MGO) and so subsequently reduces the levels of redox stress and production of species such as AGEs. AGE's form large protein aggregates, which have been shown to cause a range of redox damage and DNA modification, see Figure 1-1, (Gnerer et al. 2006b; Guix et al. 2009; Tajes et al. 2013; Stone et al. 2023)(Gnerer et al. 2006 TPI is considered a near perfect enzyme due to its catalytic efficiency, and is important in maintaining efficient adenosine triphosphate (ATP) production, although it is not an essential enzyme for sufficient ATP production (Celotto et al. 2006b; Roland et al. 2016). The structure and kinetics of TPI is discussed in more detail in Section 1.3.

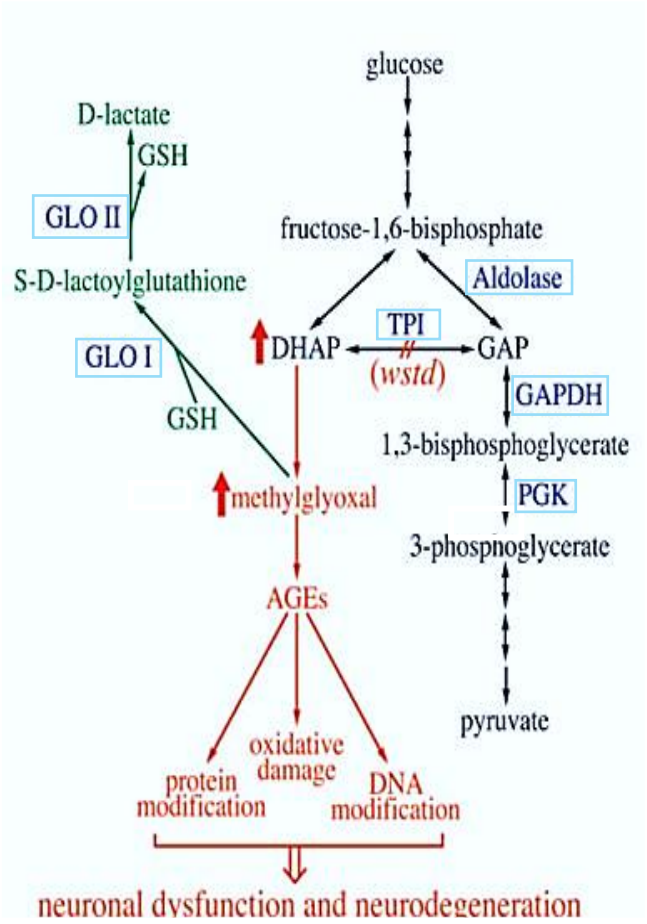

Figure 1-1: Glycolysis cascade showing the impact of dysfunctional TPI. The resultant increase in MGO and following cascade is shown in red, with the innate protective mechanism via GLO 1 shown in green. Enzymes are shown by blue boxes, glycolysis cascade is shown in black. (Gnerer et al. 2006)

TPI deficiency is characterised by an increase in DHAP particularly in red blood cells and, because of this, homozygous cases of disease lead to congenital haemolytic anaemia. Impaired immune response is also characteristic of TPI deficiency with poorer defences against infections, along with neuromuscular dysfunction including cardiomyopathy, and in the vast majority of cases neurodegeneration is seen - only two cases having been recorded without neurodegenerative symptoms. There are no effective therapies available for TPI deficiency, and the exact disease mechanism is unknown (Orosz et al. 2006; Orosz et al. 2009; Ganetzky 2015; Harris et al. 2020)(Orosz et al. 2006; Orosz et al. 2009; Ganetzky 2015; Harris et al. 2020). Outside of the main symptoms of haemolytic anaemia and neurological dysfunction specific symptoms vary from case to case. It has been reported that the intellectual disabilities are a particularly variable symptom of TPI deficiency (Ganetzky 2015). In one patient the intellectual phenotypes, namely a moderate intellectual disability

diagnosed at age 19, were significantly slower to develop than the physical phenotypes, with the patient wheelchair bound from the age of 3 (Harris et al. 2020).

Various models of impaired TPI activity have been reported in literature including multiple *Drosophila* mutant lines that attempt to mimic variants of TPI deficiency. Phenotypes similar to those seen in *Human* TPI deficiency have been shown in such models including reduced longevities and impaired motor functions (Celotto et al. 2006b; Gnerer et al. 2006; Roland et al. 2013). It must be noted that in these disease models, although dysfunctional phenotypes are observed, the impact of the dysfunctional TPI is generally not as extreme as it is in *Human* TPI deficiency where, as of 2020, only one reported case survived to 20 years of age (Harris et al. 2020). More extreme models that better mimic the *Human* disease including knock out lines have been attempted in *Drosophila,* however these more severe dysfunctions have so far proved lethal (Myers and Palladino 2023). These models should therefore be considered as minimal-moderate disease models rather than extreme.

1.2: Glutamatergic synaptic function and redox signalling

1.2.1: Synaptic function

One key mechanism to consider with disease pathologies that include symptoms of neurodegeneration is synaptic function, particularly in diseases like TPI deficiency where pathology stems from a dysfunctional synaptic enzyme, TPI (Roland et al. 2016; InterPro 2023; Stone et al. 2023). *Drosophila* glutamatergic excitatory neuromuscular junctions are often used as models to study synaptic function. In *Humans* equivalent glutamatergic excitatory synapses are present throughout the nervous system allowing comparison (Bradley and Steinert 2015; Robinson et al. 2017).

Neuromuscular junctions (NMJ) in mammalian systems utilise the excitatory neurotransmitter acetylcholine (ACh), In insects, NMJs utilise glutamate as a neurotransmitter. In this work post synaptic glutamatergic activity will be used to explore synaptic function. *Drosophila* express post synaptic glutamate receptors DGluRIIA, DGluRIIB, and DGluRIII at neuromuscular junctions, which are homologues of AMPA kainate receptors in vertebrate models, allowing direct comparison between species (Marrus et al. 2004; Bradley and Steinert 2015; Robinson et al. 2017)(Marrus et al. 2004; Bradley and Steinert 2015; Robinson et al. 2017).

At NMJs in *Drosophila* and vertebrate systems following neurotransmitter release and receptor activation on the postsynaptic cell, the post synaptic membrane is depolarised or hyperpolarised (excitatory postsynaptic potential, or inhibitory postsynaptic potential, respectively). Following sufficient depolarisation in neurons, a threshold potential is reached (-55 to -40 mV (Institute 2017)), and action potential initiated (Cruz et al. 2020). Biological resting membrane potentials generally sit around -70 to -50mV at rest (Institute 2017), and in neurons this resting potential is largely controlled by the sodium-potassium pump and K^+ leak conductance (Bradley and Steinert 2015; Institute 2017; Frank et al. 2020)(Bradley and Steinert 2015; Institute 2017; Frank et al. 2020).

Neuronal excitability in *Drosophila* is determined by the functional availability of potassium and sodium channels. An action potential is a transient depolarisation of the membrane that travels along neuronal axons and dendrites. After voltage gated sodium channels (in neurons) or voltage gated calcium channels (in muscles) depolarise the membrane, voltage gated potassium channels open and slowly repolarise the membrane potential back to rest while the voltage-gated sodium/calcium channels are closed via the inactivation gate. The direction of the action potential wave is maintained by a period of slight membrane hyperpolarisation behind the action potential, preventing the depolarising effect of Na^+/Ca^{2+} to move backwards (Institute 2017; Cruz et al. 2020). In axons, saltatory conduction allows action potentials to travel fast using an insulating myelin sheath to surround axons with regular gaps (nodes of Ranvier) allowing the action potential to 'jump' from node to node (Stampeli and Huxley 1949).

Drosophila membrane potentials are dependent on K^+ and Na^+ by the Goldman-Hodgkin-Katz equation (Jan et al. 1976):

$$\frac{PNa}{PK} = 0 - 23$$

In the Ca^{2+} mediated glutamatergic pathway in *Drosophila* when a presynaptic action potential reaches the synapse, voltage gated calcium channels open allowing an influx of Ca^{2+} ions, near the presynaptic active zone (AZ) (Kawasaki et al. 2004). In Drosophila these influxes last approximately 1 ms in wild-type larvae (Jan et al. 1977). L-type like Calcium channels, the α1 subunit encoded by cacophony locus, are present in *Drosophila* larval crawling motor neurons (as used in this work), which have been reported as showing a clear conservation of function from Drosophila to vertebrate models (Kadas et al. 2017; Kawasaki et al. 2004). An interconnected system of Ca^{2+} influx and transmitter release has been reported with transmitter release and channel function influencing each other, possibility via action of proteins such as synaptotagmin (Stanley 1997,

Yan et al. 1994). The Ca^{2+} ions bind to 'receptor molecules' on the inner cell membrane and vesicles and promote vesicle fusion, releasing glutamate into the synaptic cleft (Sudhof 2012; Cho et al. 2015). Vesicle diameters can range between 25-50 nm, containing roughly similar concentrations of neurotransmitter (Karunanithi et al. 2002). Vesicle exocytosis is controlled by SNARE, complexin, and synaptotagmin proteins, amongst others (Acuna et al. 2014; Yan et al. 1994). Synaptotagmin protein that is positioned on vesicle surfaces have been reported as a Ca^{2+} receptor molecule, sensing Ca^{2+} influx, and promote vesicle fusion at release sites near the voltage gated calcium channels. Synaptotagmin has been reported to bind to Ca^{2+} channels indirectly, possibly controlling their special organisation near to Ca^{2+} influx (Yan et al. 1994). The proximity of voltage gated calcium channels and vesicles are thought to be a key property in short term synaptic plasticity (short lived physical changes at synapse), tight coupling of the two being in the nano-domain (around 20 nm apart) and characteristic of high release probabilities; loose coupling of the two being in the micro-domain (above 100 nm distance) and characteristic of low release probability (Lee et al. 2022).

SNARE proteins, large mass oligomers, control the mechanism of vesicle exocytosis, with use of membrane anchors synaptobrevin (bound to the vesicle membrane) and syntaxin (bound to the cell membrane) see Figure 1-2 [B] (Schwarz 2006; Sudhof 2013; Bradley and Steinert 2015). SNARE proteins work alongside priming factors, namely (M)Unc13 and (M)Unc18 proteins. SNARE and membrane proteins are thought to form alpha helix structures connecting vesicles to the cell membrane (Jackson 2011; Zucker et al. 2014). Not all vesicles in the pre synaptic cell are 'release ready', i.e. docked and primed. However, following Ca^{2+} entry, vesicular release is synchronised and numerous, up to 100 vesicles can be released simultaneously (Acuna et al. 2014), but the maximum response is limited by the number of release sites and release ready vesicles.

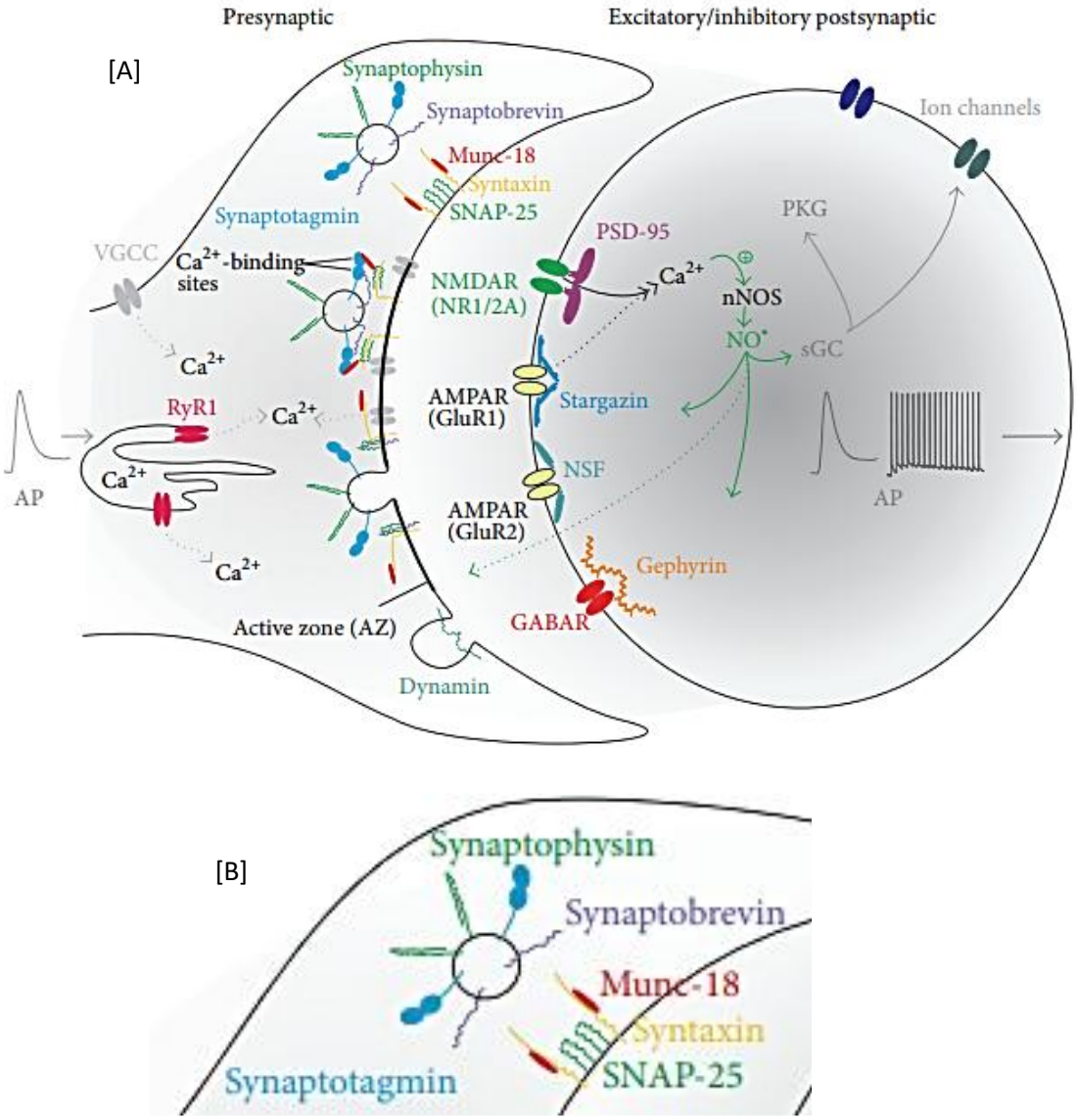

Figure 1-2: [A] Schematic of synaptic vesicle release and post synaptic activity at Ca2+ mediated glutamatergic synapses. All coloured proteins have been reported to undergo nitrergic PTM, S-Nitroslyation or 3-Nitrotyrosination, see Bradley and Steinert 2015 for full breakdown of affected residues. SNARE complexes are shown facilitating vesicle exocytosis from the presynaptic cell. Example raw electrophysiology responses for single and train stimulations are shown in dark grey on the right hand side of the post synaptic cell. Activity downstream of post synaptic stimulation via Ca^{2+} and nitric oxide synthase (NOS) is shown in the post synaptic cell, this activity is only allowed in current clamp measurements. [B] Zoomed in section of vesicle release showing SNARE proteins. Image taken from (Bradley and Steinert 2015).

Released glutamate diffuses across the synapse (≥10 µM during synaptic transmission in mammals (Wang and Reddy 2017)) to the postsynaptic neuron or muscle cell where it activates complimentary receptors creating a range of responses in the cell (Zucker et al. 2014; Martin 2016). These postsynaptic responses can be observed via electrophysiology, recording the voltage/current fluctuations in the (Roland et al. 2016) post synaptic cell. This technique is

further discussed in Section 2.2. See Figure 1-2 [A] for a schematic of synaptic activity in *Drosophila* NMJs.

1.2.2: Redox signalling and post translational modification

One common feature of almost all neurodegenerative disorders is increased redox stress, often promoted via species such as AGE (advanced glycation end products) (Pacher et al. 2007). Redox stress, produced by reactive oxygen or nitrogen species (ROS or RNS), is more severe in many neurodegenerative disorders often directly relating to post translational modifications, including in Alzheimer's disease, Parkinson's disease, and TPI deficiency (Pacher et al. 2007; Roland et al. 2016; Stone et al. 2023).

Generally, both RNS and ROS are closely linked and interdependent: e.g. The generation of peroxynitrite by reaction of nitric oxide (NO) and superoxide radicals (Nagase et al. 1997; Friebe and Koesling 2003; Miwa et al. 2003; Walker and Benzer 2004; Gnerer et al. 2006; Pacher et al. 2007; Cooper and Brown 2008; Zhang et al. 2010; Kummer et al. 2011; Hrizo et al. 2013; Mallozzi et al. 2013; Tsakiri et al. 2013; Verstegen et al. 2014; Miranda et al. 2016; Moraru et al. 2018; Picón-Pagès et al. 2019), see Figure 1-3 for a summary of redox signalling interconnections.

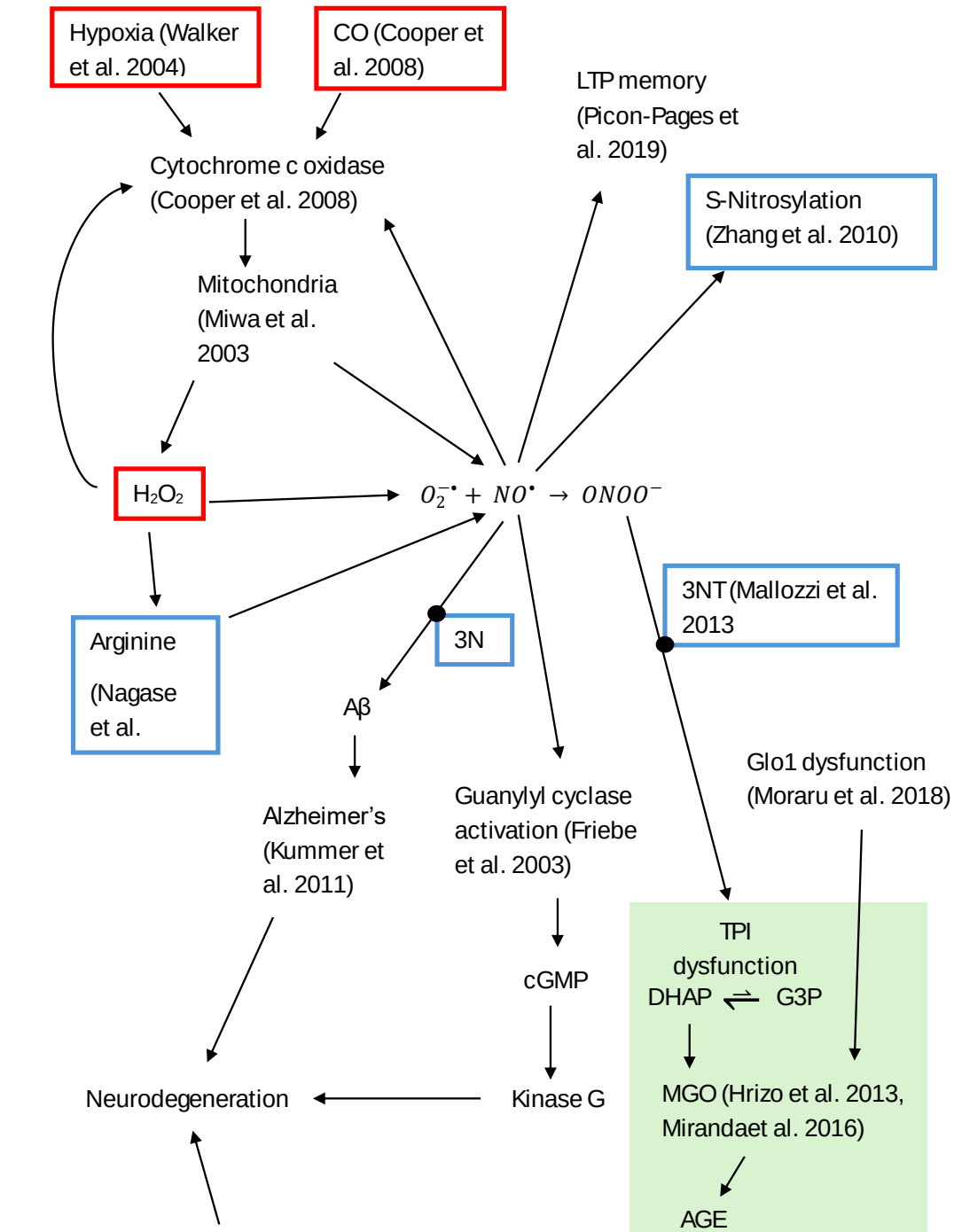

- PTM e.g. Synapsin (Verstegen et al. 2014, Tsakiri et al. 2013)
- DNA and protein modification (Gnerer et al. 2006)
- Redox stress (Pacher et al 2007)

Figure 1-3: Summary of redox signalling mechanisms and consequences from literature. ROS activity shown in red boxes, RNS activity shown in blue boxes. Impact of dysfunctional TPI shown by green highlighted box. (Nagase et al. 1997; Friebe and Koesling 2003; Miwa et al. 2003; Walker and Benzer 2004; Gnerer et al. 2006; Pacher et al. 2007; Cooper and Brown 2008; Zhang et al. 2010; Kummer et al. 2011; Hrizo et al. 2013; Mallozzi et al. 2013; Tsakiri et al. 2013; Verstegen et al. 2014; Miranda et al. 2016; Moraru et al. 2018; Picón-Pagès et al. 2019) Figure created on Microsoft Word.

One common species closely related to aberrant redox signalling in neurodegenerative diseases is NO. NO is a key molecule in paracrine and autocrine cell signalling, its high reactivity and diffusion allowing fast intra and intercellular communication, NO is also a common molecule associated with redox stress and post translational modifications (PTM) (Muller 1994; Muller 1997; Bradley and Steinert 2015; Robinson et al. 2017; Sinenko et al. 2021).

NO levels are normally maintained by NOS enzymes. In mammals there are three isoforms of NOS, which all use oxygen and L-arginine with various cofactors (Flavin adenine dinucleotide, nicotinamide adenine dinucleotide phosphate, flavin mononucleotide, and tetrahydrobiopterin), all of which bind calmodulin. Endothelial and neuronal NOS isoforms are calcium dependent (Alderton et al. 2001). NO is produced in a Ca-dependent manner within neurons by the neuronal NOS (nNOS) (Robinson et al. 2018), in endothelial cells by endothelial NOS (eNOS, to mediate muscle relaxation), or in a Ca-independent manner by the inducible NOS (iNOS, inflammatory response). Enzyme independent NO production is also known to occur *in vitro*, such as in the oxidation of L- or D-arginine with hydrogen peroxide, even in the presence of NOS inhibitors (Nagase et al. 1997). All these NOS isoforms are homologous dimers and, NOS enzymes are well conserved with clear homologues in insects, *Drosophila* NOS also showing Ca-dependence and binding calmodulin (Muller 1994; Muller 1997).

At low concentrations in physiological conditions, NO directly activates soluble guanylyl cyclase to produce cyclic guanosine monophosphate (cGMP), which in turn regulates protein kinase G activity, a key process required for neuronal development and function, and at higher concentrations it can induce PTM (Friebe and Koesling 2003; Nakamura and Lipton 2008). S-Nitrosylation, a posttranslational protein modification induced by NO, has been highlighted as a mechanism for the regulation of many processes such as control of protein functions in health and disease (Zhang et al. 2010). NO is a key player in many pathways, including the smooth muscle relaxation pathway (relaxing of smooth muscle cells) (Mateo and De Artinano 2000). NO is also important in neuronal function, affecting many downstream pathways, and having large impacts on key functions such as long-term potentiation; it is important in memory formation, and blood flow to supply oxygen and nutrients to neuronal cells (Picón-Pagès et al. 2019). NO concentration and localisation have been suggested by multiple studies to be tightly controlled within biological systems (Bredt et al. 1991; Bradley and Steinert 2015). Too high or low NO concentrations have been linked to decreased efficacy of biological systems, often based on overproduction or dysregulation by nitric oxide synthase (NOS)

enzymes (Alderton et al. 2001; Pacher et al. 2007; Adachi et al. 2010; Robinson et al. 2017; Sil et al. 2017).

Increased levels of NO have been found in mouse models of Alzheimer's disease measured live with modified carbon fiber microelectrodes, or indirectly via quantification of PTM such as S-nitrosation (Dias et al. 2016; Seneviratne et al. 2016). This was also seen indirectly via immunostaining in *Drosophila* models (Lee et al. 2016), and indirectly via quantification of nitrotyrosinated proteins in humans (Akiyama et al. 2000). In *Drosophila* models elevated NO levels have been linked to Alzheimer's disease genotypes (Lee et al. 2016), nitrergic effects on dopaminergic neurons in aged flies (Kanao et al. 2012), and NO mediated neurodegeneration in Alexander disease models (Wang et al. 2015). Inhibition of n/iNOS has been shown to reduce PTM in ageing and neurodegeneration (Sil et al. 2017; Bourgognon et al. 2021). Direct nitrotyrosination of Amyloid beta (Aβ – strongly associated with Alzheimer's disease) has also been observed with the subsequent aggregation displaying the direct impact dysregulated NO can have on neurodegeneration in Alzheimer's disease (Kummer et al. 2011).

Investigation of these redox-mediated mechanisms have been widely reported with use of applied redox stressors or antioxidants to model systems. Hydrogen peroxide (H_2O_2) has been used as a redox stressor in Drosophila models and shown to shorten lifespans (Zhu et al. 2021). Glutathione has been reported as an effective antioxidant in *Drosophila* at low concentrations (0.22 mM) improving symptoms of paraquat toxicity by survival assay (Bonilla et al. 2006). There are many stable biologically occurring NO donor sources allowing NO impact to be studied experimentally, such as S-Nitrosoglutathione. Chemical NO donors are also available, such as NOC-12, which can be used as NO carriers helping control NO availability and study NO pathways. For redox species stemming from NO such as peroxynitrite, donors are also available such as SIN-1, which steadily releases peroxynitrite in solution. This can be advantageous as it does not rely on using NO directly, which due to its high reactivity can be technically challenging. The rate of peroxynitrite release can be optimised for specific experiments, allowing a more controlled observation of its impact on physiology (Cuddy et al. 2012).

Peroxynitrite, although stable in basic solutions, is very reactive physiologically and readily reacts with proteins, predominantly on phenolic rings in tyrosine residues resulting in 3-nitrotyrosination, causing changes in protein functionality. In Alzheimer's disease the one of the key proteins affected by this modification is TPI (Picón-Pagès et al. 2019).

Many proteins are impacted by redox stress in neurodegenerative conditions, including synaptic proteins involved in vesicle-membrane fusion such as 3-

Nitrotyrosination of Munc-18, SNAP-25, Tyr 250 in Synaptophysin, and multiple Tyr residues in Synaptotagmin. S-Nitrosylation has also been shown in Synaptobrevin, of Cys 145 in Syntaxin-1, and Cys 141 in Syntaxin-4, see Figure 1-2 (Bradley and Steinert 2015). The glycolytic enzyme TPI has also been reported to undergo PTM whose main role, as previously discussed, is in the interconversion of DHAP and G3P (glyceraldehyde-3-phosphate) (Gnerer et al. 2006). Dysfunctional TPI aggravates redox stress conditions *Drosophila* models having been shown to exhibit altered redox states including increased oxidation of glutathione and NAD+ and a more oxidised mitochondrial redox state (Hrizo et al. 2013), which is expected to be via increased production of DHAP and subsequent increases in MGO, leading to increased production of AGEs (Celotto et al. 2006b; Gnerer et al. 2006b; Orosz et al. 2009; Tajes et al. 2013; Nigro et al. 2017), see Figure 1-1 and Figure 1-3.

This dysfunction has similar impacts on synaptic function although the details are currently unknown (Roland et al. 2016), this is discussed in more detail in Sections 1.3 and 1.4. Nitration and phosphorylation of proteins involved in vesicle exo-endocytosis have been shown *in vivo*, tyrosine residues in synaptic vesicle proteins like TPI and synaptophysin have been shown to be targets of reactive nitrogen species like peroxynitrite, for post translational modifications such as 3NT (Mallozzi et al. 2013).

In *Drosophila* models of disease, AGEs have been linked to redox stress and have been shown to shorten lifespans and disrupt proteostasis (Tsakiri et al. 2013), as well as facilitating various PTMs, such as glycation of Aβ exacerbating Alzheimer's disease models (Gill et al. 2019). MGO has also been reported to increase neurodegeneration and protein aggregation in *Drosophila* (Miranda et al. 2016). Increased MGO has been connected to similar pathologies as in type 2 diabetes including increased insulin resistance, and likelihood of developing obesity, a pathway of dysfunction that has been suggested in a *Drosophila* model of altered glyoxalase function (Moraru et al. 2018).

Glycolysis and connected mitochondrial function more broadly are also extensively linked to redox stress, for example, various oxidising gases including NO and carbon monoxide (CO) are known to inhibit cytochrome c oxidase (Cooper and Brown 2008). Cytochrome c oxidase plays an important role in mitochondria as the final reducing agent in the electron transport chain, so providing essential balancing of redox states (Hartline 2023).

In insects, hydrogen peroxide and superoxide are produced by mitochondria in many species including *Drosophila* (Miwa et al. 2003). In *Drosophila* mitochondrial oxidant production is promoted by drug induced inhibition (such as via potassium cyanide inhibition) of cytochrome c oxidase: cytochrome

activity is also reduced by imbalanced redox signalling via degeneration of mitochondrial cristae (Ferguson et al. 2005; Mesquita et al. 2021). Inhibition of cytochrome c oxidase in *Drosophila*, measured via oxidation of cytochrome c in a spectrophotometer, has been reported to stem from ageing as well as oxidative stress (Schwarze et al. 1998).

Hyperoxic (100 % O_2) conditions induce abnormal folding of mitochondria cristae in *Drosophila*, termed 'swirls' (Walker and Benzer 2004). Mitochondria exhibiting these swirls have significantly reduced cytochrome c oxidase activity. Cytochrome c oxidase itself is also shown to undergo morphological changes in response to hyperoxia namely it has been reported to display a previously hidden epitope, this change has been correlated with a large increase in apoptosis in *Drosophila* (Walker and Benzer 2004). Changes in cytochrome c oxidase activity in *Drosophila* have been shown to alter various behaviours and phenotypes, including dietary preferences (Mesquita et al. 2021).

Neurodegeneration and associated post translational modifications in disease and ageing, have been extensively linked to altered control over vesicle release and vesicle pool organisation. For example, dysregulated phosphorylation (a common problem within neurodegenerative conditions) of synapsin 1 in a mouse model, has been suggested to impair vesicle recruitment to the resting and recycling pools, altering the ratio and spatial separation of the pools (Verstegen et al. 2014). Dysfunctional TPI and the associated change in redox signalling has also been linked to altered vesicle dynamics with impaired vesicle recycling shown via FM1 imaging (Roland et al. 2016; Stone et al. 2023)

1.3: Triose phosphate isomerase and glyoxalase signalling

TPI and glyoxalase (Glo) are key enzymes in the glycolytic cascade. Dysfunction of both these enzymes has been linked to synaptic defects such as impaired vesicle recycling and vesicle pool control in *Drosophila* models, often relating to increased redox stress (Roland et al. 2016; Moraru et al. 2018; Stone et al. 2023). TPI is an important glycolytic enzyme, as previously mentioned its primary role is in the conversion between the two isomers DHAP and G3P, see Figure 1-1. TPI functions as a heterodimer, both monomers include an active site. A salt bridge joins the two monomers, with a catalytic lid forming over the active sites that tightly controls the surrounding hydration sphere, see Figure 1-4 [A] (Gnerer et al. 2006). TPI is considered a near perfect enzyme with diffusion limited catalysis (Celotto et al. 2006b), the equilibrium between DHAP and G3P by healthy TPI favours DHAP by 1:20 (Olah et al. 2002). Monomers of TPI are

cleared as debris via molecular chaperones from synapses so mutations that affect the dimerization of TPI can be lethal (Roland et al. 2014).

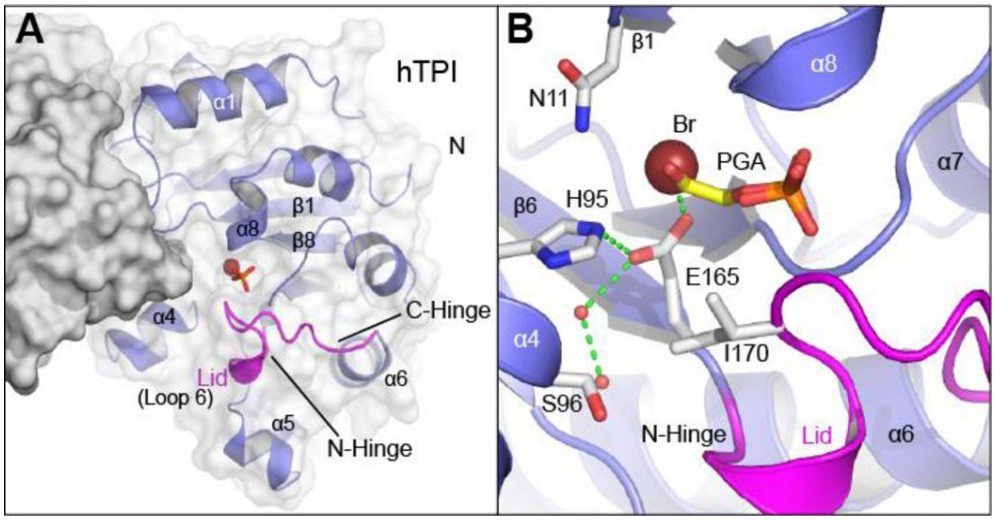

Figure 1-4: Human TPI protein structure reported by Roland et al 2014. Active site shown in colour, catalytic lid is shown in pink [A] catalytic lid within quaternary protein structure [B] Higher resolution image of the active site showing substrate docking, position of hydrogen bonds are shown with green dashes (Roland et al. 2014)

The TPI gene has high levels of conservation from bacteria to humans, the *Drosophila* to *Human* gene comparison is shown in Figure 1-5. The catalytic site and surrounding sequence are completely conserved in all known versions of the protein (InterPro 2023). Both *Human* and *Drosophila* TPI proteins contain multiple tyrosine resides a widely reported site of NO mediated PTM see Figure 1-5, so multiple possible sites for 3-nitrotyrosination (Liu et al. 2011).

```
trembl|P29613|TPIS_DROME      --MSRKFCVGGNWKMNGDQKSIAEIAKTLSSAALDPNTEVVIGCPAIYLMYARNLLPCEL   58
sp|P60174|TPIS_HUMAN          MAPSRKFFVGGNWKMNGRKQSLGELIGTLNAAKVPADTEVVCAPPTAYIDFARQKLDPKI   60
                                 **** ********* ::*:.*:  **.:* :  :**** . *: *: :**: *  ::

trembl|P29613|TPIS_DROME      GLAGQNAYKVAKGAFTGEISPAMLKDIGADWVILGHSERRAIFGESDALIAEKAEHALAE   118
sp|P60174|TPIS_HUMAN          AVAAQNCYKVTNGAFTGEISPGMIKDCGATWVVLGHSERRHVFGESDELIGQKVAHALAE   120
                              .:*.**.***::*********.*:** ** **.******* :***** **.:*. *****

trembl|P29613|TPIS_DROME      GLKVIACIGETLEEREAGKTNEVVARQMCAYAQKIKDWKNVVVAYEPVWAIGTGQTATPD   178
sp|P60174|TPIS_HUMAN          GLGVIACIGEKLDEREAGITEKVVFEQTKVIADNVKDWSKVVLAYEPVWAIGTGKTATPQ   180
                              ** *******.*:***** *.:** .*  . *:::***.:**:**********.****:

trembl|P29613|TPIS_DROME      QAQEVHAFLRQWLSDNISKEVSASLRIQYGGSVTAANAKELAKKPDIDGFLVGGASLKPE   238
sp|P60174|TPIS_HUMAN          QAQEVHEKLRGWLKSNVSDAVAQSTRIIYGGSVTGATCKELASQPDVDGFLVGGASLKPE   240
                              ******  ** **.:*:. *: * ** ******.*..****.:**:**************

trembl|P29613|TPIS_DROME      FVDIINARQ 247
sp|P60174|TPIS_HUMAN          FVDIINAKQ 249
                              *******.*
```

Figure 1-5: BLAST comparing Drosophila and Human TPI proteins. Stars mark regions of similarity. Tyrosine residues highlighted with black boxes. Met position 80/81 shown with blue box (M80T and wstd[1] Drosophila mutants), Ile at position 170 shown by pink box (I170V Drosophila mutant). Created using NIH National library of medicine, basic local alignment tool, protein blast.

Drosophila lines expressing mutated TPI proteins exhibit impaired cognitive function and longevity, similar to observations in *Human* case studies (Celotto et al. 2006b; Hrizo et al. 2013; Roland et al. 2014). Different mutations of this protein induce differing phenotypes, suggesting dysfunction from the impairment of TPI arises from more than one biological route, see Figure 1-6 (Hrizo and Palladino 2010).

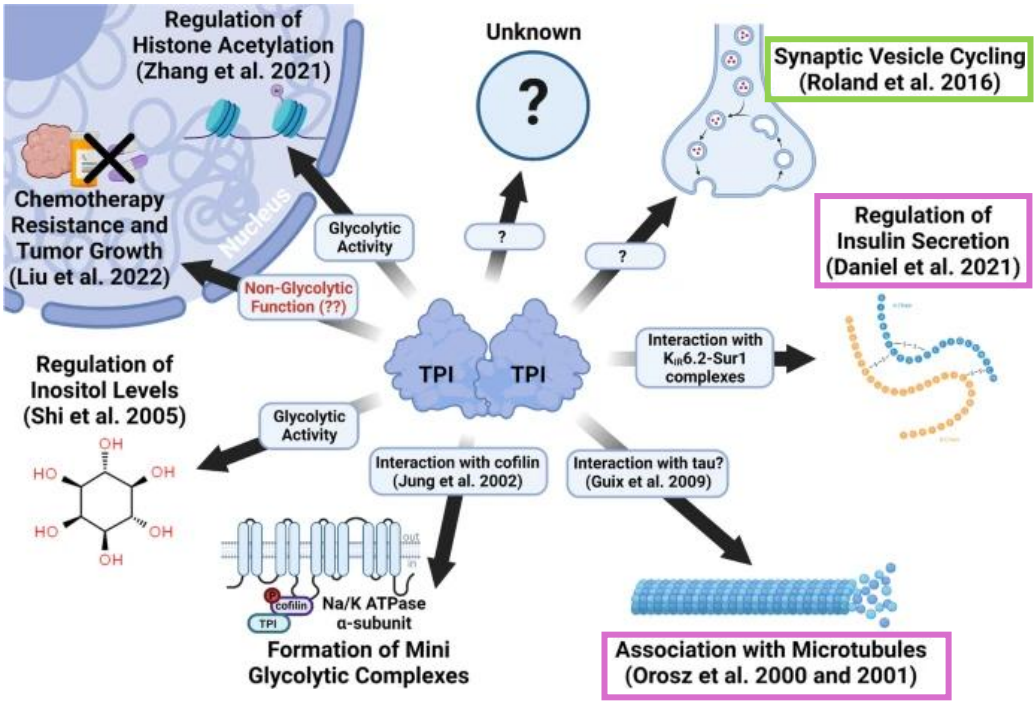

Figure 1-6: Possible routes of TPI dysfunction and implicated mechanisms collated by Hrizo and Palladino 2010. Taken from various literature sources (cited in Figure). The key highlighted mechanism for the TPI models and techniques discussed here is synaptic vesicle recycling, highlighted by green box. Also relevant, although not the focus of this work are, regulation of insulin, and association with microtubules, highlighted by pink boxes.

Various cellular mechanisms have been associated with TPI function, see Figure 1-6. One example of this is with microtubule formation where TPI was found to form a superstructure associating with microtubules, although microtubules formed in the absence of TPI did not show altered development (Olah et al. 2002). This association was shown to reduce catalytic activity in the associated TPI enzymes, it is suggested that this reduction is not problematic in wild-type systems as the catalytic efficiency is high enough the observed reduction is not pathological. However, in *Drosophila* expressing mutant TPI the catalytic efficiency is often reduced so the additional reduction with microtubule association does contribute to pathology (Olah et al. 2002).

The impact of increased MGO levels has been shown to be mitigated by the Glo system as shown in Figure 1-1. This protective system is important, as shown by the observed disease phenotypes stemming from a *Drosophila* Glo knock out

line (Moraru et al. 2018). In the literature levels of Glo have been discussed as biomarkers in brain tissue for behaviours such as anxiety in mice (Hambsch et al. 2010). As previously discussed, one hypothesis is that dysfunction in TPI and the subsequent observed neurodegeneration in various models including *Drosophila* is caused by increased levels of MGO leading to higher levels of AGEs and increased redox damage in biological systems (Scheckhuber 2019), so the activity of Glo in this system is crucial. MGO itself has been shown to reduce the levels of various Glo enzymes when in excess in cell models (Ranganathan et al. 1999), so once levels of MGO increase to a threshold value this protective system is unlikely to recover due to the positive feedback loop.

The Glo enzyme's main role is in the removal of MGO. Glo has been extensively linked to glycolytic pathologies such as type 2 diabetes via various mechanisms including increased insulin resistance, and vascular damage (Nigro et al. 2017; Moraru et al. 2018; Rabbani 2022). A Glo knock out line used in this work has been reported to show such pathologies and is discussed more in Section 1.4.1. Overexpressing Glo has been shown in some disease models to improve neurological deficits (Lu et al. 2023), protective effects of Glo activity are generally attributed to reduced MGO levels *in vivo*.

This glycolysis cascade is a target for treatment of various disorders and diseases including cancer and diabetes (Moraru et al. 2018; Enriquez-Flores et al. 2023). The work presented here suggests it could also be a target for neurodegenerative disorders. Making this pathway a target increases the importance of understanding the interplay of species and the subsequent effects that can present in this system, particularly with the development of redox stress.

1.4: *Drosophila* melanogaster model

Drosophila have been used as a model organism for many years, with over 1500 sub species, well conserved and recorded genetics, fast and well defined lifecycles see Figure 1-7, and cheap maintenance they are an ideal research model (Greenspan 2004; Nichols et al. 2012; Chyb and Gompel 2013; Hime 2013; Dahmann 2016). *Drosophila* were first used in research in 1901 by William Castle at Harvard University, and their use quickly spread and in 1906 Thomas Hunt Morgan started to use *Drosophila*, subsequently winning the Nobel Prize for his work on the *Drosophila* genetic inheritance in 1933. The use of *Drosophila* continued with work such as Hermann Muller showing mutations in *Drosophila* caused by X ray exposure in 1946, and Elizabeth Gateff and Howard Schneidermans work isolating a tumour suppressor mutation in *Drosophila* in

1967. Another Nobel prize for work on *Drosophila* was awarded in 1980 to Christiane Nusslein-Volhard and Eric Wieschaus for their work identifying genes relevant to embryonic development (Hime 2013). Work on *Drosophila* has continued to increase to this day, with the full larval brain and all neuronal connections having been mapped out in 2023 by Michael Winding et al (Winding et al. 2023).

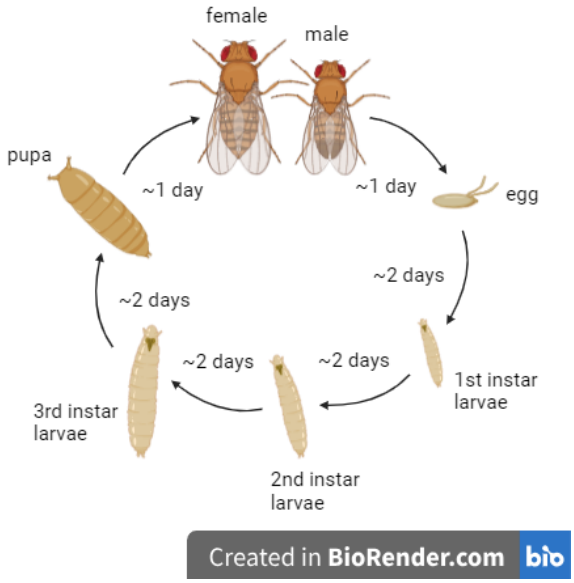

Figure 1-7: Drosophila life cycle. Female and male adults shown at top the whole cycle is approximately 10 days from egg to adult fly. Left through cycle showing; eggs (1 day), 1st instar larva (3 days), 2nd instar larva (5 days), and 3rd instar larva (7 days), pupa (9 days), and adult fly (10 days). Figure created on BioRender.

1.4.1: *Drosophila* as a model for studying TPI function

Drosophila melanogaster has been extensively used as a model for *Human* disease, due to its well conserved genetics (60 % similarity to the *Human* genome and 74 % similarity in genetic disease-associated mutations (Fernandez-Funez et al. 2015)). *Drosophila* has simpler genetics than mammalian models with only 4 chromosomes, this makes genetic manipulation easy, allowing identification of genetic targets for expression of disease dysfunction and possible treatments (Greenspan 2004).

Expression of disease relevant proteins such as Abeta (Aβ) key factor in Alzheimer's disease, beta amyloid protein precursor-like (Appl) *Drosophila* orthologue to APP (Wentzell et al. 2012), the down syndrome critical region 1

(sarah nebula), *Drosophila* orthologue to DSCR1 (Lee et al. 2016), or triosephosphate isomerase (TPI) (Gnerer et al. 2006b; Hrizo et al. 2013; Roland et al. 2014), allow neurodegeneration to be studied in *Drosophila*. Computational models can be used to compare orthologues between species and key proteins.

Drosophila models can be useful to simplify disease pathologies allowing observation of specific mechanisms isolated from the normally co-expressed dysfunctions present in real disease expression, for example Aβ42 *Drosophila* mutants express free Aβ proteins which aggregate, mimicking the pathology of Alzheimer's disease without other initiators (Fernandez-Funez et al. 2015; Nagarkar-Jaiswal et al. 2015).

Drosophila lines can express mutated proteins endogenously from eggs. Alternatively, expression of target genes can be triggered later in life, via triggers such as temperature (McGuire et al. 2004) or other conditional expression systems. Expression of mutant proteins endogenously gives the advantage of allowing disease to be observed in larvae, providing more experimental routes to observe systems, and minimising other potential causes of neurodegeneration from normal healthy ageing (Fernandez-Funez et al. 2015). However, as neurodegenerative diseases in humans are largely ageing related and start later in life these models still have limitations, so using a combination with delayed expression mutants can help to characterise disease specifics.

There are various *Drosophila* lines available containing mutated TPI proteins (Gnerer et al. 2006; Hrizo et al. 2013; Roland et al. 2014). Given the well conserved biology of both *Human* and fly TPI enzymes, these mutants provide a good model system to investigate the impact of dysfunctional TPI on synaptic activity, and subsequent neurodegeneration. One group of mutants that have been described are the so called 'wasted' lines ($wstd^1$ M81T, $wstd^2$ 4bpΔ, $wstd^3$ G41D, $wstd^4$ W89Stop), these are all caused by point mutations in the TPI gene,

see Figure 1-8 [B] and [C] (Gnerer et al. 2006). The mutant lines discussed throughout this work are described in more detail below.

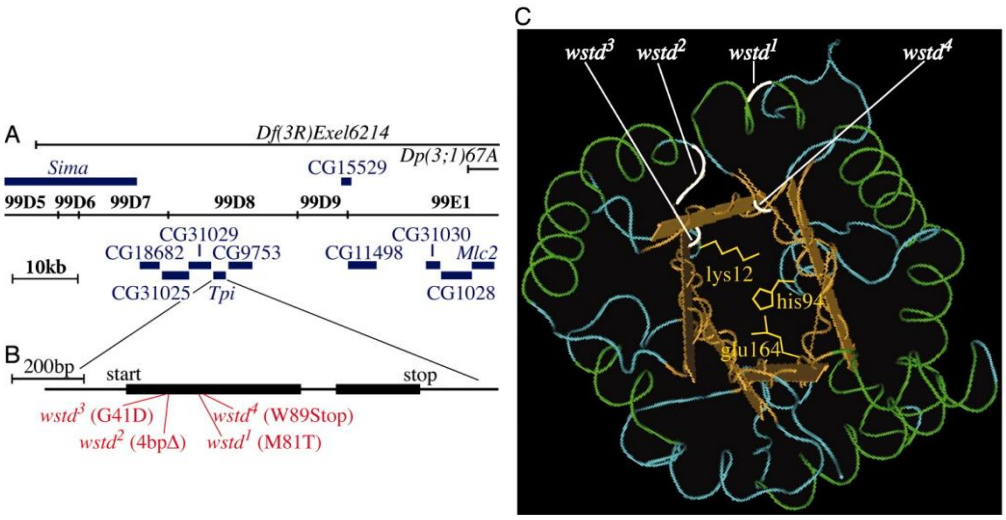

Figure 1-8: Drosophila TPI protein structure. Reported by Gnerer et al 2006. [A] Whole cytological and molecular map of the region showing position of TPI transcription unit [B] Detailed view of TPI transcription unit showing position of wasted mutations [C] TPI protein structure, quaternary proteins shaping active site shown in blue (ß sheets) and green (α helix). Active site shown in orange, key protein residues are drawn out in full (lys, his, and glu). Positions of wasted mutations are shown with white labels. (Gnerer et al. 2006)

1. wstd^1 and M80T lines

wstd^1 is a TPI *Drosophila* mutant containing a point mutation in the TPI gene Met-Thr at position 81, the M80T *Drosophila* mutant contains a point mutation Met-Thr at position 80. These wasted lines – also referred to as *Sugarkill* mutants - are characterised by reduced lifespans, age dependent neurodegeneration, temperature sensitivity (displaying a heat shock paralysis phenotype at 38°C), and aging dependent reduction of motor functions (Gnerer et al. 2006).

Similar phenotypes were found in the *Sugarkill* mutants, with the first mutant characterised sgk^1 (ND14), displaying temperature sensitivity, neurodegeneration, and reduced lifespans (Celotto et al. 2006b). The *Sugarkill* wstd^1 mutant did not show an energetic deficit in comparison to wild type lines, so ATP production is not believed to be the cause of dysfunction (Celotto et al. 2006b).

wstd^1 mutants exhibit physical signs of neurodegeneration such as vacuolar-like lesions (Gnerer et al. 2006). It is suggested in this genetic line that pathogenesis is due to the degradation of unstable TPI (Hrizo and Palladino 2010). It has been

reported that there is no energetic deficit in this line, and it has been shown to have normal mitochondrial function in adult flies at day 5, not exhibiting structural defects as in similar pathologies such as the *Drosophila* ATP6 mutants used as a model of *Human* mitochondrial dysfunction (Celotto et al. 2006b).

TPI in the two *Sugarkill* mutants (wstd^{1} and M80T) has been shown to be disproportionately degraded by proteosomes after being targeted by heat shock molecular chaperones, primarily Hsp70 and Hsp90, an effect enhanced by increased temperatures. This is unusual in neurodegenerative conditions which usually improve with increased chaperone activity, often explained as removal of protein aggregates, the *Sugarkill* TPI protein however does not show an altered solubility therefore does not cause pathology via aggregation. The degradation of TPI has been suggested to be a partial cause of pathology, however rescue via modulation of these chaperones was not possible therefore this effect can not fully explain the dysfunction exhibited by these lines (Hrizo and Palladino 2010).

These two mutants both contain point mutations between Met and Thr groups at position 80 or 81. As shown in Figure 1-5 this appears to be the same position so seemingly an identical mutation. However, these two lines show distinct phenotypes and have been reported in the literature as independent mutants (Celotto et al. 2006b; Gnerer et al. 2006b). Therefore for the context of this thesis the two lines will be discussed separately as two distinct mutations, however a PCR would be a highly beneficial future experiment to confirm how these two lines are genetically different, it is plain they will have distinct genetics as the two lines show consistent differences in phenotypes but the exact nature of these differences is unclear.

2. I170V line

Another *Drosophila* TPI mutant line reported is I170V, which contains a point mutation in the TPI gene Ile-to-Val at position 170. The mutation in this line sits in the catalytic site, and has been shown to reduce catalytic turnover and increase enzyme stability (Roland et al. 2014). I107V flies exhibited impaired recovery to mechanical and thermal stress, similar to *Sugarkill* mutants (Roland et al. 2014). The I170V mutation is not a loss of function, the mutated TPI enzyme still being functional, however, surprisingly models of TPI deficiency based on mutations at the dimer interface have been improved by addition of a catalytically null TPI allele, suggesting a functional synaptic defect that leads to pathology (Roland et al. 2016).

3. Glo(KO) line

A *Drosophila* glyoxalase (Glo) knock out has also been reported, (Moraru et al. 2018). GloKO has increased fatty acid synthase 1 activity but decreased levels of overall protein (due to altered MGO levels), increased triacylglycerol and glycogen levels in relation to total protein, increased circulating glucose and trehalose. This was seen in combination with an increased insulin resistance via a higher activation threshold of insulin pathway, and a higher circulating insulin level, all leading to an increased obesity in the Glo KO line. An increase in MGO levels and a decrease in Glo1 activity and concentration were also shown, displaying a complicated pathology in this line, the suggested mechanisms for this are shown in Figure 1-9 [C] (Moraru et al. 2018).

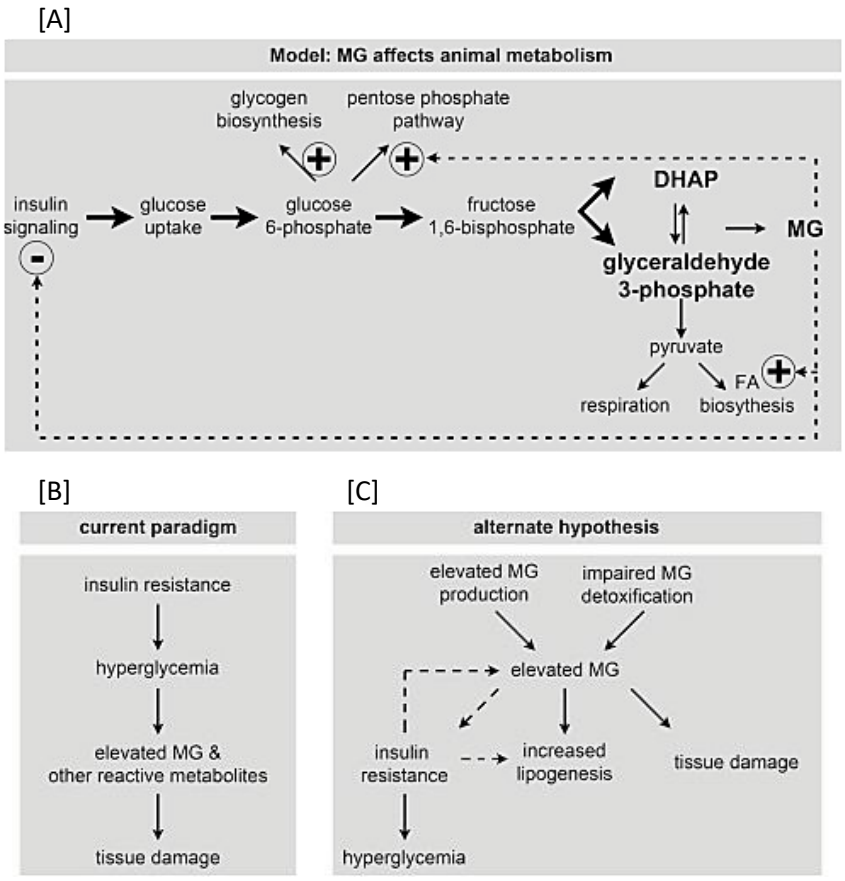

Figure 1-9: Possible model of dysfunction in Glo(KO) presented by Moraru et al. [A] Impact of increased MG (MGO) on insulin signalling (inhibitive), the pentose phosphate pathway (promotive), and fatty acid biosynthesis (promotive). [B] Current proposed theory of glyoxalase inhibition impact via insulin signalling [C] Alternate proposed mechanism of glyoxalase inhibition with elevated MG (MGO) leading to increased tissue damage and lipogenesis, as well as the previously described increased insulin resistance. (Moraru et al. 2018)

1.5: Summary

There is a growing urgency to better understand neurodegeneration and find effective clinical treatments. With current population growth and unprecedented environmental impacts such as food availability and pollution, the prevalence and impact of such conditions is on the increase worldwide.

Redox stress and dysregulation of specific proteins, including TPI, have large impacts in various forms of neurodegeneration including TPI deficiency and Alzheimer's disease. Various studies in *Drosophila* and other models have been published investigating these dysfunctions however the exact mechanisms involved are not yet fully understood.

This work will utilise *Drosophila Melanogaster* mutants expressing augmented TPI activity in comparison to wild-type lines to better understand the impacts and mechanisms of TPI dysfunction and its relation to neurodegeneration. A Glo knock out *Drosophila* line will be observed in parallel to try and expand the picture of TPI deficiency in the wider glycolysis cascade, with specific relevance to redox stress management. The influence and impact of redox states on dysfunction will be explored, and potential therapeutic targets will be suggested.

1.6: Thesis hypothesis and aims

This work aims to elucidate the mechanism of dysfunction resulting from impaired TPI activity. Current knowledge suggests that this is not due to an energetic deficit (Celotto et al. 2006b; Roland et al. 2016) but implies a glycolysis related mechanism of increased advanced glycation end product (AGE) formation, and subsequent increased redox stress. The main aims of this project were to:

- Identify functional consequences of reduced TPI activity on synaptic transmission at the *Drosophila* NMJ synapse
- Connect function consequences of TPI dysfunction to specific mechanisms involved in synaptic transmission
- Test ageing-related increases in redox signalling and identify the contributions of redox stress to neurodegeneration phenotypes in the described *Drosophila* mutant lines

- Suggest a possible mechanism for the complex pathologies reported in *Drosophila* mutants expressing dysfunctional TPI
- Suggest possible targets for treatment of neurodegeneration stemming from TPI dysfunction

Chapter 2: General materials and methods

This chapter will give detailed methods for all techniques used throughout this project. Relevant method details will also be included in the methods section at the beginning of each data chapter.

For all stock chemicals, Thermofisher Scientific, Sigma Aldrich, and the University of Nottingham stores were used.

2.1: *Drosophila*

Investigating disease phenotypes in *Drosophila* is well established and many protocols have been optimised to investigate the underlying pathology. Olfactory learning and memory assays are a common behavioural measure of basic neurological function in *Drosophila*, which is a good measure of healthy behaviour in *Drosophila* as both larvae and flies are informed primarily by their olfactory sense. For motor function quantification, climbing and crawling assays are commonly used (Nichols et al. 2012). The standard climbing assay uses 50 ml Falcon tubes with a line drawn near the top of the tube, first knocking flies to the bottom of the tube then recording how many crawl across this line in a specific time frame gives a measure of climbing ability. This technique in its simplest form does not take into account flies flying over the line, a factor that should be considered when using this method. The first version of this setup was proposed by Benzer et al (Benzer 1967) and various iterations have been suggested since. This technique however, also gives a measure of recovery from mechanical stress, which is often a phenotype for many *Drosophila* disease models including one discussed in this work, wstd[1], so this method is both a measure of climbing ability and shock recovery.

The availability of mating has been shown to have an impact on phenotypes in *Drosophila* such as longevity, with unclear impacts. Lab based *Drosophila* populations have been reported to have a reduced longevity in females that have mated, referred to as a 'cost of mating'. The inverse however has been shown in wild fly populations where female virginity was associated with reduced longevity, referred to as a 'cost of virginity' (Fowler and Partridge 1989; Markow 2011).

Drosophila larvae have a well-defined neuromuscular organisation, see Figure 2-1 [D], and large multi nuclei muscle cells, due to the fusion of multiple cells during their development (Piccirillo et al. 2013). This organisation makes

Drosophila a useful model minimising variability between experiments, as the same NMJ can be found on multiple larvae and compared through various techniques.

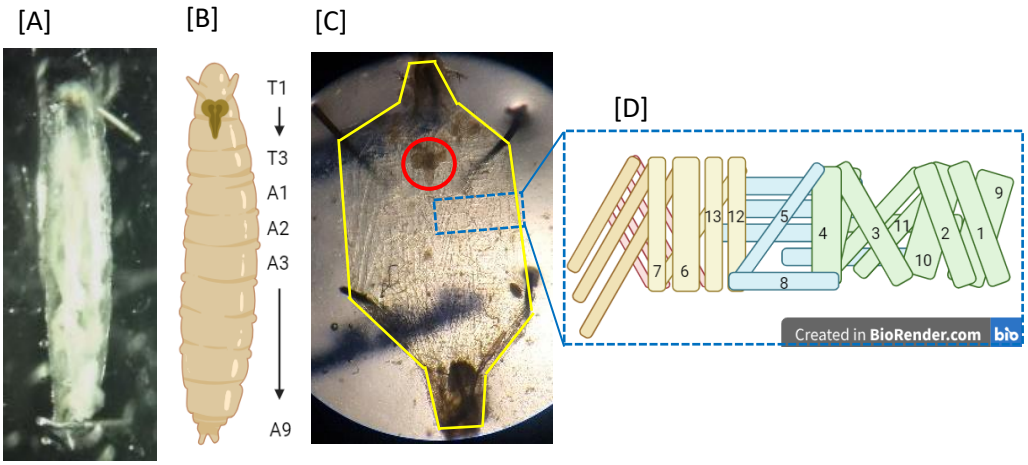

Figure 2-1: Drosophila larva anatomy. [A] Microscope image of 3rd instar Drosophila larvae pinned at head and tail [B] Drosophila larva segments labelled T1-3 and A1-9 made on BioRender [C] Microscope image of filleted 3rd instar Drosophila larva pinned open showing muscle structure, fillet is shown by yellow outline, the repeating section highlighted by blue dashed lined box, and CNS circled in red [D] Larva muscular organisation for repeating segment, muscles labelled 1-13, created on BioRender.

2.1.1: *Drosophila* maintenance

There are little to no ethical requirements for *Drosophila* research. All work was done with the 3Rs of animal work in mind, replacement, reduction, and refinement. Care was also taken to ensure flies were treated as humanely as possible, frequently tipping flies into new food vials, and keeping the number of flies per vial to a maximum of 50. Flies were kept in mixed gender populations unless unavoidable, as availability of mates can affect phenotypes (Koliada et al. 2020). All experiments were conducted on both sexes unless otherwise stated, where no significant difference was seen data was pooled, see Appendix for full breakdown of data.

Drosophila melanogaster were kept on nutrient rich agar (see Table 2.1 for food composition) at standard conditions (12 hr light cycle, 25 °C) unless otherwise stated.

Drosophila food was made by first combining dry agar and cornmeal to 1 litre of water and mixing well, separately the dry soya and yeast was added to 600 ml of cold water and mixed to a smooth paste. While stirring the agar-cornmeal mix, sugar syrup, and soya-yeast mix were added to 5 litres (+270 ml depending on humidity) of boiling water, an additional 700 ml of water was used to rinse

any remaining mix into the main pot. After cooling the propanoic acid and nipagin were incorporated, and the food mix was transferred into vials to set.

Ingredients were obtained from; Spices of India UK, Fisher, Lesaffre UK & Ireland, Brakes golden syrup, Sigma, and University if Nottingham stores.

Table 2.1: Drosophila food recipe

	Mass (g)	**Volume (ml)**
Cornmeal	536	-
Agar	42	-
Yeast	127	-
Soya flour	73	-
Sugar syrup	-	565
Propanoic acid (99.5 %)	-	35.4
20 % nipagin in EtOH	-	40
Water	-	7300 (+270)

The *Drosophila* life cycle is approximately 10 days from egg laying to adult fly, see Figure 1-7. Adult flies can live up to 6 months depending on temperature and light, at 25°C with 12hr light wild type flies live around 70 days. Flips, transferring flies into fresh food vials, were preformed either by tapping, or by anesthetizing via CO_2 then tipping flies into the new vial. Tapping is done by tapping flies to bottom of vial, quickly removing the stopper and flipping flies into a fresh vial (Nichols et al. 2012; Dahmann 2016).Experimental flies were flipped between food vials approximately once a week, stock flies were flipped once (18°C) or twice (25°C) a month. Stock vials were kept to provide a backup in case of contamination within the experimental populations. Genetic checks were done regularly, looking for marker phenotypes (see *Drosophila* lines for details Section 2.1.2.). Checks for environmental contaminants – mites, mould, debris – were also regularly done.

Some issues can arise when keeping flies, and various pests can become problematic. Mites are a common example of this, see Figure 2-2 [A] If vials become infected the mites will feed on fly pupae and eggs, slowly overwhelming fly populations in numbers and leading to dead vials as all eggs and pupae are eaten before developing. Regular flipping of flies and careful cleaning of lab surfaces minimised pest issues. Another problem that can arise in these lab populations is disease and infection, one common fungal infection

causes extreme bloating and eventually death see Figure 2-2 [B.a], flies seen to exhibit this bloating were disposed when seen and food was changed regularly.

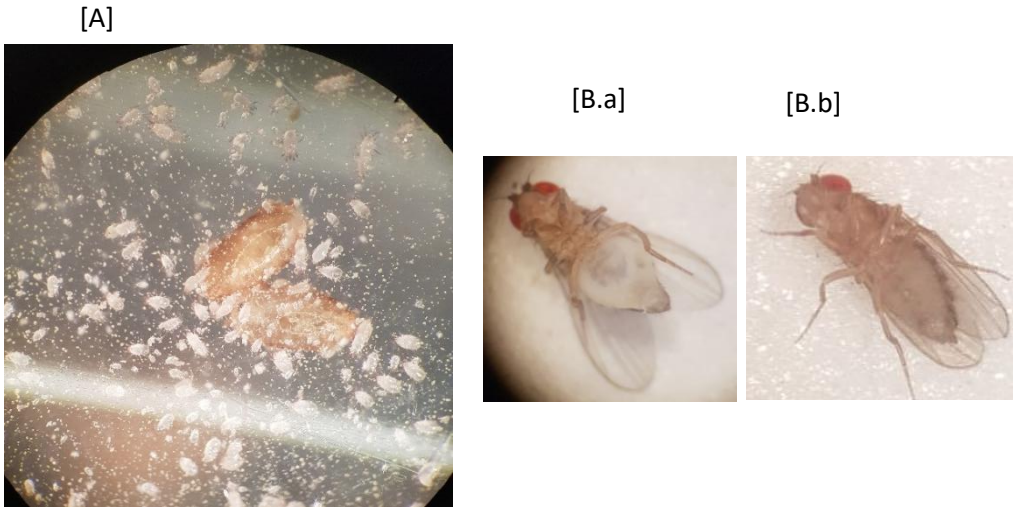

Figure 2-2: Possible problems in Drosophila maintenance. [A] Microscope image of two Drosophila pupae surrounded by mites [B.a] microscope image of female Drosophila adult fly exhibiting swelling relating to fungal infection [B.b] microscope image of a healthy adult female fly.

2.1.2: *Drosophila* genetics

1. Control lines

Wild-type control lines used were w^{1118} and Canton.S 10 (provided by Dr Joern Steinert, University of Nottingham and Dr Isabella Maiellaro, University of Nottingham, respectively). The promotor line elav-Gal4 (provided by Dr Nathan Woodling, UCL Institute of Health Ageing) was used to promote expression of the UAS constructs in neuronal tissue.

Table 2.2: Table of Drosophila control lines

Line	Cross type	Phenotype	Origin
w^{1118}	-	WT	Dr Joern Steinert University of Nottingham
Canton.S	-	WT	Dr Isabella Maiellaro University of Nottingham
elav-Gal4	Virgin females used for crosses	-	Dr Nathan Woodling UCL Institute of Health Ageing

2. TPI lines

Lines expressing mutant TPI proteins; $wstd^1$ ($dTPI^{M81T}$ provided by Prof. Ganetzky, University of Wisconsin[2]), M80T and, I170V, ($dTPI^{M80T}$ and, $hTPI^{I170V}$, provided by Prof. Michael Palladino, University of Pittsburgh), were used as disease models.

The phenotypes of the $wstd^1$ and M80T lines were checked by heat paralysis or lifespan at 29°C. The flies will paralyse when left at 38°C for 2 minutes at 6 days of age (Gnerer et al. 2006). As a secondary check flies will die in 7-20 days at 29°C (Celotto et al. 2006b), control lines will not paralyse at 38°C and will live a median of 30-40 days. The $wstd^1$ and M80T lines use a Canton.S background. The $wstd^1$ line was backcrossed into the Canton.S line to clean the genetic background. The M80T line also used a tubby body (tb) marker, individuals expressing this phenotype were discarded as they did not have the desired genetics. The I170V line was expressed over TM6 in a w^{1118} background with a tubby body (tb) marker, flies or larvae that displayed this phenotype were removed as they did not have the desired genetics. See Figure 2-3 for phenotypic markers.

3. Glo lines

Glo(KO) (M-108 Glo(KO), provided by Prof. Aurelio Teleman University of Heidelberg) was used as a model of reduced glyoxalase activity.

Glo(KO) flies have a w^{1118} background and a curly wing (cyo) marker. Flies that expressed this phenotype were removed as they did not have the desired genetics. See Figure 2-3 for phenotypic markers.

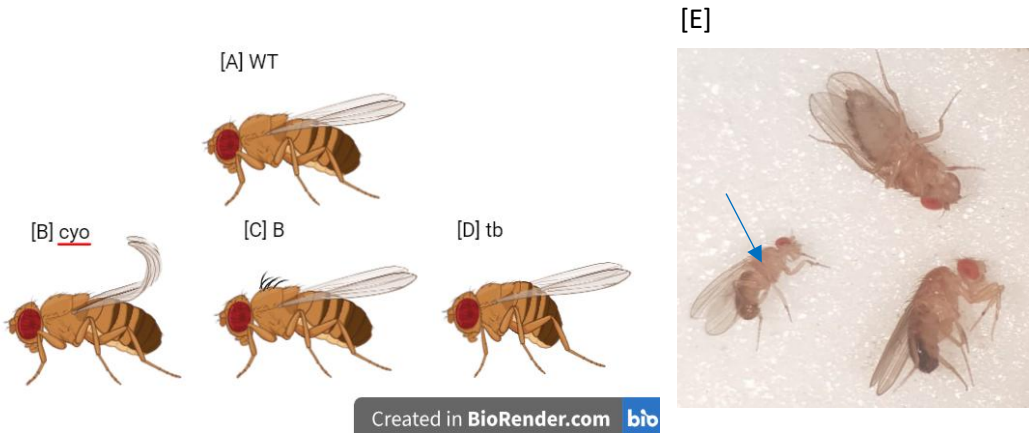

Figure 2-3: Drosophila phenotype markers. Left hand side shows cartoon flies exhibiting common phenotypic markers; [A] wild type (WT) phenotype, [B] curly wing (cyo) phenotype, [C] Bristle (B) phenotype, [D] Tubby body (tb) phenotype.Figure created on Biorender [E] Right hand side showing microscope image of tb fly (indicated by blue arrow) next to two WT flies.

Table 2.3: Table of Drosophila mutant lines

Line	Alleles	background	Mutation	Literature ref	Origin
wstd^{1} (dTPI^{M81T})	Homozygous recessive	Canton.S	Met-to-Thr substitution position 81 hypomorphic	(Gnerer et al. 2006)	Prof. Ganetzky, University of Wisconsin
M80T (dTPI^{M80T})	Heterozygous recessive, with JS10 catalytically null allele	Canton.S	Met-to-Thr point mutation position 80 /TM6 hypomorphic	(Celotto et al. 2006b)	Prof. Michael Palladino, University of Pittsburgh
I170V (hTPI^{I170V})	Heterozygous recessive, with JS10 catalytically null allele	w^{1118}	Ile-to-Val substitution position 170/TM6	(Roland et al. 2014)	Prof. Michael Palladino, University of Pittsburgh
Glo(KO)	Homozygous	w^{1118}	Glo Knock out	(Moraru et al. 2018)	Prof. Aurelio Teleman University of Heidelberg

2.2: Electrophysiology

2.2.1: Technique details

Electrophysiology is a well-established tool to observe synaptic function, allowing controlled investigation of current and voltage fluctuations both pre and post synaptically in real time *in vivo*. These fluctuations directly correlate to vesicle release at synapses, allowing investigation of electrical and biochemical activity at the synapse (The Plymouth Workshop Hanbook 1994). Using the *Drosophila* model to assess neuromuscular junctions (NMJ) has the additional advantages of quick sample preparation due to *Drosophila*'s well defined neuromuscular organisation (see Figure 2-1 [D]).

Electrophysiological methods have been used extensively to characterise neuronal function, key studies such as Hodgkin and Huxley's theory of the

action potential propagation showed the utility of using these techniques to study the nervous system. (Hodgkin and Huxley 1939).

There are many methods developed from Hodgkin and Huxley's early experiments that use real biological membranes to allow recordings under physiological conditions. One common example of this is patch clamp electrophysiology, first conducted by Neher and Sakmann (1976). Use of a virtual ground circuit clamped the potential of an isolated patch of membrane, and in combination with a two electrode clamp on the muscle fibre, the isolated membrane could be voltage clamped. Early versions of these protocols used two electrodes, one stimulating the cell and one recording current fluctuations. A schematic for this original set up is shown in Figure 2-4 [A] (Neher and Sakmann 1976). A more recent advance on this technique is two electrode voltage clamp (TEVC) which allows far more precise measurements to be made, with the biggest source of error resulting from ion leakage around the pipette.

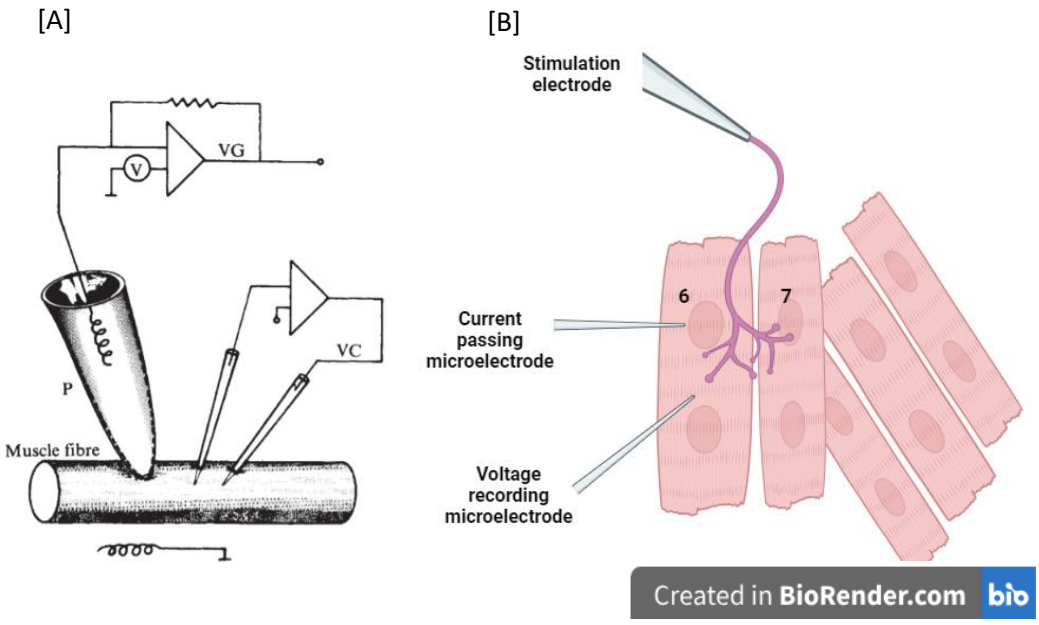

Figure 2-4: Electrophysiology technique [A] Patch clamp technique taken from Neher and Sakmann (1976) [B] TEVC technique in Drosophila 3rd instar larva recording from muscle 6. Created with Biorender

The set up for TEVC in *Drosophila* larvae is shown in Figure 2-4 [B] for recording in muscle 6. TEVC recordings allow recordings of post-synaptic currents independent of membrane potential changes. Clamping the voltage post synaptically minimises downstream activity, allowing recordings of post synaptic currents alone.

HL3 solution of specified calcium concentration is continuously perifused through the setup to ensure consistent temperature (20-25 ℃) and ion composition throughout experiments, the half time of the perfusion system being approximately 2 minutes. This setup can be further specialised exposing preparations to various drugs of interest, or altered ion compositions via the perfusion system to study the effects *in vivo*. This perfusion method can be used to deliver drugs alone, and in combination with ROS, or RNS, and various ion compositions, providing a useful system to observe synaptic activity both with, and without, acute exposure to various biological factors in real time.

HL3 used for dissections and electrophysiology, was made as shown in Table 2.4 below. All powders were weighed separately then combined, distilled water was added to make up solution to approximately 150ml, and $MgCl_2$ was added. The $MgCl_{2(aq)}$ was not added directly to the powders to minimise the chance of the reaction: $MgCl_2 + 2NaHCO_3 \rightarrow MgCO_3 + CO_2 + H_2O + 2NaCl$. The pH was measured to be 7.2±0.1, if required extra HCl or NaOH were added dropwise to adjust the pH to the required range.

Table 2.4: HL3 preparation for 300 ml

Chemical	**Concentration (mM)**	**Molar mass ($gmol^{-1}$)**	**Mass (g)**
NaCl	70	58.4	1.23
KCl	5	74.6	0.112
$MgCl_2$ (1M stock)	20	95.2	
$NaHCO_3$	10	84	0.252
Trehalose 2-hydrate	5	378	0.568
Sucrose	115	342	11.8
HEPES	5	238	0.357

For *Drosophila* larvae electrophysiological recordings, 3rd instar larvae fillets were prepared as shown in Figure 2-5, then mounted under the microscope in HL3.

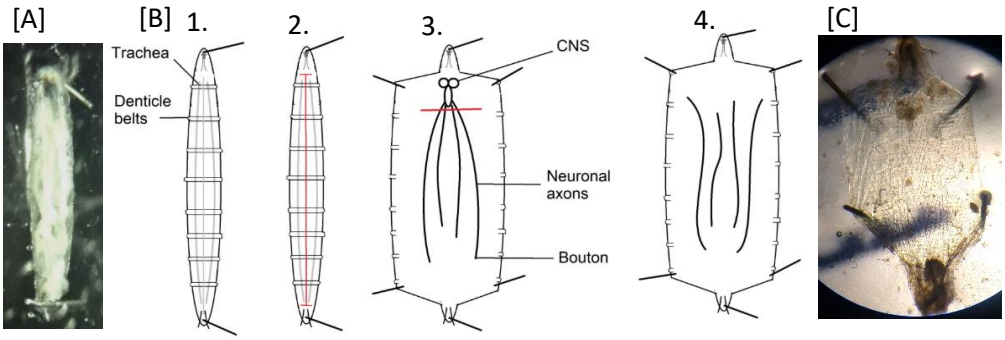

Figure 2-5: Third instar larvae dissection. [A] Microscope image of female larva pinned at head and tail [B] Schematic of dissection from left to right: 1. pinned larva at head and tail showing denticle belts and trachea for orientation. 2. head, tail and, ventral cuts shown in red. 3. Pinned out larva with guts, salivary glands and trachea removed showing CNS and neuronal axons. Direction of cut to remove CNS is shown in red. 4. Final fillet with CNS cut away. Image created on Paint [C] Microscope image of fillet at stage [B]3. with CNS still attached

Postsynaptic responses were recorded in both current clamp and two electrode voltage clamp (TEVC). Current clamp recordings were taken with two electrodes; one sharp electrode (~40-70 MΩ, containing 3 M KCl) in the postsynaptic cell, and one stimulation electrode (containing HL3 1.5 mM Ca^{2+}) which is used to aspirate the exposed end of the innervating motoneuronal axon, allowing stimulation of the NMJ. TEVC recordings were taken with three electrodes, one stimulation electrode as in current clamp, and two sharp electrodes in the post synaptic muscle cell, one recording voltage and one passing current to maintain a constant voltage in the cell, see Figure 2-6 for schematic [A] and lab setup [D]. Recordings were taken consistently from muscle 6 in segments A2/3 giving 4 possible recordings per larva. Muscle 6 forms the largest NMJ's and so the largest responses; it is also widely used in research so allowing better comparisons to be made to published data (Feng et al. 2004; Bykhovskaia and Vasin 2017).

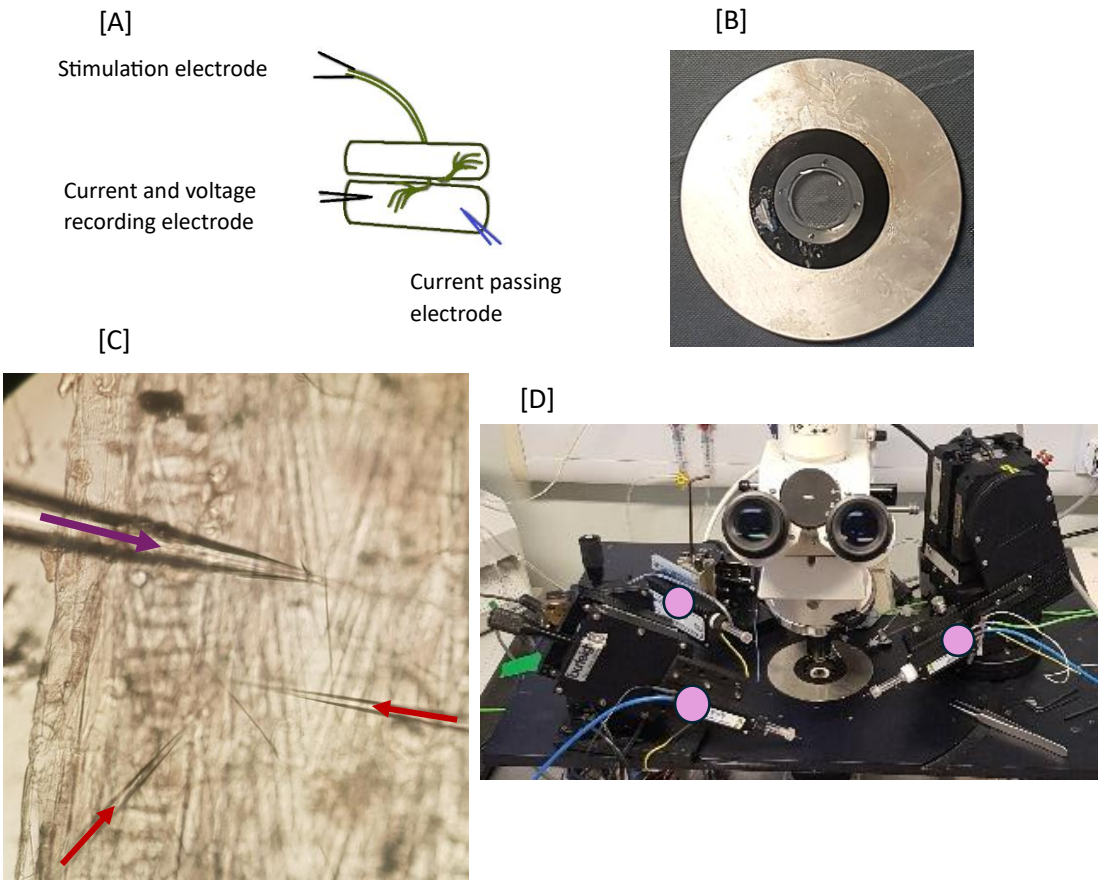

Figure 2-6: Electrophysiology lab set up [A] Electrophysiology TEVC schematic in M6 showing current passing microelectrode in blue, current and voltage recording microelectrode in black, stimulation electrode in black connected to the intubating neuron shown in green. [B] Electrophysiology recording dish, fileted larva in centre. [C] Microscope image of TEVC lab setup, microelectrodes marked with red arrows, stimulation electrode marked with a purple arrow [D] Lab setup three electrode head stages marked with pink dots

Electrophysiological experiments were performed and analysed using Clampex 10.7 software (Molecular Devices). Resistance of electrodes were tested in solution. Within current clamp and TEVC recording modes, protocols to record spontaneous excitatory junction currents and potentials (sEJC/P), and evoked excitatory junction currents and potentials (eEJC/P) were implemented to investigate synaptic activity. Recordings were taken using pClamp software with minimal filtering done in acquisition (filter was applied in Clampfit see Section 2.2.2), the acquisition frequency was 10000Hz.

Spontaneous activity was observed by recording from the muscle 'at rest' both in current clamp and TEVC, when in TEVC the holding potential was set to as close to the resting membrane potential as possible. In *Drosophila* this is generally around -60 mV, for recordings presented in this thesis membrane potentials were ensured to be between -55 mV and -65 mV. Evoked responses were recorded in a 1 Hz stimulation protocol for 20 stimulations, each stimulation lasted between 1 and 4 ms, each sweep lasted 1.2 s, the full protocol

lasted 24 s. The resulting responses were averaged, for evoked recordings voltage was clamped to -60±5 mV to maintain a consistent recording condition.

Synaptic depletion was recorded by applying train stimulations at varying frequencies (10-60 Hz for 1000 ms), see Figure 2-7. Recovery of synapses was assessed by stimulating with exponential delays between pulses for up to 38 seconds' total time, pulses were manually inputted to Clampex 10.7 with exponential rests left between stimulations.

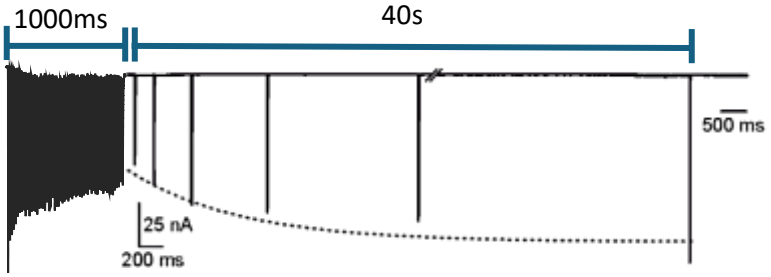

Figure 2-7: Schematic of 60 Hz train and subsequent recovery protocol, first section on the left hand side shows 60 Hz train for 1000 ms, the second section shows the recovery with exponential delays between stimulations for around 40 s. Figure made on Microsoft Word.

HL3 of various calcium concentrations to test calcium dependency was made by addition of a stock solution of 0.5 M $CaCl_2$ to 25 ml of the basic HL3 solution, see Table 2.4. Calcium concentration was 1.5 mM unless otherwise stated. To investigate the impact of calcium dependency of release, single eEJC recordings were taken in a range of calcium concentrations (0-2 mM), see Table 2.5.

Table 2.5: HL3 Calcium dilution from 0.5M stock

$[Ca^{2+}]$ (mM)	**Vol. stock for 25 ml HL3 (µl)**
0.25	12.5
0.5	25
0.75	37.5
1	50
1.25	62.5
1.5	75
1.75	87.5
2	100

For treatment with antioxidants and redox stressors, glutathione 0.22 mM (0.0043 g in 50 ml ddH_2O, (Bonilla et al. 2006)) and hydrogen peroxide 5 % (2 ml 30 % stock, 10 ml ddH_20, (Zhu et al. 2021)) were made up regularly. Additions to food every other day for 24-48 hrs were done to assess the chronic impact of treatments on physiology, H_2O_2 additions were also directly made to the perfusion system for measurement of acute effects.

Electrophysiology equipment was obtained from; Zeiss, Axon Instruments, Scientifica, and Molecular Devices.

2.2.2: Relevant statistics

Electrophysiological data was collected and processed on pClamp software (Clampfit 10.7), Gaussian filtering for spontaneous events was set at 250 Hz and for evoked events 300 Hz. Spontaneous and evoked events were identified based on saved templates which were created by manual selection of many spontaneous or evoked events. Spontaneous events were considered to be events with no stimulation and amplitudes smaller than 3nA or 3mV, evoked events were considered to be events resulting from experimental stimulation, during experimental recording these were ensured to be the maximal response possible from the muscle in question. After running these template protocols the automated selections were then checked manually, taking particular care to avoid composite spontaneous events resulting from multiple vesicle fusion so avoiding Poisson distributions (Jan et al 1976), before transferring specific data to excel for further analysis.

All statistics were run as appropriate. Shapiro-Wilk tests were used for normality tests for all data sets. Electrophysiological data was analysed using Microsoft Excel and Prism (Graph Pad Prism 10.3). ROUT outlier tests were run on all data sets and any outliers were removed. For comparative data sets such as EJC amplitudes Student t-tests were used to give statistical significance between two data sets. When more than two sets were being compared a one-way ANOVA was used, with a Tukeys multiply comparison post hoc test used when mutants were compared and a Dunnets multiple comparison post hoc test when the mutant lines were not compared. For vesicle quantal content calculations, the amplitudes of eEJCs were divided by the amplitudes of associated sEJCs, mean data is presented. For vesicle pool estimations a linear fit was fitted to a section of the end of the curve (700-1000ms), model;

$$Y = YIntercept + Slope \times X$$

and extrapolated backwards to give a Y axis value representative of the vesicle pool size (Schneggenburger et al. 1999). Mini distributions were tested for significance using Student t-tests, Kolmogorov-Smirnov test.

For train stimulations and recoveries, non-linear single exponential fits were used to give time constants (tau). For calcium dependency a non-linear sigmoidal fit was used to generate EC_{50} and HillSlope values, model;

$$Y = Bottom + \frac{(Top - Bottom)}{1 + 10^{(LogEC50 - X) - HillSlope}}$$

For Calcium dependency data was normalised to the maximal response, the $eEJC_{max}$ being equal to 1 within each data set. Robust SS and RSDR tests were used to quantify goodness of fit.

2.3: Biochemical quantification

For larval and adult fly dissections, fine forceps (0.05*0.01 mm tips, stainless steel, 11 cm), fine straight scissors (5 mm blade, 0.1 mm tips, stainless steel, 8 cm), fine angled scissors (5 mm blades, 0.1 mm tips, 45 angle, 8 cm), and blunt forceps (0.5 mm tips, stainless steel) were used, obtained from World Precision Instruments.

1. Larval dissections

Drosophila third instar larvae fillets were dissected as standard (Brent et al. 2009). Larvae were selected for age and gender then pinned down in HL3 buffer, the cuticle and muscle layer were cut, innards removed, the muscle wall was pinned back, and the CNS was removed, as shown in Figure 2-5.

2. Adult Brain dissections

For adult brain collection, full adult heads were dissected also as standard (Jove 2009). Flies were anesthetized via CO_2 then decapitated with fine scissors, freshly cut heads were placed on a pre chilled dish on ice. Heads were then dissected under HL3, using a light stereo microscope. With fine forceps the exoskeleton eyes and mouth parts were pulled away leaving the brain, see Figure 2-8. Any remaining eye tissue, trachea, or head pieces were carefully removed leaving the brain alone which can then be transferred using a cut pipette tip and ≤10µl of surrounding solution.

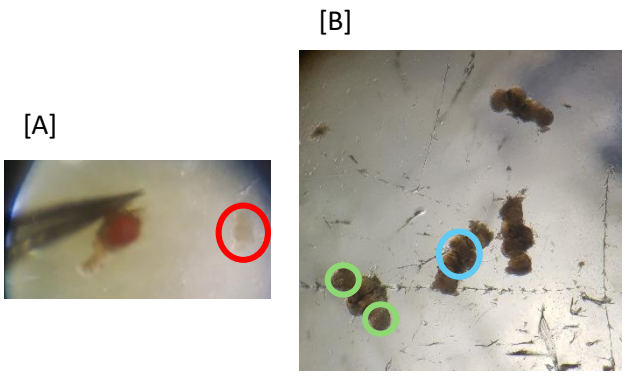

Figure 2-8: Drosophila adult brain dissection [A] Drosophila brain on the right hand side (highlighted in red), Drosophila eye and mouth parts held in fine forceps on the left hand side. [B] Four Drosophila brains, optical lobes (highlighted in green) either side of central brain region (highlighted in blue).

For lysate preparations for use in quantification of SOD activity, 50 ml of 1xlysis buffer was made up with NaCl (150 mM), Tris (50 mM, 0.303 g, pH 7.5), EGTA (2 mM, 0.038 g). 30 adult fly heads or 15 larvae fillets of known gender age and genetics were homogenised per 100 µl of lysis buffer. For Lipid peroxidation pre-made malondialdehyde (MDA) lysis buffer supplied with the assay kit was used containing 1 % Butylated hydroxytoluene (BHT) as an antioxidant. Again 30 full fly heads or 15 larvae fillets were homogenised per 100 µl of buffer. For lysates for Western blot Ripa buffer was used, 50 adult heads or 30 larvae fillets were homogenised per 40 µl of buffer.

For Western blotting, SOD activity assays, and Lipid peroxidation assays homogenates were prepared in bulk where possible. Whole adult heads or larvae fillets were collected at the appropriate ages and genders. The tissue was homogenised (Bel-Art™ ProCulture™ Cordless Homogenizer Unit) in the appropriate buffer, then centrifuged at 12,000 rpm for a minimum of 10 minutes. Table 2.5 shows relative concentrations and buffers used for different protocols.

Table 2.6: Lysate compositions for various techniques

Protocol	Buffer	Buffer volume (µl)	N (Heads/fillets)	Protein concentration (µg/ml)
Western blotting	Ripa	40	50/30	~7000
SOD absorbance assay	1X Lysis Buffer	100	30/15	~800
Lipid peroxidation fluorometric assay	MDA Lysis Buffer (BHT)	250 (2.5µl 100x)	30/15	~200

2.3.1: Lipid peroxidation and SOD activity

To measure lipid peroxidation levels *in vivo* a fluorometric assay kit that measures the concentration of malondialdehyde (MDA), a common end product of lipid peroxidation, was used following the Manufacturer's instructions (Sigma Aldrich MAK085). A dilution series was made by diluting the provided pre prepared 4.17 M MDA standard to 0.2 mM then preparing 0.4, 0.8, 1.2, 1.6, and 2 nmol dilutions for the standard curve, see Table 2.7.

Table 2.7: MDA standard curve

	0.2 mM MDA (µl)	ddH_2O (µl)	Moles (nmol)	Concentration (µM)
0	0	200	0	0
1	2	198	0.4	2
2	4	196	0.8	4
3	6	194	1.2	6
4	8	192	1.6	8
5	10	190	2	10

Sample lysates were prepared in 300 µl MDA lysis buffer containing 1*Butylated hydroxytoluene (BHT). The pre weighed bottle of thiobarbituric acid (TBA) was resuspended in 7.5 ml of glacial acetic acid, 25 ml of water was then added and

the solution was left to homogenise on a stirring plate, sonication was used when needed. To react all the MDA in the samples and standards, 600 µl of the TBA solution was added to 200 µl of each sample and standard dilution which were then incubated for 1hour at 95 °C, creating a fluorometric product. All reaction vials were rapidly cooled to room temperature in an ice bath for 10 minutes, then 200 µl from each mixture was pipetted into a one well of a 96 well clear bottomed plate. Each condition was run in triplicate for technical repeats allowing for averages to be calculated. Fluorescence intensity was measured with excitation wavelength is proportional to emission wavelength, $\lambda_{ex} = \frac{532}{\lambda_{em}}$ =553 nm, using a CLARIOstar microplate reader, where λ_{ex} is the excitation wavelength and λ_{em} is the emission wavelength.

As an indirect measure of oxidative stress levels *in vivo,* a superoxide dismutase (SOD) absorbance assay (OxiSelect™ Cell Biolabs Inc.) was used to measure the activity of SOD. Sample lysates were prepared in 100 µl of ice-cold 1xlysis buffer. A master mix was prepared as shown below in Table 2.8.

Table 2.8: SOD master mix

	Volume per well (µl)
Xanthine solution	5
Chromagen solution	5
10x assay buffer	10
Ultrapure H_2O	60

All conditions were run in triplicate in a clear bottomed 96 well plate (Purchased from Sigma Aldrich). For each well 10 µl sample or blank was added with 80 µl of the above master mix. Immediately before use 1x Xanthine oxidase was prepared from the provided 10x solution, 10 µl was added to each well, the plate was shaken gently then incubated for 1 hour at 37 °C. Absorbance was read at 490 nm on a CLARIOstar microplate reader.

To measure relative protein concentrations a Bradford Pierce assay (Purchased from Thermofisher Scientific) was used to measure levels of total protein in the samples. Bovine serum albumin (BSA) was used as a reference protein for the primarily albumin present in *Drosophila*. This allows comparative values to be calculated for Western blots, SOD, and lipid peroxidation assays to give relative values for protein concentrations *in vivo*. Sample lysates were prepared in the relevant buffer for the comparison assay (i.e. for SOD lysates 1x lysis buffer was used). A standard curve was run from the provided dilution series (0, 125, 250, 500, 750, 1000, 1500, and 2000 µg/ml), 10 µl of each condition (sample or standard dilution) was added per well, 150 µl of the protein assay reagent was

then added to each well. The plate was shaken gently for 1 minute then incubated for 5 minutes at room temperature, absorbance was read at 660 nm.

2.3.2: Immunohistochemistry

For morphology analysis neuronal area was quantified by detection of HRP (horseradish peroxidase) a marker protein spatially associated with the neuronal pile (Jan and Jan 1982). Active zones were quantified by detection of BRP (bruchpilot) an active zone protein involved in vesicle exocytosis among other functions (Knapek et al. 2011). For redox stress quantification AGE (advanced glycation end products) levels were measured (Gnerer et al. 2006; Tsakiri et al. 2013; Scheckhuber 2019), alongside caspase, a protein indicative of apoptosis (Hay and Guo 2006). For IHC experiments paraformaldehyde, 4 % (PFA) was made by addition of 4 g of PFA to 100 ml ddH_2O to make a 1.33 M solution in a fume hood. Also for IHC 1*PBS was made by dissolving one preprepared tablet (Oxoid™ Phosphate Buffered Saline Tablets) in 100 ml of ddH_2O. Triton (0.1 %, Tween (1 %), and NGS (5 %) dilutions were made from this as required, summarised in Table 2.9

Table 2.9: PBS buffers

	1*PBS	**1*PBS-T (Tween)**	**5 % NGS**	**5 % NGS-Triton**	**1*PBS-Triton**
PBS tablet	1	1	1	1	1
Tween (ml)	-	0.991	-	-	-
Triton (ml)	-	-	-	0.095	0.095
NGS (ml)	-	-	5	5	-
ddH_2O (ml)	100	99.11	95	94.91	99.91

1. Immunohistochemistry of NMJs

To visualise larval NMJ morphology immunohistochemistry was used, staining total neuronal area and active zones. First larvae were prepared as previously described, larvae fillets were then fixed in 4 % paraformaldehyde (PFA) for 15 minutes at room temperature. Fillets were unpinned, added to a prelabelled 0.5 ml Eppendorf tubes, and washed three times with 1*PBS-T (200 µl, 1 % Tween 20, 1*PBS) for 3 minutes using an Eppendorf roller. Fillets were then permeabilized with 0.1 % Triton in 1*PBS for 10 minutes on an Eppendorf roller. Fillets were washed again three times with 1*PBS-T as described previously.

The fillets were blocked in Normal Goat Serum (5 % NGS in 1*PBS-T: 5 % NGS-T) for 1 hour at room temperature on Eppendorf roller. The fillets were then incubated overnight at 4 °C in the primary antibody mouse anti-NC82 (DSHB, anti-Brp) 1:200 in 5 % NGS-T. The fillets were washed again 3 times in 1*PBS-T on roller. Fillets were then incubated for 1 hour at room temperature in secondary antibody Alexa Fluor 546 goat – anti Mouse (A11030 Invitrogen, concentration 1:400) and Alexa Fluor 488 anti-HRP (ThermoScientific, 1:400) in 5 % NGS-T. Fillets were protected from light after addition of secondary antibodies with foil for the reminder of the protocol to avoid bleaching. The fillets were washed again 3 times as described above. They were then mounted for microscope imaging, fillets were placed individually into 10 µl of mounting media on a coverslip (up to 3 larvae), a cleaned slide was then carefully placed over tissue, with gentle pressure to remove bubbles. Nail varnish was used to seal around the edges of the coverslip. Slides were kept in the dark at 4 °C. Images were taken with a Zeiss LSM 880 confocal microscope with a 40x or 60x lens then imaging area was manually cropped to NMJ size, Z stacks were taken to encompass whole NMJ area, acquisition times varied depending on size of imaging area and z stack. Images were analysed using Fiji (image J).

2. Advanced glycation end products and apoptosis

To quantify the levels of AGEs and apoptosis, larvae fillets and adult fly brains were stained for AGE and caspase (a key marker for apoptosis in *Drosophila*). Larvae and adult brains were dissected out as previously described, and immediately placed into 1*PBS in 0.5 aliquots with ≤10 µl of surrounding HL3 using a cut pipette tip. The tissue (larvae fillets or adult brains) was then fixed in 4 % paraformaldehyde (PFA) for 15 minutes at room temperature. Fillets were unpinned after fixation and added to a prelabelled 0.5 ml Eppendorf tubes. Brains were transferred between Eppendorf tubes with a pipette with the tip cut to size. The tissue was then washed for 5-10 minutes three times with 1*PBS-T (200 µl, 1 % Tween 20, 1*PBS). All steps were completed using an Eppendorf roller for fillets, for brains tubes were carefully shaken for 30 second at the start of steps, as brain tissue is too delicate for the roller. Fillets were then permeabilized with 0.1 % Triton in 1*PBS for 10 minutes on Eppendorf roller. Fillets were washed again three times with 1*PBS-T as described previously. The fillets were blocked in Normal Goat Serum (5 % NGS in 1*PBS-T) for 1 hour at room temperature on Eppendorf roller. Brains were permeabilised and blocked in one step for 30 minutes to one hour in 5 % NGS 0.3 % Triton in 1*PBS, then washed with 1*PBS-T as described previously. The tissue was then incubated overnight at 4 °C in the primary antibodies:

- Fillets - anti-AGE (clone 6D12 cosmobio, 1:200, 5 % NGS-T)

- Brains - anti-AGE (clone 6D12 cosmobio, 1:200, 5 % NGS-T), Caspase 3 (1:400, 5 % NGS – T)

The tissue was washed again for 5-10 minutes 3 times in 1*PBS-T, then incubated for 1 hour at room temperature in secondary antibodies:

- Fillets - anti-HRP (ThermoScientific, Alexa Fluor 488, 1:400, 5 % NGS-T), Goat anti-Mouse (Alexa Fluor 546, A11030 Invitrogen, 1:400, 5 % NGS – T)
- Brains - Goat anti-Mouse (Alexa Fluor 546 or 488, A11030 Invitrogen, 1:400), Goat anti-Rabbit (Alexa Fluor 660 or 647, Molecular probes, 1:200, 5 % NGS – T)

Tissue was protected from light after addition of secondary antibodies with foil for the reminder of the protocol to avoid bleaching. Tissue was washed again for 5 minutes 3 times as described above, in 1*PBS-T for the first wash, then 1*PBS for the remaining two. Tissue was then mounted for microscope imaging. Fillets were placed individually into 10 µl of mounting media on a coverslip (up to 3 larvae per coverslip), a cleaned slide was then carefully placed over tissue, with gentle pressure to remove bubbles. Brains were transferred with ≤10 µl of surrounding 1*PBS using a cut pipette tip into a small drop of mounting media on a cleaned slide, cover slips were carefully placed over tissue (one per brain, up to 3 brains per slide) gentle pressure was applied to minimise bubbles. Nail varnish was used to seal around the edges of the coverslips, slides were kept in the dark at 4 °C. Images were taken with a Zeiss LSM 880 confocal microscope with a 40x or 60x lens then imaging area was manually cropped to NMJ or brain size, Z stacks were taken to encompass whole NMJ or brain area, acquisition times varied depending on size of imaging area and Z stack. Images were analysed using Fiji (image J).

2.3.3: Western blotting

To measure TPI protein levels, Western blots were performed on young (5 days old), and old (20 days) adult heads and 3rd instar larvae fillets. 50 heads or 30 fillets were homogenised in 40 µl of Ripa buffer and centrifuged at 12,000 for 10 mins. The supernatant was collected and a BSA assay was run to quantify protein concentration.

A solution of 10*SDS Page running buffer was made by addition of; Tris base (Trizma, 30.3 g), Glycine (144 g in 1500 ml ddH_2O), SDS (10 g), made up to 1 L with ddH_2O, pH checked to be 8.3, adjusted if necessary. 1*SDS dilutions were

made as needed. 5*SDS loading buffer was made with addition of; Tris (250 mM), SDS (10 %), Glycerol (30 %), Bromophenol blue (5 %), volume was adjusted with ddH_2O to be 10 ml.

Transfer buffer solution was made by addition of; Tris (3.03 g), Glycine (14.4 g), ddH_2O (800 ml), Methanol (200 ml). 10*TBS solution was made by addition of; Tris (24 g), NaCl (88 g), and ddH_2O to make up volume to 1 L, pH was checked and adjusted if needed to 7.6.

TBST (0.1 % tween) solution was made up by addition of 10*TBS (100 ml), Tween (1 ml), and ddH_2O (900 ml). 5 % Marvel and TBST solution was made by addition of Marvel milk powder (0.25 g) and TBST (5 ml).

Samples were prepared as 20 µg protein per loading volume in 1xLamini buffer. Samples were heated at 95 °C for 5 mins then centrifuged at 12,000 rpm for 5 mins, the supernatant was collected. The gel operator was set up with precast gels (Purchased from Bio-RAD), the tank was then filled with 1xSDS PAGE starting in centre ensuring no leaks then allowed to overflow to halfway up outer compartment. Samples and reference ladder were loaded, and the gel was run at 35 mA for one gel or 70 mA for two gels, for 1 hr (using Bio-RAD PowerPac), until reference reached the bottom of the gel.

Two pieces of Whatman paper and two sponges were soaked in transfer buffer (10 mins). The cassette was then assembled with a Pvdf membrane (prewashed in methanol, ddH_2O, and transfer buffer in succession, used for TPI Western blot), or a nitrocellulose membrane (used for Glo Western blot, does not require pre-wash), and a gel sheet as shown in Figure 2-9.

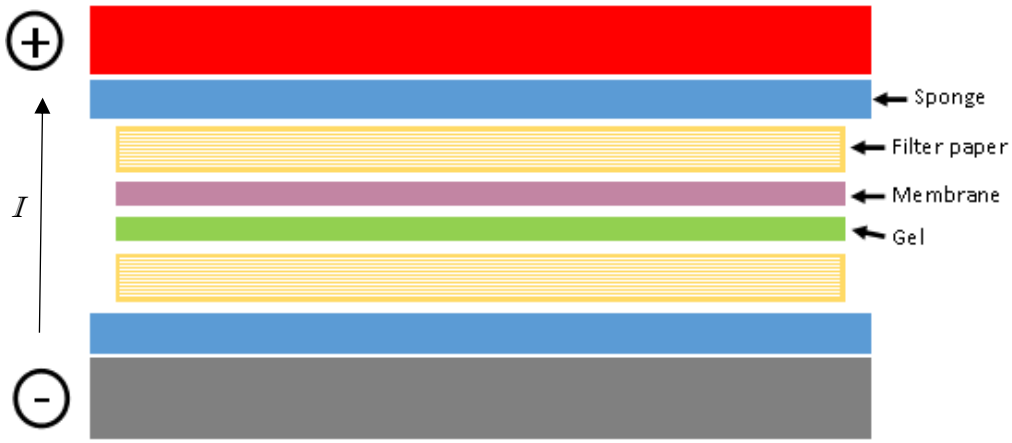

Figure 2-9: Western blotting cassette set up. From top to bottom: positive cassette side (red), pre-soaked sponge (blue), pre-soaked Whatman filter paper (yellow), Membrane (purple), gel (green), pre-soaked Whatman filter paper (yellow), pre-soaked sponge (blue), negative cassette side (grey). Black arrow showing direction of current (I). Figure created on Microsoft publisher.

A roller was used to gently press air bubbles out, then the cassette was closed, locked, and placed in the Bio-RAD transfer tank, this was repeated for a second cassette. An ice block was placed on the negative side of the cassette and the tank was filled with cold transfer buffer 1xSDS P. The transfer was run at 350 mA for 1 hr. The cassettes were opened from the positive side so the membrane was on top. The membrane corner was cut next to the reference ladder for orientation. If required Ponceau stain was used at this stage to confirm protein transfer, which was generally done during optimisation but left out for remaining runs. Membranes were then rolled and placed into a sterile Falcon tube with the protein side facing in. Membranes were washed with TBST (0.1 % tween) for 5-10 mins until the ponceau stain was nearly gone (this wash step was only needed if ponceau stain was used). They were then blocked with incubation of 5 % milk (made from marvel milk powder bought at Tesco, used for TPI blots), or BSA 5 % in TBST (used for Glo blots) for 1 hr. Incubation of primary antibodies were run at 4 °C overnight (in BSA for Glo WB), Anti-TIM (Santa-Cruiz, 1:2000), anti-Glo (phospho-Glo1(Y136) generated by Dr Teleman's lab, German Cancer Research Centre (DKFZ), Heidelberg University), anti-Glo (Santa Cruiz (D-5) sc-133214), anti-tubulin (Sigma-Aldrich T5168-2ML, 1:2000). The following day the membranes were washed three times with TBST, then incubated with secondary antibodies, 680RD Licor (Dnk-MS IgG abcam 216778, 1:5000 for TPI WB) or anti-IgG (GeneTex, Rabbit Anti-Guinea Pig IgG antibody (HRP), or m-IgG Fc BP-CFL 488 sc-533653 for Glo WB), for 60 min in dark. Membranes were imaged using Bio-RAD Imagelab and analysed with Image J.

2.3.4: Relevant statistics

All statistics were run as appropriate. Shapiro-Wilk tests were used for normality tests for all data sets. Bradford assay results were analysed following the assay protocol, the blank readings were subtracted and BSA concentration was calculated by comparison to the standard curve.

Lipid peroxidation results were analysed as described in the protocol. For all data points triplicate recordings were averaged then blank readings were subtracted to account for background. A standard curve was created with values for known concentrations of MDA standard, and the relative levels of MDA in samples were found in comparison to the standard curve using an equation of a straight line;

$$y = ax + c$$

Results were normalised to total protein concentration by the Bradford assay.

SOD results were analysed following the assay protocol, the blank readings were subtracted, and relative SOD activity was calculated normalising to relevant control line result. Results were normalised to total protein concentration by the Bradford assay.

IHC results were analysed in Image J. Images were stacked and any background was removed. Total neuronal pile and active zone areas were assessed by intensity measurements of HRP area for neuronal, and BRP area for active zones. The ratio of BRP:HRP total % areas is reported, along with single BRP to total HRP area as active zone: total neuronal area ratio. BRP count was done by automated analysing and count of particles, manually adjusting to optimise the selection of BRP signals. Bouton count was done manually, counting the branching number per NMJ for each confocal image individually. AGE and caspase were quantified by intensity measurements. In larvae this was done with measurement of a saved selection size both in the centre of muscle tissue in muscle 6/7, and by manually centring a nucleus from muscle 6/7 within the saved selection. For adult brains selection was made per image by hand selecting the central region of the brain excluding optical lobes.

Western blotting was quantified in image J. Images were made greyscale, and a selection area per protein band was saved to fit the largest well signal in the line. The saved selection was moved to surround each well signal separately, and intensity of the signal was taken as the sample measurement, along with the intensity of saved selection in the area directly above or below the well signal as a corresponding blank reading for the well. The sample measurements were adjusted by subtraction of the associated blank reading. Then the measurements of experimental protein (TPI) were normalised to total protein

by division of adjusted TPI protein reading by the adjusted paired tubulin protein readings.

For comparisons between data sets Student t-tests were used to give statistical significance between two data sets. When more than two sets were being compared a one-way ANOVA was used, with a Tukeys multiply comparison post hoc test used when mutants were compared and a Dunnets multiple comparison post hoc test when the mutant lines were not compared.

2.4: Behavioural studies

Treatments with antioxidant (glutathione) and redox stressor (hydrogen peroxide) were used as compensators or exacerbators of the disease dysfunctions. For dietary treatments glutathione 0.22 mM (0.0043 g in 50 ml ddH_2O (Bonilla et al. 2006)) and hydrogen peroxide 5 % (2 ml 30 % stock, 10 ml H_20 (Zhu et al. 2021)) were made up regularly.

2.4.1: Longevity

Flies were collected for longevity in 24 hr hatching windows counted and placed in vials of approximately 50 flies per vial (6.5x2.5 cm). The number of deaths were recorded every other day starting from day 10 (day of adult fly emergence from pupa) until all the population were dead. Treatments of 150 µl of solution (5 % H_2O_2 (Zhu et al. 2021), 0.22 mM Glutathione (Bonilla et al. 2006), or ddH_2O) were given every other day, non-treated vials were given drops of water if food looked dry but was not in need of changing. Treated vials were kept horizontally to minimise flies getting stuck in liquid or wet food.

2.4.2: Circadian rhythm

Sleep tubes (4 inches, TriKinetics Inc., catalog number: PPT5x65 Polycarbonate) were prepared with food filling one end (1 inches), one tube per fly was prepared. The food filled ends of tubes were capped with paraffin wax, see Figure 2-10 [D]. The fly food used in experiments was (2,25 g of agar, 7,5 g of sucrose, made up with ddH_2O to 115 ml). Young (6-8 day) or old (16-19 day) male flies were collected and placed into tubes with a paintbrush, one fly per tube, the open ends were plugged with small sections of pipe cleaner 0.5 cm in

length. Tubes were then mounted into monitor racks, rubber bands were used to secure the tubes in place. Tubes were aligned so the centre of each tube aligns to the centre of the *Drosophila* activity monitor, ensuring the position of infrared beams in tubes, see Figure 2-10 [B]. Flies were left to acclimatise to the environment for 3 days before experiment was started. The monitor range (number of monitor racks set up) used was 35, the monitor racks were placed into an incubator (Percival, DR 36VL) set to 25 °C. Racks were then connected to the computer and power supply. DAMSystem311 software (DAMFileScan, Tricineticks DAM system) was used to track flies crossing infrared beams over the set time periods, with set light cues. Experiments were run for 1 or 5 days in 12 hr light-dark cycle or 24 hr dark.

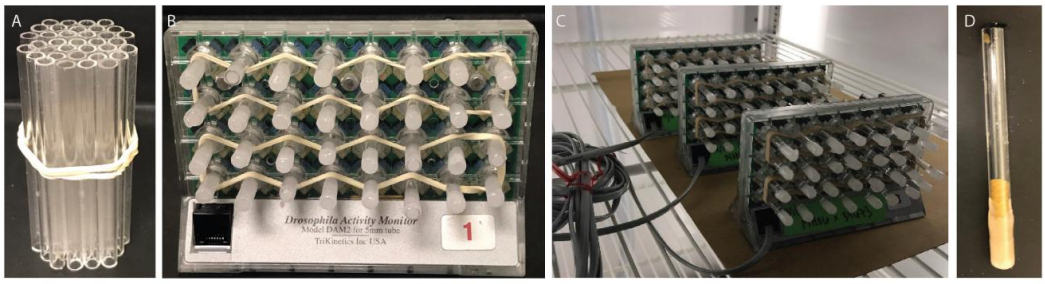

Figure 2-10: Sleep tubes and circadian setup. [A] bundle of sleep tubes without food [B] sleep tubes in monitor racks with rubber bands in place [C] Racks arranged and connected to computer and power supply [D] Sleep tube with food and wax cap (Driscoll et al. 2019)

2.4.3: Learning and memory

Reciprocal training assays were run to investigate learning and memory in w^{1118}, Canton. S, M80T, I170V, and $wstd^{1}$ lines. Assay protocols previously described by Michels et al, were used as a basis for these experiments (Michels et al. 2017). Fructose was used as a reward and n-amyl acetate (AM) or octan-1-ol, were used as smell conditions in comparison to distilled water. Trials were run on standard 9.2 cm petri dishes coated with 1 % agarose, made by addition of agar powder to distilled water which was heated and stirred until all powder was dissolved, the solution was poured into eight petri dishes per 100 ml and left to set. For the sugar training 36 g of fructose was added per 50 ml of the 1 % hot agarose before pouring into petri dishes, care was taken to minimise the temperature before this addition to avoid caramelisation while still getting full incorporation of the sugar. Petri dishes were marked with two lines 1 cm apart along the diameter and labelled according to the condition. The n-amyl acetate and Octan-1-ol odours were made by addition of 10 µl of n-amyl acetate or Octan-1-ol to 490 µl of paraffin oil, this was mixed in a vortex for approximately

30 seconds. The odours or control were added dropwise to circles of filter paper (a standard holepunch was used to collect paper circles), saturated paper circles were placed on the respective side(s) of the petri dishes. For experimental trials fifteen 3rd instar larvae were placed in the central 1 cm strip and left for 4 minutes after which the larvae's placement on the petri dish was noted. Experiments were run with first an innate preference test with an odour on one side of the dish and a control (water) on the other side. Then three conditioning phases were run where the odour was placed on both sides of the dish either with sugar agar (positive conditioning) or normal agar (negative conditioning). Finally, a learning and memory test was run in the same manner as the innate test with odour on one side and control opposite on a normal agar dish, the resulting count of larvae was used to calculate preference index (PI) values relative to the innate preference. All trails were conducted at room temperature and standard lab lighting.

2.4.4: Motor function

To assess motor function crawling and climbing assays were run. For crawling assays an arena was set up with 6 zones, the zones were kept moist with ddH_2O to avoid larvae drying out. A camera was positioned above the arena so all 6 zones were in view, a clean single 3rd instar larvae of the appropriate line and gender was added to each zone with a paintbrush. The background and lighting were optimised to best image larvae, this was crucial to ensure the software was able to continuously track larvae. A copper wire was used to border each zone, a current of 2 A (6 V) was run through this wire, giving a temperature of approximately 49 °C to deter larvae from the edges of their zones without causing damage. See Figure 2-11 [A] for experimental setup. The larvae movements were tracked with Any Maze 7.2 for 10 minutes following a 30 second acclimatisation period, absolute turning angles, average speed, and total distance travelled were recorded.

[A]

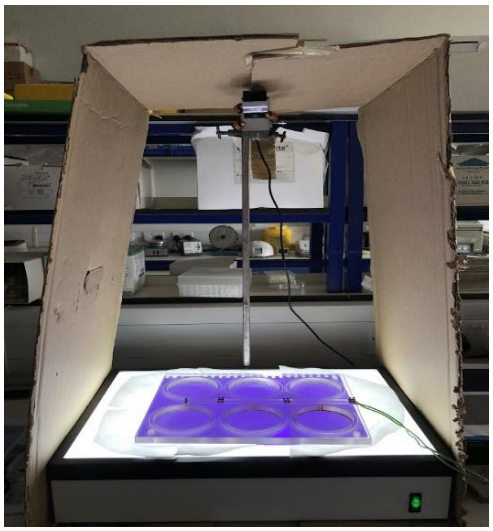

[B]

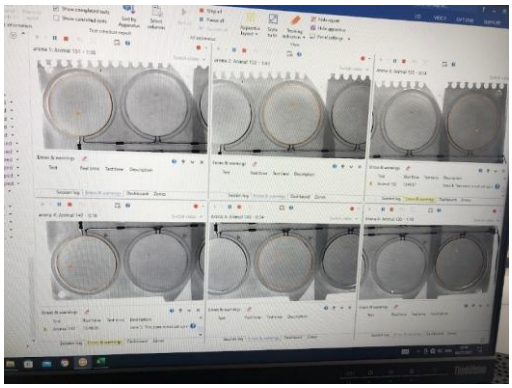

Figure 2-11: Larval crawling lab setup [A] Experimental set up for larval crawling arena back lit with purple backing sheet to provide contrast, cardboard walls and ceiling to avoid directional light [B] Software view of larval crawling setup, six arenas shown.

Adult fly climbing assays were run as standard (Madabattula et al. 2015) see Figure 2-12. Flies of appropriate age, gender, and line were collected, three 50 ml Falcon tubes per condition were then set up containing 10 flies each. Flies were rendered unconscious with CO_2 to transfer then left for 30 minutes to an hour to recover and acclimatise to the tubes. Falcon tubes were prepared with a line drawn at a height of 5 cm from the base of the tube as the threshold. For each experiment flies were tapped as gently as possible to the base of the tubes (multiple tubes can be tapped at once by placing all in a stand and tapping the stand) and a timer was started for 90 seconds. A camera was setup to record all tubes and the number of flies to cross the threshold in each tube was recorded. Results were displayed as average percent of flies to cross the threshold.

[A] [B]

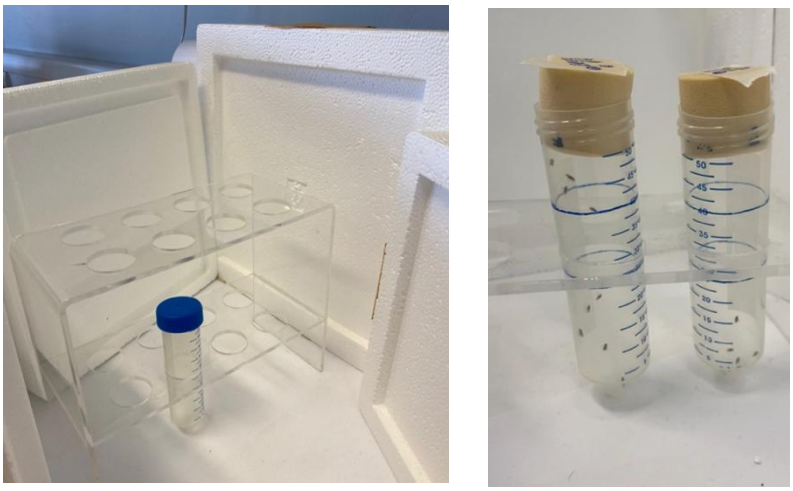

Figure 2-12: Experimental setup for adult climbing standard protocol [A] Open arena with Falcon tube tray [B] Two tubes mid experiment with threshold marked in blue pen

2.4.5: Relevant statistics

All statistics were run as appropriate, ROUT outlier tests were run on all data sets and any outliers were removed. Data for longevity studies was recorded in excel as raw numbers of flies, prism was then used to plot Kaplan Meier survival curves, median lifespans were recorded, and log-rank (Mantel-Cox) and Gehan-Breslow-Wilcoxon tests were used to compare data sets for statistical significance.

Circadian data was sorted into 1 min bins on *Drosophila* activity monitor software (DAMFileScan) MATLAB was then used to eliminate dead or immobile flies. Data was then analysed in Prism to compare data sets as standard, (Driscoll et al. 2019; Breda et al. 2020). Shapiro-Wilk tests were used for normality tests for all data sets. Kruskal Wallis ANOVAs were used to test differences between the three lines in young flies, with Dunn post-hoc tests. Mann Whitney Students t-tests were used to test differences between the two lines in old flies.

For learning and memory assays Innate preference was reported as the average of $Pref_{innate}$ values between all trials:

$$Pref_{innate} = \frac{no.larvae\ on\ AM\ side - no.larvae\ on\ control\ side}{total\ larvae}$$

Learnt preference was reported as averaged PI values from all trials:

$$PI = \frac{Pref(odour\ rewarded) - Pref(control\ rewarded)}{2}$$

Where no significant innate preference was seen and positive PI values were found in individual larvae, they were assumed to have learnt the odour association.

Behavioural studies used $Pref_{innate}$ and PI calculations to quantify preferential behaviour of lines in relation to odours and rewards, both innate and learnt. Shapiro-Wilk tests were used to test for normality, mean data was compared with t-tests for two data sets or one-way ANOVA for multiple data sets.

Motor function, crawling data was tested for normality with the D'Agostino and Pearson omnibus test and reported with 95 % confidence intervals

For larval crawling and adult climbing data Shapiro-Wilk tests were also used to test for normality. For parametric data sets mean data was compared with t-tests for two data sets or one-way ANOVA for multiple data sets to test for statistical significance. When sex or treatment was compared as well as genetic lines a two-way ANOVA was used. For nonparametric data sets Kruskal-Wallis and Mann-Whitney tests were used.

2.5: Methods for Appendix data

2.5.1: *Drosophila* lines

1. Glo lines

UAS-Glo flies (UAS-Glo1, provided by Prof. Aurelio Teleman University of Heidelberg) were expressed over TM6 in a w^{1118} background with a bristle marker (B), flies expressing extra humeral bristles were discarded. UAS-Glo were crossed with Gal4 to provide an F1 generation that overexpressed the Glo1 protein.

Table 2.10: Drosophila mutants

	Alleles	**Mutation**	**Literature reference**	**Origin**
UAS-Glo	Homozygous	UAS-Glo construct (not expressed)	Not reported	Prof. Aurelio Teleman University of Heidelberg
Glo(OE)	-	Glo Overexpression	Not reported	-

1. Gal4-UAS system

The Gal4-UAS system was used to over express target proteins with UAS-TPI and UAS-Glo lines crossed with elav-Gal4 to promote expression in neuronal tissue, see Figure 2-13. Crosses were set up by collecting virgin female Gal4 flies and young male UAS-X parent flies into new vials. Virgin females and young males were collected by first setting up a hatching vial for both lines with no adults in but plenty of pupating larvae, newly hatched adults were then collected at regular intervals. Virgins were identified by dark spots on the abdomen (meconium from byproducts of pupal metabolism) and still furled wings, both signs of very young age and so virginity, flies in cases where the only hatched flies in the vial were female were also assumed to be virgins and collected. Once enough flies from both lines were collected (minimum of 5 each) the vials were combined. The F1 (first generation) from this cross containing the intended genetics were collected as they emerged for up to 13 days after the parents were first placed in the vial. Parents were continuously flipped into new vials to provide continuous F1 generations and to ensure none of the F1 generation hatched into the parent population so contaminating the cross. The F1 generation can be checked by disease and marker phenotypes, when multiple phenotypes are observed the cross was unsuccessful, most commonly due to contamination of cross vial with unwanted individuals.

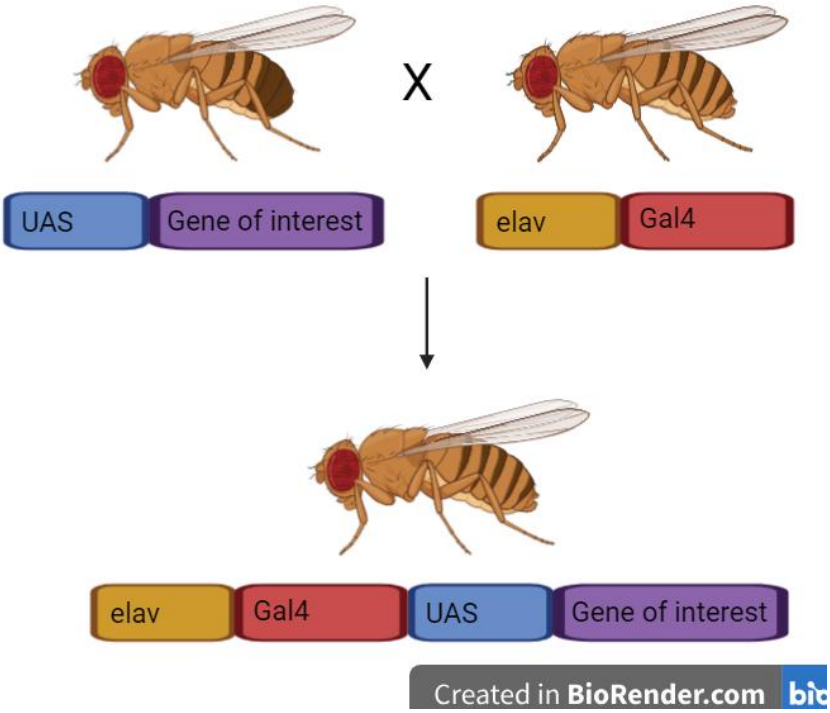

Figure 2-13: Schematic of Gal4 -UAS system. Parent lines on top line; UAS – X young males, containing but not expressing gene of interest, and elav-Gal4 virgin females. F1 generation on bottom line expressing gene of interest in targeted neuronal tissue via elav driver. Figure created on Biorednder.

Figure 2-14: When crosses go wrong. F1 generation TPI OE line, red white and yellow eye phenotypes all shown. Most likely due to incorrect selection of parents, or contamination of one or both parent lines. Cross would be discarded, parent lines cleaned and checked for phenotypic markers before reattempting cross. Image was taken on stereomicroscope.

2.5.2: Relevant statistics

All statistics were run as appropriate, ROUT outlier tests were run on all data sets and any outliers were removed. Spontaneous events, evoked events and train stimulations with subsequent recovery protocols were run for the Glo(OE) line, along with longevity experiments and a Western blot to measure for Glo expression. Electrophysiology and longevity experiments were analysed as previously described in Sections 2.2.2 and 2.4.5. Western blot data was not analysed as experiments were unsuccessful. For comparisons between data sets Student t-tests were used to give statistical significance between two data sets. When more than two sets were being compared a one-way ANOVA was used, with a Tukeys multiply comparison post hoc test used when all lines were compared and a Dunnets multiple comparison post hoc test when the mutant lines were not compared.

Chapter 3: Results for synaptic function in TPI mutants

3.1: Aims and hypothesis

The aim of the work presented in this chapter is to quantify basic synaptic function of excitatory glutamatergic neuromuscular junctions (NMJ) in 3rd instar larvae. Amplitudes and frequencies of spontaneous events, alongside amplitudes of evoked events and impact of external calcium concentration were used to investigate pathology in mutant *Drosophila* lines.

These experiments elucidate synaptic function for three triose phosphate isomerase (TPI) mutants, wstd[1], M80T, and I170V, and a glyoxalase (Glo) knock out line, Glo(KO), in comparison to relevant wild type controls. The comparison between the pathology of different mutant lines should give an insight into the mechanism of dysfunction at NMJs.

The hypothesis was that the lines expressing dysfunctional TPI would show impaired synaptic functionality when compared to controls, as suggested previously (Roland et al. 2016; Stone et al. 2023).

3.2: Introduction

Synaptic function is a key readout to elucidate the impact of disease models on neuronal physiology. Spontaneous events, reflecting single vesicle release from ready releasable pools, and single evoked events, reflecting coordinated release of all ready releasable vesicles, provide specific information on synaptic functions such as vesicle endo and exocytosis, allowing a detailed analysis of the mechanisms leading to dysfunction in disease models (Poodry and Edgar 1979; Koenig et al. 1983; Bykhovskaia and Vasin 2017; Robinson et al. 2018).

Spontaneous events are a key measurement of synaptic activity, amplitudes of spontaneous events directly correlate to the size (volume) of individual vesicles and the frequency of these events provides an insight to the position and availability of pre-synaptic vesicles (Akbergenova et al. 2007; Bruns et al. 2000). Evoked events give an insight into vesicle fusion and release probability, the mean peak eEJC values given by:

$$I = Np_{vr}q$$

Where N is the number of independent ready release vesicles, p_{vr} is the vesicular release probability, and q is the quantal peak size at a given calcium concentration (Silver 2003; Robinson et al. 2018).

Calcium dependency of release is also an important parameter to define when investigating synaptic function. Glutamatergic neuromuscular junctions (NMJs) in *Drosophila* are calcium mediated, action potentials (APs) triggering calcium influx via pre-synaptic calcium channels which then facilitate vesicle fusion (Cho et al. 2015; Yan et al. 1976). Varying external calcium concentration therefore, provides an indication to whether dysfunction impact is pre-synaptic or post-synaptic in synaptic transmission.

TPI has been suggested to impact on synaptic function in multiple ways. For example TPI has been linked to increasing the activity of sodium-potassium pumps in combination with the actin binding protein cofilin. Both proteins are shown to locate together to membranes via Rho activator lysophosphatidic acid suggesting the TPI-cofilin construct interacts with the Na^+/K^+ pump (Jung et al. 2002), and to impaired vesicle cycling at the *Drosophila* NMJ (Roland et al. 2016), further detail can be found in chapter 1.

Impaired TPI function has also been linked to increased levels of redox stress in *Drosophila* models of neurodegeneration, and TPI has been shown *in vitro* to undergo various post translational modifications (PTM) such as deamidation (Gnerer et al. 2006; Enriquez-Flores et al. 2020), and 3-nitrotyrosination (3NT) (Mallozzi et al. 2013). Multiple key proteins required for physiological synaptic transmission and glycolysis have also been shown to undergo such PTMs (Bradley and Steinert 2015; Robinson et al. 2018; Scheckhuber 2019), providing a possible indirect route of dysfunction via increased redox stress stemming from dysfunctional TPI.

As Glyoxalase (Glo) is a protective enzyme in the same redox pathway as TPI - see Figure 1-1 - reduced glyoxalase function is anticipated to impact on the same mechanisms as dysfunctional TPI, likely in an interdependent manner with one dysfunction feeding into the other. As the Glo protective pathway mitigates redox stress it is also expected that dysfunctional glyoxalase will also lead to increased redox stress. One mechanism therefore, that could be impacted by dysfunctional Glo as well as dysfunctional TPI, is synaptic activity.

3.3: Methods

Electrophysiology allows investigation of cellular function by measuring current and voltage fluctuations across synapses. In this chapter current clamp and two electrode voltage clamp (TEVC) recordings were performed, taken from 3rd instar *Drosophila* larvae in muscle 6, segments A2 and 3. *Drosophila* larvae dissection and muscle structure are shown in Figure 2-5 and 2-1 [D].

Current clamp recordings require a single sharp electrode (40-70MΩ) containing 3M KCl in the post synaptic muscle cell, this is a technically easier set up than TEVC, but will include post synaptic activity from the muscle cell in the recorded responses see Figure 3-1 [A]. TEVC recordings require a secondary sharp electrode in the muscle (see Figure 3-1 [C]), this allows clamping of the voltage in the post synaptic muscle cell, ensuring observed responses are due solely to the initial binding of neurotransmitters and not due to downstream activity such as further depolarisation or muscle contraction.

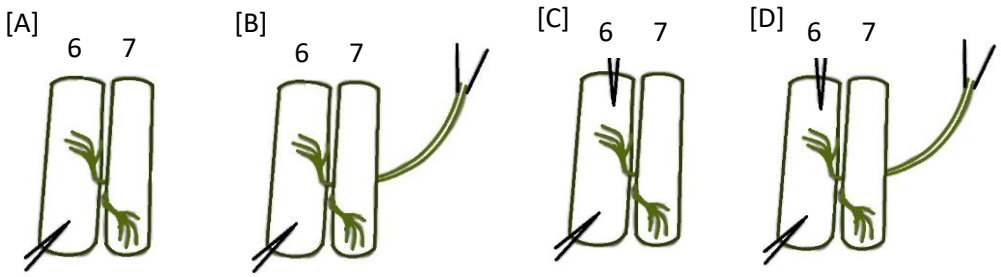

Figure 3-1: Electrophysiology experimental schematics. Muscles 6 and 7 of filleted Drosophila 3rd instar larvae. [A] current clamp spontaneous excitatory junction current recordings, [B] current clamp evoked excitatory junction current recordings, [C] TEVC spontaneous excitatory junction potential recordings, [D] TEVC evoked excitatory junction potential recordings. Figure created in Paint.

For evoked recordings the same setup of microelectrodes was used with an additional stimulation (suction) electrode holding the exposed end of the innervating motoneuron (see Figure 3-1 [B] and 3-1 [D]).

Spontaneous and evoked recordings are reported in current clamp (sEJP and eEJP) and two voltage clamp (sEJC and eEJC).

Protocols were set up on Clampex 10.7 (Molecular Devices), for spontaneous recordings, current and voltage were recorded from the post synaptic muscle for 120s. For single evoked recordings stimulations were set at 1Hz.

Data is expressed as mean±SEM, time constants are reported as best fit values. Where multiple comparisons are made, a one-way ANOVA was used to test statistical significance, and where only two values are compared students t tests

were used. N values are reported as N = animal number and, n = muscle number.

3.4: Sex differences

Sex was not found to affect the sEJC or eEJC amplitudes for any of the mutant or control lines, see Figure 3-2 and 3-3. Therefore, electrophysiology data was pooled for all experiments.

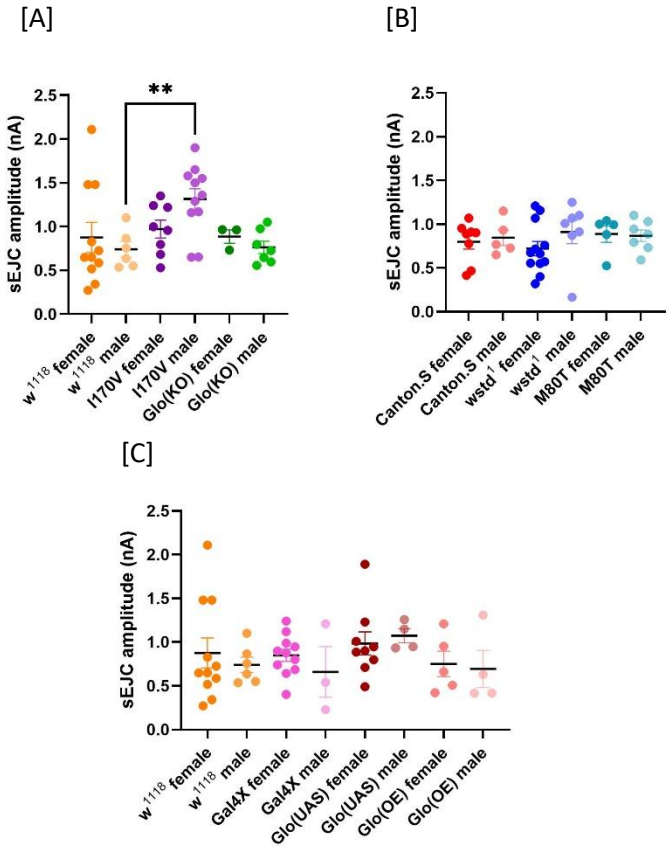

*Figure 3-2: sEJC data split by sex [A] w^{1118} female: 0.88±0.2 nA, w^{1118} male: 0.74±0.09 nA, I170V female: 0.97±0.1 nA, I170V male: 1.3±0.1 nA, Glo(KO) female: 0.89±0.08 nA, Glo(KO) male: 0.76±0.07 nA, [B] Canton.S female: 0.80±0.08 nA, Canton.S male: 0.85±0.09 nA, $wstd^1$ female: 0.72±0.08 nA, $wstd^1$ male: 0.91±0.1 nA, M80T female: 0.89±0.09 nA, M80T male: 0.87±0.07 nA [C] w^{1118} female: 0.88±0.2 nA, w^{1118}male: 0.74±0.09 nA, Gal4 female: 0.85±0.07 nA, Gal4 male: 0.66±0.3 nA, UAS-Glo female: 0.98±0.1 nA, UAS-Glo male: 1.1±0.08 nA, Glo(OE) female: 0.75±0.1 nA, Glo(OE) male: 0.74±0.09 nA . Data was compared with unpaired students t-test for male-female pairs, one-way ANOVA was used to compare all males or all females within each plot, **p<0.005.*

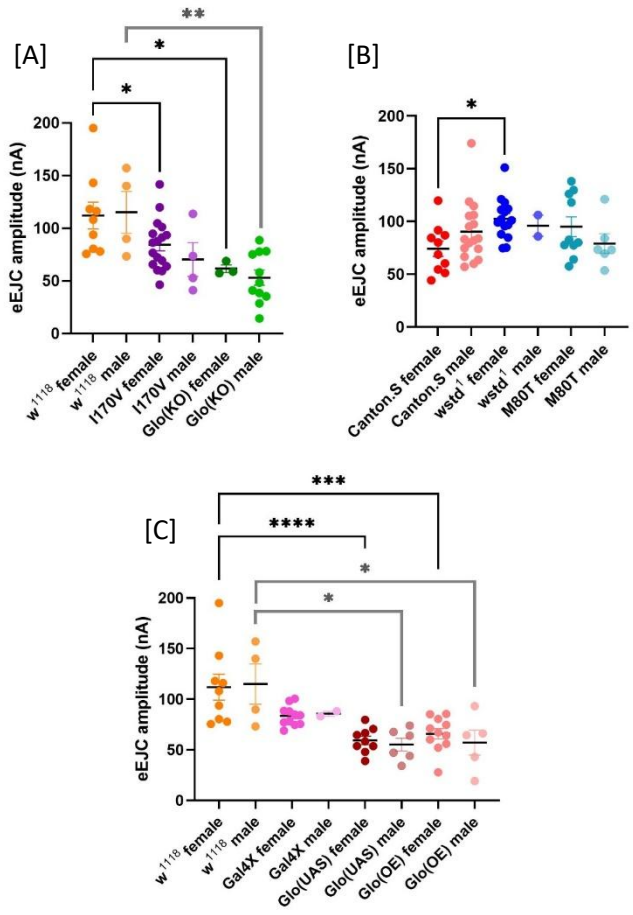

*Figure 3-3: eEJC data split by sex [A] w^{1118} female: 110±10 nA, w^{1118} male: 120±20 nA, I170V female: 84±6 nA, I170V male: 70±20 nA, Glo(KO) female: 62±4 nA, Glo(KO) male: 53±7 nA, [B] Canton.S female: 74±7 nA, Canton.S male: 90±7 nA, $wstd^1$ female: 100±5 nA, $wstd^1$ male: 96±10 nA, M80T female: 95±9 nA, M80T male: 79±9 nA, [C] w^{1118} female: 110±10 nA, w^{1118}male: 120±20 nA, Gal4 female: 84±3 nA, Gal4 male: 86±3 nA, UAS-Glo female: 59±4 nA, UAS-Glo male: 55±6 nA, Glo(OE) female: 66±5 nA, Glo(OE) male: 57±10 nA. Data was compared with unpaired students t-test for male-female pairs, one-way ANOVA was used to compare all males or all females within each plot. Significance between female lines are shown in black, male comparisons are shown in grey, *p<0.05, **p<0.005, ***p<0.0005, ****p<0.0001.*

3.5: Spontaneous events were altered in wstd^{1} and I170V mutants

3.5.1: Amplitudes and frequency

The amplitudes of sEJP events showed a lack of significant differences for most lines. Except in the wstd^{1} line which showed significantly increased amplitudes compared to Canton.S, 1.3±0.2 nA vs 0.70±0.1 nA, see Figure 3-4 [C].

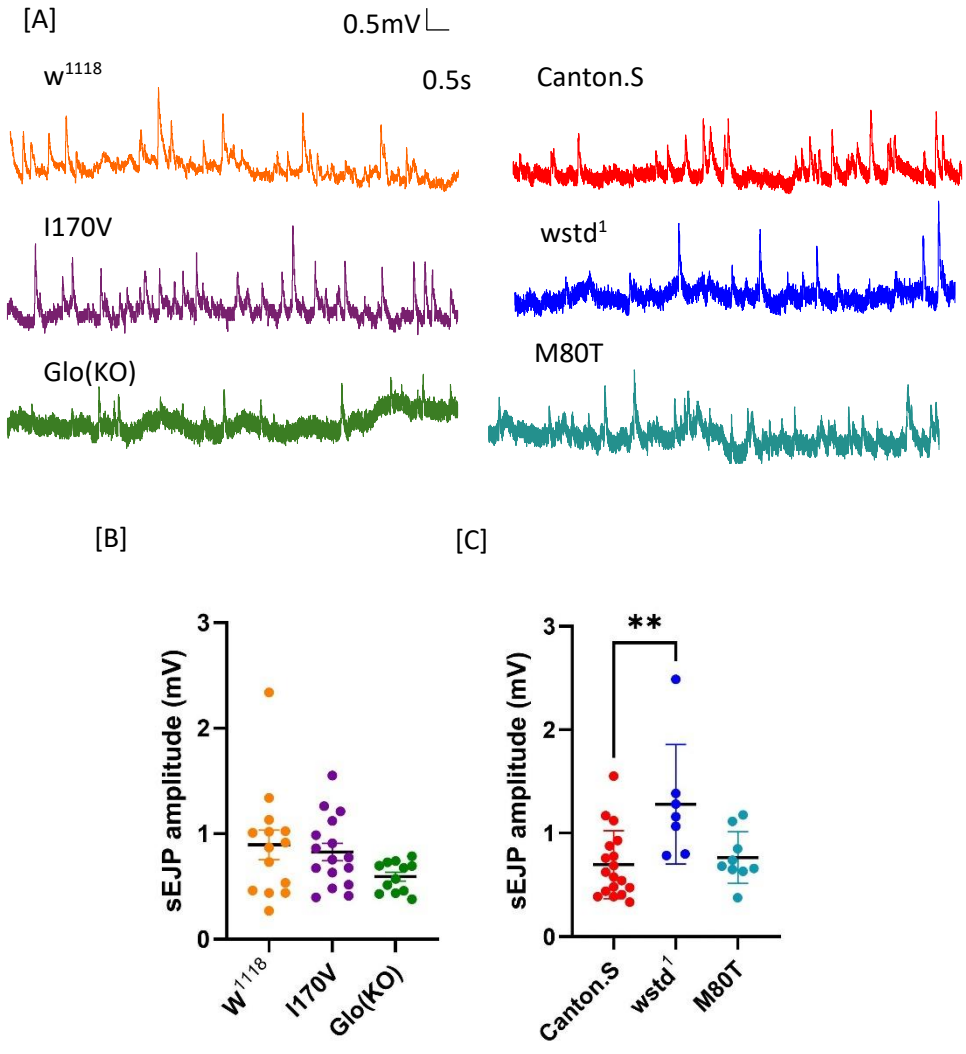

*Figure 3-4: Current clamp data sEJP amplitudes. Data is expressed as mean±SEM [A] Example raw sEJP trace for 10 s for all lines. [B] Amplitudes from control lines: w^{1118}: 0.89±0.1 mV, TPI mutant line: I170V: 0.83±0.08 mV, and Glo mutant line: Glo(KO): 0.59±0.04 mV. [B] Amplitudes of control line: Canton.S: 0.70±0.08 mV, and TPI mutant lines: wstd^{1}: 1.3±0.2 mV, M80T: 0.76±0.08 mV. Statistical analysis used was one-way ANOVA, n≥7, N≥4, p**<0.005*

The amplitudes of sEJC events were not altered with mutations of TPI: I170V, wstd^{1}, and M80T showing no significant difference in comparison to their respective control, w^{1118}, see Figure 3-5 [B] and [C]. The glyoxalase knock out line also showed no difference in comparison to its control. The only significant difference seen between all genetic lines was between the TPI mutant line I170V which showed significantly higher amplitudes, 1.2±0.2 nA, to the glyoxalase knock out line which showed lower amplitudes 0.77±0.1 nA.

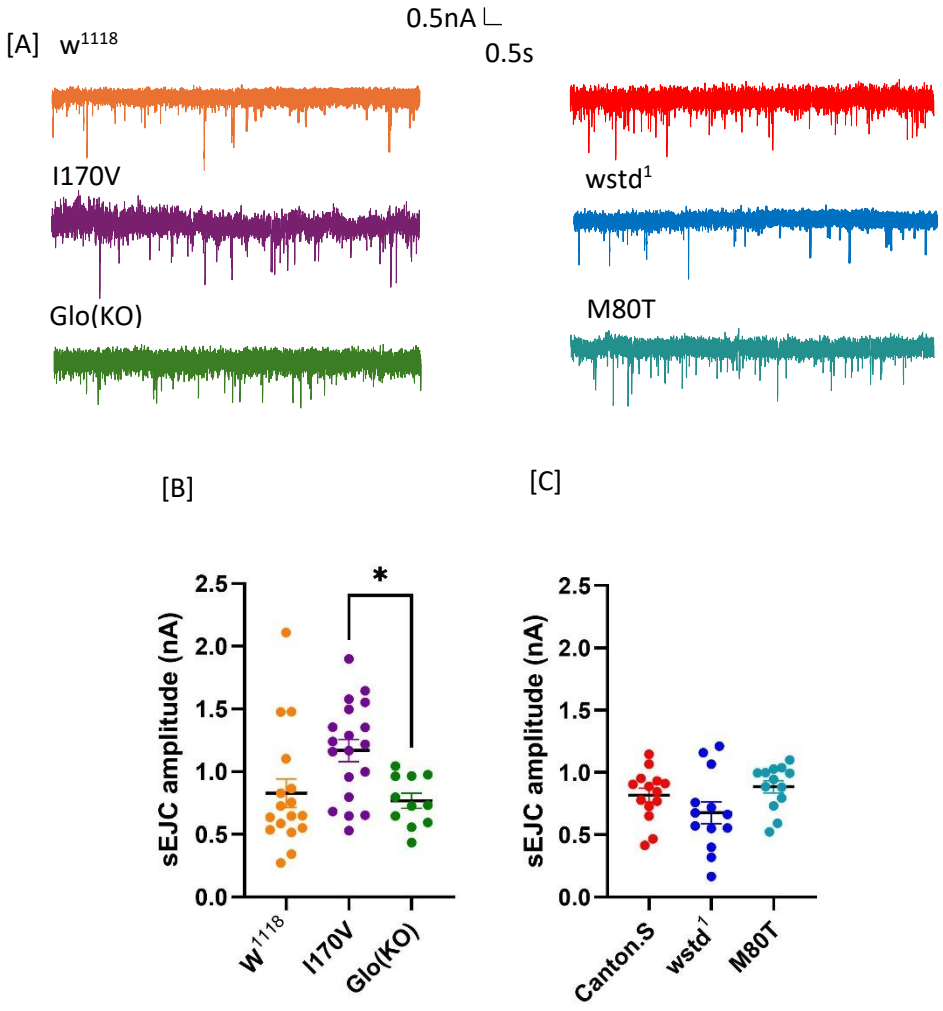

Figure 3-5: TEVC data sEJC amplitudes. Data expressed as mean±SEM [A] Example raw sEJC trace for 10s for all lines [B] Amplitudes of controls; w^{1118}: 0.8±0.1 nA, TPI mutant line; I170V: 1.2±0.2 nA, and Glo mutant line; Glo(KO): 0.77±0.06 nA, [C] Amplitudes of control; Canton.S: 0.87±0.05 nA, and TPI mutant lines; wstd^{1}: 0.67±0.09 nA, M80T: 0.92±0.05 nA. Statistical analysis used was one-way ANOVA, n≥10, N≥4, p<0.05*

The frequencies of sEJP events showed a significant difference between I170V and w^{1118} showing higher frequencies of, 2.1±0.2 s^{-1} compared to in w^{1118}, 1.2±0.2 s^{-1}, see Figure 3-6 [B]. The frequency of sEJC events was not seen to be significantly affected in mutant lines, see Figure 3-7.

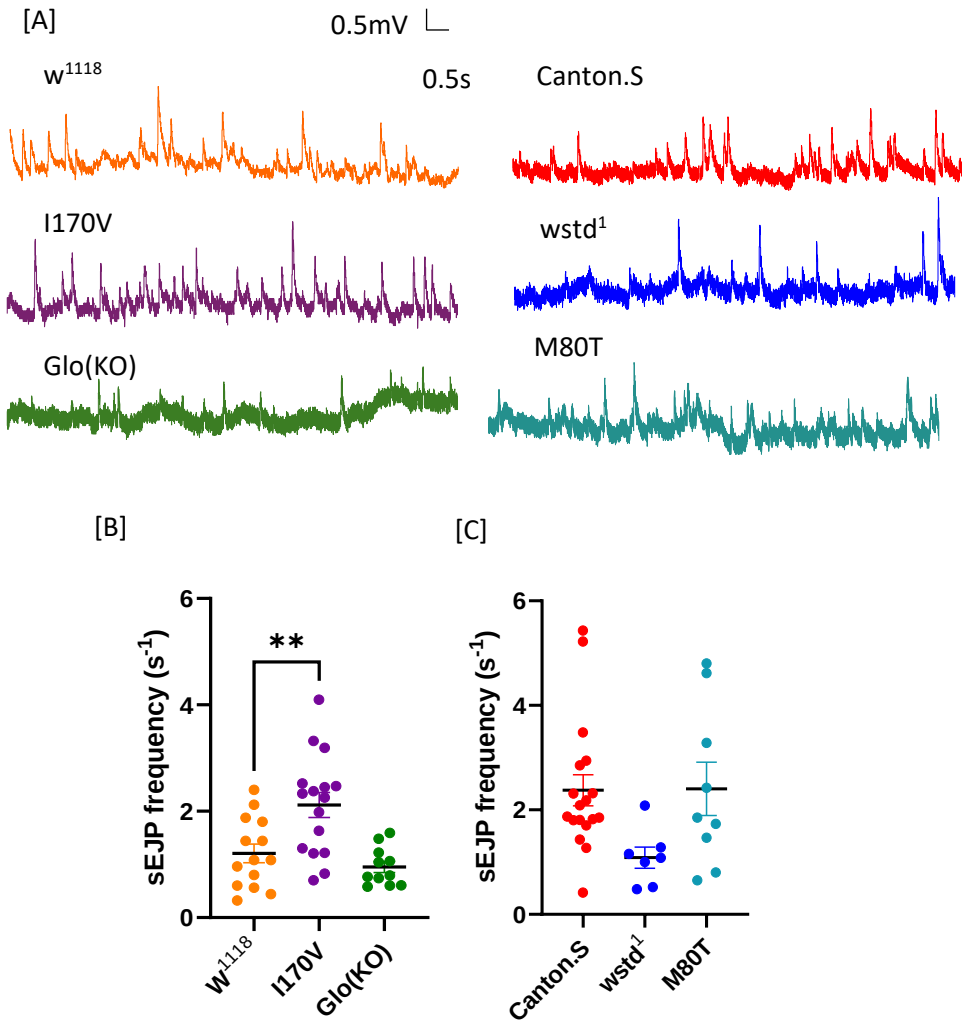

*Figure 3-6: Current clamp data sEJP frequencies. Data is expressed as mean±SEM [A] Example raw sEJP trace for 10 s for all lines. [B] Frequencies of control lines; w^{1118}: 1.2±0.2 s^{-1}, TPI mutant lines; I170V: 2.1±0.2 s^{-1}, and Glo mutant line; Glo(KO): 1.1±0.2 s^{-1}. [C] Frequencies of control line; Canton.S: 2.4±0.3 s^{-1}, and TPI mutant lines; $wstd^{1}$: 1.1±0.2 s^{-1}, M80T: 2.4±0.5 s^{-1}. Statistical analysis used was one-way ANOVA, n≥7, N≥4, p**<0.01.*

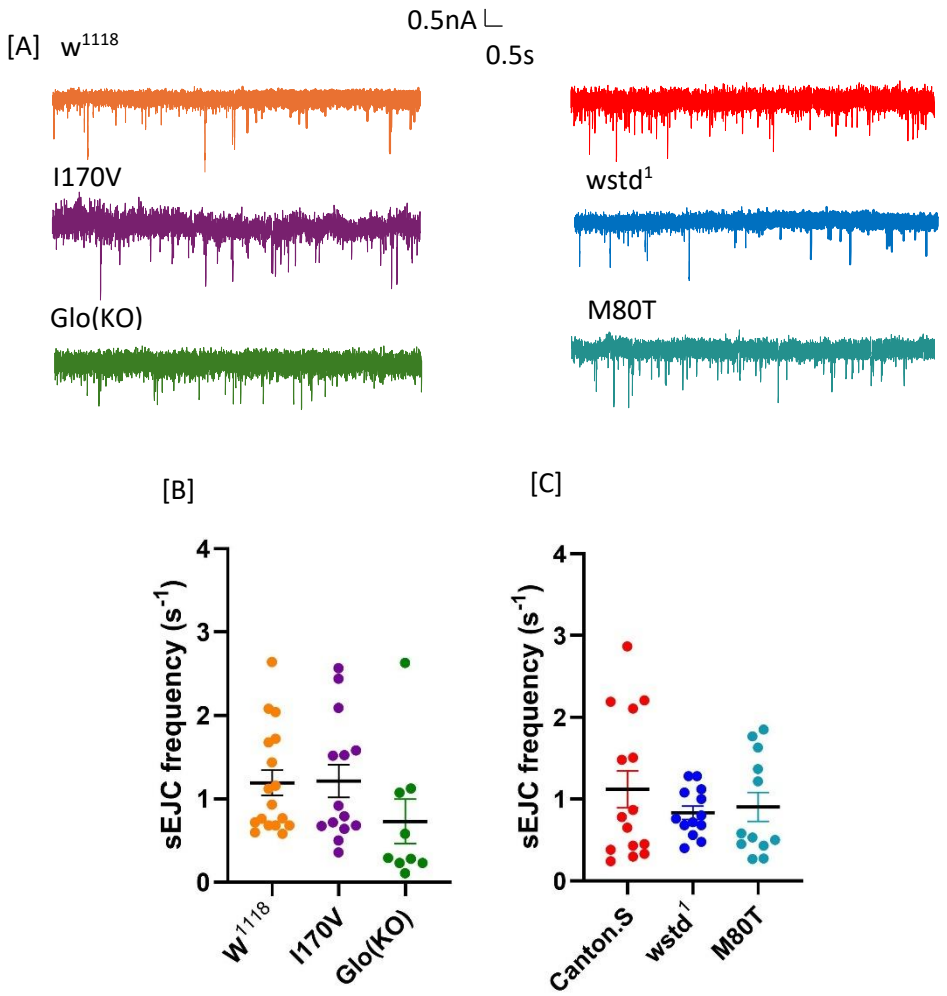

Figure 3-7: TEVC data sEJC frequencies. Data is expressed as mean±SEM, [A] Example raw sEJC trace for 10 s for all lines. [B] Amplitudes from control lines; w^{1118}: 1.2±0.2 s^{-1}, TPI mutant line; I170V: 1.3±0.3 s^{-1}, and Glo mutant line; Glo(KO): 1.1±0.4 s^{-1}. [C] Amplitudes of control line; Canton.S: 1.8±0.3 s^{-1}, and TPI mutant lines; $wstd^{1}$: 0.83±0.08 s^{-1}, M80T: 1.0±0.2 s^{-1}. Statistical analysis used was one-way ANOVA, n≥10, N≥4

3.5.2: Distribution of spontaneous events

The distribution of the amplitudes of spontaneous events is a good measure of the spread of available vesicles. (Roland et al. 2016)

The I170V line showed a right shifted distribution of spontaneous amplitudes, see Figure 3-8, found to be significant. This is mirrored in the mean sEJC amplitude comparisons which tend towards higher amplitudes in I170V compared to w^{1118}, see Figure 3-5 [B].

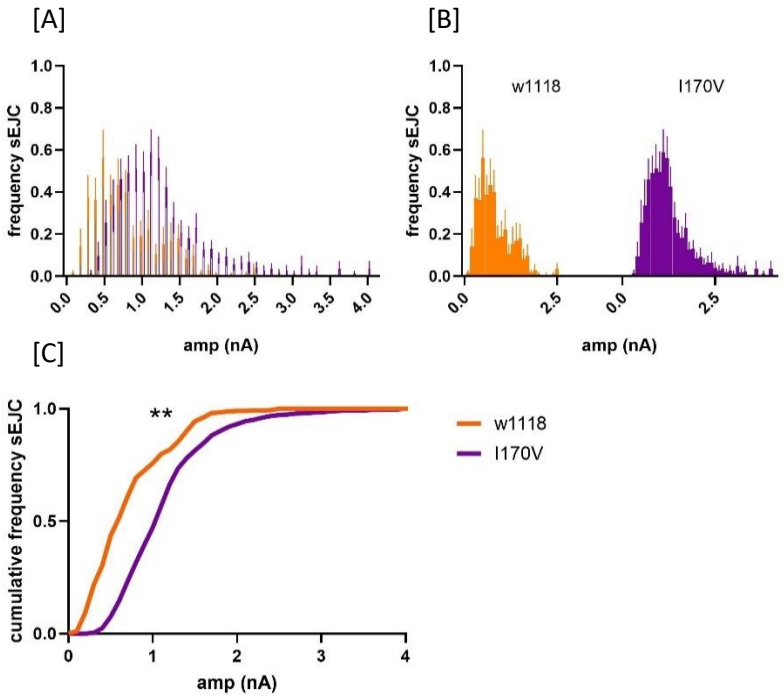

*Figure 3-8: TEVC data sEJC amplitude distributions for control line w^{1118} (orange) and TPI mutant line I170V (purple). [A] Normalised amplitude distributions, data overlapped. [B] Normalised amplitude distributions, data separated out. [C] Normalised cumulative amplitude distributions, found to be significantly different, Students t-test, Kolmogorov-Smirnov test, **p<0.01, n≥10, N≥4.*

The $wstd^1$ and M80T lines showed no differences in spontaneous amplitude distribution compared to controls, see Figure 3-9.

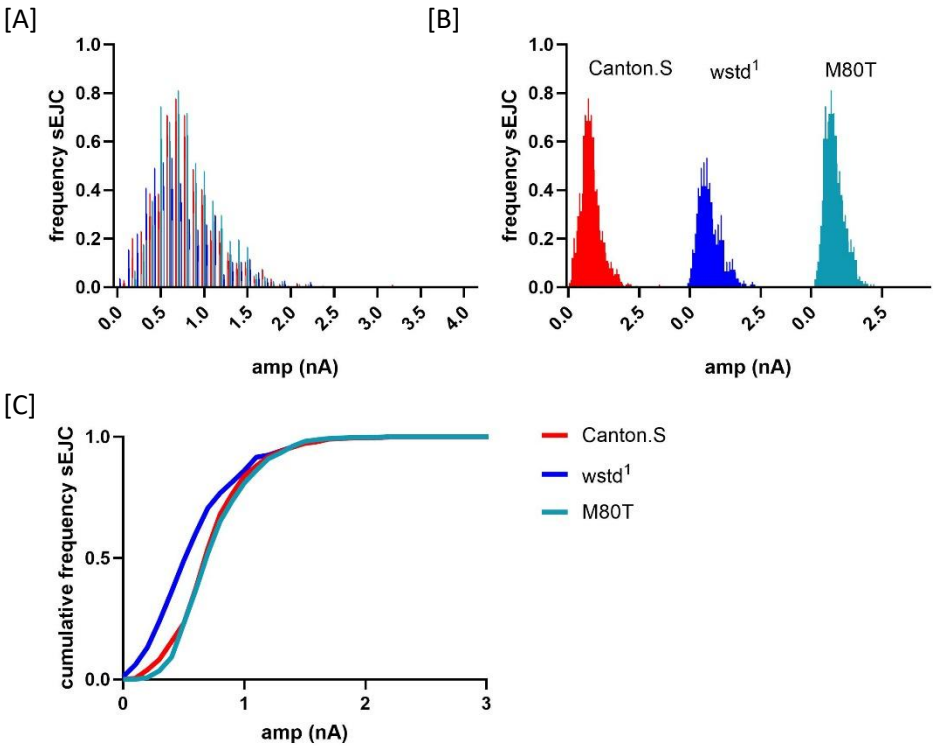

Figure 3-9: TEVC data sEJC amplitude distributions for control line Canton.S (red) and TPI mutant lines wstd[1] (blue) and M80T (cyan). [A] Normalised amplitude distributions, data overlapped. [B] Normalised amplitude distributions data separated out. [C] Normalised cumulative amplitude distributions, not found to be significantly different, Students t-test, Kolmogorov-Smirnov test, p>0.05, n≥10, N≥4.

The relative amplitude distribution for the Glo(KO) was not found to be significantly altered. The Glo(KO) line shows a narrower distribution than w^{1118} see Figure 3-10.

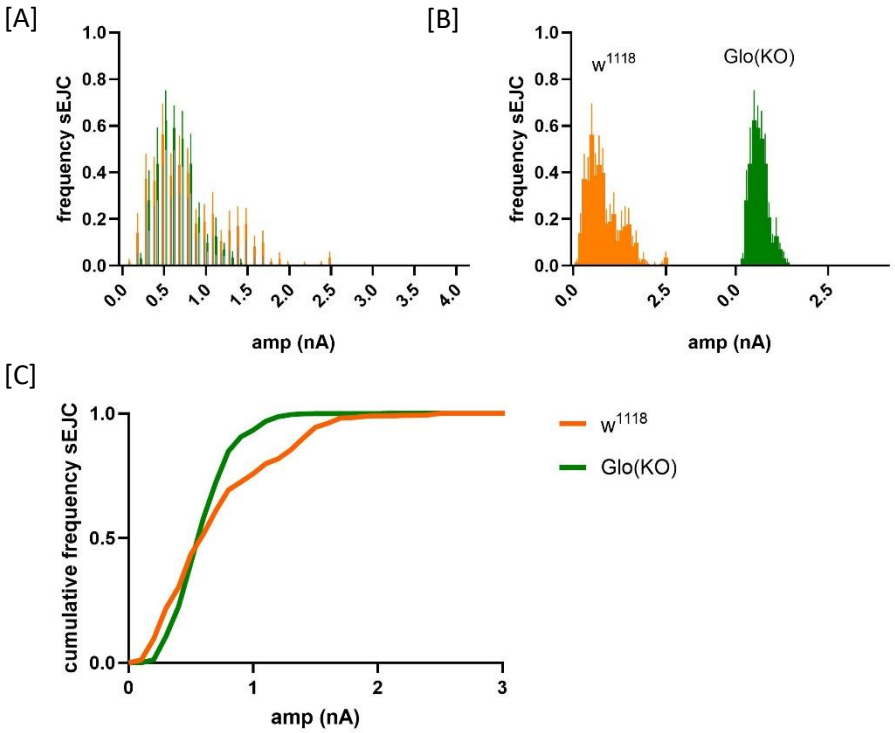

Figure 3-10: TEVC data sEJC amplitude distributions for control line w^{1118} (orange), and Glo mutant line Glo(KO) (green). [A] Normalised amplitude distributions, data overlapped. [B] Normalised amplitude distributions, data separated out. [C] Normalised cumulative amplitude distribution, not found to be significantly different, Students t-test, Kolmogorov-Smirnov test, p>0.05, n≥10, N≥4.

3.6: Evoked responses and quantal content were altered in I170V, $wstd^1$, and Glo(KO) mutants

Single evoked events represent the release of the entire available vesicle population, so gives another insight to the availability and arrangement of pre-synaptic vesicles.

eEJC amplitudes were reduced in the TPI mutant I170V, 82±6 nA, along with the Glo(KO) line, 62±9 nA, in comparison to the control line w^{1118}, 110±9 nA. No differences were seen in the $wstd^1$ or M80T mutants, see Figure 3-11 [B].

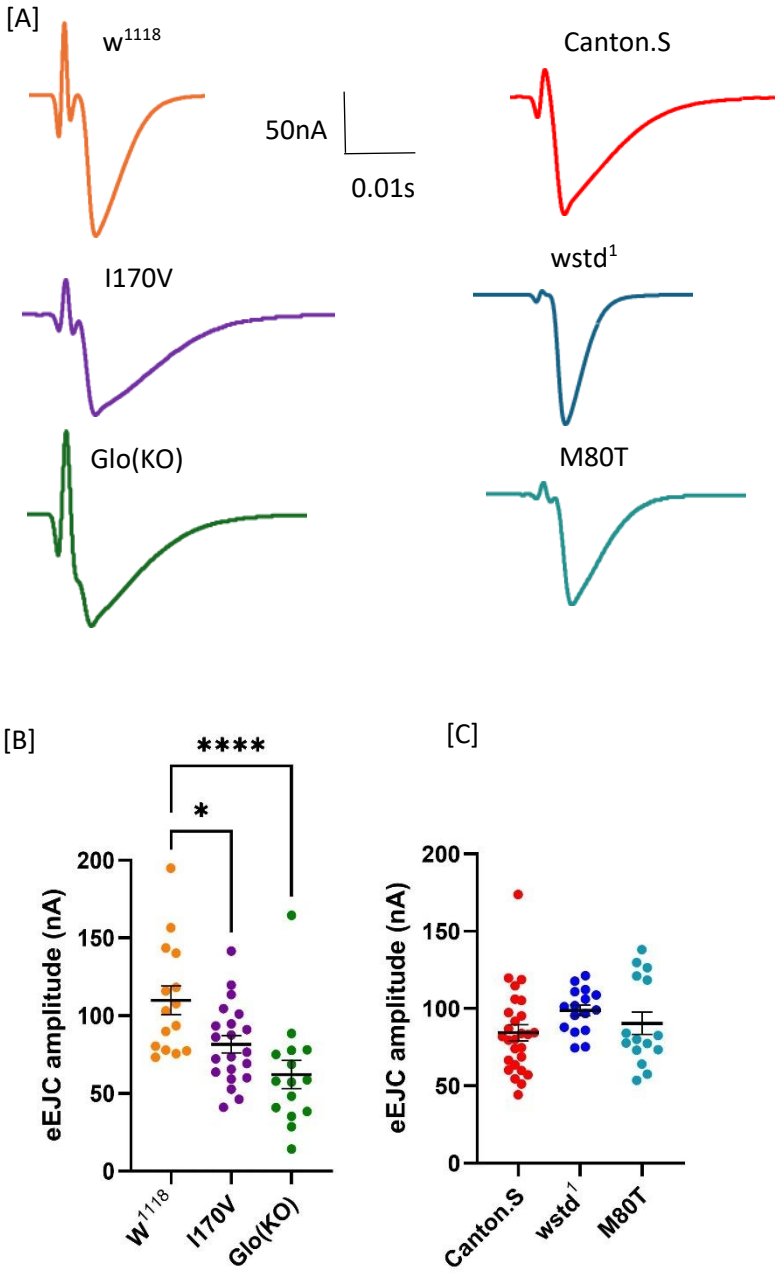

Figure 3-11: TEVC data eEJC amplitudes, data expressed as mean±SEM [A] Example raw eEJC trace, average of 20 responses from one recording for all lines. [B] Amplitudes for control lines; w^{1118}: 110±9 nA, TPI mutant line; I170V: 82±6 nA, and Glo mutant lines; Glo(KO): 62±9 nA, [B] Amplitudes of control line; Canton.S: 84±5 nA, and TPI mutant lines; $wstd^{1}$: 99±4 nA, M80T: 90±7 nA. Statistical analysis used was one-way ANOVA, p<0.05, p****<0.0001, n≥15, N≥7.*

Quantal content calculations (eEJC amplitude divided by sEJC amplitude) give an estimation of the average number of vesicles involved in a single evoked response.

The TPI mutant I170V showed a reduced quantal content in comparison to the control w^{1118}, 59±4 vs 191±21 see Figure 3-12 [A], this is expected from the significantly smaller eEJC amplitudes. The Glo(KO) line also showed a reduced quantal content, 97±30, compared to w^{1118}, 190±20, see Figure 3-12 [A]. This again fits with the significantly reduced eEJC amplitudes, see Figure 3-11 [B].

The TPI mutant $wstd^{1}$ showed the opposite effect with significantly larger quantal contents, 167±18 vs 101±13 in Canton.S, see Figure 3-12 [B]. The M80T TPI mutant line did not show any differences compared to Canton.S, as expected given the lack of differences found in spontaneous and evoked amplitudes.

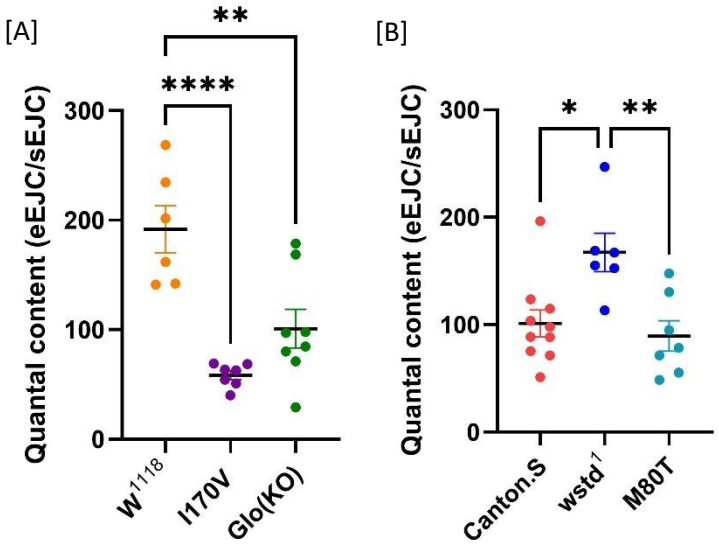

Figure 3-12: Quantal content eEJC amplitudes divided by sEJC amplitudes, data expressed as mean±SEM [A] Quantal content for control lines; w^{1118}: 190±20, TPI mutant line; I170V: 59±4, and Glo mutant lines; Glo(KO): 97±30. [B] Quantal content for control line; Canton.S: 101±10, and TPI mutant lines; $wstd^{1}$: 170±20, M80T: 90±10. Statistical analysis used was one-way ANOVA, n≥6, N≥4, p<0.05, p**<0.005, p****<0.0001.*

3.7: Calcium dependency was altered in wstd^{1} and I170V mutants

Drosophila excitatory glutamatergic NMJs are calcium dependent, action potentials reaching the boutons of NMJs stimulate calcium influx which goes on to stimulate the release of vesicles and downstream muscular responses. Identifying changes in calcium dependency could help locate the point of dysfunction leading to altered synaptic activity.

Calcium dependency of eEJC events was found to be altered in I170V and wstd^{1} compared to their respective controls, see Figure 3-13.

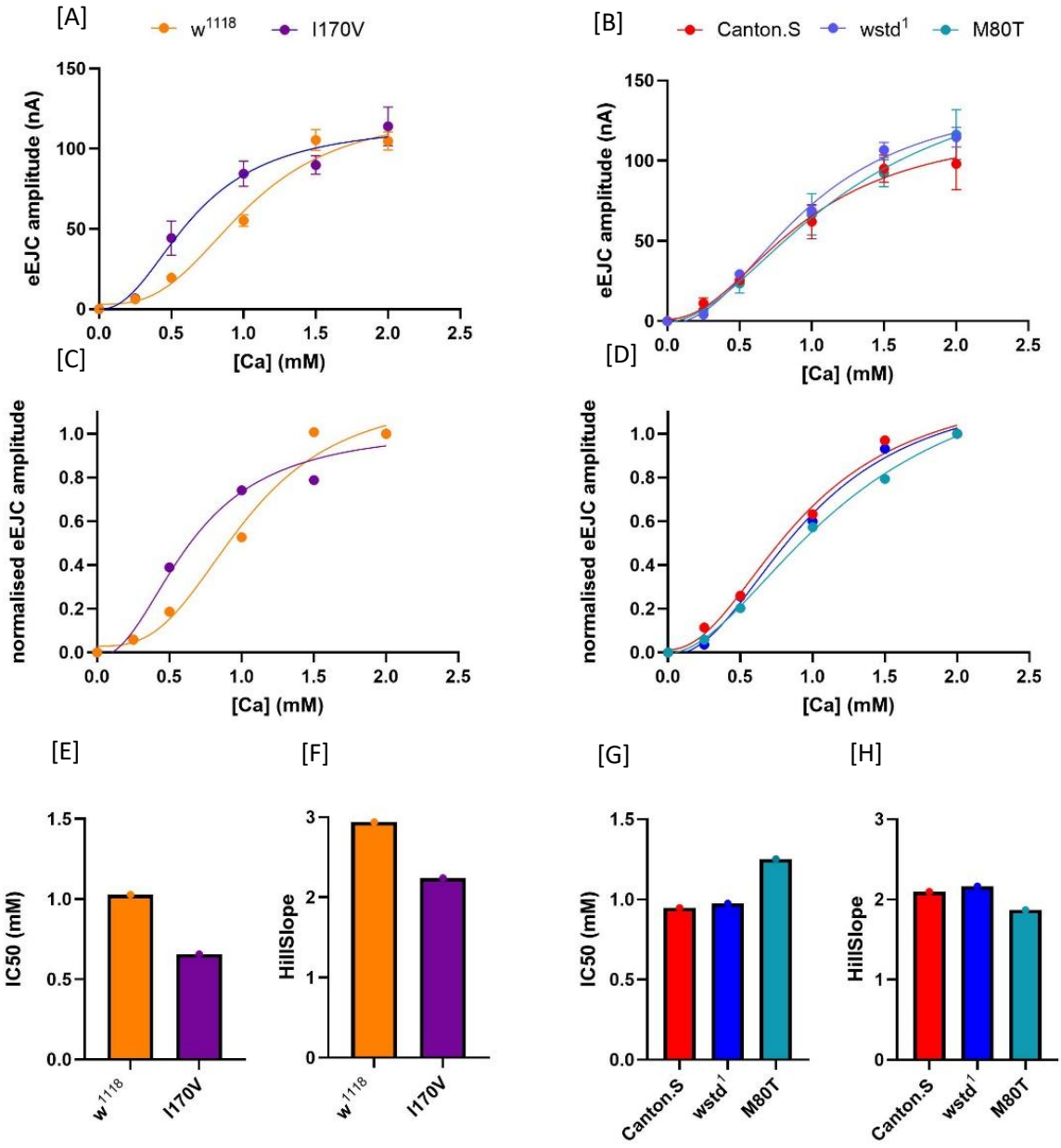

*Figure 3-13: Calcium dependency [A] eEJC, data expressed as mean±SEM EC_{50} values, control line; w^{1118}: 1.03 mM, TPI mutant line; I170V: 0.66 mM. Student t test showed significance ****p<0.0001 [B] eEJC, data expressed as mean±SEM EC_{50} values, control line; Canton.S: 0.95 mM, TPI mutant lines; $wstd^1$: 0.97 mM, M80T: 1.3 mM. One-way ANOVA of EC_{50} values between $wstd^1$ vs Canton.S found significance ***p<0.0005, M80T vs Canton.S was not significant. [C] Normalised eEJC, data expressed as mean values for w^{1118} and I170V, student t test found significance ****p<0.0001. [D] Normalised eEJC, data expressed as mean values for Canton.S, $wstd^1$, and M80T, one-way ANOVA found no significance. [E] EC_{50} values from mean data for w^{1118} (1.03) and I170V (0.657) single value so no statistics ran. [F] HillSlope values from mean data for for w^{1118} (2.94) and I170V (2.24) single value so no statistics ran. [G] EC_{50} values from mean data for Canton.S (0.947), $wstd^1$ (0.974), and M80T (1.25) single value so no statistics ran. [H] HillSlope values from mean data for Canton.S (2.10), $wstd^1$ (2.16), and M80T (1.87) single value so no statistics ran. n≥5, N≥5.*

3.8: Discussion

Synaptic function in the TPI and glyoxalase mutants was altered in comparison to control lines, see Table 3.1.

Table 3.1: Summary of significantly altered synaptic activity in mutant lines compared to control lines

	wstd[1]	**M80T**	**I170V**	**Glo(KO)**
Spontaneous events	sEJP amplitude increased **p<0.005	ns	sEJP frequency increased **p<0.01 sEJC amplitude distribution shifted left **p<0.01	ns
Evoked events	ns	ns	eEJC amplitude decreased *p<0.05	eEJC amplitude decreased ****p<0.0001
Quantal content	Quantal content increased *p<0.05	ns	Quantal content decreased ****p<0.0001	Quantal content decreased **p<0.005
Calcium dependency	eEJC curve shifted left ***p<0.0005	ns	eEJC normalised and non normalised curves shifted left ****p<0.0001	N/A

The data from the TPI mutant I170V suggests that in the I170V line the content of evoked events is reduced. This could be due to altered vesicle formation or altered recycling mechanisms leading to smaller available vesicle pools (Kuromi and Kidokoro 1998; Akbergenova and Bykhovskaia 2007). These mechanisms involve various proteins that have been discussed previously as targets of redox stress, such as SNARE complexes (Akbergenova and Bykhovskaia 2007; Mallozzi et al. 2013; Acuna et al. 2014). TPI itself has also been linked to vesicle movement and is also known to be impacted by redox stress (Guix et al. 2009; Roland et al. 2016; Enriquez-Flores et al. 2023; Stone et al. 2023). As single vesicle sizes did not significantly differ in this line it is possible that dysfunction stems from altered vesicle organisation rather than formation: again various proteins involved in this mechanism are predicted to be impacted by redox stress (Ramaswami et al. 1994; Kuromi and Kidokoro 1998; Akbergenova and Bykhovskaia 2007; Mallozzi et al. 2013; Reddy-Alla et al. 2017).

The data from the TPI mutant wstd[1] suggests that more vesicles are being released per single evoked event compared to controls, the increase sEJP amplitudes – with controlled V_m between -55 mV to -65 mV - also suggests that single vesicles may be larger although no increase in the eEJC amplitudes does not support this.

The data from the TPI mutant M80T showed no differences in spontaneous or evoked events, or in calcium dependency. This is unexpected given previously reported dysfunction in this line, see Chapter 1 Section 1.4.1 for more details (Roland et al. 2016).

The data from the Glyoxalase mutant Glo(KO) suggests that the number of vesicles released per single evoked event is reduced in this line. Given the lack of change in spontaneous amplitudes – i.e. the same amount of neurotransmitter per vesicle - this is more likely to be due to an altered vesicle organisation, with fewer vesicles in the ready releasable pool and more in the reserve pool (Richmond and Broadie 2002; Akbergenova and Bykhovskaia 2007). Or alternatively an altered release probability, both appear more likely than an altered vesicle formation (Koenig et al. 1983; Ramaswami et al. 1994; Kuromi and Kidokoro 1998; Richmond and Broadie 2002; Akbergenova and Bykhovskaia 2007; Sudhof 2013).

The quantal content, and availability of vesicles for spontaneous release rely on vesicle recycling, which in turn is dependent on a range of proteins to function normally, many of which could be impacted by increased redox stress at the synapse, including SNARE proteins among others (Akbergenova and Bykhovskaia 2007; Mallozzi et al. 2013; Acuna et al. 2014), see Figure 1-2 [A]. Vesicle recycling – endocytosis and exocytosis – are also dependent on vesicle docking, fusion, and trafficking, the complexity of these mechanisms may be being reflected by the differing phenotypes arising from the different TPI mutations. The organisation of vesicle pools has been reported to be maintained by synapsin (Akbergenova and Bykhovskaia 2007), one of the proteins predicted to be affected by redox stress.

The spread of data sets in some experiments could suggest a type 1 statistics error, this could be due to individual variation in the dysfunction within lines due to the complexity of the cascade, so requiring larger data sets to confirm significance. Alternatively, this could be due to distinct populations within lines with defined variants such as sex, further sub division of data would be prudent, however the subdivisions by sex shown here also show large spreads, so do not seem to define this variation.

Overall this data suggests that both the TPI and Glyoxalase proteins are key in healthy functioning of glutamatergic excitatory NMJs, but whether this is a

direct impact or working via the associated redox pathways is not yet clear. The seemingly different mechanisms of dysfunction in the TPI mutant lines was unexpected and suggests there are multiple pathways of disease stemming from TPI dysfunction.

3.9: Future directions

As previous work has suggested, impaired vesicle dynamics is a key phenotype of *Drosophila* TPI mutants (Gnerer et al. 2006; Mallozzi et al. 2013; Roland et al. 2016; Stone et al. 2023), the work presented in this chapter suggests this dysfunction stems from various routes. More detailed electrophysiology would be beneficial to further probe these synapses. A more detailed analysis including investigation of; rising phases, falling phases, area under the curve, width at half height of peak, and time to peak would be beneficial (Erxleben et al. 1988; Bruns et al. 2000). However in the data collected for this thesis, the signal-noise ratio was not sufficient to yield reliable analysis of response curve shapes. The variation in decay characteristics in eEJC recordings could suggest stimulation of multiple motor axons (Jan et al. 1976), as the protocol here selectively recorded maximal response from each NMJ, all the eEJC recordings should be a composite response from all available motor axons. Variation therefore may indicate a pathology or compensation mechanism with altered ratios of motor axon function in *Drosophila* mutant lines. More in depth electrophysiological experiments are discussed in the next chapter providing a more detailed analysis of synaptic activity, and possible origins of dysfunction.

Chapter 4: Results for vesicle dynamics are altered in all mutants

4.1: Aims and hypothesis

The work presented in this chapter aimed to investigate high frequency train stimulation and subsequent recovery stimulations in the triose phosphate isomerase (TPI) and glyoxalase (Glo) mutant lines, and quantify the resultant synaptic activity. This chapter will also assess evoked excitatory junction currents (eEJCs) in the presence of hydrogen peroxide (H_2O_2), a known oxidative stressor.

It was expected that depletion following train stimulations and subsequent recoveries would be altered in mutant lines, as *Drosophila* TPI mutants have previously been reported to exhibit altered synaptic activity (Gnerer et al. 2006; Mallozzi et al. 2013; Roland et al. 2016; Stone et al. 2023). The only line shown here that has been previously described by these parameters is wstd^1 which was reported to show enhanced depletion with high frequency train stimulation (Stone et al. 2023), more detail is given in Chapter 1. The treatment of H_2O_2 was expected to worsen disease phenotypes taking them further from the control values, and potentially also to inhibit normal healthy activity in control lines, making the H_2O_2 treated control phenotypes closer to the disease model phenotypes (Gnerer et al. 2006; Guix et al. 2009; Hrizo et al. 2013; Stone et al. 2023).

4.2: Introduction

High frequency train stimulations (10Hz-60Hz) provide information on how synapses function for high frequency synaptic transmission, the normal firing rate for crawling in *Drosophila* larvae being approximately 1Hz. The following recovery protocol, stimulating muscle with exponentially increasing time gaps between pulses, then allows the flexibility and resilience of these synapses to be tested. Wild type lines have been reported to exhibit depletion to a constant plateau that corresponds to the available vesicle recycling and to recover fully to normal function even after high frequency train stimulation (Poodry and Edgar 1979; Kuromi and Kidokoro 1998; Robinson et al. 2018). We have also previously reported that train stimulations in wstd^1 show increased depletion and slower recovery than control lines (Stone et al. 2023). None of the other

lines described here have been tested by this measure, although the impaired vesicle dynamics reported in *Sugarkill* mutants (wstd^{1} and M80T) imply train and recovery protocols will show altered activity in these lines compared to controls, a suggestion that can be investigated via these detailed electrophysiology experiments (Roland et al. 2016; Stone et al. 2023).

Given previous work on similar models from the literature the most commonly suggested mechanism of dysfunction is via redox stressors and post translational modifications by species such as advanced glycation end products (AGEs), (Gnerer et al. 2006; Hrizo et al. 2013; Roland et al. 2014; Stone et al. 2023). To confirm or rule out the primary impact of redox stress, models treated with antioxidants and redox stressors could be used. Evoked and spontaneous events in the presence of H_2O_2 for the control line w^{1118} and Glo(KO) is shown here to begin to investigate this possibility, although data sets are small some trends are described.

4.3: Methods

The method for setting up TEVC for eEJCs are as described previously in chapter 2.

HL3 at various calcium concentrations was made up in a dilution series as described in Table 2.5 Solution was transferred by perfusion for 5 minutes to ensure complete change of solution.

For acute impact of redox stressors hydrogen peroxide was added to HL3 containing the standard 1.5 mM Calcium to make up a 5 % solution of H_2O_2 (Zhu et al. 2021), this was then perfused through the prep for a minimum of 5 minutes. For chronic exposure parent flies were placed in food vials for 1-2 days then removed and a solution of 5 % H_2O_2 (150 µl a day) was added to food vials for 48 hrs. Leaving 1-2 days laying and hatching time before addition of H_2O_2 was necessary as premature H_2O_2 exposure prevented eggs from hatching.

Train recordings were set at various frequencies (10, 20, 30, 40, 50, and 60 Hz) for 1 s, the firing rate for crawling in larvae being 1 Hz. The recovery protocol for all trains contained eleven single stimulations separated by exponentially increasing delay periods between stimulations, protocols were manually created on Clampex 10.7. The time course for recoveries were based on the frequency of the associated train, all recovery protocols were run for approximately 40 s.

For analysis non-linear fits were used. For train fits only trains that showed depletion were included, for some trains this required fitting after the initial potentiation phase, model;

$$Y = (Y0 - Plateau) \times \exp(-K \times X) + Plateau$$

Where Y0 is Y when t=0, Plateau is Y value at t=∞, and K is the rate constant.

For recovery protocols fits were taken from the start of synaptic recovery, excluding initial points that may show further depletion. Tau comparisons for train and recoveries show values from individual recordings, not mean data.

N values are given as N = animal number and n = muscle number.

4.4: Evoked responses to train stimulations and subsequent recovery protocols were altered in all mutants

4.4.1: Train stimulations and recovery protocols

Train stimulations between 10-60 Hz for 1000 ms were used to induce vesicle depletion at the neuromuscular junctions (NMJs). Normalised plots of mean eEJC amplitudes are shown for train stimulations and recoveries. Recovery plots are shown both as normalised to the first peak in the train stimulation, and as normalised to the end peak of the recovery. This provides a measure of the ability of the synapse to recover and allows quantification of the rate of recovery.

1. Data for I170V line

At 10 Hz stimulation the TPI mutant I170V showed no significant difference in train stimulation by depletion, 74±3 % compared to 70±3 %, or time course, 550±80 ms compared to 380±80 ms, in comparison to controls. Following the 10 Hz train, I170V showed a less complete recovery, 107±5 % vs 120±8 % in w^{1118} reflected by the time constants, 12000±2000 ms compared to 7300±1000 ms in w^{1118}, see Figure 4-1 [D].

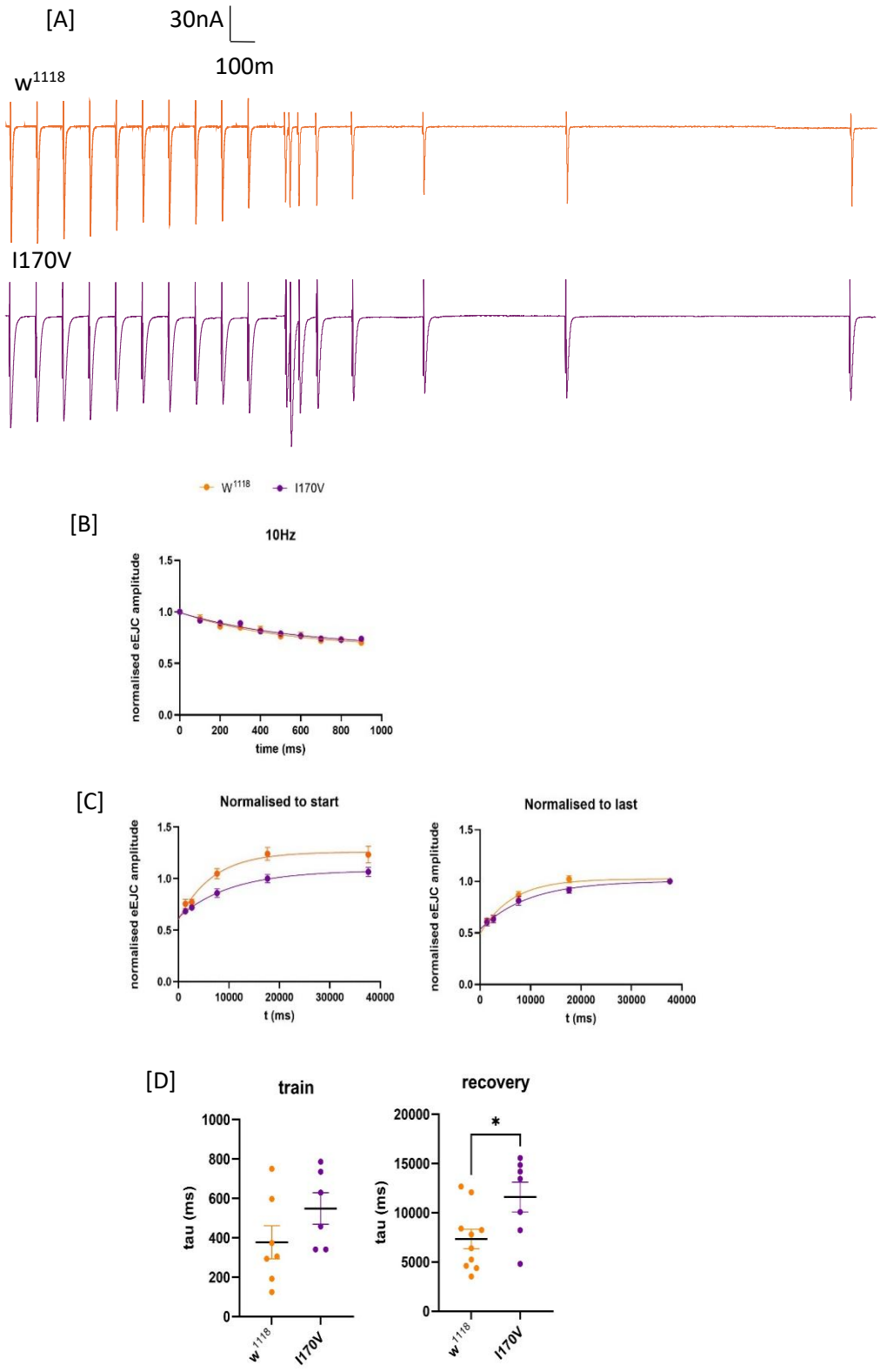

*Figure 4-1: Normalised 10 Hz train stimulations for I170V, data expressed as mean±SEM [A] Example raw traces of train and first 2.5 s of recovery from one recording for w^{1118} and I170V [B] 10 Hz train mean data, time constants for train; w^{1118}: 380±80 ms, I170V: 550±80 ms. Final amplitudes of; w^{1118}: 70±3 %, I170V: 74±3 %, [C] Recovery from 10 Hz train, normalised to first peak of train and last peak of recovery, time constants for recoveries; w^{1118}: 7300±1000 ms, I170V: 12000±2000 ms. Degree of recovery normalised to the first amplitude in the preceding train; w^{1118}: 120±8 %, I170V: 107±5 %. [D] time constants plotted mean±SEM, *p<0.05. Curves were fitted with non linear fits and student t tests were used to compare data sets for statistical significance n≥7. N≥5*

At 20 Hz I170V was seen to have a reduced depletion, amplitudes reducing to 99±5 % compared to 95±7 % in w^{1118} see Figure 4-2 [A], no difference in time constants for train, 290±60 ms compared to 210±10 ms see Figure 4-2 [C], or recovery, 7600±1000 ms compared to 11000±2000 ms see Figure 4-2 [C], were found for 20 Hz. No differences were found in extent of recovery at 20 Hz, 99±5 % compared to 95±7 %, see Figure 4-2 [B].

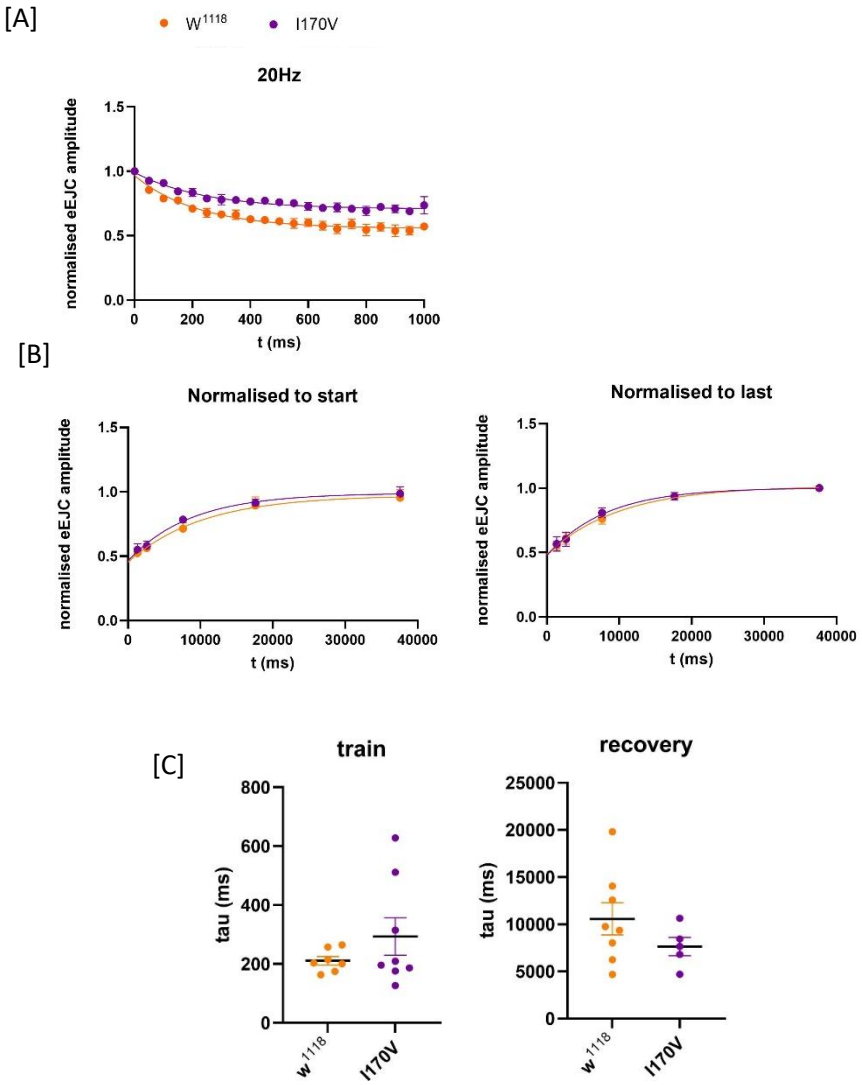

Figure 4-2: Normalised 20 Hz train stimulation for I170V, data expressed as mean±SEM [A] 20 Hz mean data, time constants for train; w^{1118}: 210±10 ms, I170V: 290±60 ms. Final amplitudes of; w^{1118}: 57±2 %, I170V: 74±7 %. [B] Recovery from 20 Hz train normalised to first peak in train and last peak in recovery, time constants for recovery; w^{1118}: 11000±2000 ms, I170V: 7600±1000 ms. Degree of recovery normalised to the first amplitude in the preceding train; w^{1118}: 95±7 %, I170V: 99±5 %. [C] time constants plotted mean±SEM. Curves were fitted with non linear fits and student t tests were used to compare data sets for statistical significance n≥8, N≥6.

At 30 Hz no differences were found for the I170V mutant; trains depleting to 66±4 % compared to 63±2 % see Figure 4-3 [A], with time constants of 320±70 ms compared to 206±30 ms see Figure 4-3 [C]. Extent of recovery in I170V was 92±10 % compared to 94±6 % see Figure 4-3 [B], with time constants of 6300±700 ms compared to 6300±700 ms. See Figure 4-3 [C].

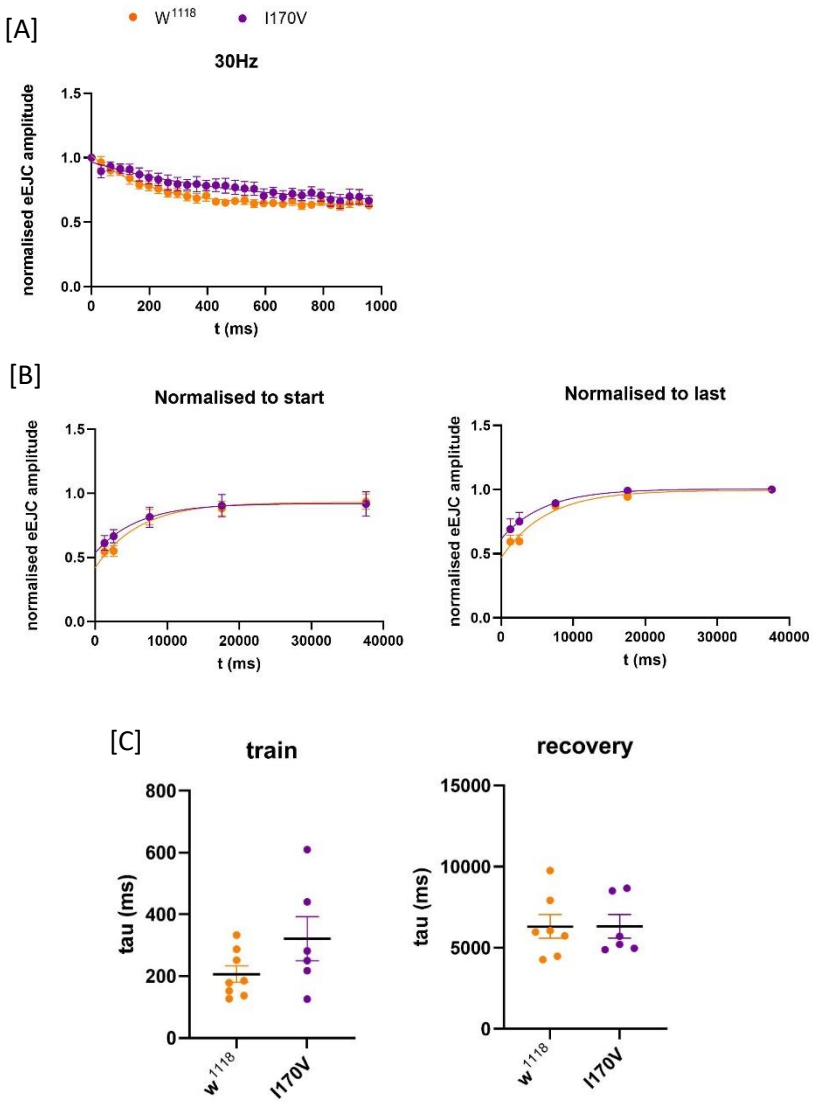

Figure 4-3: Normalised 30 Hz train stimulation for I170V, data expressed as mean±SEM [A] 30 Hz train mean data, time constants for train; w^{1118}: 206±30 ms, I170V: 320±70 ms. Final amplitudes of; w^{1118}: 63±2 %, I170V: 67±4 %. [B] Recovery from 30 Hz train normalised to first peak of train and last peak of recovery, time constants for recovery; w^{1118}: 6300±700 ms, I170V: 6300±700 ms. Degree of recovery normalised to the first amplitude in the preceding train; w^{1118}: 94±6 %, I170V: 92±9 %. [C] time constants plotted mean±SEM. Curves were fitted with non linear fits and student t tests were used to compare data sets for statistical significance n≥7, N≥5.

At 40 Hz and 50 Hz both lines I170V and w^{1118} deplete in a similar manner to a similar point. Trains depleting to 72±7 % compared to 70±4 % at 40 Hz, and 58±5 % compared to 64±5 % at 50 Hz see Figure 4-4 [A] and 4-5 [A]. With time

constants of 180±30 ms compared to 380±100 ms at 40 Hz, and 200±50 ms compared to 320±90 ms at 50 Hz see Figure 4-4 [C] and 4-5 [C]. At 40 Hz and 50 Hz I170V again showed a less complete recovery, 92±8 % vs 126±20 % at 40 Hz and 92±4 % vs 108±10 % at 50 Hz see Figure 4-4 [B] and 4-5 [B]. With time constants significantly decreased at 40 Hz, 5300±1000 ms compared to 10300±1000 ms. But no significant differences at 50 Hz, 9200±2000 ms compared to 7500±700 ms for recovery, see Figure 4-4 [C] and Figure 4-5 [C].

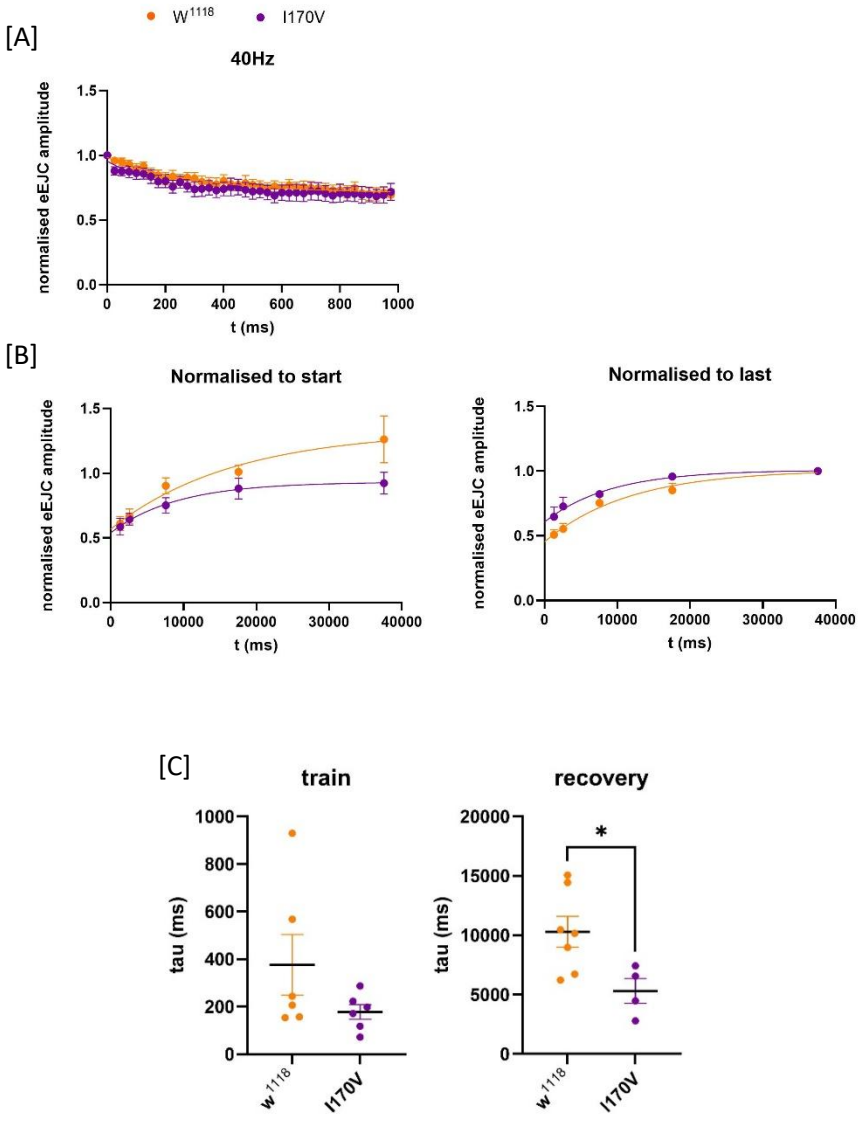

Figure 4-4: Normalised 40 Hz train stimulation for I170V, data expressed as mean±SEM [A] 40 Hz train mean data, time constants for train; w^{1118}: 380±100 ms, I170V: 180±30 ms. Final amplitudes of; w^{1118}: 70±4 %, I170V: 72±7 %. [B] Recovery from 40 Hz train, normalised to first peak of train and last peak of recovery, time constants for recovery; w^{1118}: 10300±1000 ms, I170V: 5300±1000 ms. Degree of recovery normalised to the first amplitude in the preceding train; w^{1118}: 130±20 %, I170V: 92±8 %. [C] time constants plotted mean±SEM. Curves were fitted with non linear fits and student t tests were used to compare data sets for statistical significance n≥8, N≥5.

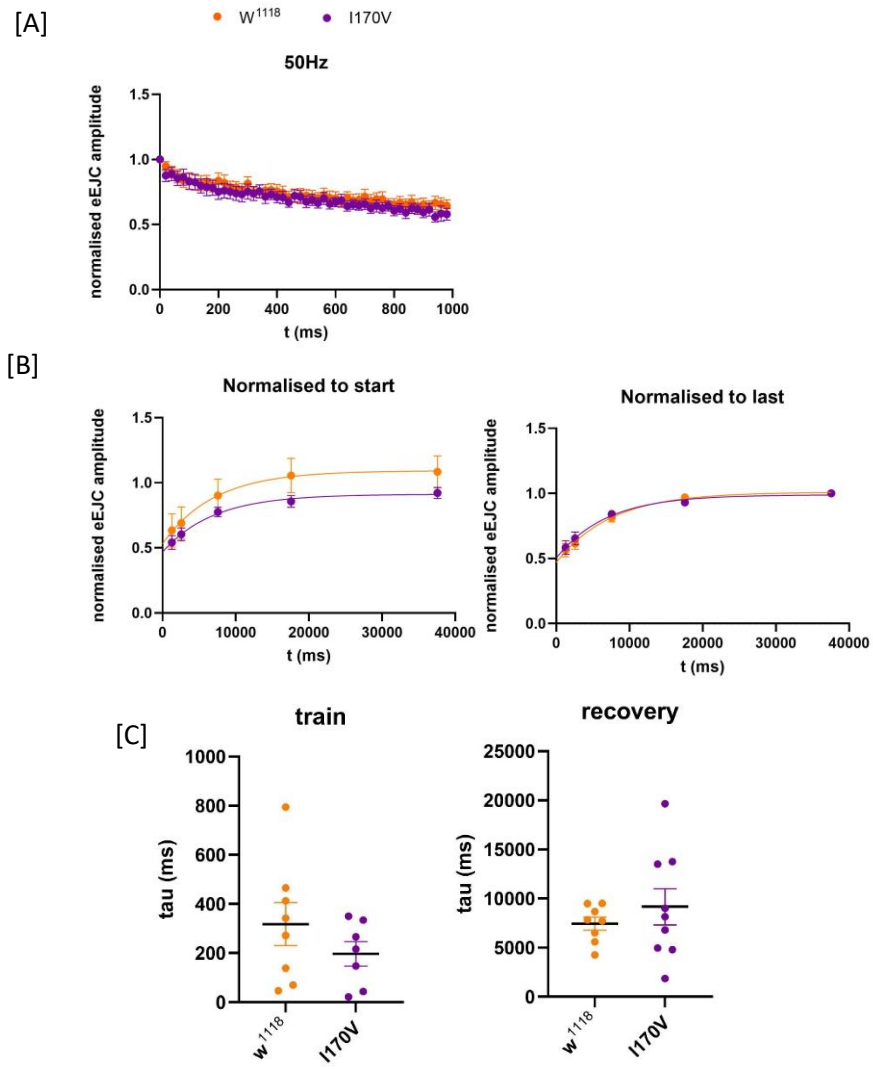

Figure 4-5: Normalised 50 Hz train stimulation for I170V, data expressed as mean±SEM [A] 50 Hz train mean data, time constants for train; w^{1118}: 320±90 ms, I170V: 200±50 ms. Final amplitudes of; w^{1118}: 64±5 %, I170V: 58±5 %. [B] Recovery for 50 Hz train normalised to first peak in train and last peak in recovery, time constants for recovery; w^{1118}: 7500±700 ms, I170V: 9200±2000 ms. Degree of recovery normalised to the first amplitude in the preceding train; w^{1118}: 108±10 %, I170V: 92±4 %. [C] time constants plotted mean±SEM. Curves were fitted with non linear fits and student t tests were used to compare data sets for statistical significance n≥9, N≥6.

At 60 Hz I170V showed no change in depletion, 49±7 % compared to 56±4 % see Figure 4-6 [A], with time constants of 350±200 ms compared to 220±20 ms see Figure 4-6 [C]. Although the 60 Hz train did show some different behaviour in consistency of the train stimulation, with various stimulations throughout the train not reaching the same amplitude as surrounding peaks. No changes in I170V recovery were seen at 60 Hz, extent of recovery reaching 96±7 % compared to 97±4 % see Figure 4-6 [B], with time constants of 8900±1000 ms compared to 6600±900 ms, see Figure 4-6 [C].

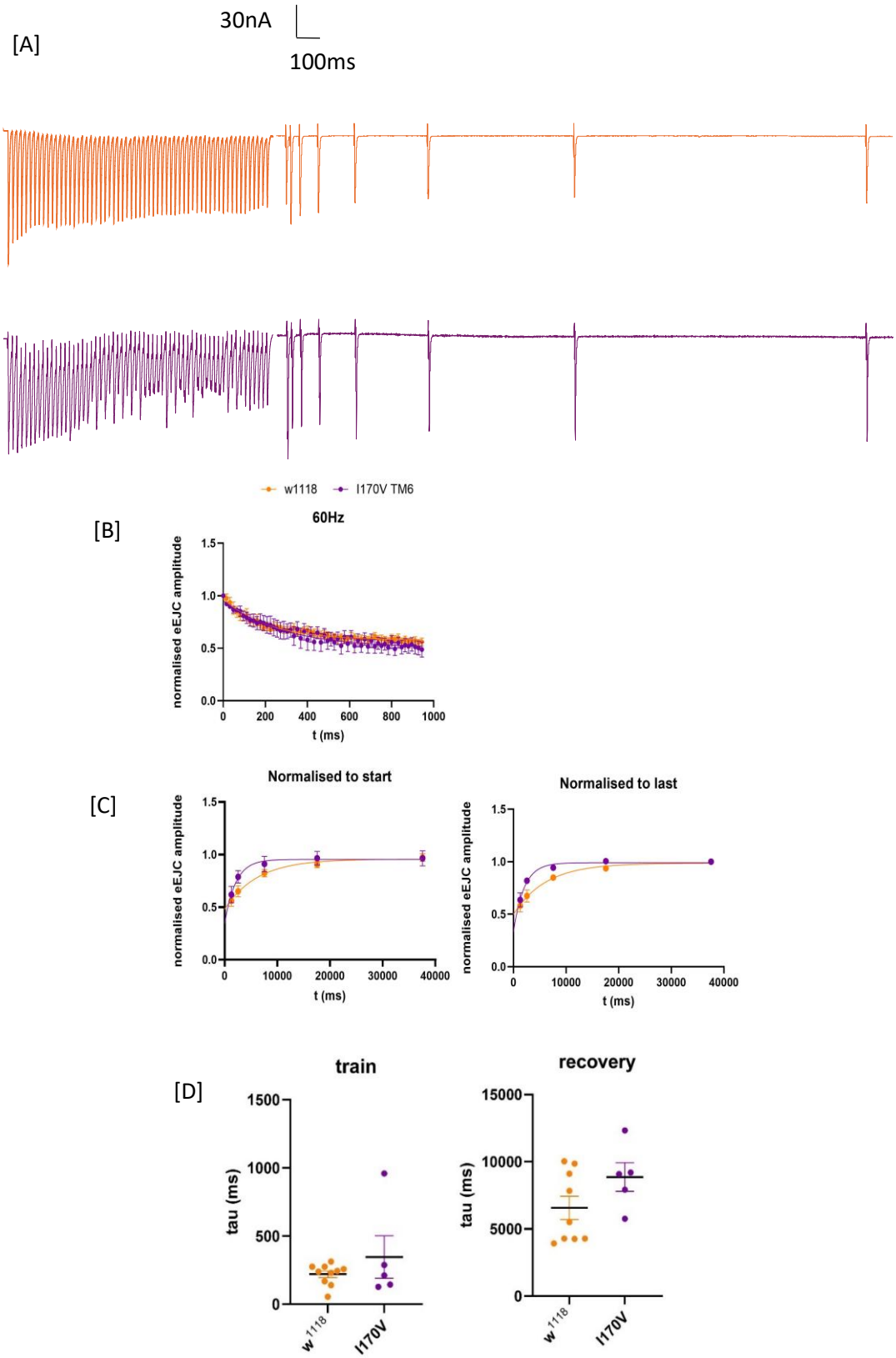

Figure 4-6: Normalised 60 Hz train stimulation for I170V, data expressed as mean±SEM [A] Example raw traces of train and first 2.5 s of recovery from one recording for w^{1118} and I170V [B] 60 Hz train mean data, time constants for train; w^{1118}: 220±20 ms, I170V: 350±200 ms. Final amplitudes of; w^{1118}: 56±4 %, I170V: 49±7 %. [C] Recovery from 60 Hz train normalised to first peak of train and last peak of recovery, time constants for recovery; w^{1118}: 6600±900 ms, I170V: 8900±1000 ms. Degree of recovery normalised to the first amplitude in the preceding train; w^{1118}: 97±4 %, I170V: 96±7 %. [D] time constants plotted mean±SEM. Curves were fitted with non linear fits and student t tests were used to compare data sets for statistical significance n≥6, N≥5.

2. Data for *Sugarkill*, wstd^{1} and M80T lines

At 10 Hz the M80T line shows a tendency to deplete further reflected in the reduced time constant, depleting to 75±4 % in wstd^{1}, 71±10 % in M80T compared to 69±2 % in Canton.S see Figure 4-7 [A], with time constants of 370±40 ms in wstd^{1}, 270±30 ms in M80T compared to 560±100 ms in Canton.S see Figure 4-7 [C]. Extent of recovery following the 10 Hz train was found to be similar in wstd^{1} and M80T compare to Canton.S, 120±10 % in wstd^{1}, 91±3 % in M80T compared to 99±8 % in Canton.S see Figure 4-7 [B], with time constants of 9600±1000 ms in wstd^{1}, 8600±2000 ms in M80T compared to 6900±800 ms in Canton.S, see Figure 4-7 [C].

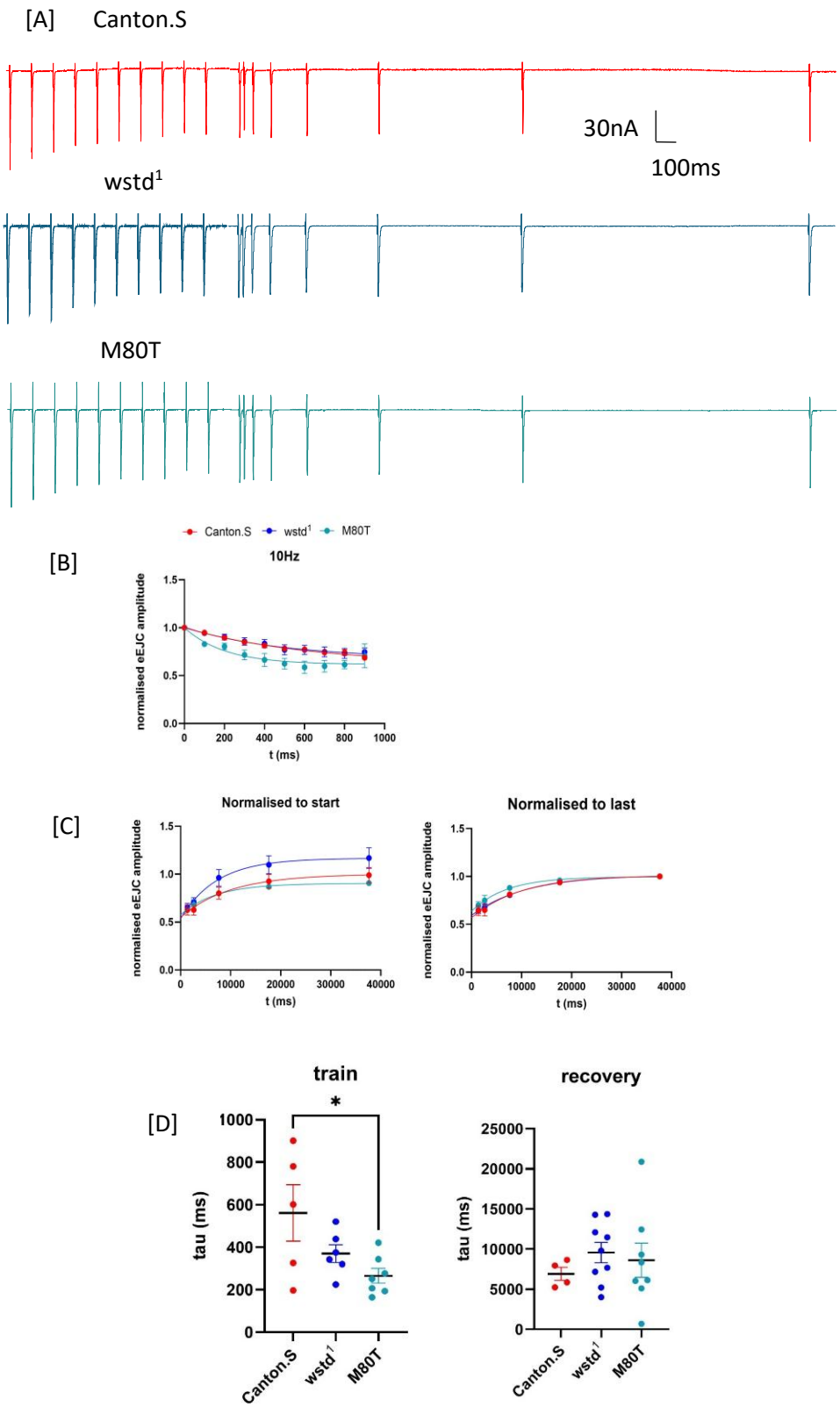

*Figure 4-7: Normalised 10 Hz train stimulation for wstd[1] and M80T, data expressed as mean±SEM [A] Example raw traces of train and first 2.5 s of recovery from one recording for Canton.S, wstd[1] and, M80T [B] 10 Hz train mean data, time constants for train; Canton.S: 560±100 ms, wstd[1]: 370±40 ms, M80T: 270±30 ms. Final amplitudes of; Canton.S: 69±2 %, wstd[1]: 75±4 %, M80T: 71±10 %. [C] Recovery from 10 Hz train, normalised to first peak in train and last peak in recovery, time constants for recovery; Canton.S: 6900±800 ms, wstd[1]: 9600±1000 ms, M80T: 8600±2000 ms. Degree of recovery normalised to the first amplitude in the preceding train; Canton.S: 99±8 %, wstd[1]: 120±10 %, M80T: 91±3 %. [D] time constants plotted mean±SEM. Curves were fitted with non linear fits and student t tests were used to compare data sets for statistical significance, *p<0.05, n≥7, N≥5.*

At 20 Hz no significant differences were seen in the two *Sugarkill* mutants. Trains depleted to 74±9 % in wstd^1, 64±8 % in M80T compared to 70±8 % in Canton.S see Figure 4-8 [A], with time constants of 150±20 ms in wstd^1, 230±50 ms in M80T compared to 300±50 ms in Canton.S see Figure 4-8 [C]. Extent of recovery following 20 Hz train was 104±9 % in wstd^1, 87±6 % in M80T compared to 87±6 % in Canton.S see Figure 4-8 [B], with time constants of 7300±1000 ms in wstd^1, 10100±2000 ms in M80T compared to 9400±2000 ms in Canton.S, see Figure 4-8 [C].

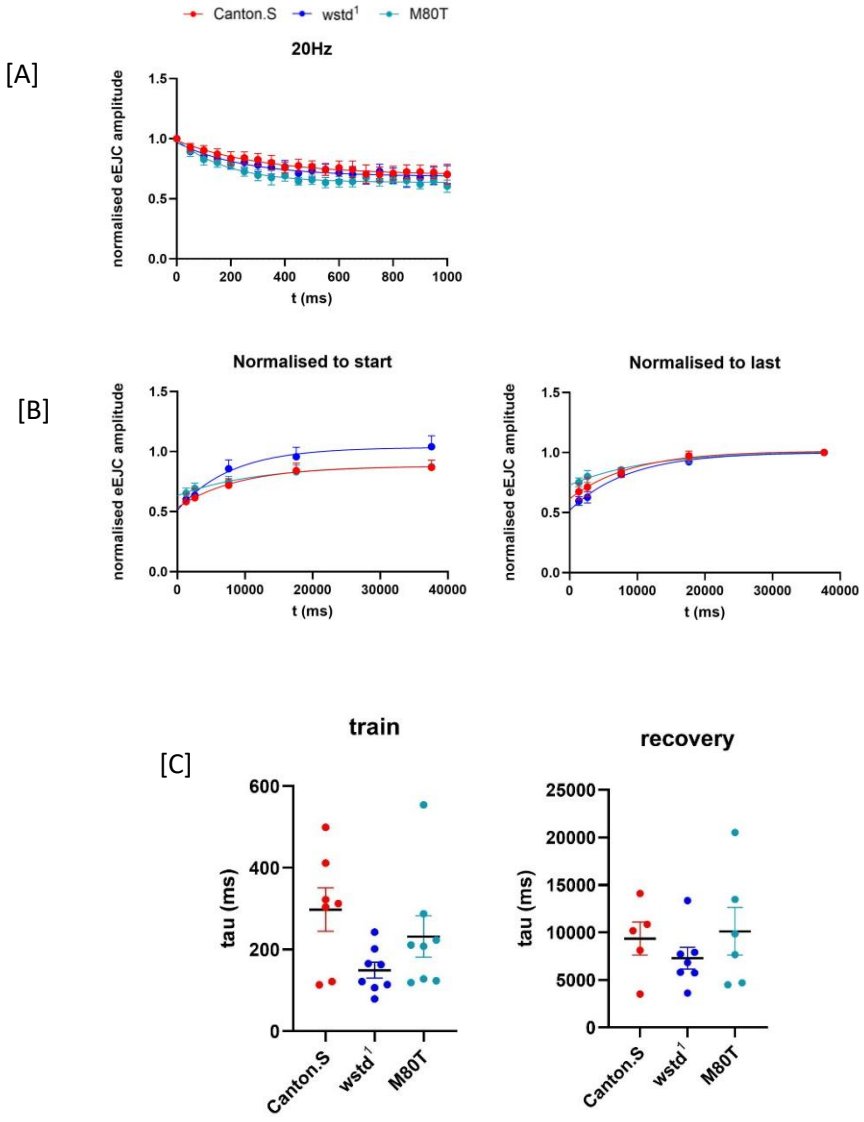

Figure 4-8: Normalised 20 Hz train stimulation for wstd^1 and M80T, data expressed as mean±SEM [A] Canton.S: 300±50 ms, wstd^1: 150±20 ms, M80T: 230±50 ms. Plateaus of; Canton.S: 70±8 %, wstd^1: 70±7 %, M80T: 60±5 %. [B] Recovery from 20 Hz train, normalised to first peak in train and last peak in recovery, time constants for recovery; Canton.S: 9400±2000 ms, wstd^1: 7300±1000 ms, M80T: 10100±2000 ms. Degree of recovery normalised to the first amplitude in the preceding train; Canton.S: 87±6 %, wstd^1: 104±9 %, M80T: 87±6 %. [C] time constants plotted mean±SEM. Curves were fitted with non linear fits and student t tests were used to compare data sets for statistical significance n≥7, N≥5.

At 30 Hz the two *Sugarkill* mutants continued to show little differences to control. Trains depleting to 61±4 % in wstd^{1}, 60±8 % in M80T, compared to 63±9 % in Canton.S see Figure 4-9 [A], with time constants of 170±40 ms in wstd^{1}, 160±30 ms in M80T compared to 320±80 ms in Canton.S see Figure 4-9 [C]. Extent of recovery following 30 Hz train was 95±5 % in wstd^{1}, 86±4 % in M80T compared to 86±8 % in Canton.S see Figure 4-9 [B], with time constants of 7200±1000 ms in wstd^{1}, 5500±400 ms in M80T compared to 9200±900 ms in Canton.S, see Figure 4-9 [C].

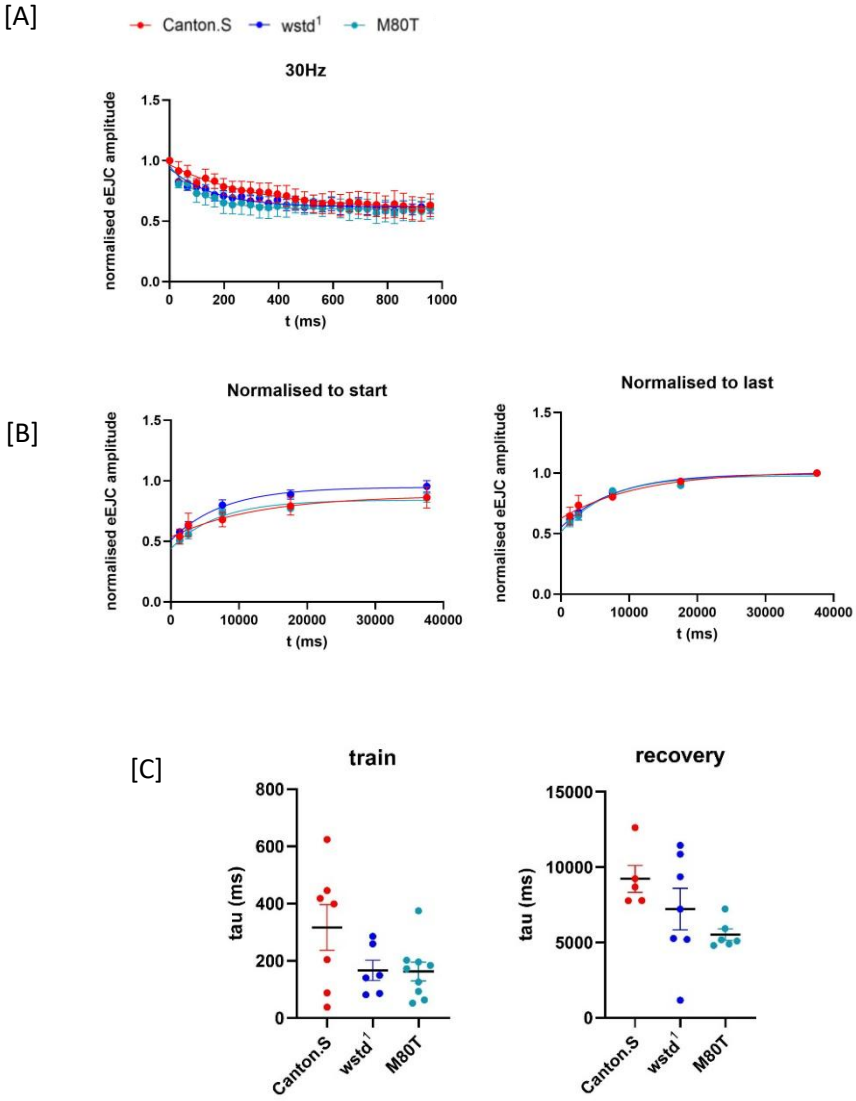

Figure 4-9: Normalised 30 Hz train stimulation for wstd^{1} and M80T, data expressed as mean±SEM, [A] 30 Hz train mean data, time constants for train; Canton.S: 320±80 ms, wstd^{1}: 170±30 ms, M80T: 160±30 ms. Final amplitudes of; Canton.S: 63±9 %, wstd^{1}: 61±4 %, M80T: 60±8 %. [B] Recovery from 30 Hz train, normalised to first peak of train and last peak in recovery, time constants for recovery; Canton.S: 9200±900 ms, wstd^{1}: 7200±1000 ms, M80T: 5500±400 ms. Degree of recovery normalised to the first amplitude in the preceding train; Canton.S: 86±9 %, wstd^{1}: 95±5 %, M80T: 86±4 %. [C] time constants plotted mean±SEM. Curves were fitted with non linear fits and student t tests were used to compare data sets for statistical significance n≥7, N≥5.

At 40 Hz M80T shows reduced depletion, 51±4 % in wstd^1, 81±10 % in M80T compared to 57±9 % in Canton.S see Figure 4-10 [A], with time constants of 140±30 ms in wstd^1, 340±100 ms in M80T compared to 240±90 ms in Canton.S see Figure 4-10 [C]. Extent of recovery following 40 Hz train was reduced in the *Sugarkill* lines, 97±2 % in wstd^1, 93±5 % in M80T compared to 107±20 % in Canton.S see Figure 4-10 [B], time constants were not found to be altered, 7500±1000 ms in wstd^1, 6900±3000 ms in M80T compared to 8500±800 ms in Canton.S, see Figure 4-10 [C].

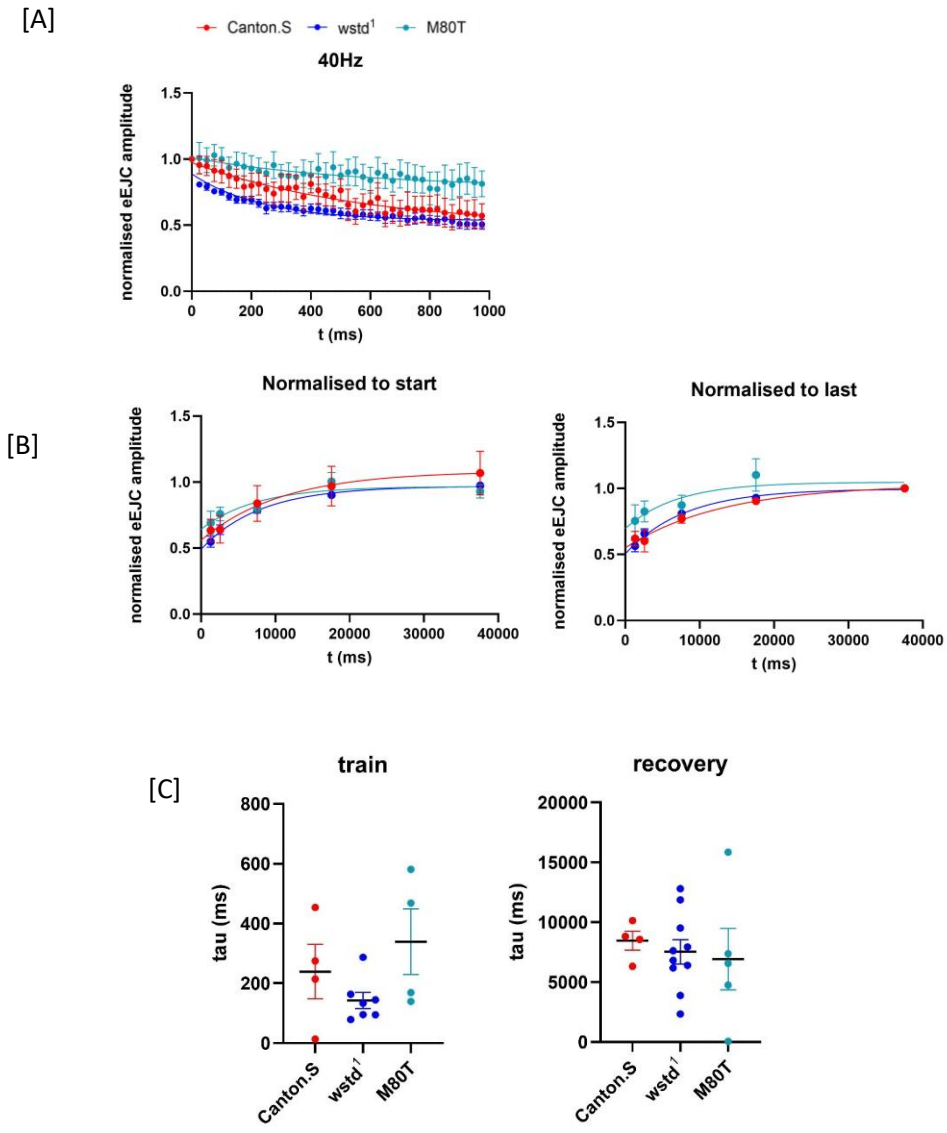

Figure 4-10: Normalised 40 Hz train stimulation for wstd^1 and M80T, data expressed as mean±SEM, [A] 40 Hz train mean data, time constants for train; Canton.S: 240±90 ms, wstd^1: 140±30 ms, M80T: 340±100 ms. Final amplitudes of; Canton.S: 57±9 %, wstd^1: 51±4 %, M80T: 81±10 %. [B] Recovery from 40 Hz train normalised to first peak of train and last peak of recovery, time constants for recovery; Canton.S: 7900±1000 ms, wstd^1: 7500±1000 ms, M80T: 6900±3000 ms. Degree of recovery normalised to the first amplitude in the preceding train; Canton.S: 107±20 %, wstd^1: 97±2 %, M80T: 93±5 %. [C] time constants plotted mean±SEM. Curves were fitted with non linear fits and student t tests were used to compare data sets for statistical significance n≥6, N≥5.

At 50 Hz amplitudes depleted to; 46±7 % in wstd^1, 70±10 % in M80T compared to 58±6 % in Canton.S see Figure 4-11 [A], time constants were unaltered, 30±30 ms in wstd^1, 290±200 ms in M80T compared to 250±60 ms in Canton.S see Figure 4-11 [C]. Extent of recovery was reduced in both *Sugarkill* mutants, 94±6 % in wstd^1, 93±8 % in M80T compared to 108±10 % in Canton.S see Figure 4-11 [B], with time constants of 7500±1000 ms in wstd^1, 11000±3000 ms in M80T compared to 24000±10000 ms in Canton.S, see Figure 4-11 [C].

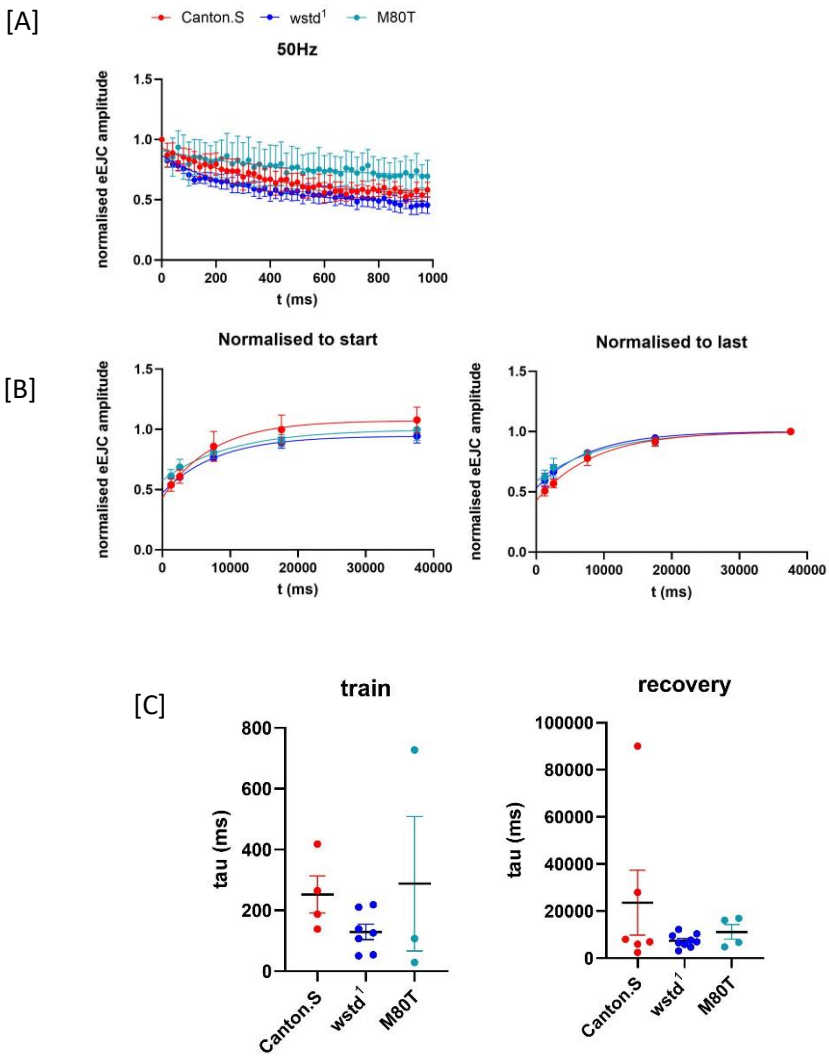

Figure 4-11: Normalised 50 Hz train stimulation for wstd^1 and M80T, data expressed as mean±SEM [A] 50 Hz train mean data, time constants for train; Canton.S: 250±60 ms, wstd^1: 130±30 ms, M80T: 290±200 ms. Final amplitudes of; Canton.S: 58±6 %, wstd^1: 46±7 %, M80T: 72±8 %. [B] Recovery from 50 Hz train normalised to first peak in train and last peak of recovery, time constants for recovery; Canton.S: 24000±10000 ms, wstd^1: 7500±1000 ms, M80T: 9700±3000 ms. Degree of recovery normalised to the first amplitude in the preceding train; Canton.S: 108±10 %, wstd^1: 94±6 %, M80T: 93±8 %. [C] time constants plotted mean±SEM. Curves were fitted with non linear fits and student t tests were used to compare data sets for statistical significance n≥6, N≥5.

At 60 Hz stimulation trains depleted to 41±7 % in wstd^1, 47±10 % in M80T compared to 50±8 % for Canton.S see Figure 4-12 [A], time constants were not significantly altered in either *Sugarkill* mutant, 230±60 ms in wstd^1, 204±40 ms

compared to 260±90 ms in Canton.S see Figure 4-12 [C]. Extent of recovery following 60 Hz was reduced in both *Sugarkill* mutants, 85±6 % in wstd^{1}, 93±4 % in M80T compared to 110±10 % in Canton.S see Figure 4-12 [B], time constants were unaltered, 10600±2000 ms in wstd^{1}, 10200±3000 ms in M80T compared to 8500±800 ms in Canton.S, see Figure 4-12 [C].

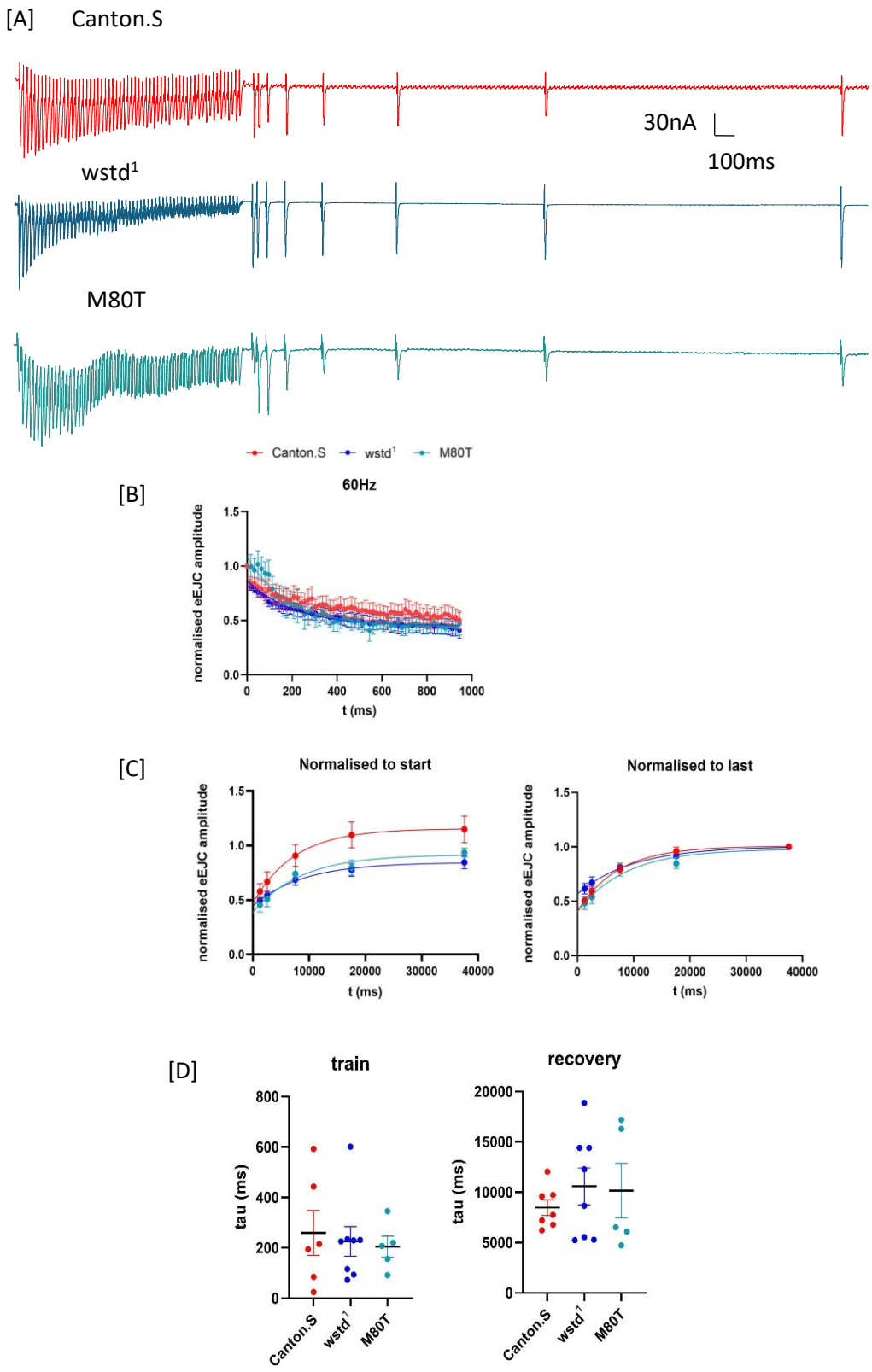

Figure 4-12: N*ormalised 60 Hz train stimulation for wstd[1] and M80T, data expressed as mean±SEM [A] Example raw traces of train and first 2.5 s of recovery from one recording for Canton.S, wstd[1] and, M80T [B] 60 Hz train mean data, time constants for train; Canton.S: 260±90 ms, wstd[1]: 230±60 ms, M80T: 204±40 ms. Final amplitudes of; Canton.S: 50±8 %, wstd[1]: 41±7 %, M80T: 54±9 %. [C] Recovery for 60 Hz train, normalised to first peak of train and last peak of recovery, time constants for recovery; Canton.S: 8500±800 ms, wstd[1]: 10600±2000 ms, M80T: 10080±2000 ms. Degree of recovery normalised to the first amplitude in the preceding train; Canton.S: 110±10 %, wstd[1]: 85±6 %, M80T: 92±5 %. [D] time constants plotted mean±SEM. Curves were fitted with non linear fits and student t tests were used to compare data sets for statistical significance n≥7, N≥5.*

3. Data for Glo(KO) line

At 10 Hz the glyoxalase knock out line seemed to show significantly reduced levels of depletion with unaltered amplitudes at the end of the train relative to the start, 99±6 %, compared to 70±3 % for w^{1118} see Figure 4-13 [A], time constants of 630±600 ms for Glo(KO) compared to 380±80 ms for w^{1118} see Figure 4-13 [C]. Extent of recovery was 120±10 % for Glo(KO) compared to 120±8 % for w^{1118} see Figure 4-13 [B], time constants of 10700±1000 ms for Glo(KO) compared to 7300±1000 ms for w^{1118}, see Figure 4-13 [C]. Recovery from the 10 Hz train was altered in Glo(KO) as expected from the lack of depletion in the train, see Figure 4-13 [A].

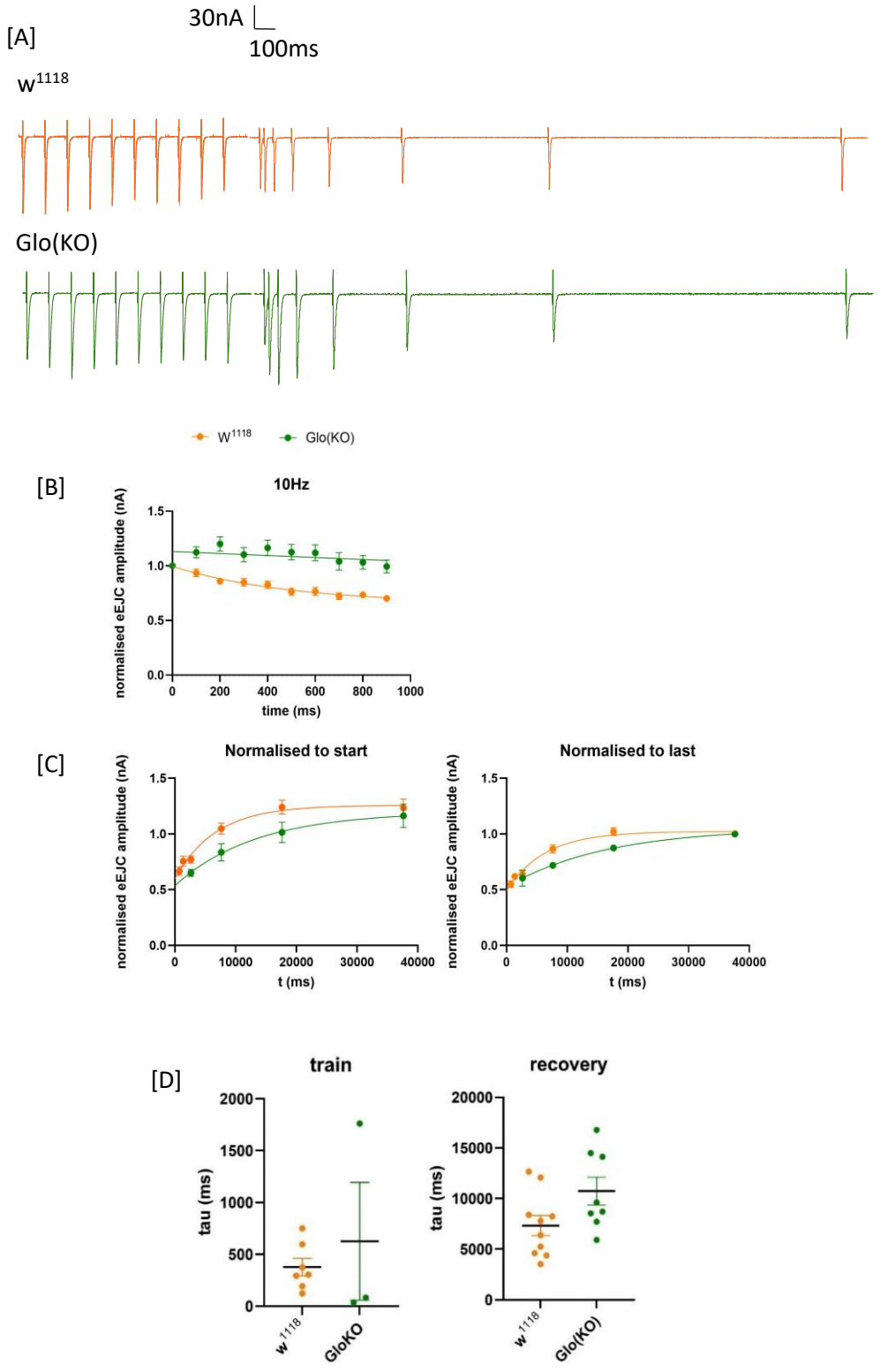

Figure 4-13: Normalised 10 Hz train stimulations for Glo(KO), data expressed as mean±SEM [A] Example raw traces of train and first 2.5 s of recovery from one recording for w^{1118} and Glo(KO) [B] 10 Hz train mean data,time constants for train; w^{1118}: 380±80 ms, Glo(KO): 630±600 ms. Plateau values of; w^{1118}: 70±3 %, Glo(KO): 99±6 %, [C] recovery from 10 Hz train normalised to first peak of train and to last peak of recovery, time constants for recovery; w^{1118}: 7300±1000 ms, Glo(KO): 10700±1000 ms. Degree of recovery normalised to the first amplitude in the preceding train; w^{1118}: 120±8 %, Glo(KO): 120±10 %, [D] time constants plotted mean±SEM. Curves were fitted with non linear fits and student t tests were used to compare data sets for statistical significance n≥9, N≥5.

As at 10 Hz, the Glo(KO) line showed reduced levels of depletion at 60 Hz in comparison to control, although depletion is seen here unlike at 10 Hz, 86±30 % for Glo(KO) compared to 56±4 % for w^{1118} see Figure 4-14 [A]. Time constants were not altered, 380±100 ms for Glo(KO) compared to 220±20 ms for w^{1118} see Figure 4-14 [C]. Extent of recovery was increased, 110±16 % in Glo(KO) compared to 97±4 % for w^{1118} see Figure 4-14 [B], reflected by the increased time constant, 17000±4000 ms in Glo(KO) compared to 6600±900 ms in w^{1118}, see Figure 4-14 [C].

The Glo(KO) line also shows an initial potentiation phase in train stimulation, more notably at 60 Hz than 10 Hz, this is expected from the lower release indicated by the reduced single eEJC amplitude, an effect that is not observed in w^{1118}, see Figures 4-13 and 4-14.

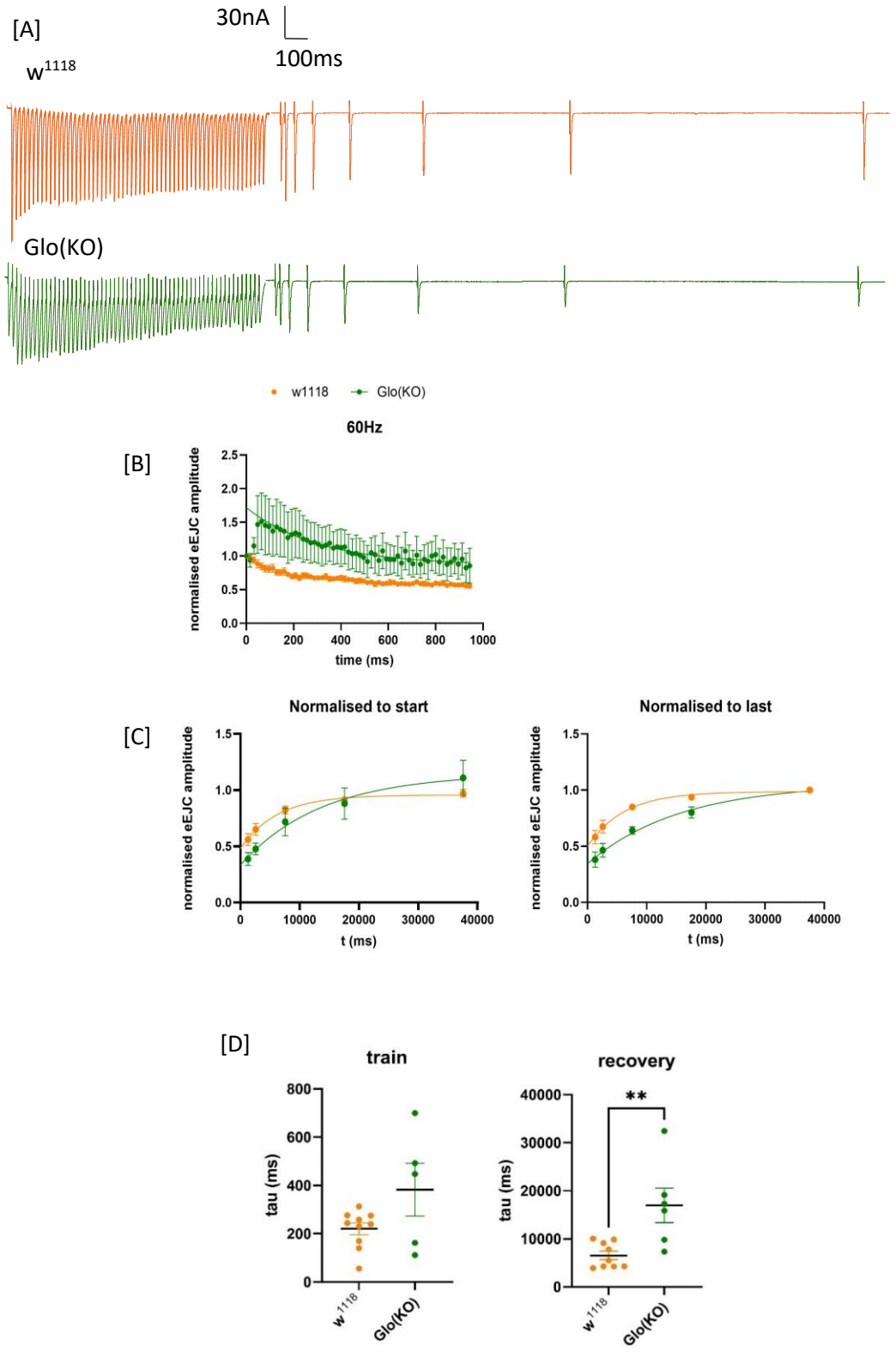

Figure 4-14: Normalised 60 Hz train stimulation for Glo(KO), data expressed as mean±SEM [A] Example raw traces of train and first 2.5 s of recovery from one recording for w^{1118} and Glo(KO) [B] 60 Hz train mean data, time constants for train; w^{1118}: 220±20 ms, Glo(KO): 380±100 ms. Final amplitudes of; w^{1118}: 56±4 %, Glo(KO): 86±20 %. [C] Recovery from 60 Hz train normalised to first peak of train and to last peak of recovery, mean time constants for recovery; w^{1118}: 6600±900 ms, Glo(KO): 17000±4000 ms, Degree of recovery normalised to the first amplitude in the preceding train; w^{1118}: 97±4 %, Glo(KO): 110±20 %. [D] time constants plotted mean±SEM. Curves were fitted with non linear fits and student t tests were used to compare data sets for statistical significance n≥9, N≥4.

4.4.2: Vesicle pool estimations

Vesicle pool estimations were seen to be increased for wstd^{1} compared to Canton.S, 930±100 nA vs 450±100 nA, however the M80T and I170V lines showed no significant differences to controls, see Figure 4-15 [B].

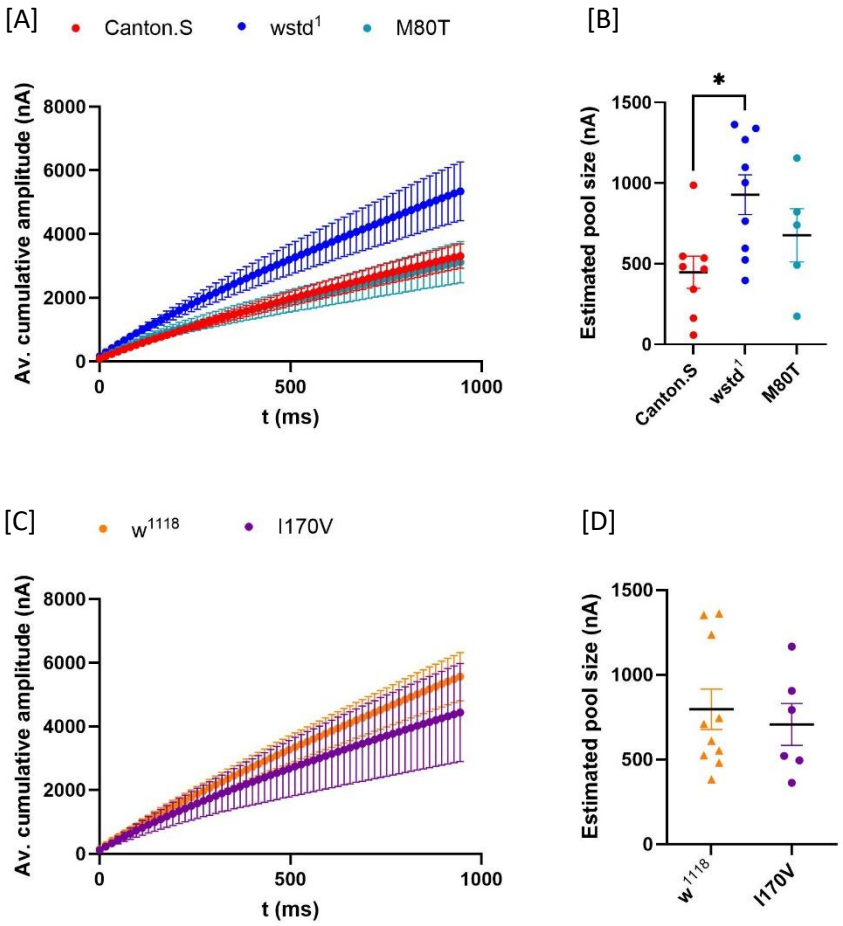

*Figure 4-15: Total available vesicle pool size estimations, cumulative amplitudes from 60 Hz train were plotted, back extrapolation to the y axis from 700-1000 ms steady state section of plotted data gives an estimation of the available vesicle pool size [A] mean cumulative amplitudes from 60 Hz train stimulation error is SEM. For mutant lines wstd^{1} and M80T vs Canton.S [B] Plotted vesicle pool estimates for; wstd^{1}: 930±100 nA, and M80T: 640±100 nA vs Canton.S: 450±100 nA, each point plotted represents a pool estimate for an individual 60 Hz train stimulation [C] mean cumulative amplitudes from 60 Hz train stimulation error is SEM. For mutant line I170V vs w^{1118} [D] Plotted vesicle pool estimates for; I170V: 706±100 nA, vs w^{1118}: 800±100 nA, each point plotted represents a pool estimate for an individual 60 Hz train stimulation. One-way ANOVA Dunnetts multiple comparisons test used to test between wstd^{1}, M80T, and Canton.S *p<0.05, unpaired students t test used to compare between I170V and w^{1118}, ns.*

4.5: Treatment with redox stressors altered eEJCs in w^{1118} and Glo(KO) lines

As TPI dysfunction and deficiency has been linked to redox stress and enhanced ROS levels (Seigle et al. 2008; Guix et al. 2009; Hrizo et al. 2013; Roland et al. 2019; Hrizo et al. 2021; Stone et al. 2023), the following experiments aim at assessing effects of direct application of redox stress synaptic function.

H_2O_2 (5 % (Zhu et al. 2021)) perfusion was run for 5 minutes before starting experiments, eEJC and sEJC responses were then recorded over a 3000s period with constantly maintained perfusion. This gave a measure of acute exposure on synapses. Chronic exposure was also investigated via addition of H_2O_2 to food in vials for 48 hrs prior to experiments.

Investigating synaptic activity in the presence of redox stressors gives valuable information on how phenotypes alter in environments of high redox stress. As the expected route of dysfunction in mutant lines is heavily related to redox stress, the impact of additional redox stress should promote dysfunction in control lines and enhance dysfunction in mutant lines.

Preliminary electrophysiology with constant perfusion of 5 % H_2O_2 (Zhu et al. 2021) throughout whole experiment showed a seemingly two stage decrease in amplitude of evoked events over time, the effect appeared slower in Glo(KO) than w^{1118} see Figure 4-16 [A]. Paired spontaneous events showed no changes throughout the experiment, see Figure 4-16 [B]. As these results were only preliminary statistics were unable to be run, therefore trends highlighted in Figure 4-16 [A] are predictions not statistical fits.

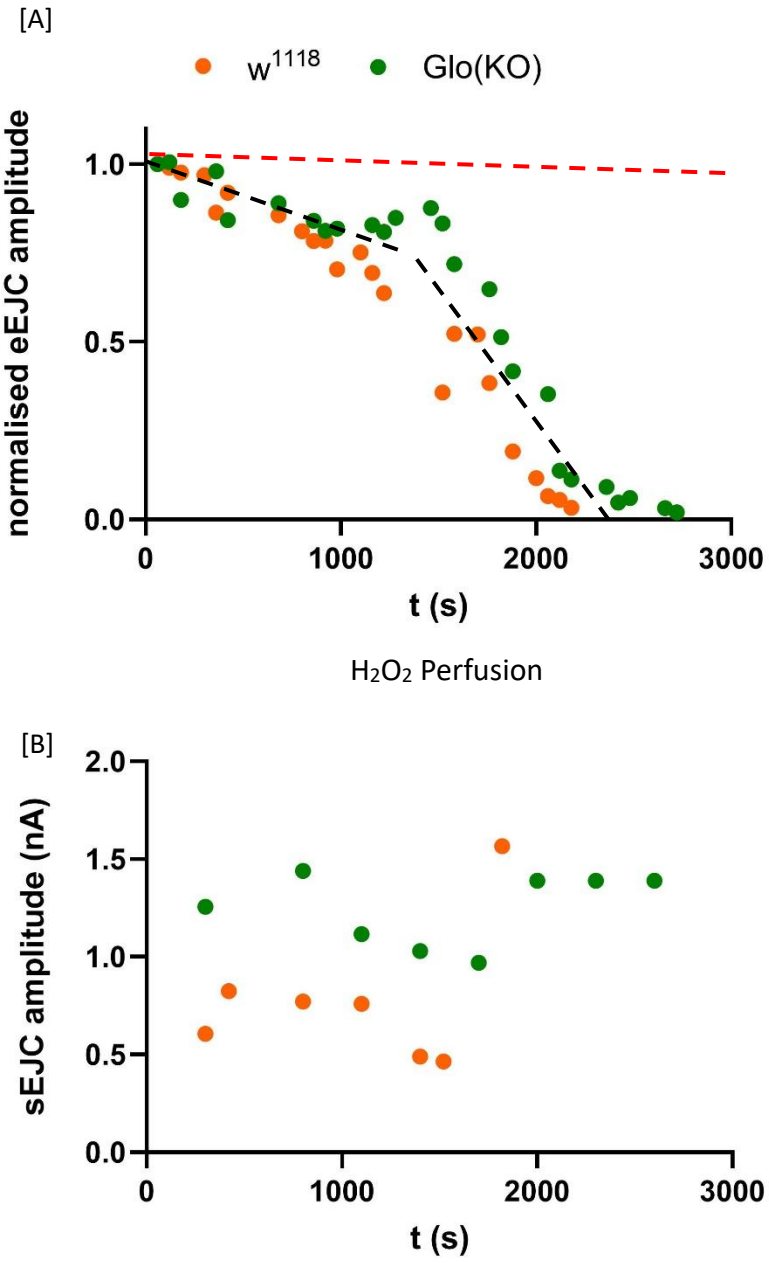

Figure 4-16: Acute H_2O_2 exposure over 3000 s stimulation with constant H_2O_2 perfusion recordings started 5 min after perfusion start [A] eEJC amplitudes for w^{1118} and I170V, black dotted lines showing apparent two stage response; initial slow reduction in amplitude and second faster depletion stage, red dotted line showing expected wild type response (Robinson et al. 2018) [B] sEJC amplitudes for w^{1118} and I170V

Measurements of eEJCs following treatments with 5 % H_2O_2 (Zhu et al. 2021) additions to food showed a decrease in eEJC amplitude in w^{1118}, 34 % reduction compared to non-treated control see Figure 4-17.

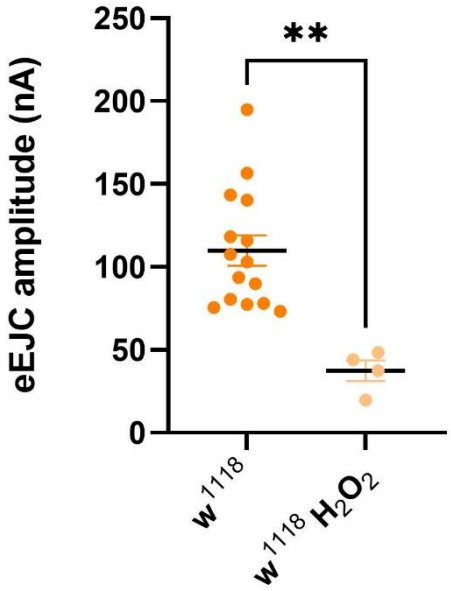

*Figure 4-17: eEJC recordings of 3rd instar larvae fillets with chronic H_2O_2 exposure. Larvae fed with 5 % H_2O_2 for 48hr prior to experiments. Data is presented as mean eEJC±SEM; w^{1118}: 109±9 nA, w^{1118} H_2O_2 : 37±6 nA, n≥4 N≥3 Unpaired students t test used to test for statistical significance **p<0.005*

4.6: Discussion

As shown in the previous chapter, this chapter corroborates the conclusion that synaptic activity is altered in the TPI and glyoxalase mutant lines. Train stimulations give an indication of overall available vesicle pool size and vesicle recycling kinetics, recovery protocols giving an indication of vesicle recycling kinetics and synaptic resilience see Table 4.1 for summery.

Table 4.1: Summary of train, recovery, and redox stress effects on eEJC data in mutant lines in comparison to controls

	wstd[1]	**M80T**	**I170V**	**Glo(KO)**
Train stimulation	Time constant for 20 Hz train was found to be reduced *p<0.05. Increased depletion was seen at 40, 50, and 60 Hz	Increased depletion seen at 10 Hz, time constant for 10 Hz train was reduced *p<0.05. Reduced depletion seen at 40 and 50 Hz. Potentiation seen at start of 60 Hz train	Reduced depletion seen at 20 Hz	No depletion at 10 Hz, minimal depletion at 60 Hz, potentiation at start of trains
Recovery from train	More complete recoveries were seen at 10, 20 and 30 Hz. Less complete recoveries were seen at 40, 50 and 60 Hz	Less complete recoveries were seen at 30, 40, 50, and 60 Hz.	Less complete recoveries seen at 10, 40 and 50 Hz.	Time constant for recovery from 60 Hz train increased **p<0.005
Effect of redox stress	N/A	N/A	N/A	Reduced eEJC amplitudes were found when treated with acute H_2O_2

Train and recovery protocols showed less complete recoveries for the I170V line. With reduced depletion following the 20 Hz train compared to the control line w^{1118}, although these differences were not consistent with some protocols showing no significant differences such as in the 60 Hz train and recovery. Time constants for recovery following 50 and 60 Hz trains were increased, although this was not found to be significant. This could support the hypothesis from the previous chapter that vesicle dynamics are altered in TPI mutant lines (Roland et al. 2016; Stone et al. 2023).

The $wstd^{1}$ line showed altered depletion and recovery through all frequencies although the direction of change depended on the frequency. Low frequency stimulation led to more complete recovery, higher level of facilitation, than control and at high frequency stimulation this effect was reversed. The previous chapter suggested vesicles in this line were larger and more were released per single evoked event. This is supported in this chapter by the increased vesicle pool sizes. This could explain why at low frequency recovery was possible where at high frequency recovery was limited, as with larger vesicles – suggested by the increased sEJP amplitudes - and more vesicles being released following initial stimulation the system could not maintain firing at high frequency. This also could suggest altered vesicle recycling in this line, impaired recycling could explain the inability to recover following high frequency trains, again fitting with the previous suggestion of altered vesicle dynamics (Roland et al. 2016; Stone et al. 2023).

The M80T line also showed altered depletion and recovery at all frequencies. Although this did not follow the same pattern as $wstd^{1}$, some effects were comparable, such as the less complete recoveries following high frequency trains, 30-60 Hz. The M80T line also showed reduced depletion at 40 and 50 Hz and potentiation at the start of the 60 Hz train. Both reduced depletion and potentiation are comparable to the Glo(KO) line suggesting M80T also shows a lower release, although no significant difference in eEJC does not corroborate this. No significant results were found in the previous chapter however this data does suggest that vesicle release or organisation in this line is altered, in keeping with the results for $wstd^{1}$ and I170V.

In the Glo(KO) line no depletion was seen following the 10 Hz train, recovery following this train showed an increased time constant, although this was not found to be significant. Potentiation was seen in this line at the start of both 10 and 60 Hz trains, reflecting the lower release from the reduced eEJC amplitudes. Throughout the 60 Hz train Glo(KO) showed depletion, although not to the extent as w^{1118}. Recovery from the 60 Hz train was seen to be more increased compared to w^{1118}, suggesting a faster recycling mechanism in this line. This data with the conclusions drawn from the last chapter support the hypothesis

of an altered vesicle organisation and release in this line, similar to the TPI mutants possibly suggesting a connected mechanism.

As expected, chronic exposure of H_2O_2 as a redox stressor reduced eEJC amplitudes in w^{1118} (Nagase et al. 1997; Miwa et al. 2003; Fukai and Ushio-Fukai 2011; Bradley and Steinert 2015; Robinson et al. 2018). Also as expected acute exposure with perfusion of H_2O_2 lowered eEJC amplitudes over time for both w^{1118} and Glo(KO), a seeming two stage response is seen with an initial slow reduction then a sharper reduction starting around 1,400 s, this could be due to an initially compensated response which becomes redundant after further exposure to H_2O_2. The kinetics of the reduction however were significantly altered in the Glo(KO) line, which reinforces the previous suggestion that Glo(KO) expresses altered vesicle dynamics. Glo(KO) has also been reported to have an increased resilience to oxidative stress induced by a 3 % H_2O_2 treatment for 1 week (Moraru et al. 2018), which could be a different explanation for the altered kinetics for amplitude reduction in this line. The general reduction in eEJC amplitudes with H_2O_2 treatment confirms the assumption that enhanced redox stress does impair synaptic transmission.

Again the data spreads in some experiments could suggest type 1 errors, as discussed in Section 3.8 this requires either larger data sets or further sub division of data sets to confirm significance shown here.

4.7: Future work

The data presented here could benefit from further analysis investigating; rising phases of single events in trains and recoveries, fall phase of single events in trains and recoveries, and frequency of failures (Erxleben et al. 1988; Bruns et al. 2000; Castillo et al. 1954). However the data presented in this thesis did not have sufficient signal:noise ratios to allow reliable analysis, additionally experiments showing failures were excluded from recordings so analysis is not possible with the current data. To further investigate the altered activity seen here more precise investigation of vesicle organisation in synapses would be invaluable, such as with electron microscopy. More detailed electrophysiology with redox stress treatment would also be beneficial, as the synaptic phenotypes shown in these lines do not appear to be consistent between mutants.

Completing the preliminary studies presented here for electrophysiological recordings with treatments of redox stressors would be a beneficial future set of experiments. Completing data sets, including TPI mutant lines for chronic

H_2O_2 exposure, and including relevant controls without treatment for acute exposure would be highly informative. Including *Drosophila* lines, possibly bi-transgenic, containing a TPI point mutation and a glyoxalase overexpression, could also give a better suggestion as to whether the increased oxidative stress from impaired TPI function is the key driver of pathology, and if glyoxalase is a potential therapeutic target.

Another beneficial addition to this data would be quantification of proteins associated with redox stress, this would give confirmation of the current hypothesis that dysfunction stems from altered redox stress. Quantifying the TPI protein levels would also be useful to determine the presence and state of catalysis for this enzyme in the mutant lines.

The following chapters begin to address some of these questions.

Chapter 5: Results for TPI expression and redox stress are altered in all mutants

5.1: Aims and hypothesis

In this chapter the expression of triose phosphate isomerase (TPI) will be quantified, along with the expression of markers for redox stress, advanced glycation end products (AGE), and caspase – a marker for apoptosis. To further investigate redox stress, lipid peroxidation and the activity of superoxide dismutase (SOD) were investigated in all *Drosophila* lines. Morphology of neuromuscular junctions (NMJs) will also be quantified by horseradish peroxidase (HRP) - a marker neuronal tissue, and bruchpilot (BRP) - a marker for active zones in *Drosophila* labelling.

TPI levels in wstd[1] and M80T are expected to be reduced, the I170V mutant is expected to have normal levels of TPI based on previously reported data (Seigle et al. 2008; Hrizo and Palladino 2010; Roland et al. 2014). The expectation was that species associated with enhanced redox stress such as AGE, Caspase, lipid peroxidation, and SOD activity would be increased in the TPI deficient lines in comparison with controls as TPI dysfunction has been reported to increase redox stress (Roland et al. 2016; Moraru et al. 2018; Stone et al. 2023).

5.2: Introduction

Quantifying the expression of proteins such as TPI will help assess the innate conditions present in all *Drosophila* lines at various time points in the animal's life, the levels of TPI seen in Western blots being related to the state of catalysis, and the efficiency of translation, among other factors (Orosz et al. 2009; Hrizo et al. 2013; Roland et al. 2014; Roland et al. 2019; Myers and Palladino 2023). Quantification of other proteins such as AGEs will give an indication of the levels of redox stress present at synapses (Guix et al. 2009; Tsakiri et al. 2013; Scheckhuber 2019).

Morphological characterisation of NMJs in larvae is commonly done by staining for HRP, a protein associated spatially with neuronal tissue and BRP, an active zone protein associated spatially with active zones, areas of high synaptic activity. Alterations in NMJ morphology in *Drosophila* have been shown to be altered by ND diseases such as Alzheimer's disease (Torroja et al. 1999). BRP function has also been shown to be strongly linked to olfactory memory via

facilitation of vesicle release, along with synapsin a protein present in SNARE complexes that has been discussed previously as a potential target of post translational modifications stemming from redox stress (Knapek et al. 2011; Bradley and Steinert 2015).

Levels of TPI have been previously quantified in the *Sugarkill* line M80T, which have been reported to have lower cellular TPI levels than controls (Seigle et al. 2008). The removal of TPI has previously been suggested to be due to proteasomal degradation (Hrizo and Palladino 2010). I170V has been reported to have no change in TPI levels (Roland et al. 2014).

Although many suggestions have been made that increased levels of dihydroxyacetone phosphate (DHAP) and subsequently of methylglyoxal (MGO) and species such as AGE underlie the pathology of TPI mutants none of these chemical species have been directly quantified in these lines. Caspase, a marker for apoptosis, along with AGE quantification, SOD activity, and lipid peroxidation quantification, give indications to the levels of cellular damage often associated with elevated redox stress (Fukai and Ushio-Fukai 2011; Hrizo et al. 2013; Sinenko et al. 2021).

5.3: Methods

Western blots were run as described in chapter 2, blots were run with 20µg total protein of female flies or larvae per well. All mutant and control lines contained the more common allele variant of the TPI enzyme, TPI-S (Oakeshott. J et al. 1984).

SOD activity and lipid peroxidation levels were quantified by use of pre-prepared fluorometric assay kits, full method details can be found in chapter 2. All experiments were run in triplicate with each plotted point representing one experiment. Statistics were not possible to run on all data sets for lipid peroxidation as the technique did not yield consistently reliable results, any results that came out as zero or negative were excluded due to technical issues.

Immunohistochemistry was run for HRP, BRP, AGE, and caspase quantification on 3rd instar larvae and 20 day old adult flies, detailed methods and analysis details are described in Chapter 2, Section 2.3.

N values are defined in Figure captions.

5.4: TPI expression was altered in all TPI mutants

TPI protein levels *in vivo* were quantified by Western blot, the two *Sugarkill* mutants wstd^{1} and M80T showed a decrease in TPI protein levels, as confirming previous data for *Sugarkill* mutants (Seigle et al. 2008). Relative expression: 0.59±0.1 and, 0.43±0.05 in wstd^{1} and M80T larvae respectively compared to Canton.S, see Figure 5-1 [C]. This effect becomes more significant in adult flies, which could suggest a correlation with ageing, however the 5 day old flies and 20 day old flies show little difference, 0.099±0.03, 0.084±0.04 in wstd^{1} and M80T 5 day old flies respectively compared to Canton.S, and 0.088±0.03, 0.065±0.01 in wstd^{1} and M80T 20 day old flies respectively compared to Canton.S, see Figure 5-2 [C] and 5-3 [C].

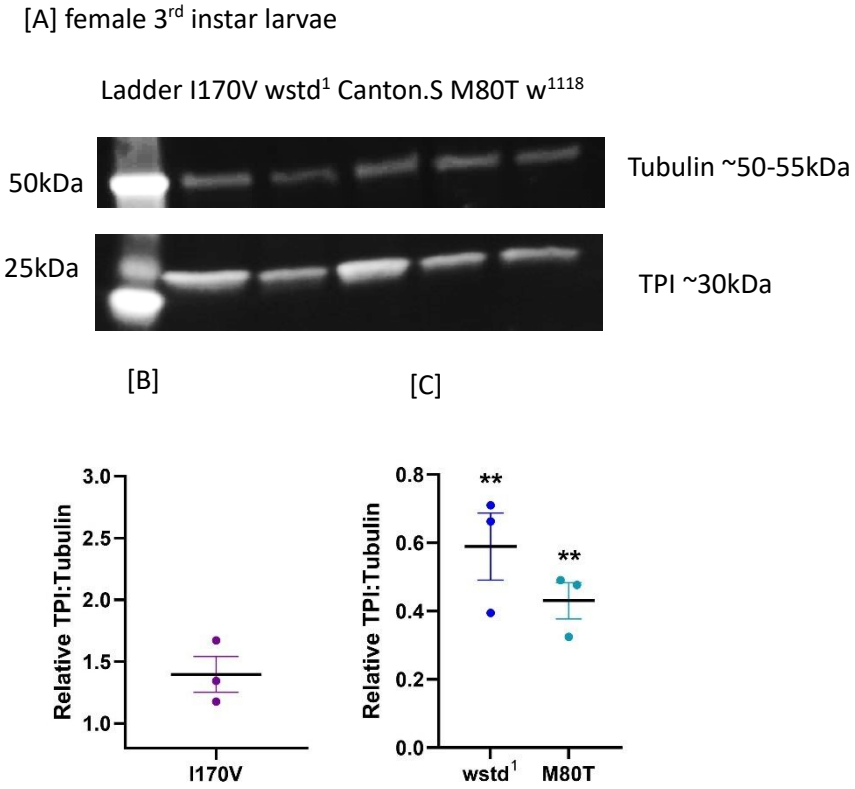

*Figure 5-1: Western blot for TPI expression in female 3rd instar larvae, data is expressed as normalised to paired control values, mean±SEM statistics were run in comparison to normalised control values. [A] Example blot for I170V, wstd^{1}, Canton.S, M80T and, w^{1118} [B] Normalised to w^{1118}; I170V: 1.4±0.1 [C] Normalised to Canton.S; wstd^{1}: 0.59±0.1, M80T: 0.43±0.05. **p<0.05, n=40 (animals), N=3 (experimental runs), one-way ANOVA and student t-tests.*

The I170V mutant line showed the opposite effect with no difference in TPI levels seen in larvae confirming previously reported data (Roland et al. 2014), a difference seen at 5 days, 1.6±0.2 compared to w^{1118}, which is enhanced at 20 days, 1.8±0.2 compared to w^{1118}, see Figure 5-2 [B] and 5-3 [B].

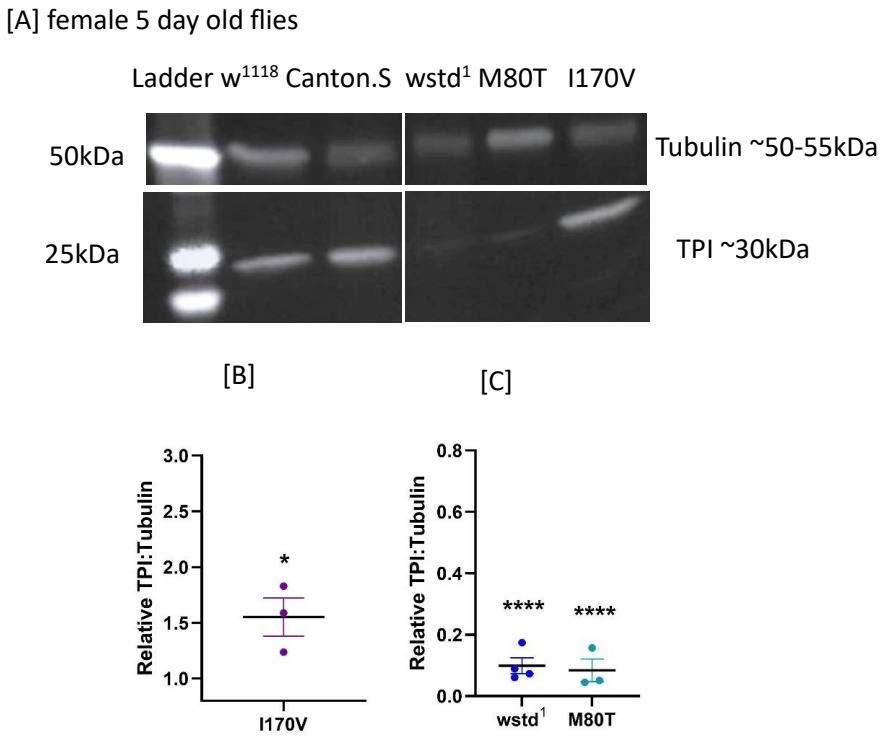

*Figure 5-2: Western blot for TPI expression in female 5 day old flies, data is expressed as normalised to paired control values, mean±SEM, statistics were run in comparison to normalised control values. [A] Example blot for I170V, wstd[1], Canton.S, M80T and, w[1118] [B] Normalised to w[1118]; I170V: 1.6±0.2. [C] Normalised to Canton.S; wstd[1]: 0.099±0.03, M80T: 0.084±0.04. *p≤0.05, ****p<0.0001, n=40 (animals), N=3 (experimental runs), one-way ANOVA and student t-tests.*

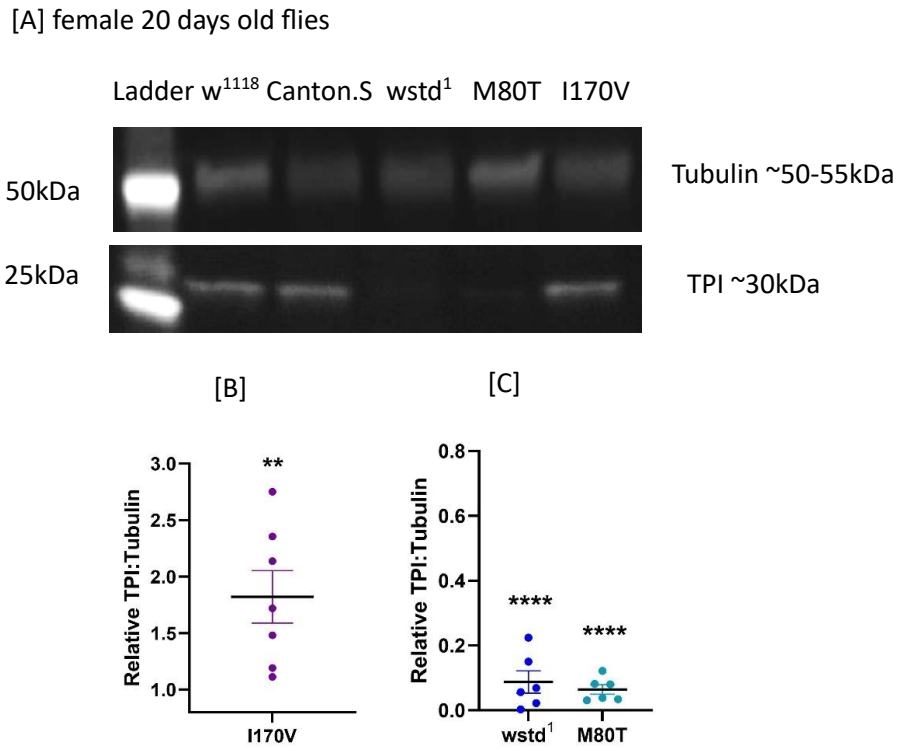

*Figure 5-3: Western blot for TPI expression in female 20 day old flies, data is expressed as normalised to paired control values, mean±SEM, statistics were run in comparison to normalised control values. [A] Example blot for I170V, wstd[1], Canton.S, M80T and, w[1118] [B] normalised to w[1118]; I170V: 1.8±0.2. [C] normalised to Canton.S; wstd[1]: 0.088±0.03, M80T: 0.065±0.01. **p<0.005, n=40 (animals), N=3 (experimental runs), one-way ANOVA and student t-tests.*

5.5: Redox stress was unaltered in all mutants

5.5.1: No change in SOD activity was found in TPI mutants

The activity of SOD was quantified by biochemical fluorometric assay. Higher SOD activity, as a consequence of compensatory upregulation, may indicate higher levels of redox stress under physiological conditions (Miao and Clair 2009; Fukai and Ushio-Fukai 2011), and has been connected with longer lifespans in *Drosophila* (Aigaki et al. 2002). Conversely, lower levels of SOD may indicate higher levels of oxidative stress in pathology due to failed compensation by SOD (Miao and Clair 2009). SOD activity was not seen to be significantly different in any of the three TPI mutant lines relative to their respective controls. No significant differences seen compared to Canton.S, see Figure 5-4.

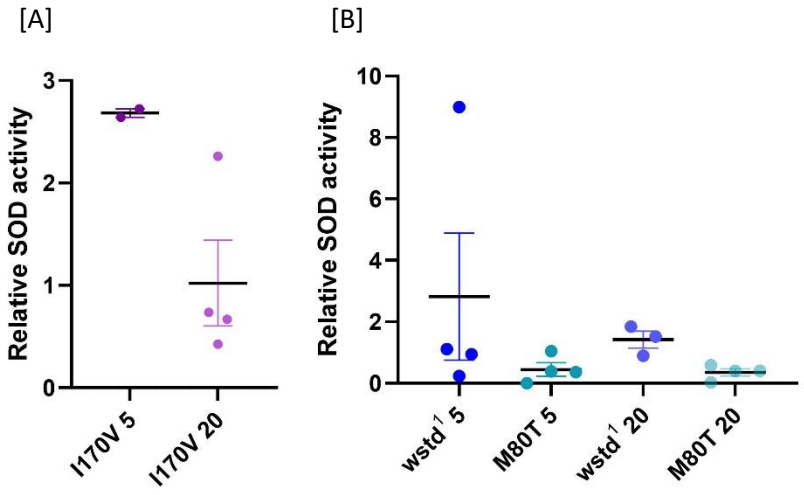

Figure 5-4: Relative SOD activity (U/g) normalised to paired control data expressed as mean±SEM, statistics were run in comparison to normalised control values. [A] Normalised to w^{1118}; I170V 5 day old flies: 2.7± 0.04, I170V 20 day old flies: 1± 0.4 [B] Normalised to Canton.S; $wstd^{1}$ 5 day old flies: 2.8±2, $wstd^{1}$ 20 day old flies: 1.4± 0.3, M80T 5 day old flies: 0.45± 0.2, M80T 20 day old flies: 0.36±0.1. p>0.05, n=15 (animals), N≥2 (experimental runs, runs done in triplicate), one-way ANOVA and student t-tests

5.5.2: No change in lipid peroxidation was found in TPI mutants

Quantification of lipid peroxidation was done by biochemical fluorometric assay. Peroxidation of lipids is a common post translational modification caused by redox stress, so will correlate to levels of redox stress. No significant differences were seen in the levels of lipid peroxidation between any of the *Drosophila* lines, see Figure 5-5.

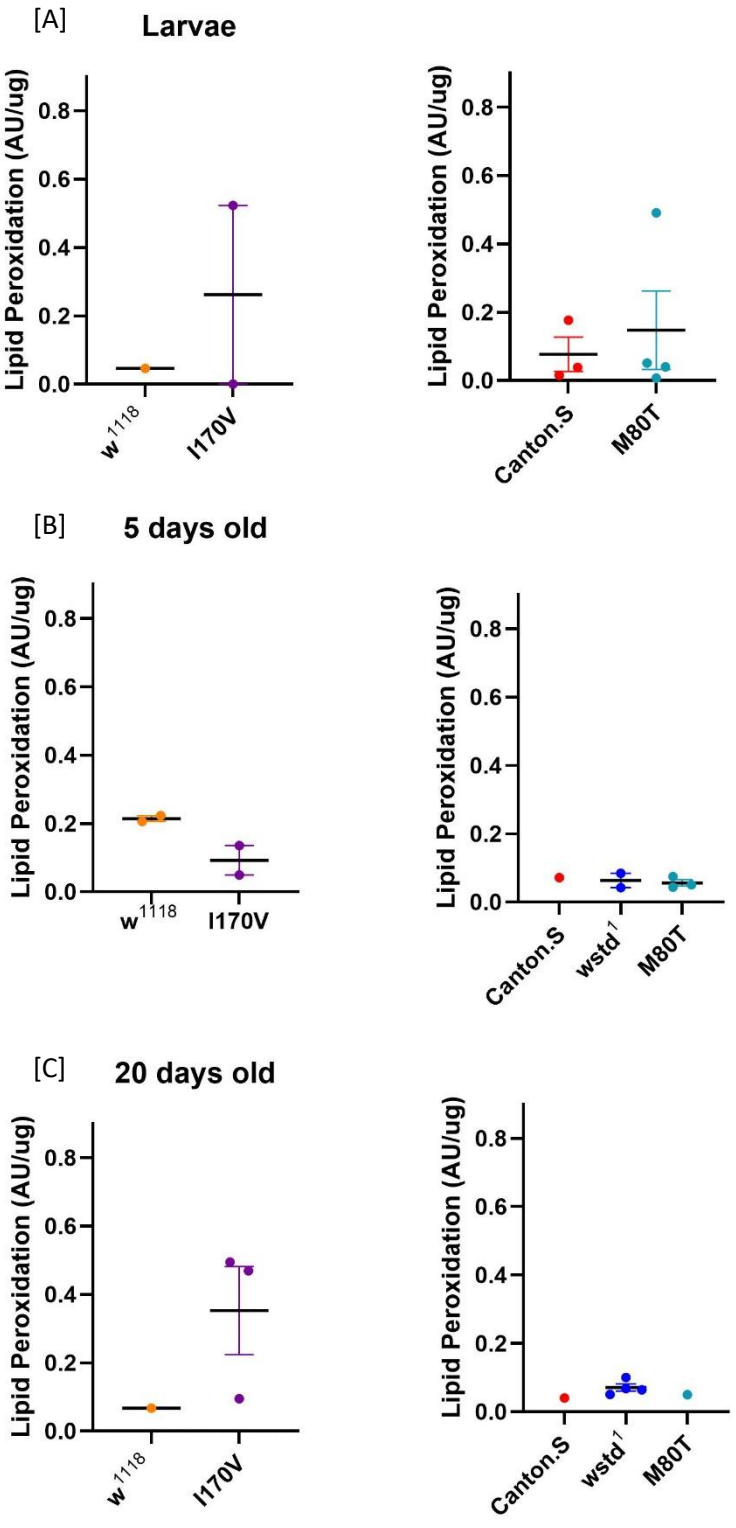

Figure 5-5: Lipid peroxidation levels, data expressed as mean±SEM, error not given when only one data point [A] 3rd instar larvae; w^{1118}: 0.046 AU/ug, I170V: 0.26±0.3 AU/ug, Canton.S: 0.077±0.05 AU/ug, M80T: 0.15±0.1 AU/ug. [B] 5 day old adult flies; w^{1118}: 0.21±0.008 AU/ug, I170V: 0.092±0.04 AU/ug, Canton.S: 0.071 AU/ug, $wstd^1$: 0.063± 0.02 AU/ug, M80T: 0.056± 0.009 AU/ug [C] 20 day old adult flies; w^{1118}: 0.067 AU/ug, I170V: 0.35±0.1 AU/ug, Canton.S: 0.40 AU/ug, $wstd^1$: 0.071±0.01 AU/ug, M80T: 0.050 AU/ug. Where two or more data points were available, students t tests were used to compare two lines, one-way ANOVA tests were used to compare three lines, p>0.05, n=15 (animals), N ≥1 (experimental runs, runs done in triplicate), no statistics were run on data sets with only one data point.

5.6: Levels of AGE and NMJ morphology was altered in wstd^{1} and I170V mutants

AGE expression is a useful readout as it has been widely reported to be a common early sign of redox stress, both in relation to TPI deficiency and more broadly in disease (Gnerer et al. 2006; Guix et al. 2009; Hrizo et al. 2013; Tsakiri et al. 2013; Gill et al. 2019; Scheckhuber 2019; Stone et al. 2023).

5.6.1: NMJ morphology

Drosophila 3rd instar larvae NMJs were stained for neuropile area (HRP, blue) and active zones (BRP, yellow) to investigate any possible morphological impacts of TPI dysfunction. Active zones were quantified by measure of BRP intensity a protein spatially associated with active zones in *Drosophila* NMJs (Knapek et al. 2011). The I170V mutant showed an increased number of boutons per NMJ compared to the control line w^{1118}, 49±7 boutons compared to 28±3 boutons in w^{1118}, see Figure 5-6 [E]. The distribution of BRP in I170V was not found to be statistically significant.

[A]

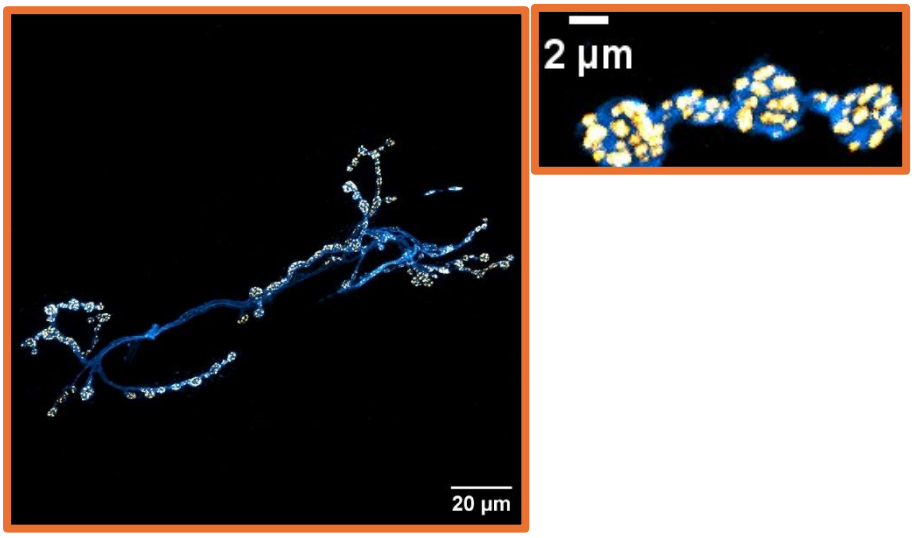

[B]

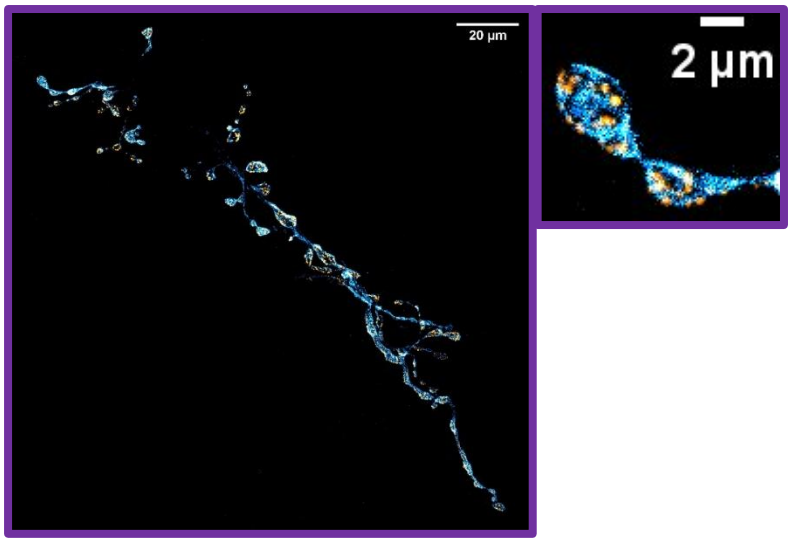

[C] [D] [E] [F]

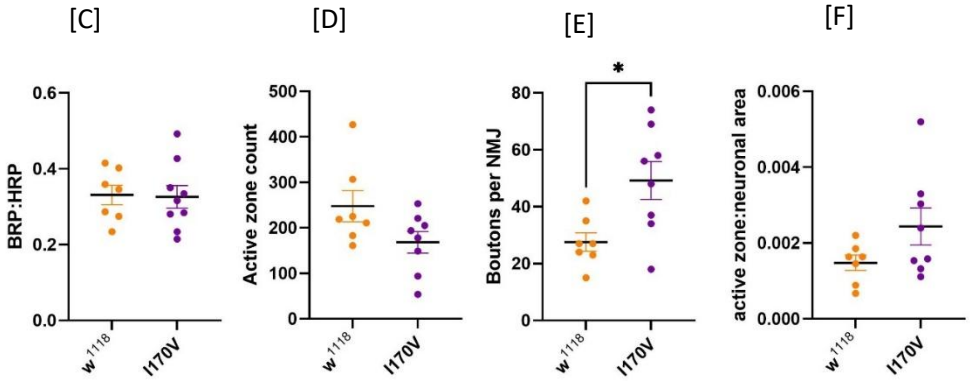

*Figure 5-6: Morphological analysis of A2/3 M6/7 NMJs from 3rd instar Drosophila larvae, neuronal area (HRP) shown in blue active zones (BRP) shown in yellow, data expressed as mean±SEM. [A] w^{1118} confocal image full NMJ and enhanced bouton [B] I170V confocal image full NMJ and enhanced bouton, [C] BRP:HRP ratio; w^{1118}: 0.33 ± 0.03, I170V: 0.33 ± 0.03 [D] Active zone count; w^{1118}: 250 ± 30, I170V : 170 ± 20 [E] Single active zone to total neuronal area ratio; w^{1118}: 0.0015 ± 0.0002, I170V: 0.0024 ± 0.0005 [F] Bouton count; w^{1118}: 28 ± 3, I170V: 49 ± 7. *p<0.05. n≥7 (muscle), N≥3 (animal), student t-tests.*

The two *Sugarkill* mutants M80T and wstd^{1} showed differences in NMJ morphology with M80T displaying larger individual active zones, 0.26±0.01 in wstd^{1} and, 0.42±0.06 in M80T, and area of active zones relative to total neuronal area, 0.0014±0.0002 in wstd^{1} and, 0.0021±0.0002 in M80T, see Figure 5-7 [D] and [G]. However, neither of these *Sugarkill* mutants showed any differences to the control line Canton.S.

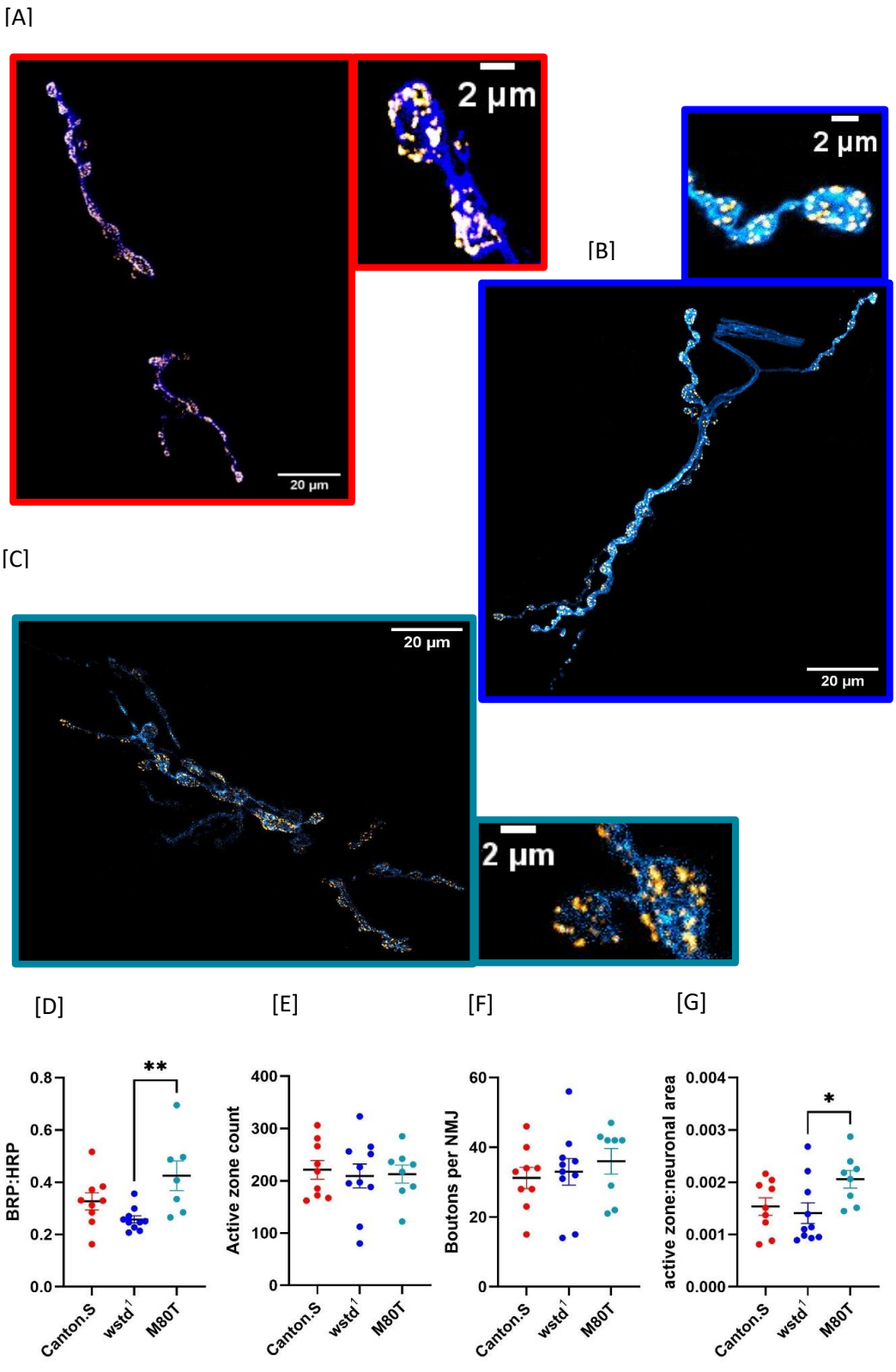

*Figure 5-7: Morphological analysis of A2/3 M6/7 NMJs from 3rd instar Drosophila larvae, neuronal area (HRP) shown in blue active zones (BRP) shown in yellow, data expressed as mean±SEM. [A] Canton.S full NMJ and enhanced bouton, [B] wstd^{1} full NMJ and enhanced bouton, [C] M80T full NMJ and enhanced bouton, [D] BRP:HRP ratio; Canton.S: 0.33±0.03, wstd^{1}: 0.26±0.01, M80T: 0.42±0.06 [E] Active zone count; Canton.S: 220±20, wstd^{1}: 210±20, M80T: 210±20 [F] Single active zone to total neuronal area ratio; Canton.S: 0.0015 ± 0.0002, wstd^{1}: 0.0014±0.0002, M80T: 0.0021±0.0002 [G] Bouton count; Canton.S: 31±3, wstd^{1}: 33±4, M80T: 36±4. *p<0.05, **p<0.01, p<0.05, N≥3 (animal), n≥7 (muscle), one-way ANOVA used to compare all lines in respect to control.*

5.6.2: Oxidative stress in larvae and adult flies

I170V larvae showed significantly increased intensity between nuclei in muscle tissue, 25000±2000 in I170V compared to 15000±2000 in w^{1118}, see Figure 5-8 [D]. No differences were seen in intensity of AGE in $wstd^{1}$ or M80T larvae compared to Canton.S, see Figure 5-9.

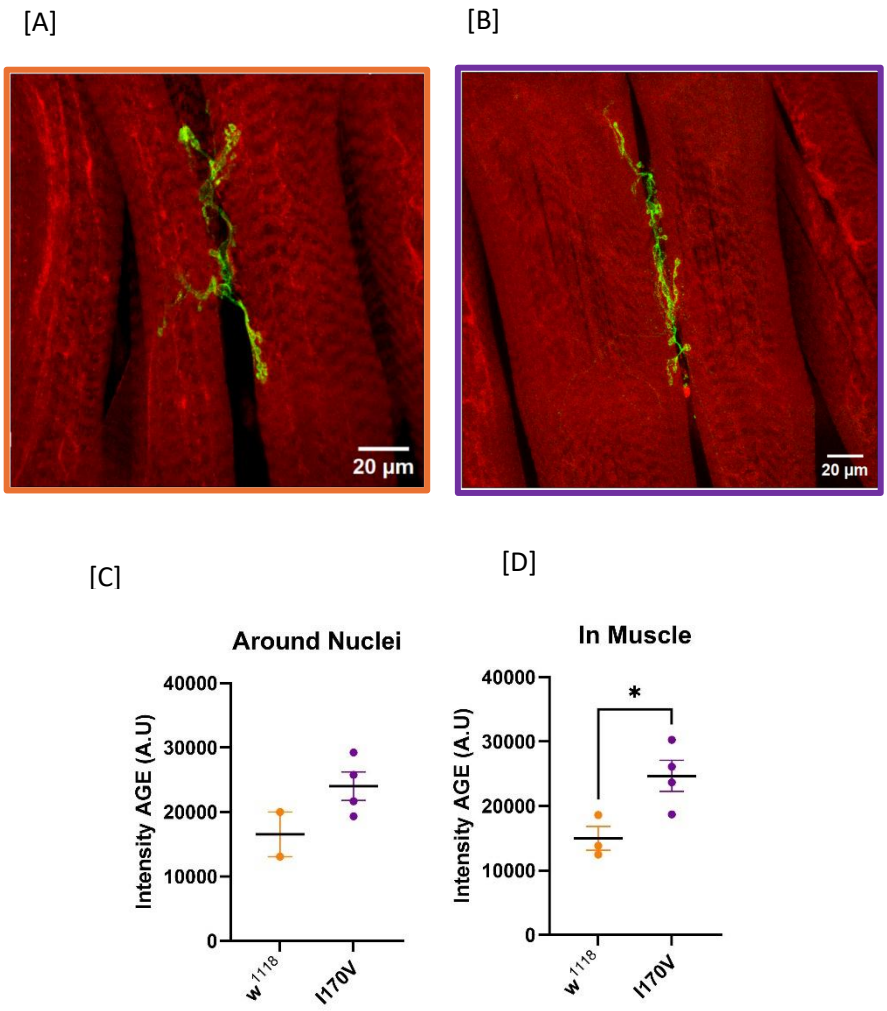

*Figure 5-8: AGE studies in 3rd instar larvae, AGE shown in red, neuronal areas shown in green, data expressed as mean±SEM [A-B] Representative confocal images A2/3, Muscle 6/7 3rd instar Drosophila larval NMJs, [C] Intensity of AGE in saved selection (selection size) around a nucleus in muscle 6/7; w^{1118}: 17000±3000 A.U., I170V: 24000±2000 A.U.. [D] Intensity of AGE in saved selection (selection size) in muscle 6/7; w^{1118}: 15000±2000 A.U., I170V: 25000±2000 A.U.. *p≤0.05, n≥2 (muscle), N≥2 (animal), student t-tests.*

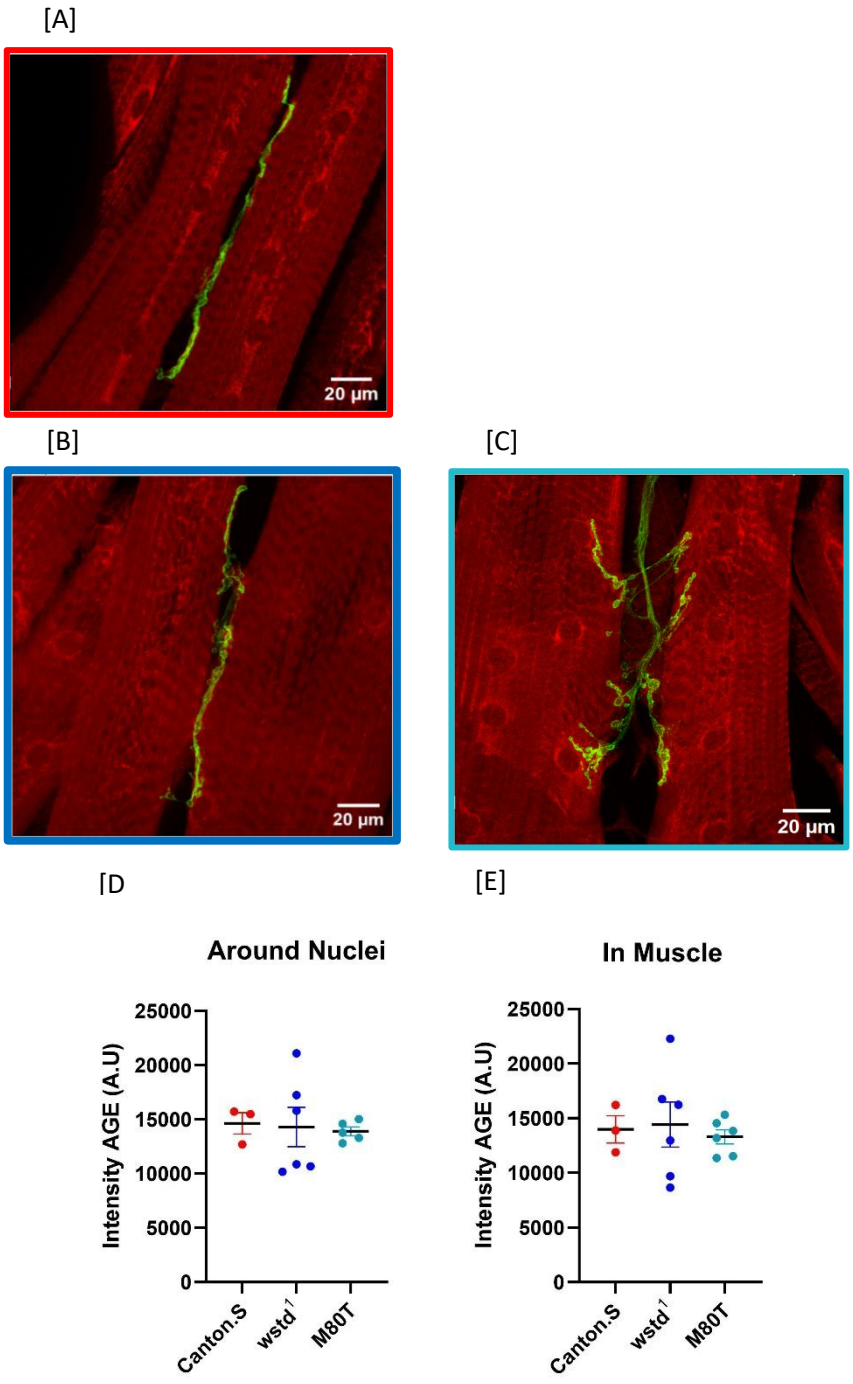

Figure 5-9: AGE studies in 3rd instar larvae, AGE shown in red, neuronal areas shown in green, data expressed as mean±SEM [A-C] Representative confocal images A2/3, Muscle 6/7 3rd instar Drosophila larval NMJs, [D] Intensity of AGE in saved selection (selection size) around a nucleus in muscle 6/7; Canton.S: 15000±1000 A.U., wstd1: 14000±2000 A.U., M80T: 14000±400 A.U.. [E] Intensity of AGE in saved selection (selection size) in muscle 6/7; Canton.S: 14000±1000 A.U., wstd1: 14000±2000 A.U., M80T: 13000±600 A.U.. p>0.05, n≥3 (muscle), N≥2 (animal), one-way ANOVA.

Analysis of AGE and caspase levels in 20 day old fly brains showed no differences between I170V and w^{1118}, see Figure 5-10.

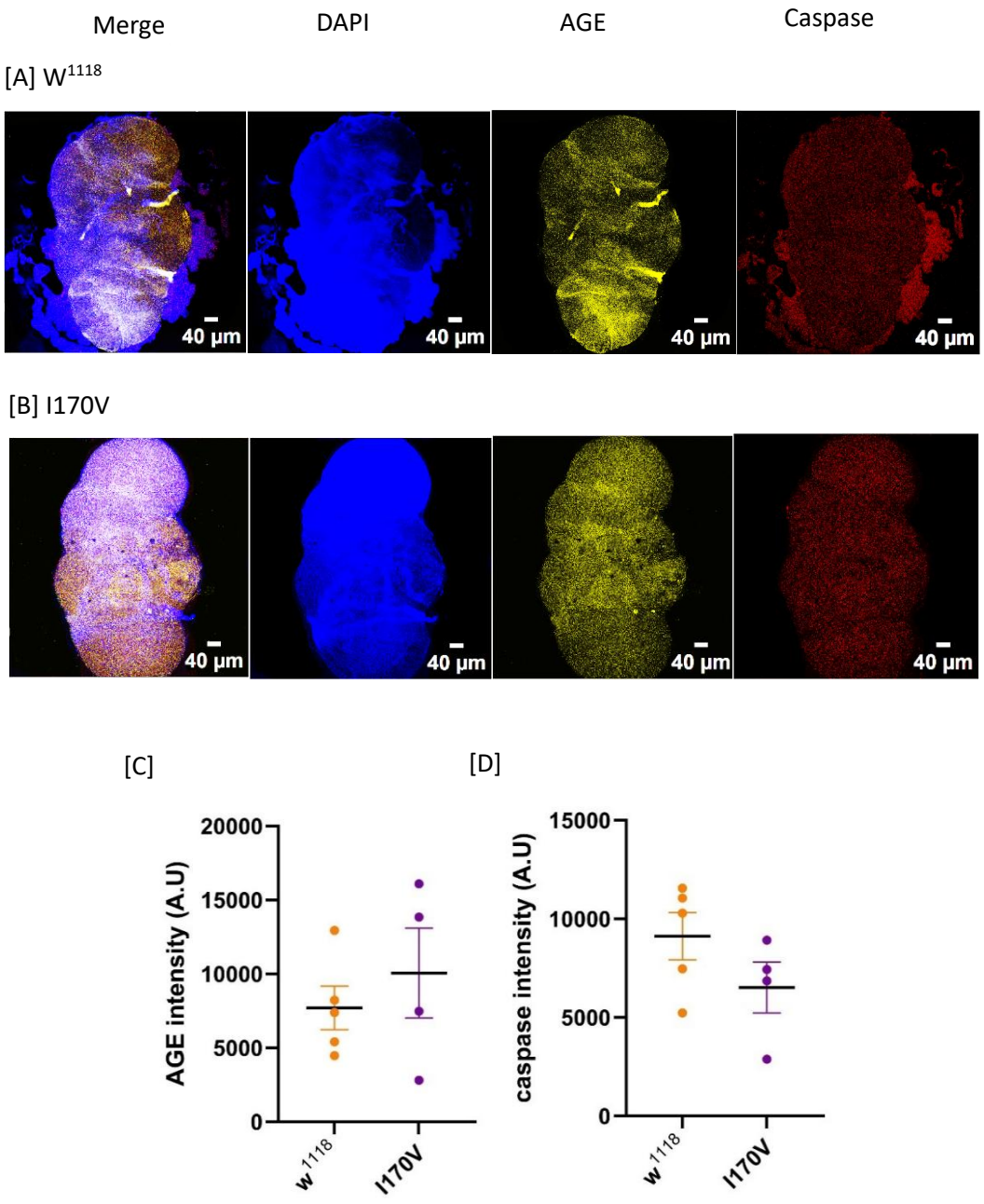

Figure 5-10: AGE and caspase studies in 20 day old flies, DAPI shown in blue, AGE shown in yellow, caspase shown in red, data expressed as mean±SEM [A-B] Example confocal images of w^{1118} and I170V. [C] Intensity of AGE in central brain region excluding optic lobes; w^{1118}: 7800±1500 A.U., I170V: 10000±3000 A.U.. [D] Intensity of caspase a measure of apoptosis in central brain region excluding optic lobes; w^{1118}: 9100±1000 A.U., I170V: 6500±1000 A.U.. p>0.05, N≥4 (animal), student t-tests.

AGE intensity was found to be significantly increased in wstd^{1} 18000±4000 compared to 3000±1000 in Canton.S see Figure 5-11 [D]. Caspase intensity was not significantly altered in wstd^{1}, 18000±4000 compared to 2700±500 in Canton.S, or M80T , 7200±3000 compared to 2700±500 in Canton.S, see Figure 5-11.

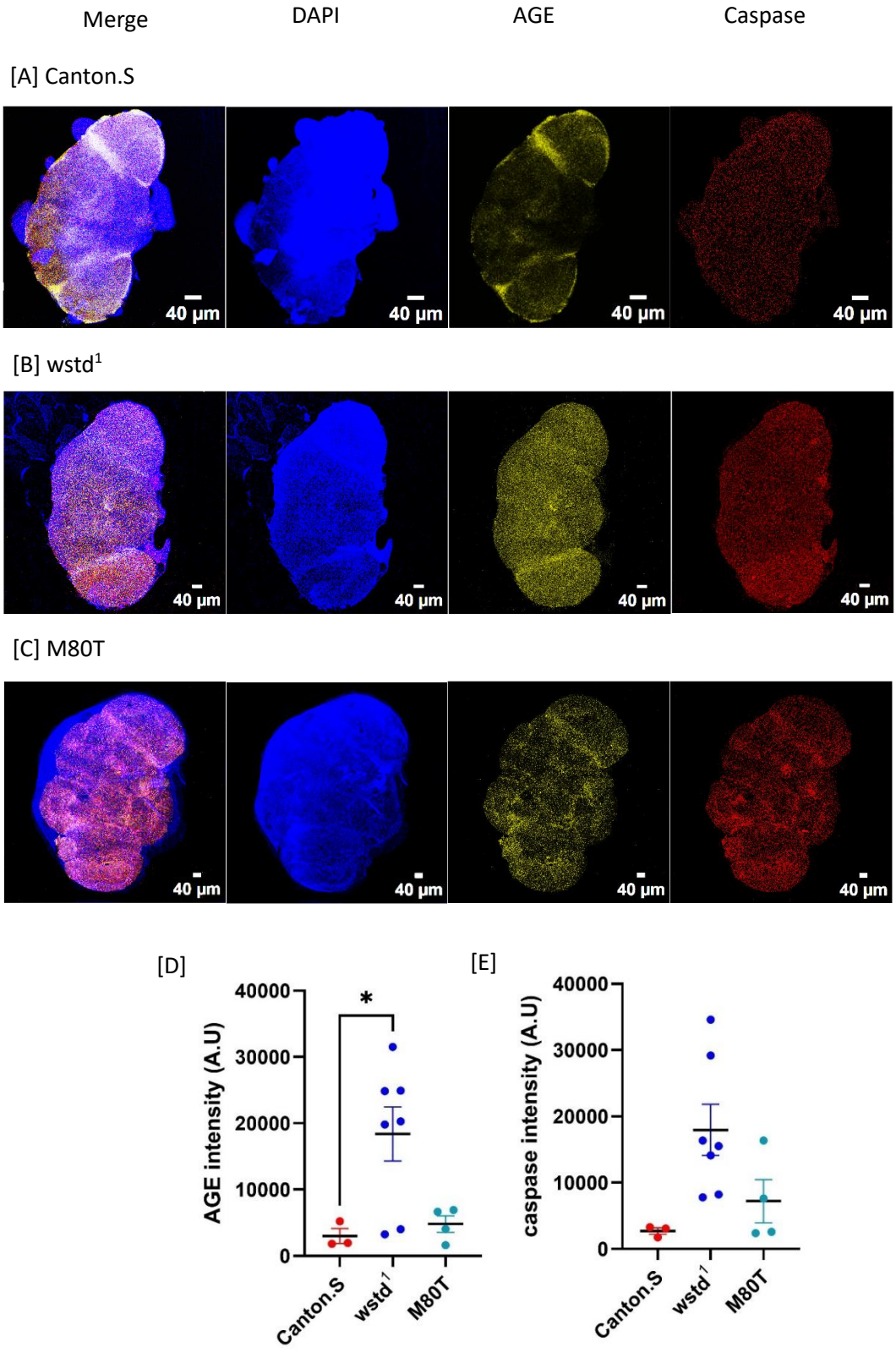

*Figure 5-11: AGE and caspase studies in 20 day old flies, DAPI shown in blue, AGE shown in yellow, caspase shown in red, data expressed as mean±SEM [A-C] Example confocal images for Canton.S, wstd[1] and, M80T. [D] Intensity of AGE in central brain region excluding optic lobes; Canton.S: 3000±1000 A.U., wstd[1]: 18000±4000 A.U., M80T: 4800±1000 A.U.. [E] Intensity of caspase a measure of apoptosis in central brain region excluding optic lobes; Canton.S: 2700±500 A.U,, wstd[1]: 18000±4000 A.U., M80T: 7200±3000 A.U.. *p≤0.05, N≥3 (animal), one-way ANOVA.*

5.7: Discussion

The data presented here suggests that the mechanism of dysfunction, at least in part, stems from an altered TPI expression. In wstd[1] and I170V this was paired with altered AGE expression and in I170V altered NMJ morphology. The results for this chapter are summarised in Table 5.1.

Table 5.1: Summarized significant results for protein expression in mutant lines

	wstd[1]	**M80T**	**I170V**
TPI expression	TPI expression was found to be reduced in larvae **p<0.005, and adults 5 and 20 days ****p<0.0001	TPI expression was found to be reduced in larvae **p<0.005, and adults 5 and 20 days ****p<0.0001	TPI expression was found to be higher in 5 day old flies *p<0.05, and 20 day old flies **p<0.005
NMJ morphology	ns	ns	Bouton count was increased *p<0.05
AGE	AGE in 20 day adults was increased *p<0.05	ns	AGE was increased in muscle tissue in larvae *p<0.05

The I170V line shows an increase of TPI protein that appears to correlate with age, the statistical significance increasing from larvae where the difference was not significant, to 5 day old adults where results were significant, and 20 day old adults where results were highly significant. The data for TPI expression at 20 days in this line however did show a large amount of variability, this range implies a complicated pathology with a variety of phenotypes in individuals. The observed increase in TPI expression is counter to previously published results on this line that showed no significant differences in protein expression (Roland et al. 2014). However the reported results come from 1-2 day old flies so it is possible the increase had not yet become significant. This could suggest reduced clearance of the TPI monomers from the synapse in this line, possibly due to a stronger dimerization in the mutated TPI (Roland et al. 2014).

In I170V lipid peroxidation in 20 day old flies, was not found to be significantly altered. The data set presented here is not large or consistent enough to draw definitive conclusions, further studies would therefore be required to confirm the observed tendency.

The increased AGE seen in I170V larvae muscle tissue indicates increased levels of redox stress, however this effect was lost in adult flies with the increase in mean AGE values not showing significance. The higher expression of TPI seen in adult flies but not in larvae could therefore be a compensation mechanism for the increase in redox stress. The I170V line also showed no significant difference in caspase levels in 20 day old adults.

The decrease in TPI protein expression in wstd^{1} and M80T fits with previously published work (Seigle et al. 2008) although the significance found in young flies here is larger than previously published and could be explained by the younger age used by Seigle et al, 2 vs 5 days old. The wstd^{1} and M80T lines showing no difference in TPI protein levels between 5 and 20 day old flies could suggest a biological plateau, or a technical plateau, being unable to differentiate between the low values. This supports the idea of increased protein clearance in these lines.

The observed increase in AGE, in 20 day old wstd^{1} flies indicates an increase in redox stress supporting the hypothesis that the dysfunctional TPI enzyme promotes redox stress via increase in DHAP levels.

Redox stress would be expected to increase in all TPI and Glo mutants based on reported data on these lines (Hrizo et al. 2013; Roland et al. 2016; Moraru et al. 2018; Stone et al. 2023), see Chapter 1 for details.

5.8: Future directions

Quantification of the redox stress in these lines could be better supported by repeating the SOD and lipid peroxidation assays to reduce the error margins. It would also be prudent to repeat these measures with multiple techniques, for example running Western blots for AGE expression may give a more sensitive result than the immunohistochemistry data presented here.

Aside from improving the quantification of the measures presented here, such as low n values, quantification of specific proteins that could be targeted by redox stress, such as the proteins that make up SNARE complexes, would be invaluable. As previous chapters have suggested a dysfunction of key proteins for vesicle dynamics could be the cause of dysfunction in the TPI mutant lines.

Investigating whole animal physiology would also be useful to assess the impact of these changes on overall animal health, this is addressed in the next chapter.

Chapter 6: Results for behaviour are altered in all mutants

6.1: Aims and hypothesis

The aim of this chapter is to quantify altered behaviour stemming from dysfunctional triose phosphate isomerase (TPI) or glyoxalase (Glo), and to quantify the impact of antioxidants and oxidative stressors on these phenotypes.

Lifespan is a good measure to assess whole animal health and so the extremity of the disease model. Lifespans of the TPI deficient mutants are expected to be reduced compared to control lines (Gnerer et al. 2006; Hrizo et al. 2013), and the GloKO line is expected to have increased lifespans based on previous data (Moraru et al. 2018).

Treatments with antioxidants are expected to improve overall health, with treatments of oxidative stressors expected to reduce health, these experiments could therefore give an indication to whether this could be a possible therapeutic route. As the TPI phenotype is expected to be closely related to increased redox stress it is anticipated that they already exhibit changes associated with increased redox stress. As Glyoxalase1 reduces glutathione for use as an antioxidant in *Drosophila*, the GloKO line would not be expected to be able to use the additional glutathione. The GloKO line is expected to have a better resilience to oxidative stress with H_2O_2 treatment as previously reported, where an increase in MGO was suggested to have beneficial effects. The exact nature of these effects are not fully described, but are linked to pathology similar to type 2 diabetes, see Section 1.4 for more detail (Moraru et al. 2018),.

It is expected that learning and memory and motor activity will be impaired in wstd^1 mutants as we have previously shown (Stone et al. 2023).

6.2: Introduction

Analysing and quantifying behaviour provides information of how genetic mutations and environmental conditions impact on whole animal physiology. In this chapter data on longevity, motor activity, and learning and memory will be provided.

Longevity experiments were conducted to assess the lifespan of the mutant lines under various conditions, including treatment with antioxidants and oxidative stressors to investigate the state of redox stress in the various lines. wstd^{1} and M80T lines have been reported to have reduced lifespans, an effect which is enhanced by increased environmental temperature (Gnerer et al. 2006; Hrizo et al. 2013). Higher temperatures generally have been shown to worsen the TPI *Sugarkill* phenotypes (wstd^{1} and M80T). This is suggested to be due to increased activity of molecular chaperones which promote degradation of TPI *Sugarkill*, (Hrizo and Palladino 2010). This effect is also seen in wild type flies although the extent of degradation and levels of chaperones are enhanced in *Sugarkill* flies (Hrizo and Palladino 2010). The I170V line in counter, has been reported to have no change in lifespan compared to control lines (Roland et al. 2014).

The GloKO line has been reported to have increased lifespans compared to control lines, and has also been reported to show increased resilience to oxidative stress induced by a 3 % H_2O_2 treatment for 1 week (Moraru et al. 2018).

Glutathione treatments were used to examine the impacts of an antioxidant on the disease phenotypes. The effect of such antioxidants are not acute, glutathione antioxidant properties relying on absorption through digestion to cells and reduction before it can be functional. Therefore glutathione was not used in electrophysiological perfusion treatments, as the oxidative stressor H_2O_2 was, instead glutathione treatment was only used in addition to food.

Glutathione could present an alternate effect alongside its antioxidant properties, as various glutathione containing compounds, such as S-fluorenylmethoxycarbonyl glutathione, have been known to inhibit glyoxalase enzymes in calf and rat models (Chyan et al. 1994), and as glutathione treatments are used in addition to food, it is not clear what form the glutathione is in when/if it reaches the intended synapses, so this addition could be having an impact on glyoxalase 1, the key enzyme of the innate protective mechanism in the relevant glycolysis pathway (Hambsch et al. 2010; Nigro et al. 2017; Rabbani 2022), possibly leading to increased levels of redox stress.

Circadian rhythm gives an indication of the activity and sleep. These are two broad physiological parameters, the dysfunction of which has been linked to ND disease in *Drosophila* (He et al. 2017). This behaviour is controlled by clock genes and generally cycles around the 24hr day. The circadian clock in *Drosophila* has been described, where ecolsion activity for normal healthy *Drosophila* was shown to peak midday (Konopka and Benzer 1971). Various post translational modifications are key in control of the circadian clock in

Drosophila, both in activation of clock proteins and in their degradation allowing stimulation and inhibition of relevant pathways at specific time points throughout the 24hr day (Breda et al. 2020). Healthy normal circadian rhythms exist in 12hr light-dark cycles. In *Drosophila* this is regulated by photosensitive clock proteins; temperature sensitive clock proteins are also present with cycles as little as 2°C having been shown to impact *Drosophila* rhythms (Breda et al. 2020). Clock proteins in *Drosophila* have also been reported to be involved in regulation of ageing (Robinson and Robinson 2004). Circadian rhythm in *Drosophila* has also been linked to redox stress sensitivity in the context of ND (Spiers et al. 2019). The impact of dysfunctional TPI on circadian rhythms in *Drosophila* has not been reported, however given the connection with redox stress and ND (He et al. 2017; Roland et al. 2016; Moraru et al. 2018; Stone et al. 2023) it is expected expression of dysfunctional TPI will impact on circadian rhythm.

Learning and memory via classical or operant conditioning, by association of an activity with either a positive or negative stimulus to encourage or discourage the action, is a common measure of cognition in animal models. This is a particularly accurate measure in Drosophila larvae which primarily exhibit foraging activity and are highly motivated by their olfactory sense (Nichols et al. 2012) making conditioning via olfactory memory cues a good measure of animal learning ability. We have previously reported that $wstd^{1}$ shows impaired learning and memory, and unaffected larval crawling behaviour compared to control lines (Stone et al. 2023).

Circadian rhythm gives an indication of the activity and sleep. This behaviour is controlled by clock genes and generally cycles around the 24hr day. The circadian clock in *Drosophila* has been described, where ecolsion activity for normal healthy *Drosophila* was shown to peak midday (Konopka and Benzer 1971). Various post translational modifications are key in control of the circadian clock in *Drosophila*, both in activation of clock proteins and in their degradation allowing stimulation and inhibition of relevant pathways at specific time points throughout the 24hr day (Breda et al. 2020). Healthy normal circadian rhythms exist in 12hr light-dark cycles, observing 24 hr light and 24 hr dark alongside the standard 12 hr light-dark 24 hr day gives a good indication whether this control is functioning normally in our mutant lines. In *Drosophila* this is regulated by photosensitive clock proteins; temperature sensitive clock proteins are also present with cycles as little as 2°C having been shown to impact *Drosophila* rhythms (Breda et al. 2020). Clock proteins in *Drosophila* have also been reported to be involved in regulation of ageing (Robinson and Robinson 2004).

6.3: Methods

Longevity was recorded every other day with controlled temperatures, light, and humidity. Vials were kept with 30-50 mixed sex flies per vial. Longevity was recorded at; 25 °C on a 12 hr light cycle as standard condition, 25 °C on a 24 hr light cycle to investigate any changes based in circadian rhythm cycles, 29 °C on a 12 hr light cycle to investigate impacts of higher temperature on dysfunction, 25 °C on a 12 hr light cycle with 5 % H_2O_2 (Zhu et al. 2021) to investigate the impact of enhanced redox stress, 25 °C on a 12 hr light cycle with 0.22 mM Glutathione (Bonilla et al. 2006) to investigate the impact of antioxidant availability, and 25 °C on a 12 hr light cycle with H_20 as a control for treated longevity. Statistical analysis used was Kaplan-Meier survival analysis, with two post hoc tests. Log rank Mantel-Cox tests, which compare complete data sets weighting all deaths equally over lifetimes, and Gehan-Breslow-Wilcoxon tests, which compare data sets giving extra weight to early deaths.

All treatments (H_2O_2, Glutathione, and water) were added as 150 µl solution additions to vials every other day. Treatments were made every 48 hrs until the end of experiments. For treated larvae, treatments were begun 24 hours after adults had been added to vials to allow egg laying and 1st instar development.

Circadian rhythm data was collected for the TPI mutants I170V, young and old male flies, and wstd^1 young male flies, in comparison to the Canton.S control line. Experiments were run both in 12 hr light-dark cycles and in 24 hr dark. Data was collected at 25 °C, flies were individually monitored in sleep tubes. The wstd^1 flies were not observed at old age as they did not survive long enough into the experiments.

Motor activity was assessed via standard methods. For larval crawling, tracking larvae around an agar plate, and for adult climbing tracking how many flies climb upwards over a pre-defined barrier in Falcon tubes, see chapter 2 for full details.

Learning and memory was assessed with operant conditioning, so associating a voluntary action and a stimulus, in this case moving towards an odour to find food (Michels et al. 2017). Experiments were conducted at room temperature and standard lab lighting, see chapter 2 for full details.

N values are defined in Figure captions.

6.4: Longevity was altered in all mutants

Longevity was assessed to investigate impact of TPI and Glo mutations on whole lifespan of animals. If disease is effectively mimicked in these lines it would be expected that lifespans would be reduced as in *Human* disease (Goedert and Spillantini 2006; Orosz et al. 2006). Median lifespans are compared, Kaplan-Meier survival analysis with Log rank Mantel-Cox tests and Gehan-Breslow-Wilcoxon tests are reported in figure captions for survival comparisons.

6.4.1: Lifespans at 25 °C and 29 °C

Longevity at 25 °C with a 12 hr light cycle was significantly reduced in wstd^{1} and M80T with median lifespans of 30 and 28 days *vs* 50 days in Canton.S, supporting previously reported findings where at 22 °C wstd^{1} flies survived to 41 days compared to 54 days in wild type flies, M80T lines at 25 were reported to show a 55% decrease in lifespan compared to controls (Celotto et al. 2006. Gnerer et al. 2006; Hrizo et al. 2013) see Figure 6-1 [A]. The I170V line and

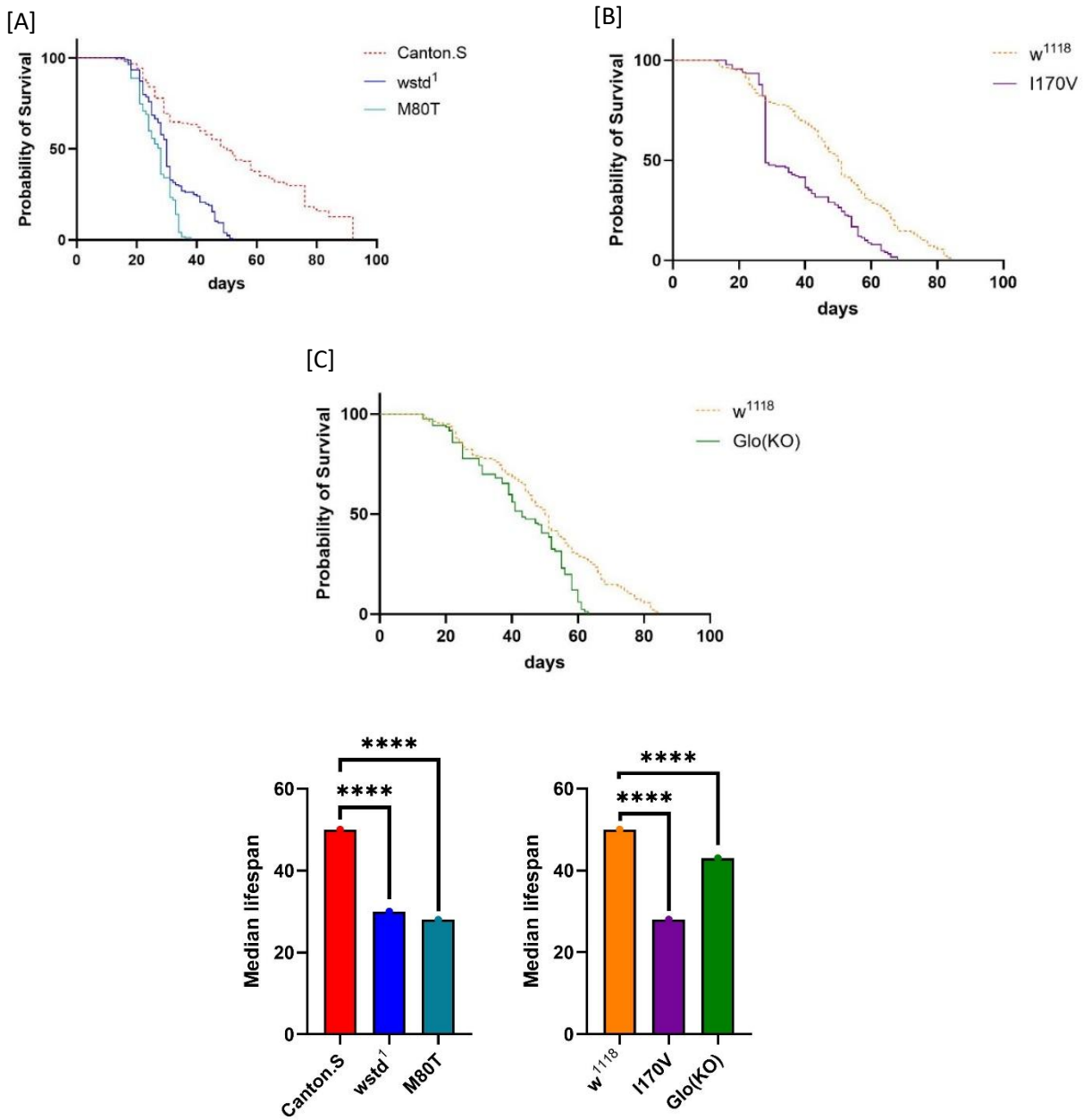

*Figure 6-1: Longevity 25 °C 12 hr light dark cycle median survival; [A] Canton. S: 50, wstd^{1}: 30, ****p<0.0001 and ****p<0.0001, M80T: 28, ****p<0.0001 and ****p<0.0001 [B] w^{1118}: 50, I170V: 28, ****p<0.0001 and ****p<0.0001 [C] w^{1118}: 50, Glo(KO): 43, ****p<0.0001 and ****p<0.0001 N≥107, Kaplan-Meier survival analysis, log rank Mantel-Cox test and Gehan-Breslow-Wilcoxon tests used for significance respective p values given after comparisons above.*

GloKO line also showed reduced lifespans 28 and 43 days vs 50 days in w^{1118}, see Figure 6-1 [B] and [C]. For I170V this is unexpected as this line has previously been reported to have no change in lifespan compared to controls (Roland et al. 2014), the Glo(KO) result is also unexpected as previous studies have reported the Glo(KO) line to exhibit increased longevity at 25 °C with approx. 70 days compared to approx. 50 days in controls.

Survival at 29 °C with a 12 hr light cycle showed reduced longevity from 25 °C survival in all lines; w^{1118} 29 day survival, 40 % decrease, Canton.S 68 day survival, 74 % decrease, I170V 40 day survival, 63 % decrease, $wstd^{1}$ 17 day survival, 40 % decrease, M80T 14 day survival, 35 % decrease. The Sugerkill lines still showed reduced lifespans at 29 °C compared to Canton.S, the I170V line however did not show any difference to w^{1118} at 29 °C unlike at 25 °C see Figure 6-2.

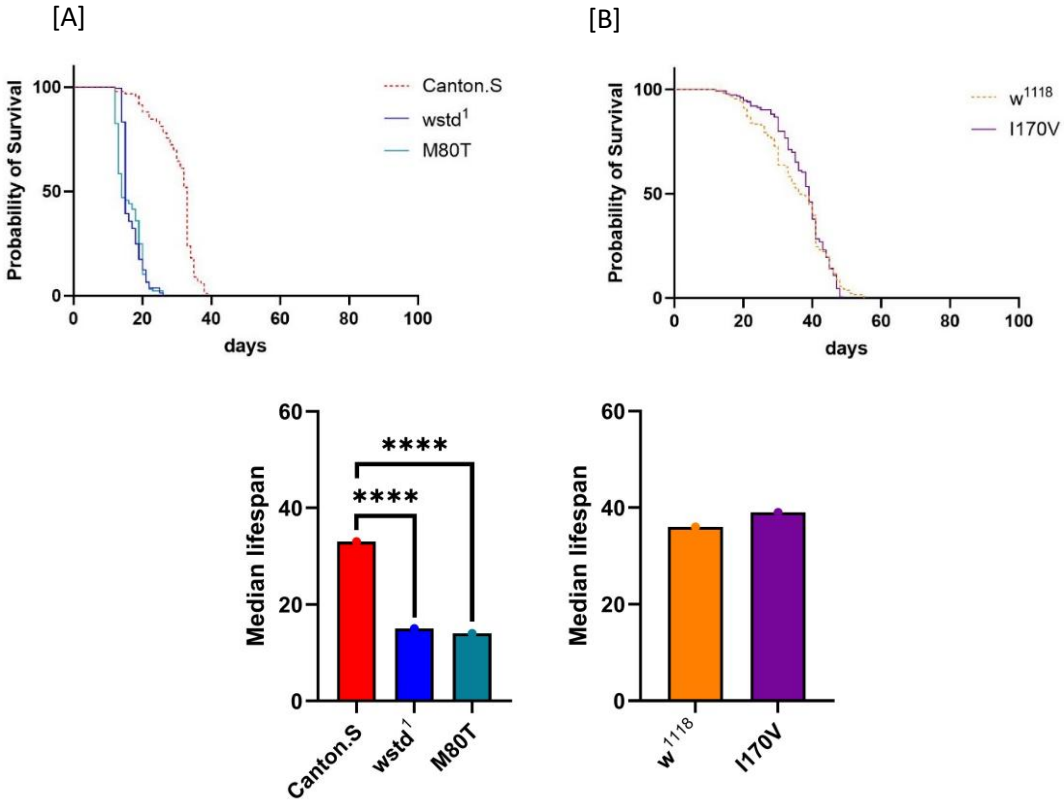

*Figure 6-2: Longevity 29 °C 12 hr light dark cycle median survival; [A] Canton.S: 33, $wstd^{1}$: 15, ****p<0.0001 and ****p<0.0001, M80T: 14, ****p<0.0001 and ****p<0.0001 [B] w^{1118}: 36, I170V: 39, ns and ns. N≥89, Kaplan-Meier survival analysis, log rank Mantel-Cox test and Gehan-Breslow-Wilcoxon tests used for significance respective p values given after comparisons above.*

6.4.2: Lifespans with glutathione and H_2O_2 treatment

There were no differences seen between water treatment and glutathione treatment within any of the *Drosophila* lines except in the Glo(KO) line with reduction of lifespan, from median lifespans of 58 days with water treatment, to 48 days with glutathione treatment. Comparisons to controls for the *Sugarkill* lines continued to show reduced lifespans, 25 days and 24 days for $wstd^1$ and M80T respectively compared to 52 days in Canton.S. The I170V line did not show any differences in lifespan compared to w^{1118} unlike at 25 °C. The Glo(KO) line showed an increased lifespan more significantly with water treatments than glutathione, 58 days with water treatment and 48 days with glutathione treatment compared to in w^{1118} with 44 days with water treatment and 47 days with glutathione treatment, see Figure 6-3.

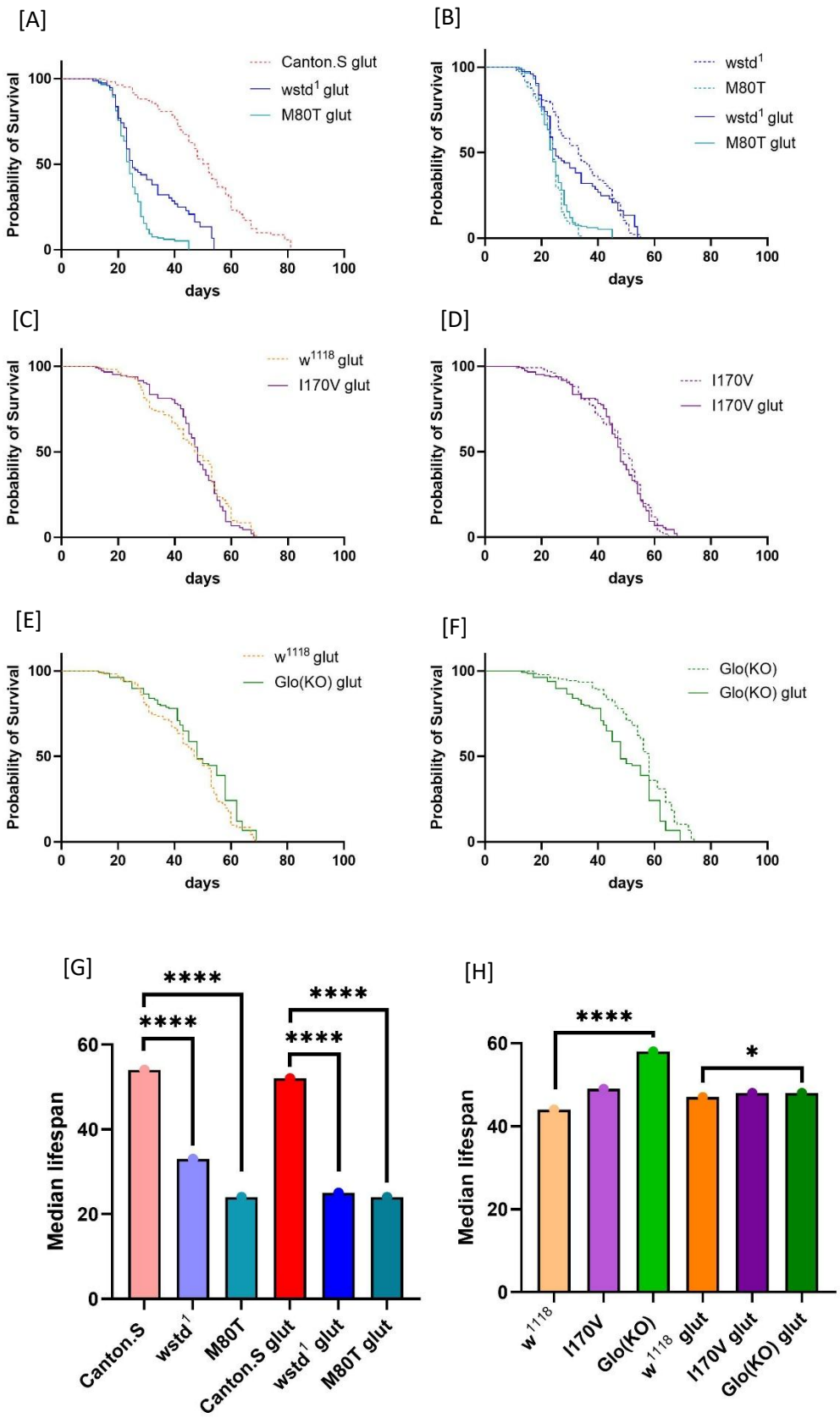

*Figure 6-3: Longevity 25 °C 12 hr light dark cycle glutathione (0.22 mM) treatment with water treated controls (dotted lines) median survivals; [A] Canton.S glut: 52, wstd[1] glut: 25, ****p<0.0001 and ****p<0.0001, M80T glut: 24, ****p<0.0001 and ****p<0.0001 [B] wstd[1]: 33, M80T: 24, wstd[1] glut: 25, ns and ns, M80T glut: 24, ns and ns. [C] w[1118] glut: 47, I170V glut: 48, ns and ns [D] I170V: 49, I170V glut: 48, ns and ns [E] w[1118] glut: 47, Glo(KO) glut: 48, *p<0.05 and ns [F] Glo(KO): 58, Glo(KO) glut: 48, ***p<0.001 and ***p<0.001 N≥99, Kaplan-Meier survival analysis, log rank Mantel-Cox test and Gehan-Breslow-Wilcoxon tests used for significance respective p values given after comparisons above.*

Treatment with H_2O_2 led to reduced longevity compared to water treatment in; w^{1118} 28 vs 44, 37 % reduction, Canton.S 36 vs 54, 34 % reduction, I170V 32 vs 49, 35 % reduction and, GloKO 26 vs 58, 56 % reduction, and $wstd^1$, 23 vs 33, 31 % reduction. In M80T the lifespan was found to be altered by Grehan-Breslow-Wilcoxon but median lifespans were unaffected, 25 vs 24, see Figure 6-4.

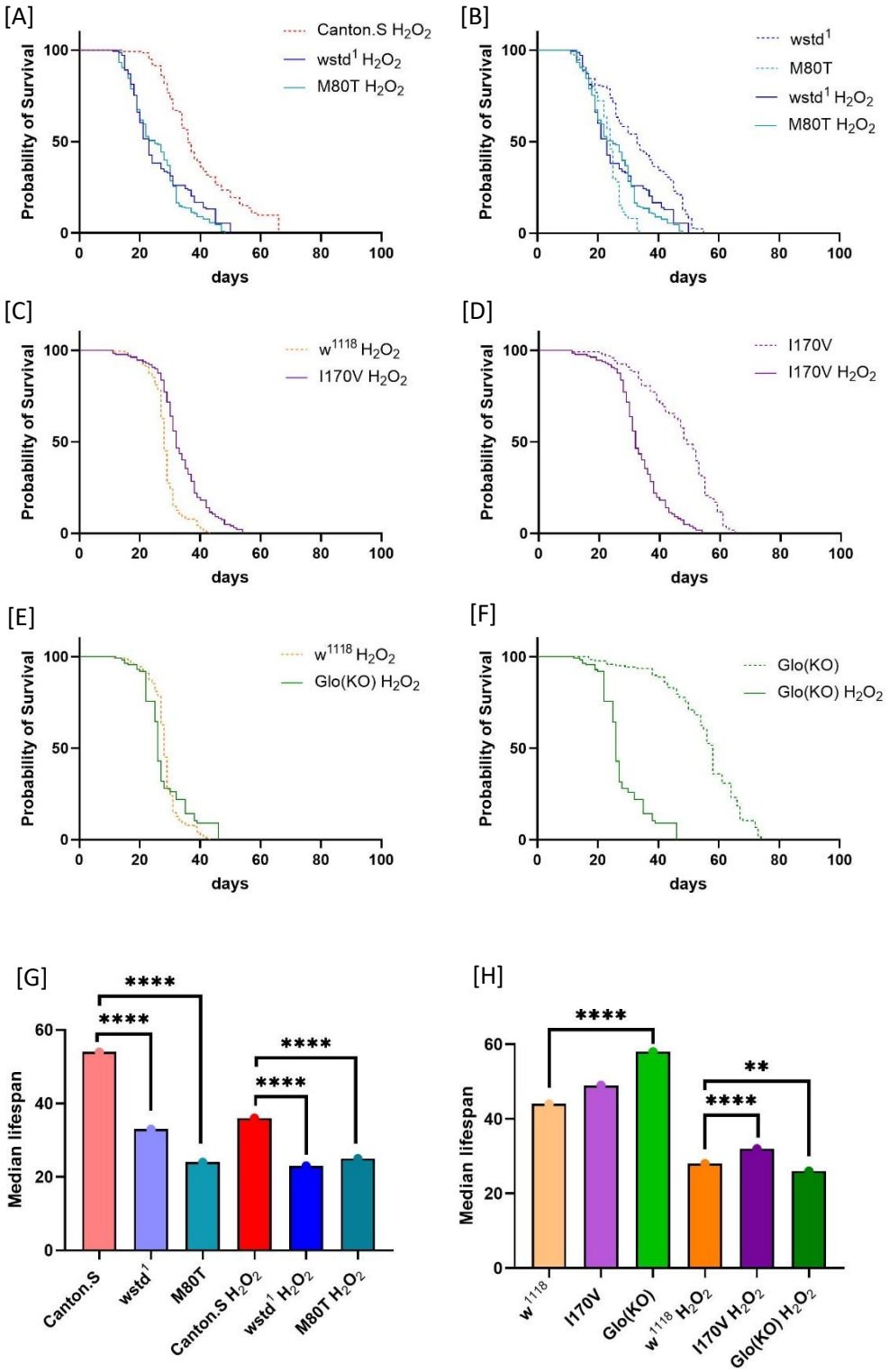

*Figure 6-4: Longevity 25 °C 12 hr light dark cycle H_2O_2 (5 %) treatment with water treated controls (dotted lines) median survival; [A] Canton.S H_2O_2: 36, wstd^1 H_2O_2: 23, ****p<0.0001 and ****p<0.0001, M80T H_2O_2: 25, ****p<0.0001 and ****p<0.0001, [B] wstd^1: 33, M80T: 24, wstd^1 H_2O_2: 23, ****p<0.0001 and ****p<0.0001, M80T H_2O_2: 25, ***p<0.0005 and ns. [C] w^{1118} H_2O_2: 28, I170V H_2O_2: 32, ****p<0.0001 and ****p<0.0001 [D] I170V: 49, I170V H_2O_2: 32, ****p<0.0001 and ****p<0.0001 [E] w^{1118} H_2O_2: 28, Glo(KO) H_2O_2: 26, ns and **p<0.005 [F] Glo(KO): 58, Glo(KO) H_2O_2: 26, ****p<0.0001 and ****p<0.0001 N≥97, Kaplan-Meier survival analysis, log rank Mantel-Cox test and Gehan-Breslow-Wilcoxon tests used for significance respective p values given after comparisons above.*

6.5: Circadian rhythm is altered in wstd^1 and I170V mutants

Circadian rhythm experiments are useful to assess whole animal physiology and homeostasis *in vivo*. The circadian clock control is a broad phenotypic read out that is affected by various mechanisms, regulated by clock genes as described in more detail in Section 6.2 (Dubowy and Sehgal 2017), therefore it is a good measure of overall animal health.

6.5.1: Circadian rhythm in young flies

1. Recordings for 7-9 day old flies on day 4 of experiment

Circadian rhythm for young flies showed differences for both TPI mutants in comparison to the control line. In 12 hr light-dark cycle on day 4 for young flies (7-9 days old) wstd^1 showed significantly less sleep and activity over ZT 24 hrs, the I170V line showed similar behaviour to Canton.S, see Figure 6-5 [A] and [B]. Total sleep was seen to be increased in both TPI mutants in the light 12 hrs for I170V, 540±20, and for wstd^1, 690±10, compared to Canton.S 490±10. Total sleep was also significantly reduced for young I170V flies in the dark 12 hrs, 620±10 compared to Canton.S 680±9, see Figure 6-5 [C]. Mean sleep duration was found to be significantly reduced in the dark 12 hrs for wstd^1, 90±30 compared to Canton.S 340±70 see Figure 6-5 [D]. Sleep episodes were not found to be altered in either mutant line. Activity count per time awake was found to be reduced for both TPI mutants in the dark 12 hrs for I170V, 1.7±0.07 and wstd^1 1.1±0.2 compared to Canton.S 2.6±0.4 see Figure 6-5 [F]. Latency was also reduced in the dark 12 hrs for wstd^1, 2.6±1 compared to Canton.S 19±4, see Figure 6-5 [G].

[A]

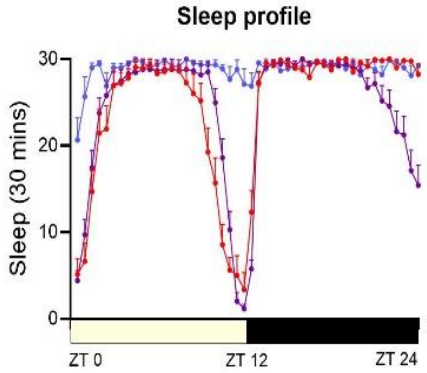
Sleep profile
Sleep (30 mins)
30
20
10
0
ZT 0
ZT 12
ZT 24

[B]

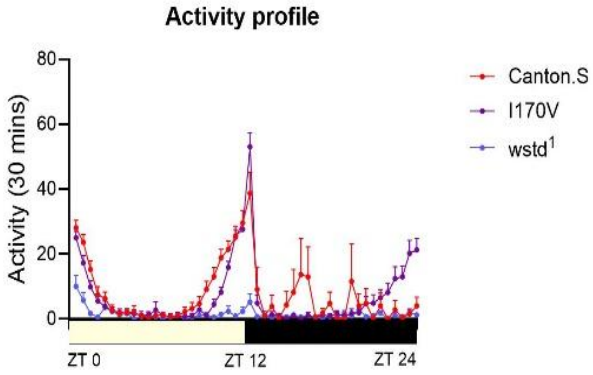
Activity profile
Activity (30 mins)
80
60
40
20
0
ZT 0
ZT 12
ZT 24
Canton.S
I170V
wstd1

[C]

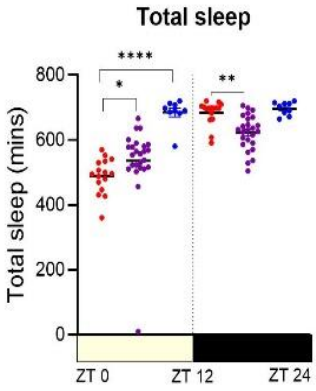
Total sleep
Total sleep (mins)
****
*
**
800
600
400
200
0
ZT 0
ZT 12
ZT 24

[D]

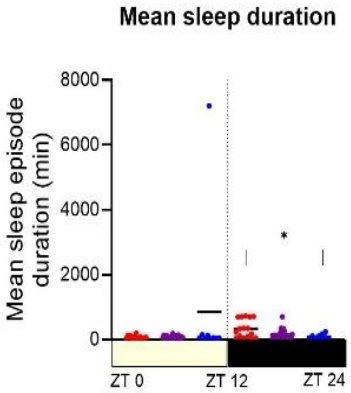
Mean sleep duration
Mean sleep episode duration (min)
8000
6000
4000
2000
0
*
ZT 0
ZT 12
ZT 24

[E]

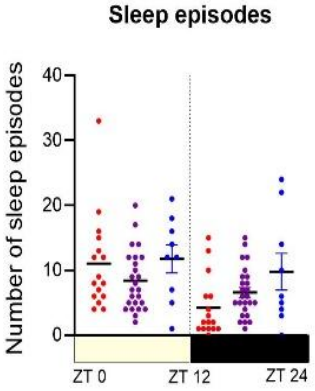
Sleep episodes
Number of sleep episodes
40
30
20
10
0
ZT 0
ZT 12
ZT 24

[F]

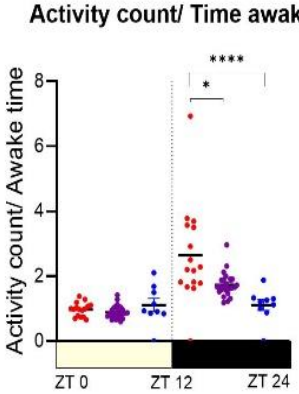
Activity count/ Time awake
Activity count/ Awake time
****
*
8
6
4
2
0
ZT 0
ZT 12
ZT 24

[G]

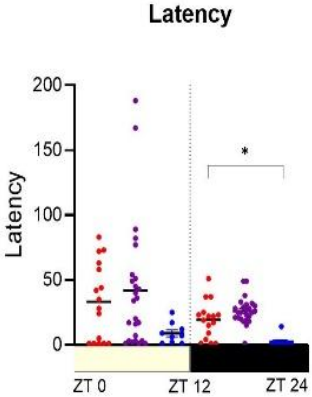
Latency
Latency
200
150
100
50
0
*
ZT 0
ZT 12
ZT 24

*Figure 6-5: Circadian data, for young male flies 7-9 days old, 12hr light-dark cycle, 25 °C, data shown over ZT 24 hr period, N=35. [A] Sleep profile, wstd[1] was found to be significantly different to Canton.S **p<0.005, I170V showed no significant difference [B] Activity profile, wstd[1] was found to be altered compared to Canton.S, ***p<0.001, I170V was not found to be significantly altered [C] Total sleep in light 12 hr; Canton.S: 490±10, I170V: 540±20, wstd[1]: 690±10, was found to be altered for wstd[1] and I170V ****p<0.0001, and I170V *p<0.05. Total sleep in dark 12 hr; Canton.S: 680±9, I170V: 620±10, wstd[1]: 700±7. I170V was found to be significantly altered in dark 12 hr for I170V **p<0.005 [D] Mean sleep episode duration in the light; Canton.S: 69±10, I170V: 80±9, wstd[1]: 860±800. Mean sleep episode duration in dark; Canton.S: 340±70, I170V: 150±30, wstd[1]: 90±30, mean sleep duration in the dark for wstd[1] was found to be altered compared to Canton.S *p<0.05 [E] Number of sleep episodes in the light; Canton.S: 11±2, I170V: 8.4±0.9, wstd[1]: 12±2. Sleep episodes in the dark; Canton.S: 4.3±1, I170V: 6.6±0.8, wstd[1]: 9.8±8. Sleep episodes were not found to differ between lines [F] Activity count per awake time in the light; Canton.S: 0.97±0.05, I170V: 0.89±0.04, wstd1:1.1±0.2. Activity count per time awake in the dark; Canton.S: 2.6±0.4, I170V: 1.7±0.07, wstd1: 1.1±0.2. Activity count per time awake was found to differ in dark 12 hr for wstd[1] ****p<0.0001 and I170V *p<0.05 [G] Latency in the light; Canton.S: 33±7, I170V: 42±10, wstd[1]: 8.9±3. Latency in the dark; Canton.S: 19±4, I170V: 26±2, wstd1: 2.6±1. Latency was found to differ in dark for wstd[1] *p<0.05. Comparisons were made using one-way ANOVA Kruskal-Wallis test, normality was tested for using Shapiro Wilk tests.*

In 24 hr dark for young flies on day 4 (7-9days old) wstd[1] still showed reduced sleep and activity over ZT 24 hrs, I170V still was not significantly different, see Figure 6-6 [A] and [B]. Total sleep was not found to be significantly altered in either mutant line. Mean sleep duration was found to be reduced in the second 12 hrs for wstd[1], 17±10 compared to Canton.S 76±11 see Figure 6-6 [D]. Sleep episodes and activity per time awake were not found to be significantly altered in either mutant line. Latency was not found to be significantly altered in either mutant see Figure 6-6 [E] and [F].

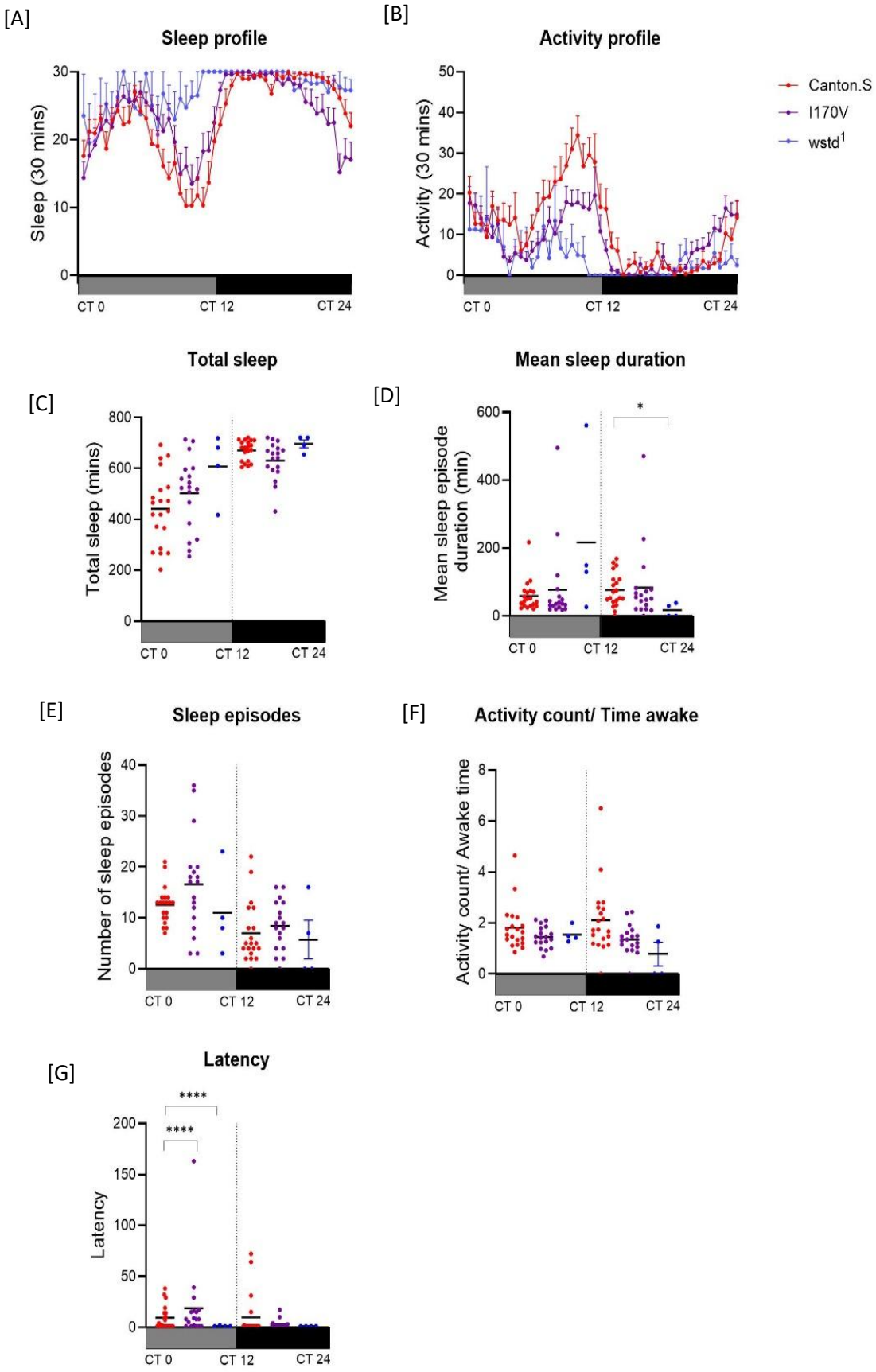
[A]
Sleep profile
Sleep (30 mins)
CT 0
CT 12
CT 24
[B]
Activity profile
Activity (30 mins)
Canton.S
I170V
wstd1
[C]
Total sleep
Total sleep (mins)
[D]
Mean sleep episode duration
Mean sleep episode duration (min)
[E]
Sleep episodes
Number of sleep episodes
[F]
Activity count/ Time awake
Activity count/ Awake time
[G]
Latency
****
****

*Figure 6-6: Circadian data, for young male flies 7-9 days old, 12 hr dark-dark cycle, 25 °C, data shown over ZT 24 hr period, N=35. [A] Sleep profile, wstd^1 was found to be significantly different to Canton.S ***p<0.0005, I170V was not found to be significantly altered [B] Activity profile, wstd^1 was found to be altered compared to Canton.S, ****p<0.0001, I170V was not found to be significantly altered [C] Total sleep in the first 12 hr; Canton.S: 440±30, I170V: 502±30, wstd^1: 606±70. Total sleep in the second 12 hr; Canton.S: 670±9, I170V: 630±20, wstd^1: 700±10. Total sleep was not found to be altered in either mutant [D] Mean sleep episode duration in first 12 hr; Canton.S: 59±10, I170V: 77±30, wstd^1: 220±200. Mean sleep episode duration in second 12 hr; Canton.S: 76±11, I170V: 84±30, wstd^1: 17±10. Mean sleep episode duration in second 12 hrs for wstd^1 was found to be altered compared to Canton.S *p<0.05 [E] Number of sleep episodes in the first 12 hr; Canton.S: 13±0.8, I170V: 17±2, wstd^1: 11±4. Number of sleep episodes in the second 12 hr; Canton.S: 7.0±1, I170V: 8.4±1, wstd^1: 5.8±4. Number of sleep episodes were not found to differ for either mutant [F] Activity count per awake time in first 12 hr; Canton.S: 1.8±0.2, I170V: 1.4±0.1, wstd^1: 1.5±0.2. Activity count per awake time in second 12 hr; Canton.S: 2.1±0.3, I170V: 1.4±0.1, wstd^1: 0.78±0.5. Activity count per awake time was not found to differ for either mutant [G] Latency in the first 12 hr; Canton.S: 9.3±3, I170V: 19±9, wstd^1: 1.3±0.3. Latency in second 12 hr; Canton.S: 10±5, I170V: 2.7±1, wstd^1: 1±0. Latency was not found to differ for either mutant. Comparisons were made using one-way ANOVA Kruskal-Wallis test, normality was tested for using Shapiro Wilk tests.*

2. Recordings for 11-13 day old flies on day 8 of experiment

In 12 hr light-dark cycle on day 8 for young flies (11-13days old) wstd^1 continued to show a reduced sleep and activity, I170V continued to show similar behaviour to control, see Figure 6-7 [A] and [B]. Total sleep was found to be increased in light 12hrs for wstd^1, 707±2 and I170V 550±20 compared to Canton.S 500±10, and was found to be significantly reduced in the dark 12hrs for I170V, 630±10 compared to Canton.S 680±8 see Figure 6-7 [C]. Mean sleep duration was significantly increased in the light 12hrs for wstd^1, 270±100 compared to Canton.S 69±9, and significantly reduced in the dark 12hrs for wstd^1, 140±30 and I170V 180±20 compared to Canton.S 400±50 see Figure 6-7 [D]. Sleep episodes were found to be significantly increased in the dark 12 hrs for I170V, 5.7±0.6 compared to Canton.S 3.7±0.9 see Figure 6-7 [E]. Activity count per time awake was found to be decreased in dark 12hrs for wstd^1, 0.96±0.2 compared to Canton.S 2.3±0.3 see Figure 6-7 [F]. Latency was significantly increased in light 12hrs for I170V, 29±5, compared to Canton.S 8.4±2, and significantly decreased in dark 12hrs for wstd^1, 1.1±0.06 compared to Canton.S 23±3, see Figure 6-7 [G].

[A]

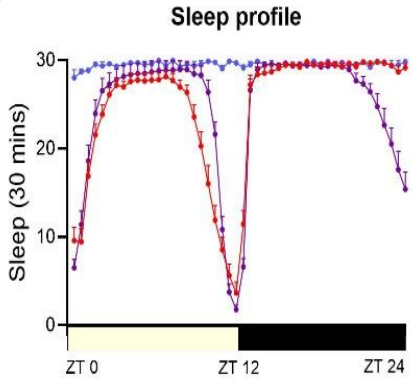
Sleep profile
Sleep (30 mins)
30
20
10
0
ZT 0
ZT 12
ZT 24

[B]

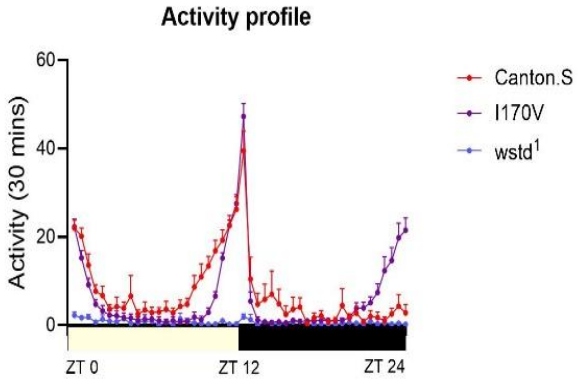
Activity profile
Activity (30 mins)
60
40
20
0
ZT 0
ZT 12
ZT 24
Canton.S
I170V
wstd1

[C]

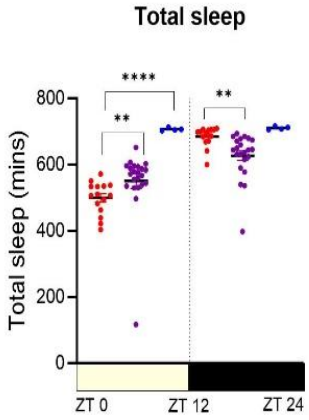
Total sleep
Total sleep (mins)
800
600
400
200
0
****
**
**
ZT 0
ZT 12
ZT 24

[D]

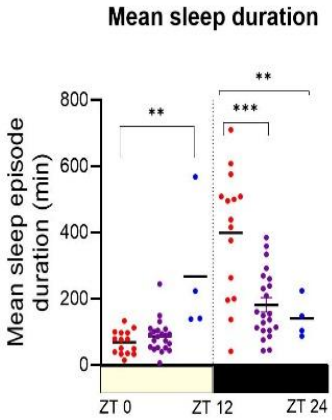
Mean sleep duration
Mean sleep episode duration (min)
800
600
400
200
0
**
**
***
ZT 0
ZT 12
ZT 24

[E]

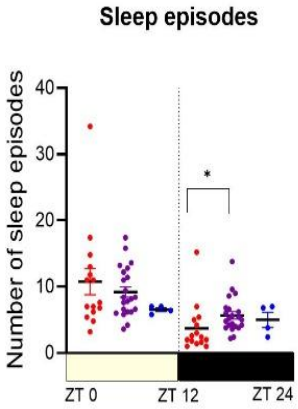
Sleep episodes
Number of sleep episodes
40
30
20
10
0
*
ZT 0
ZT 12
ZT 24

[F]

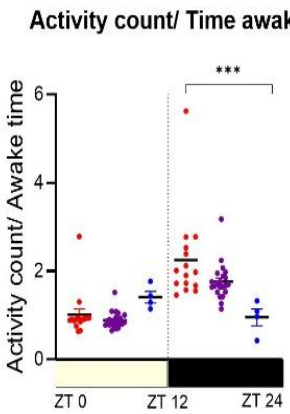
Activity count/ Time awake
Activity count/ Awake time
6
4
2
0
***
ZT 0
ZT 12
ZT 24

[G]

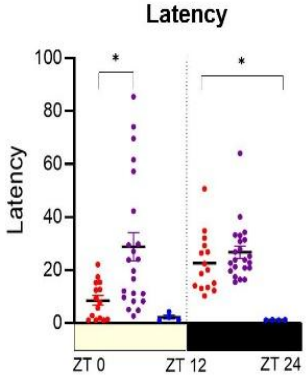
Latency
Latency
100
80
60
40
20
0
*
*
ZT 0
ZT 12
ZT 24

*Figure 6-7: Circadian data, for young male flies 11-13 days old, 12 hr light-dark cycle, 25 °C, data shown over ZT 24 hr period, N=35. [A] Sleep profile, wstd^1 was found to be significantly different to Canton.S ***p<0.0005, I170V showed no significant difference [B] Activity profile, wstd^1 was found to be altered compared to Canton.S, ****p<0.0001, I170V was not found to be significantly altered [C] Total sleep in light ; Canton.S: 500±10, I170V: 550±20, wstd^1: 707±2. Total sleep in dark; Canton.S: 680±8, I170V: 630±10, wstd^1: 710±2. Total sleep in the light were found to be significantly altered for wstd^1 ****p<0.0001 and I170V **p<0.005, and in dark for I170V **p<0.005 compared to Canton.S [D] Mean sleep episode duration in the light; Canton.S: 69±9, I170V: 87±10, wstd^1: 270±100. Mean sleep episode duration in dark; Canton.S: 400±50, I170V: 180±20, wstd1: 140±30. Mean sleep episode duration was altered in light for wstd^1 **p<0.005, and in dark for wstd^1 *p<0.05 and I170V **p<0.005 [E] Number of sleep episodes in the light; Canton.S: 11±2, I170V: 9.2±0.8, wstd^1: 6.6±0.3. Number of sleep episodes in the dark; Canton.S: 3.7±0.9, I170V: 5.7±0.6, wstd^1: 5.0±1. Number of sleep episodes in the dark in I170V was found to be altered *p<0.05 [F] Activity count per awake time in the light; Canton.S: 1.0±0.1, I170V: 0.89±0.04, wstd^1: 1.4±0.1. Activity count per time awake in dark; Canton.S: 2.3±0.3, I170V: 1.8±0.09, wstd^1: 0.96±0.2. Activity count per time awake was found to differ in dark for wstd^1 ***p<0.001 [G] Latency in the light; Canton.S: 8.4±2, I170V: 29±5, wstd^1: 2.2±0.7. Latency in the dark; Canton.S: 23±3, I170V: 27±2, wstd^1: 1.1±0.06. Latency was found to differ in light for I170V *p<0.05 and in dark for wstd^1 *p<0.05. Comparisons were made using one-way ANOVA Kruskal-Wallis test, normality was tested for using Shapiro Wilk tests.*

In 24 hr dark on day 8 for young flies (11-13 days old) wstd^1 continued to show reduced sleep and activity, I170V showed better retention of sleep profile than Canton.S, however activity was not significantly altered, see Figure 6-8 [A] and [B]. Total sleep was found to be reduced in I170V in the second 12 hrs, 630±20, compared to Canton.S 680±7 see Figure 6-8 [C]. Mean sleep duration was found to be reduced in the first 12 hrs I170V, 35±4, compared to Canton.S 330±90 see Figure 6-7 [D]. Sleep episodes were found to be significantly increased in the first 12 hrs for I170V, 18±1, compared to Canton.S 7.9±1 see Figure 6-7 [E]. Activity count per time awake was not found to be significantly altered in either mutant. Latency was found to be significantly increased in the first 12 hrs for I170V, 14±4 compared to Canton.S 6.1±2, see Figure 6-8 [G].

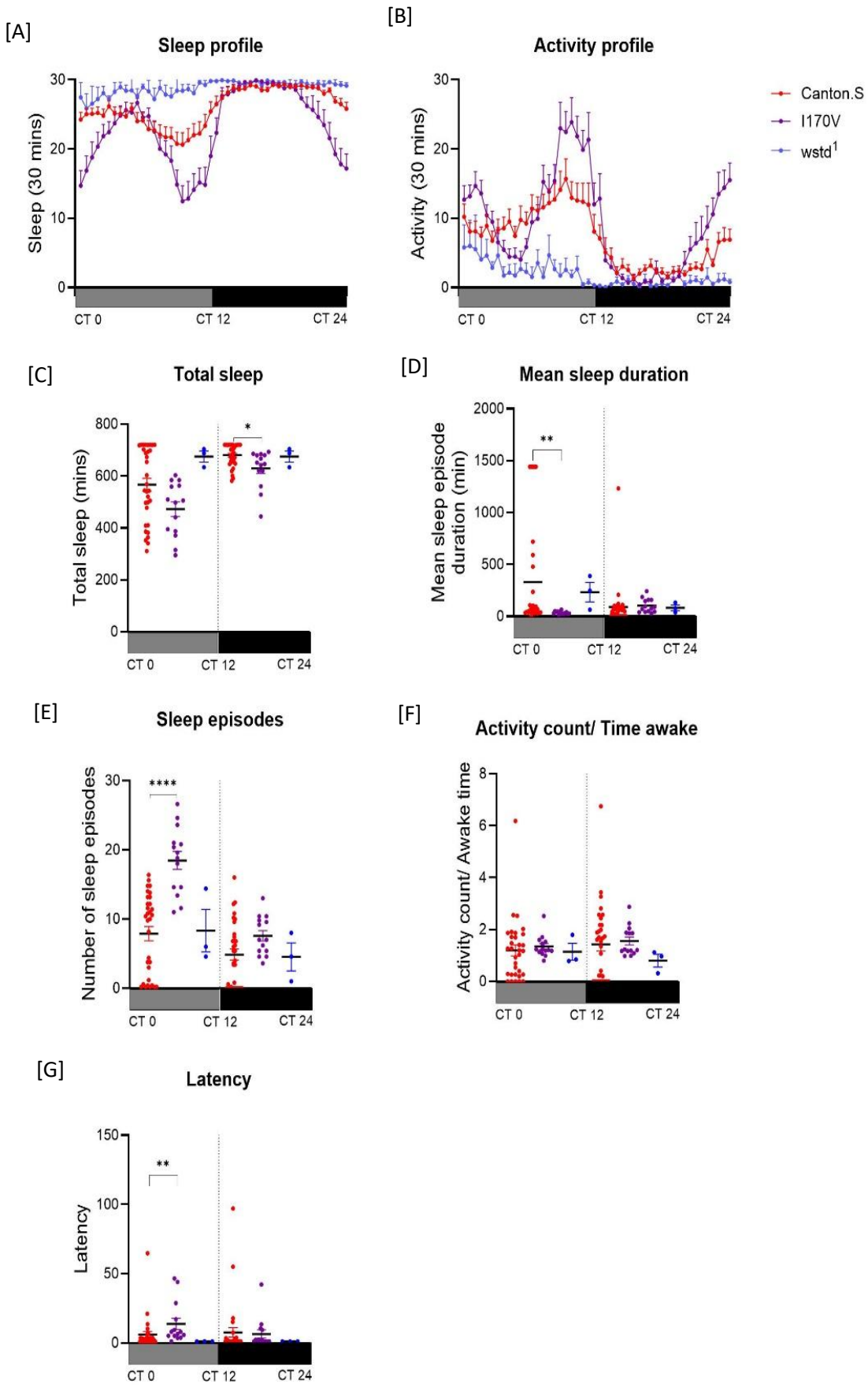
[A]
Sleep profile
Sleep (30 mins)
30
20
10
0
CT 0
CT 12
CT 24
[B]
Activity profile
Activity (30 mins)
Canton.S
I170V
wstd1
[C]
Total sleep
Total sleep (mins)
800
600
400
200
*
[D]
Mean sleep duration
Mean sleep episode duration (min)
2000
1500
1000
500
**
[E]
Sleep episodes
Number of sleep episodes
****
[F]
Activity count/ Time awake
Activity count/ Awake time
8
6
4
2
[G]
Latency
150
100
50

*Figure 6-8: Circadian data, for young male flies 11-13 days old , 12 hr dark-dark cycle, 25 °C, data shown over ZT 24 hr period, N=35. [A] Sleep profile, wstd[1] ***p<0.0005 and I170V ***p<0.0005 were found to be significantly different to Canton.S [B] Activity profile, wstd[1] ****p<0.0001 was found to be altered compared to Canton.S, I170V was not found to be significantly altered [C] Total sleep in first 12 hr; Canton.S: 570±20, I170V: 470±30, wstd[1]: 680±20. Total sleep in second 12 hr; Canton.S: 680±7, I170V: 630±20, wstd[1]: 680±20 in second 12 hrs was found to be significantly altered in I170V *p<0.05 [D] Mean sleep episode duration in first 12 hr; Canton.S: 330±90, I170V: 35±4, wstd[1]: 230±90. Mean sleep episode duration in second 12 hr; Canton.S: 91±40, I170V: 103±18, wstd[1]: 82±30. Mean sleep episode duration in first 12 hrs for I170V was found to be altered compared to Canton.S **p<0.005 [E] Number of sleep episodes in first 12 hr; Canton: 7.9±1, I170V: 18±1, wstd1: 8.3±3. Number of sleep episodes in second 12 hr; Canton.S: 4.9±0.8, I170V: 7.6±0.8, wstd[1]: 4.5±2. Number of sleep episodes was found to differ significantly for I170V in first 12 hrs ****p<0.0001 [F] Activity count per awake time in the first 12 hr; Canton.S: 1.2±0.2, I170V: 1.3±0.1, wstd[1]: 1.1±0.3. Activity count per time awake in second 12 hr; Canton.S: 1.4±0.3, I170V: 1.6±0.2, wstd[1]: 0.80±0.2. Activity count per time awake was not found to differ significantly in either mutant [G] Latency in first 12 hr; Canton.S: 6.1±2, I170V: 14±4, wstd[1]: 1.1±0.07. Latency in the second 12 hr; Canton.S: 7.6±3, I170V: 6.4±3, wstd[1]: 1±0. Latency was found to differ in first 12 hrs for I170V **p<0.005. Comparisons were made using one-way ANOVA Kruskal-Wallis test, normality was tested for using Shapiro Wilk tests.*

6.5.2: Circadian rhythm for old flies

1. Recordings for 17-19 day old flies on day 4 of experiment

In 12 hr light-dark cycle on day 4 for old flies (17-19 days old) I170V sleep and activity profiles over ZT 24 hrs did not show any differences to the control, see Figure 6-9 [A] and [B]. Total sleep was found to be increased in the light 12 hrs in I170V, 620±10 compared to Canton.S 550±10. Total sleep was found to be reduced in the dark 12 hrs for I170V, 650±9 compared to Canton.S 700±2 see Figure 6-9 [C]. Mean sleep duration was found to be reduced in the dark 12 hrs in I170V, 240±40 compared to Canton.S 603±40 see Figure 6-9 [D]. Sleep episodes were found to be increased in light 12 hrs for I170V, 8.9±0.7 compared to Canton.S 7.1±0.6. And in the dark 12 hrs for I170V, 4.9±0.7 compared to Canton.S 1.5±0.2 see Figure 6-9 [E]. Activity count per time awake was found to be reduced in the light 12 hrs for I170V, 0.85±0.05 compared to Canton.S 1.0±0.05. And in the dark 12 hrs for I170V, 1.7±0.08 compared to Canton.S 2.0±0.09 see Figure 6-9 [F]. Latency was found to be increased in the light 12 hrs for I170V, 20±5 compared to Canton.S 7.5±3, see Figure 6-9 [G].

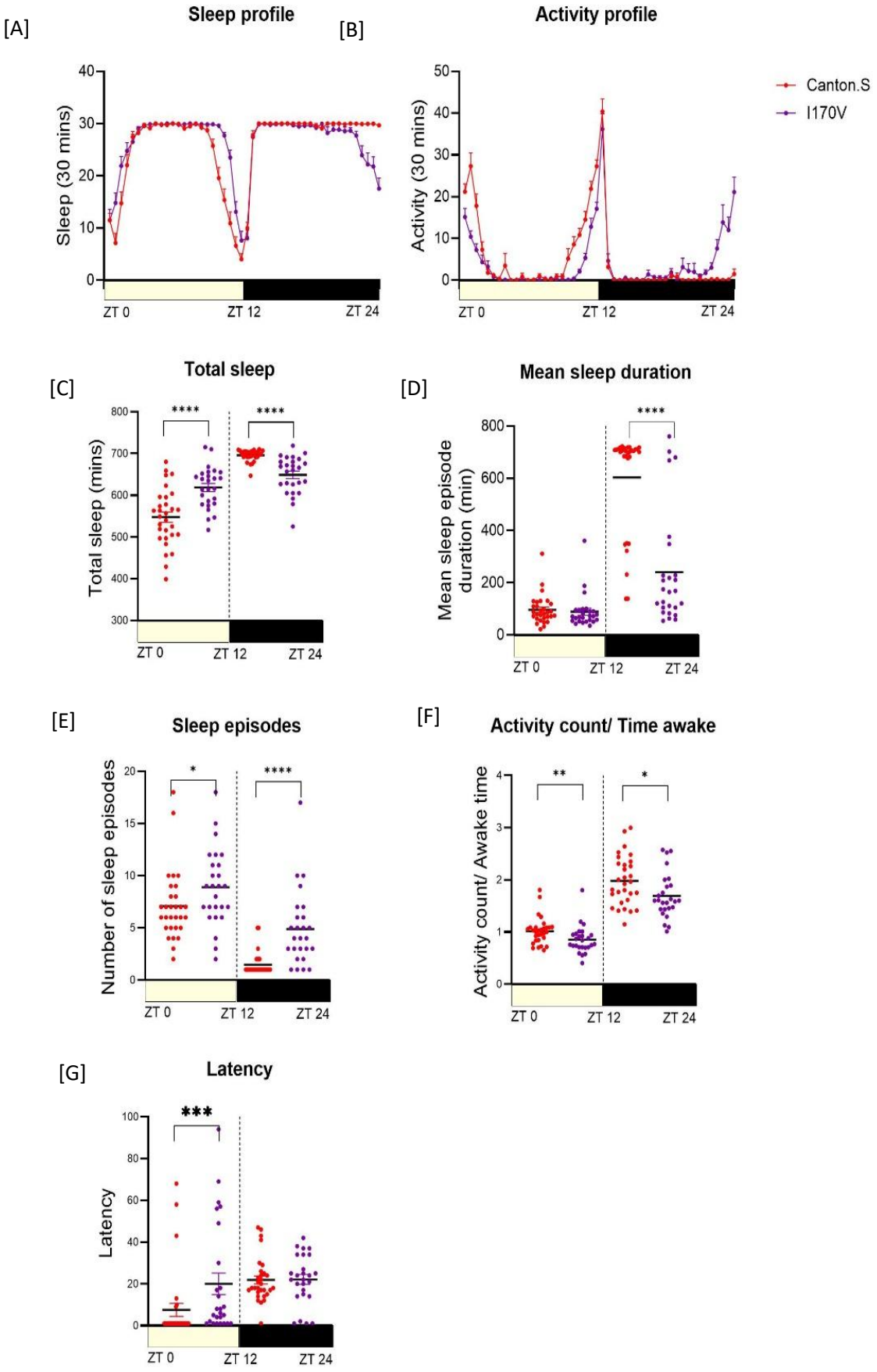
[A]
Sleep profile
Sleep (30 mins)
ZT 0
ZT 12
ZT 24
[B]
Activity profile
Activity (30 mins)
Canton.S
I170V
[C]
Total sleep
Total sleep (mins)
****
[D]
Mean sleep duration
Mean sleep episode duration (min)
[E]
Sleep episodes
Number of sleep episodes
*
[F]
Activity count/ Time awake
Activity count/ Awake time
**
[G]
Latency
***

*Figure 6-9: Circadian data, for old male flies 17-19 days old, 12 hr light-dark cycle, 25 °C, data shown over ZT 24 hr period, N=35. [A] Sleep profile, I170V was not found to be different [B] Activity profile, I170V was not found to be different [C] Total sleep in light; Canton.S: 550±10, I170V: 620±10. Total sleep in dark; Canton.S: 700±2, I170V: 650±9. Total sleep in light and dark was found to be altered in I170V ****p<0.0001 [D] Mean sleep episode duration in the light; Canton.S: 97±10, I170V: 89±10. Mean sleep episode duration in dark; Canton.S: 603±40, I170V: 240±40. Mean sleep episode duration in dark for I170V was found to be significant ****p<0.0001 [E] Number of sleep episodes in the light; Canton.S: 7.1±0.6, I170V: 8.9±0.7. Number of sleep episodes in the dark; Canton.S: 1.5±0.2, I170V: 4.9±0.7. Number of sleep episodes was significantly altered in I170V in the light *p<0.05 and the dark ****p<0.0001 [F] Activity count per awake time in the light; Canton.S: 1.0±0.05, I170V: 0.85±0.05. Activity count per time awake in dark; Canton.S: 2.0±0.09, I170V: 1.7±0.08. Activity count per time awake was altered in I170V in the light **p<0.01 and the dark *p<0.05 [G] Latency in the light; Canton.S: 7.5±3, I170V: 20±5. Latency in dark; Canton.S: 22±2, I170V: 22±2. Latency was found to differ in light for I170V ***p<0.0005. Comparisons were made using student t test Mann-Whitney test, normality was tested for using Shapiro Wilk tests.*

In 24 hr dark on day 4 for old flies (17-19 days old) I170V sleep and activity profiles over ZT 24 hrs did not show any differences to the control, see Figure 6-10 [A] and [B]. Total sleep was found to be decreased in the second 12 hrs for I170V, 580±10 compared to Canton.S 650±10 see Figure 6-10 [C]. Mean sleep episode duration was found to be decreased in first 12 hrs for I170V, 30±2 compared to Canton.S 54±10. And in the second 12 hrs for I170V, 65±7 compared to Canton.S 350±60 see Figure 6-10 [D]. Sleep episodes were found to be increased in first 12 hrs for I170V, 20±1 compared to Canton.S 12±0.9. And in the second 12 hrs for I170V, 11±0.8 compared to Canton.S 4.0±0.7 see Figure 6-10 [E]. Activity count per time awake was not found to differ for I170V. Latency was found to be significantly increased in first 12 hrs for I170V, 9.8±3 compared to Canton.S 1.1±0.1, see Figure 6-10 [G].

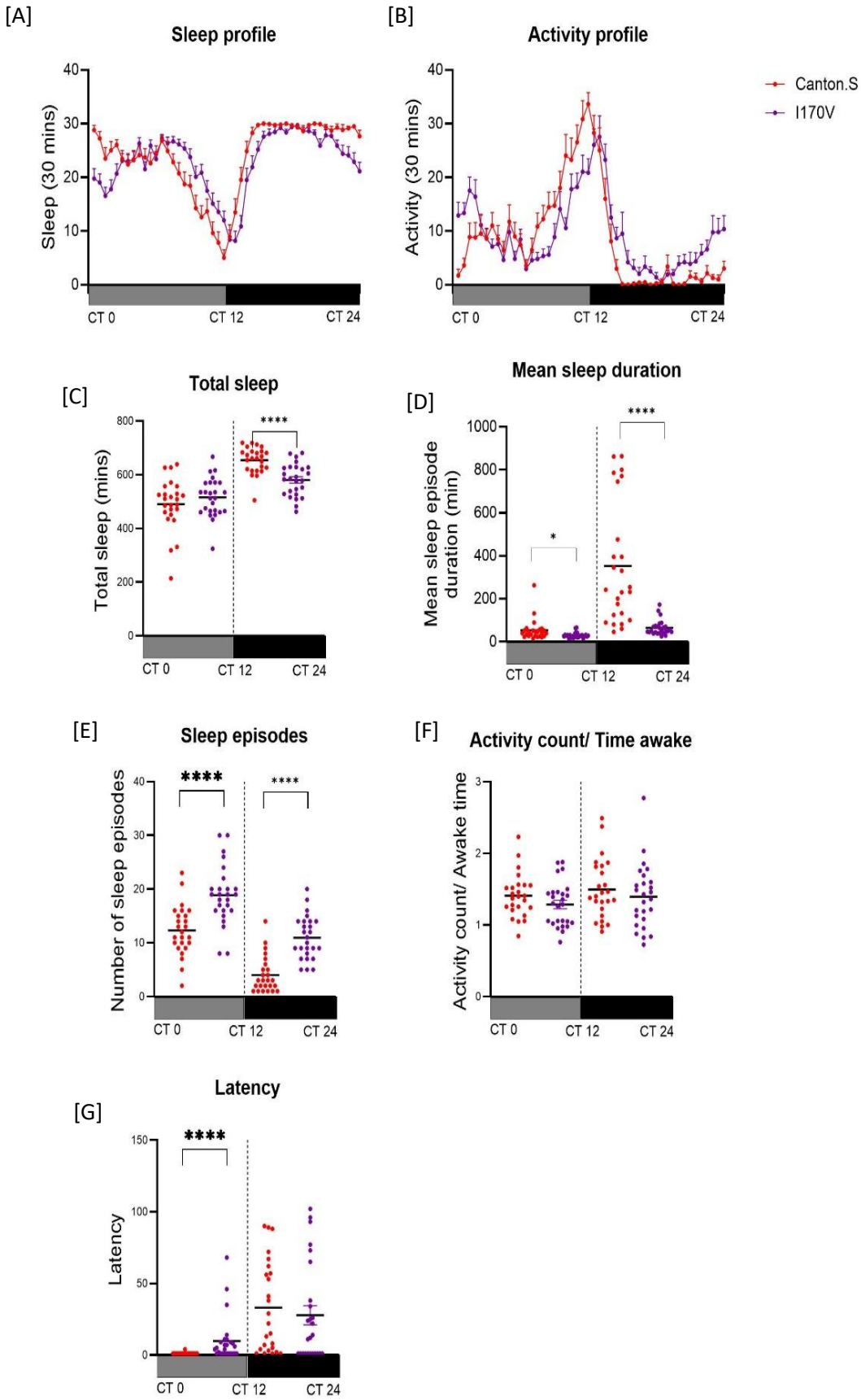
[A]
Sleep profile
Sleep (30 mins)
CT 0
CT 12
CT 24
[B]
Activity profile
Activity (30 mins)
Canton.S
I170V
[C]
Total sleep
Total sleep (mins)
****
[D]
Mean sleep duration
Mean sleep episode duration (min)
*
****
[E]
Sleep episodes
Number of sleep episodes
****
****
[F]
Activity count/ Time awake
Activity count/ Awake time
[G]
Latency
Latency
****

*Figure 6-10: Circadian data, for old male flies 17-19 days old, 12 hr dark-dark cycle, 25 °C, data shown over ZT 24 hr period, N=35. [A] Sleep profile, I170V was not found to be different [B] Activity profile, I170V was not found to be different [C] Total sleep in the first 12 hr; Canton.S: 490±20, I170V: 520±10. Total sleep in the second 12 hr; Canton.S: 650±10, I170V: 580±10. Total sleep in the second 12 hrs for I170V was found to be altered ****p<0.0001[D] Mean sleep episode duration in first 12 hr; Canton.S: 54±10, I170V: 30±2. Mean sleep episode duration in second 12 hr; Canton.S: 350±60, I170V: 65±7. Mean sleep episode duration was found to be altered for I170V in first 12 hrs *p<0.05 and in second 12hrs ****p<0.0001 [E] Number of sleep episodes in the first 12 hr; Canton.S: 12±0.9, I170V: 20±1. Number of sleep episodes in second 12 hr; Canton.S: 4.0±0.7, I170V: 11±0.8. Number of sleep episodes was altered for I170V in the first 12 hrs ****p<0.0001 and in the second 12 hrs ****p<0.0001 [F] Activity count per awake time in first 12 hr; Canton.S: 1.4±0.06, I170V: 1.3±0.06. Activity count per time awake in second 12 hr; Canton.S: 1.5±0.08, I170V: 1.4±0.09. Activity count per time awake was not found to differ for I170V [G] Latency in first 12 hr; Canton.S: 1.1±0.1, I170V: 9.8±3. Latency in second 12 hr; Canton.S: 33±6, I170V: 28±7. Latency was found to differ in first 12 hrs for I170V ****p<0.0001. Comparisons were made using student t test Mann-Whitney test, normality was tested for using Shapiro Wilk tests.*

2. Recordings for 21-23 day old flies on day 8 of experiment

In 12 hr light-dark cycle on day 8 for old flies (21-23 days old) I170V sleep and activity profiles over ZT 24 hrs did not show any differences to the control, see Figure 6-11 [A] and [B]. Total sleep was found to be increased in light 12 hrs for I170V, 620±9 compared to Canton.S 530±10, and was found to be reduced in dark 12 hrs for I170V, 660±8 compared to Canton.S 690±3 see Figure 6-11 [C]. Mean sleep duration was found to be decreased in the dark 12 hrs for I170V, 230±30 compared to Canton.S 560±30 see Figure 6-11 [D]. Sleep episodes were found to be increased in the light 12 hrs I170V, 10±0.6 compared to Canton.S 7.7±0.7. And in the dark 12 hrs for I170V, 5.3±0.8 compared to Canton.S 1.7±0.1 see Figure 6-11 [E]. Activity count per time awake was found to be decreased in the light 12 hrs I170V, 0.82±0.04 compared to Canton.S 0.96±0.03. And in the dark 12 hrs for I170V, 1.6±0.07 compared to Canton.S 1.9±0.08 see Figure 6-11 [F]. Latency was found to be increased in the light 12 hrs for I170V, 13±3 compared to Canton.S 3.3±1, see Figure 6-11 [G].

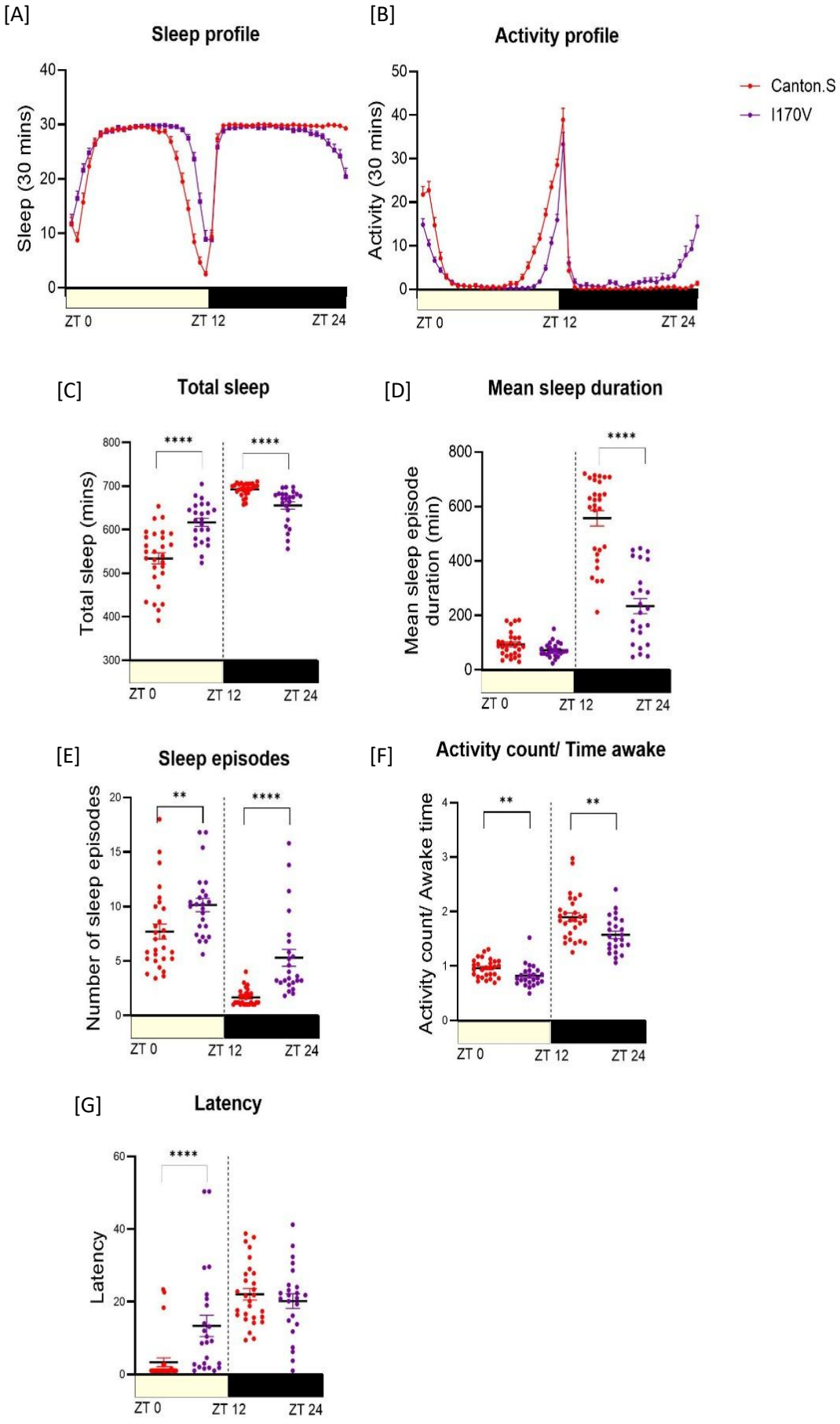
[A]
Sleep profile
Sleep (30 mins)
ZT 0
ZT 12
ZT 24
[B]
Activity profile
Activity (30 mins)
Canton.S
I170V
[C]
Total sleep
Total sleep (mins)
[D]
Mean sleep duration
Mean sleep episode duration (min)
[E]
Sleep episodes
Number of sleep episodes
[F]
Activity count/ Time awake
Activity count/ Awake time
[G]
Latency
Latency

*Figure 6-11: Circadian data, for old male flies 21-23 days old, 12 hr light-dark cycle, 25 °C, data shown over ZT 24 hr period, N=35. [A] Sleep profile, I170V was not found to be different [B] Activity profile , I170V was not found to be different [C] Total sleep in light; Canton.S: 530±10, I170V: 620±9. Total sleep in dark; Canton.S: 690±3, I170V: 660±8. Total sleep was found to be altered for I170V in light ****p<0.0001 and in dark ****p<0.0001 [D] Mean sleep episode duration in light; Canton.S: 94±8, I170V: 73±5. Mean sleep episode duration in dark; Canton.S: 560±30, I170V: 230±30. Mean sleep episode duration was found to be altered in I170V in dark ****p<0.001 [E] Number of sleep episodes in light; Canton.S: 7.7±0.7, I170V: 10±0.6. Number of sleep episodes in dark; Canton.S: 1.7±0.1, I170V: 5.3±0.8. Number of sleep episodes was found to be altered for I170V in the light **p<0.005 and in dark ****p<0.0001 [F] Activity count per awake time in the light; Canton.S: 0.96±0.03, I170V: 0.82±0.04. Activity count per time awake in dark; Canton.S: 1.9±0.08, I170V: 1.6±0.07. Activity count per time awake was found to be altered in I170V in light **p<0.005 and in dark **p<0.005 [G] Latency in light; Canton.S: 3.3±1, I170V: 13±3. Latency in dark; Canton.S: 22±2, I170V: 20±2. Latency was found to differ for I170V in the light ****p<0.0001. Comparisons were made using student t test Mann-Whitney test, normality was tested for using Shapiro Wilk tests.*

In 24 hr dark on day 8 for old flies (21-23 days old) I170V sleep and activity profiles over ZT 24 hrs did not show any differences to the control, see Figure 6-12 [A] and [B]. Total sleep was found to be increased in the first 12 hrs I170V, 560±10 compared to Canton.S 500±10. And decreased in the second 12 hrs for I170V, 590±10 compared to Canton.S 660±7 see Figure 6-12 [C]. Mean sleep duration was found to be decreased in the first 12 hrs for I170V, 39±4 compared to Canton.S 51±5. And the second 12 hrs for I170V, 56±6 compared to Canton.S 290±30 see Figure 6-12 [D]. Sleep episodes were found to be increased in the first 12 hrs I170V, 17±0.9 compared to Canton.S 12±0.8. And in the second 12 hrs for I170V, 13±0.9 compared to Canton.S 3.6±0.4 see Figure 6-12 [E]. Activity per time awake was not found to be altered for I170V. Latency was found to be increased in the first 12 hrs for I170V, 5.7±2 compared to Canton.S 1.6±0.3. And decreased in the second 12 hrs for I170V, 14±3 compared to Canton.S 27±5, see Figure 6-12 [G].

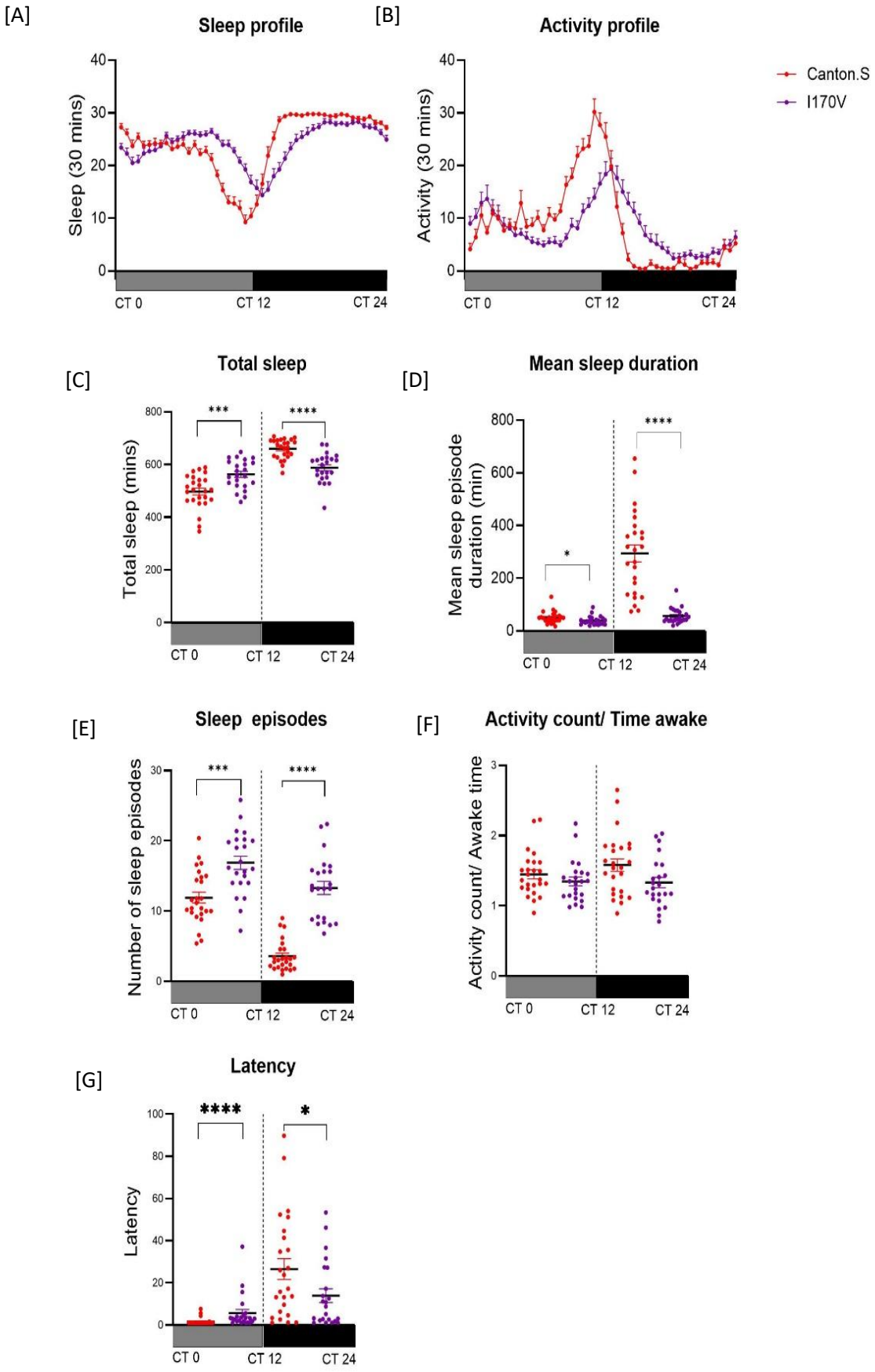
[A]
Sleep profile
Sleep (30 mins)
CT 0
CT 12
CT 24
[B]
Activity profile
Activity (30 mins)
Canton.S
I170V
[C]
Total sleep
Total sleep (mins)
[D]
Mean sleep duration
Mean sleep episode duration (min)
[E]
Sleep episodes
Number of sleep episodes
[F]
Activity count/ Time awake
Activity count/ Awake time
[G]
Latency
Latency

*Figure 6-12: Circadian data, for old male flies 21-23 days old, 12 hr dark-dark cycle, 25 °C, data shown over ZT 24 hr period, N=35. [A] Sleep profile, I170V was not found to be different [B] Activity profile, I170V was not found to be different [C] Total sleep in first 12 hr; Canton.S: 500±10, I170V: 560±10. Total sleep in second 12 hr; Canton.S: 660±7, I170V: 590±10. Total sleep was found to be altered in I170V in the first 12 hrs ***p<0.0005 and in the second 12 hrs ****p<0.0001 [D] Mean sleep episode duration in first 12 hr; Canton.S: 51±5, I170V: 39±4. Mean sleep episode duration in second 12 hr; Canton.S: 290±30, I170V: 56±6. Mean sleep episode duration was found to be altered in I170V in first 12 hrs *p and second 12 hrs ****p [E] Number of sleep episodes in first 12 hr; Canton.S: 12±0.8, I170V: 17±0.9. Number of sleep episodes in second 12 hr; Canton.S: 3.6±0.4, I170V: 13±0.9. Number of sleep episodes was found to differ for I170V in first 12 hrs ***p<0.0005 and second 12 hrs ****p<0.0001 [F] Activity count per awake time in first 12 hr; Canton.S: 1.4±0.06, I170V: 1.3±0.06. Activity count per time awake in second 12 hr; Canton.S: 1.6±0.09, I170V: 1.3±0.07. Activity count per time awake was not found to differ for I170V [G] Latency in first 12 hr; Canton.S: 1.6±0.3, I170V: 5.7±2. Latency in second 12 hr; Canton.S: 27±5, I170V: 14±3. Latency was found to differ for I170V in the first 12 hrs ****p<0.0001 and second 12 hrs *p<0.05. Comparisons were made using student t test Mann-Whitney test, normality was tested for using Shapiro Wilk tests.*

6.6: Motor activity was altered in TPI mutants

6.6.1: Larval locomotion

Assessing larvae crawling ability is a common method of quantifying motor activity, wild type larvae have been reported to crawl an average of 3 cm per minute (Nichols et al. 2012).

Larval crawling behaviour was seen to differ in M80T showing significantly increased total distance travelled 0.49±0.03 m vs 0.15±0.02 m see Figure 6-13 [B]. wstd^{1} and I170V showed no significant change in crawling behaviour total distances of; 0.21±0.02 m in wstd^{1} vs 0.15±0.02 m in Canton.S, and 0.19±0.02 m in I170V vs 0.13±0.01 m in w^{1118}, see Figure 6-13.

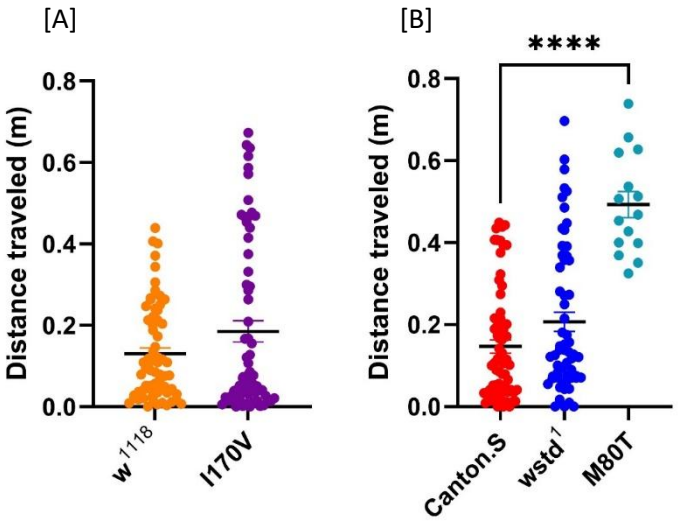

*Figure 6-13: Crawling data for 3rd instar larvae raised at 25 °C, total distance travelled in 10 minutes. Mean values of; [A] Canton.S: 0.15±0.02 m, wstd¹: 0.21±0.02 m, M80T: 0.49±0.03 m. [B] w¹¹¹⁸: 0.13±0.01 m, I170V: 0.19±0.02 m. Nonparametric students t test, Mann Whitney test used to test significance between two data sets, one-way ANOVA, Kruskal-Wallis test used to test statistical significance between three data sets, D'Agostino and Pearson test was used to test normality, N≥15, ****p<0.0001.*

Splitting data by sex shows no significant differences between sexes, see Figure 6-14. No significant differences were observed in turning angle of larvae, see Figure 6-15.

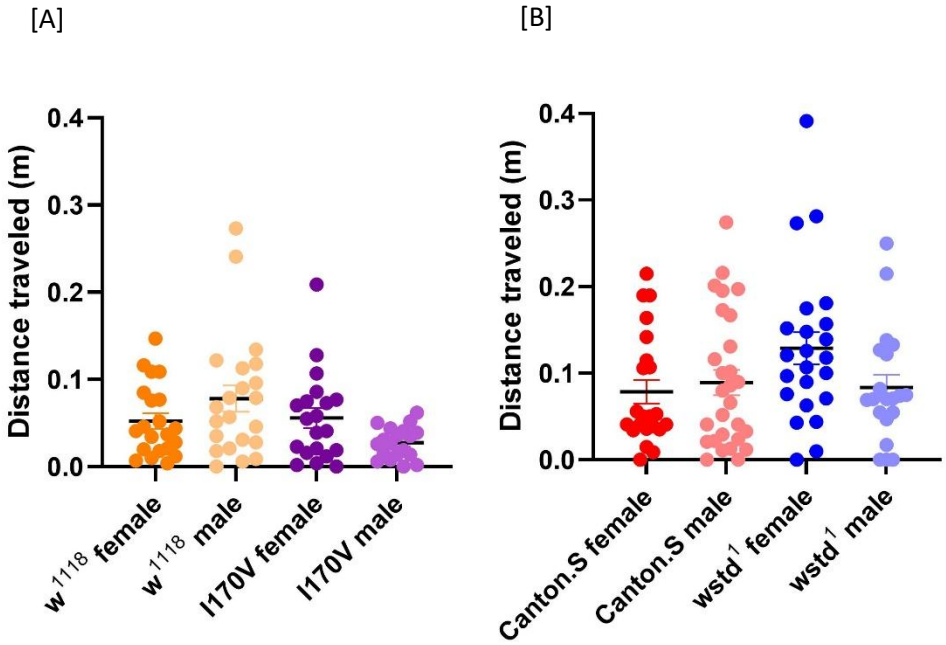

Figure 6-14: Crawling data for 3rd instar larvae raised at 25°C, total distance travelled over 10 minutes. Mean values of; [A] Canton.S female: 0.079±0.01 m, Canton.S male: 0.089±0.01 m, wstd¹ female: 0.13±0.02 m, wstd¹ male: 0.084±0.01 m. [B] w¹¹¹⁸ female: 0.052±0.009 m, w¹¹¹⁸ male: 0.078±0.02 m, I170V female: 0.056±0.01 m, I170V male: 0.027±0.004 m. Two-way ANOVA used to test statistical significance, D'Agostino and Pearson test was used to test normality, N≥22.

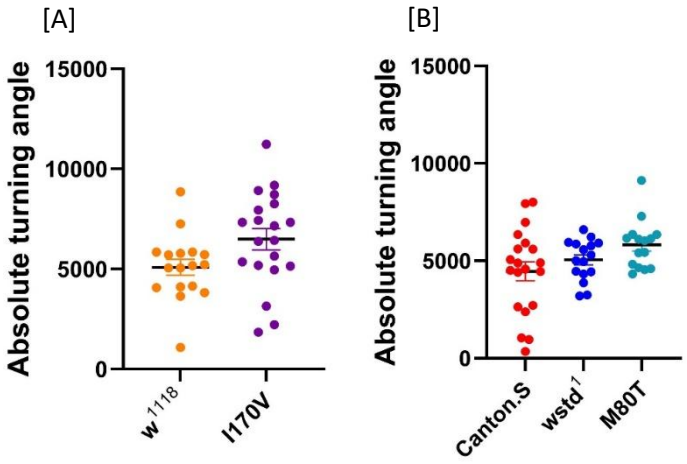

Figure 6-15: Crawling data for 3rd instar larvae raised at 25°C, absolute turning angle over 10 minutes. Mean values of; [A] Canton.S: 4500±500, wstd¹: 5100±300, M80T: 5800±300. [B] w¹¹¹⁸: 6500±900, I170V: 6500±500. One-way ANOVA used to test statistical significance, D'Agostino and Pearson test was used to test normality, N≥15.

Treatment of H_2O_2 showed no effect on distance travelled, although w^{1118} untreated did show a reduced distance travelled compared to $wstd^1$, 0.26±0.02 m in w^{1118} compared to 0.43±0.03 m in $wstd^1$, an effect that increased with treatment, see Figure 6-16 [A]. Absolute turning angle did show an effect of treatment with $wstd^1$ treated with H_2O_2 turning significantly less than the untreated group, 3200±200 with treatment compared with 5100±300 without, see Figure 6-16 [B].

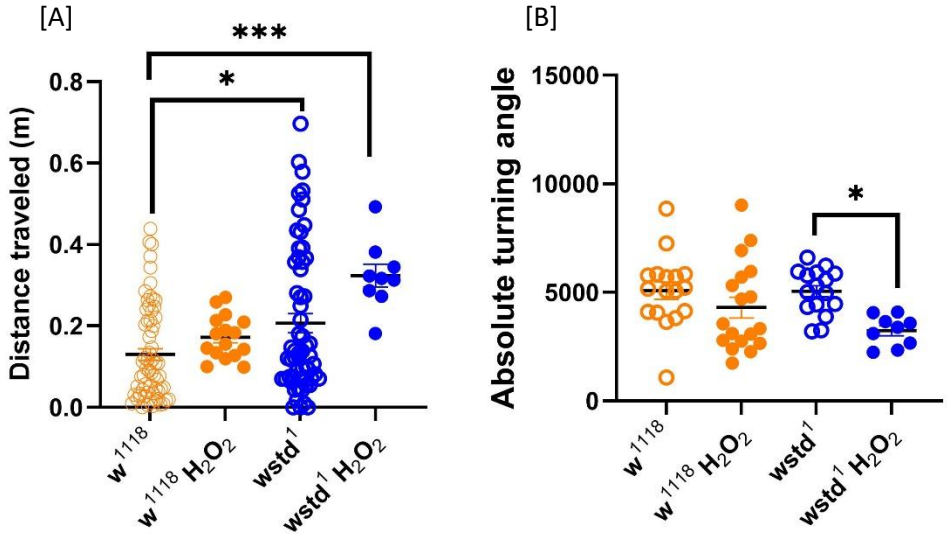

*Figure 6-16: Crawling data for 3rd instar larvae raised at 25°C with H_2O_2 treatments, distance travelled and absolute turning angle over 10 minutes. Mean values of; [A] w^{1118}: 0.26±0.02, w^{1118} H_2O_2 : 0.22±0.03, $wstd^1$: 0.43±0.03, $wstd^1$ H_2O_2: 0.32±0.03 [B] w^{1118}: 6500±900, w^{1118} H_2O_2: 4300±500, $wstd^1$: 5100±300, $wstd^1$ H_2O_2: 3200±200. Two-way ANOVA used to test statistical significance, *p<0.05, ***p<0.001 D'Agostino and Pearson test was used to test normality, N≥9.*

6.6.2: Negative geotaxis

The ability of adult flies to climb up the side of vials gives a good idea of motor function and control.

Male flies are seen to be significantly less active in climbing in the w^{1118} and M80T lines, 40±4 % vs 63±6 % and 7.8±2 % vs 59±6 % respectively see Figure 6-17, for this reason data is showed separated by sex.

The I170V line shows significantly increased climbing activity compared to w^{1118} in both females and males, 92±5 % vs 63±6 % and 91±3 % vs 40±4 % respectively. $wstd^{1}$ and M80T both show a decrease in climbing activity in both females and males, $wstd^{1}$ females 39±8 % vs 93±3 %, $wstd^{1}$ males 37±9 % vs 92±2 % and, M80T females 59±6 % vs 93±3 %, M80T males 7.8±2 % vs 92±2 %, see Figure 6-17.

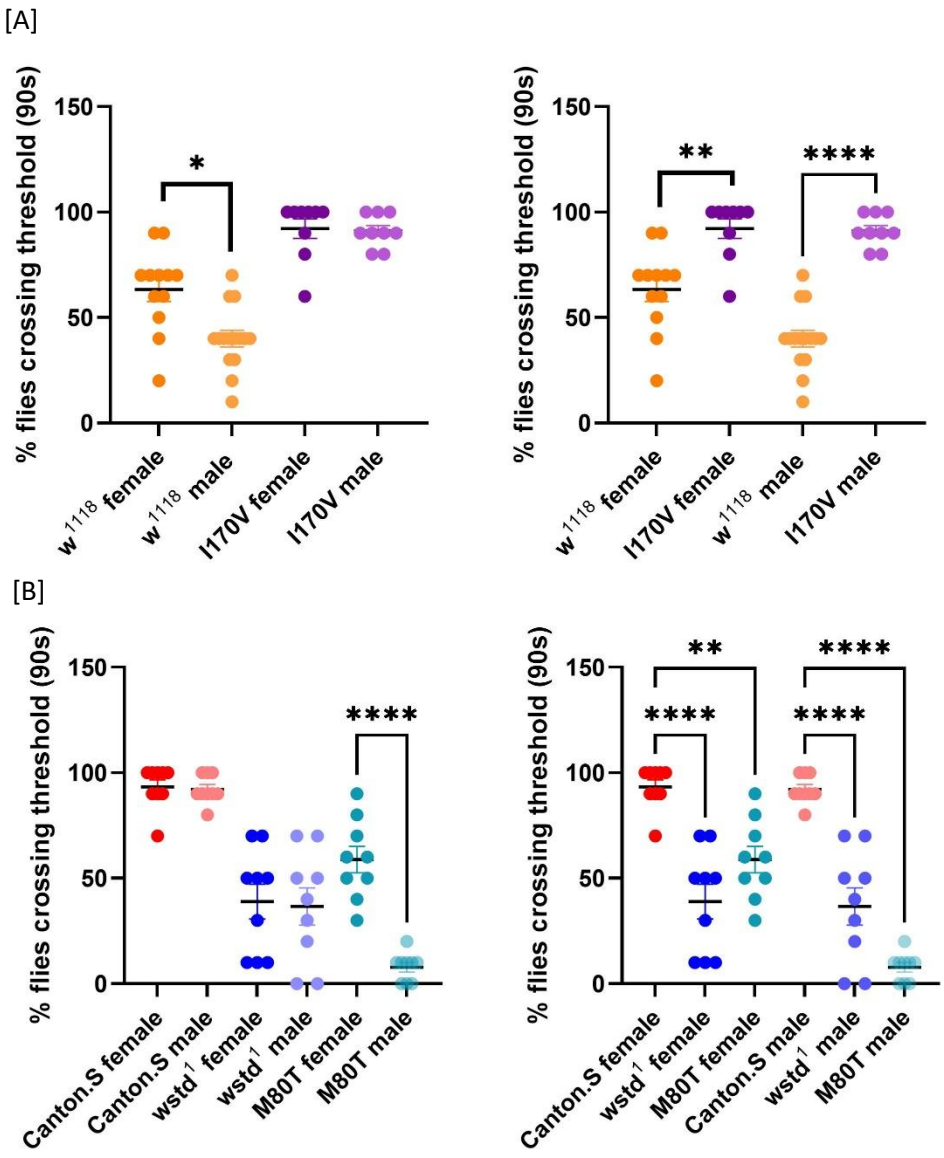

*Figure 6-17: 5 day old adult fly climbing mean % of flies crossing threshold in 90s mean data ± SEM, data is expressed twice to aid visualisation of comparisons, [A] w^{1118} female: 63±6 %, w^{1118} male: 40±4 %, I170V female: 92±5 %, I170V male: 91±3 %, [B] Canton.S female: 93±3 %, Canton.S male: 92±2 %, $wstd^{1}$ female: 39±8 %, $wstd^{1}$ male: 37±9 %, M80T female: 59±6 %, M80T male: 8±2 %. Two-way ANOVA used to test for statistical significance, *p<0.05, **p<0.01, ****p<0.0001, N≥9.*

These differences are maintained at 21 days of age, with I170V still showing increased climbing activity compared to w^{1118}, although as extreme, 92±4 % vs 73±2 %, and $wstd^{1}$ and M80T both showing reduced climbing activity. In $wstd^{1}$ this is comparable to results at 5 days of age, 31±10 % vs 73±2 %, in M80T the effect is more pronounced than the 5 days old data with no flies making it over the threshold in the time, see Figure 6-18 [B]. Male I170V flies at 21 days

showed increased climbing compared to the male w^{1118} flies, 92±7 % compared to 72±3 % in w^{1118} see Figure 6-18 [A].

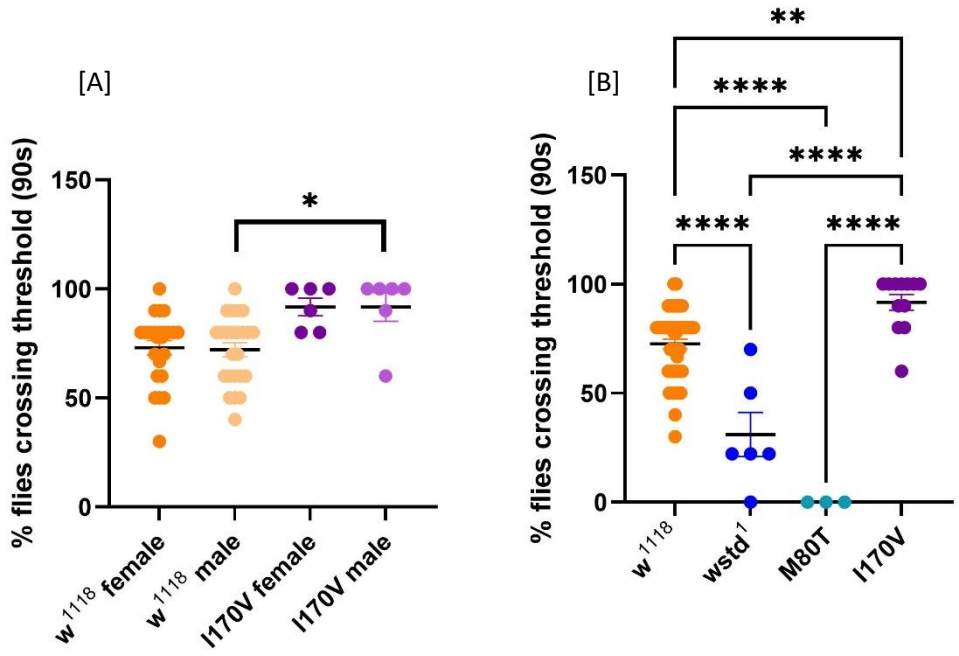

*Figure 6-18: 21 day old adult fly climbing data expressed as mean % of flies crossing threshold [A] Sex differences; w^{1118} female: 73±3 %, w^{1118} male: 72±3 %, I170V female: 92±4 %, I170V male: 92±7 % [B] Combined sex data; w^{1118}: 73±2 %, $wstd^{1}$: 31±10 %, M80T: 0±0 %, I170V: 92±4 %. Two-way ANOVA used to test for significance [A], one-way ANOVA used to test for statistical significance [B], *p<0.05, **p<0.01, ****p<0.0001, N≥3.*

6.7: Learning and memory was not altered in mutants

Learning and memory was assessed by Pavlovian conditioning as measure of cognitive function in *Drosophila* 3rd instar larvae. Data is expressed as PI values, values away from zero indicate learning has occurred, the larger the value the larger the effect, positive associations show as positive values, negative associations show as negative values. The association taught here was between the odorant n-amyl acetate and sucrose, the wild type phenotype has been previously reported as exhibiting a positive learning association.

Learning and memory capability in the TPI mutant lines did not show the expected impairment with $wstd^{1}$ and M80T showing no significant differences to Canton.S, and I170V line showing no impairment in comparison to w^{1118}, see Figure 6-19.

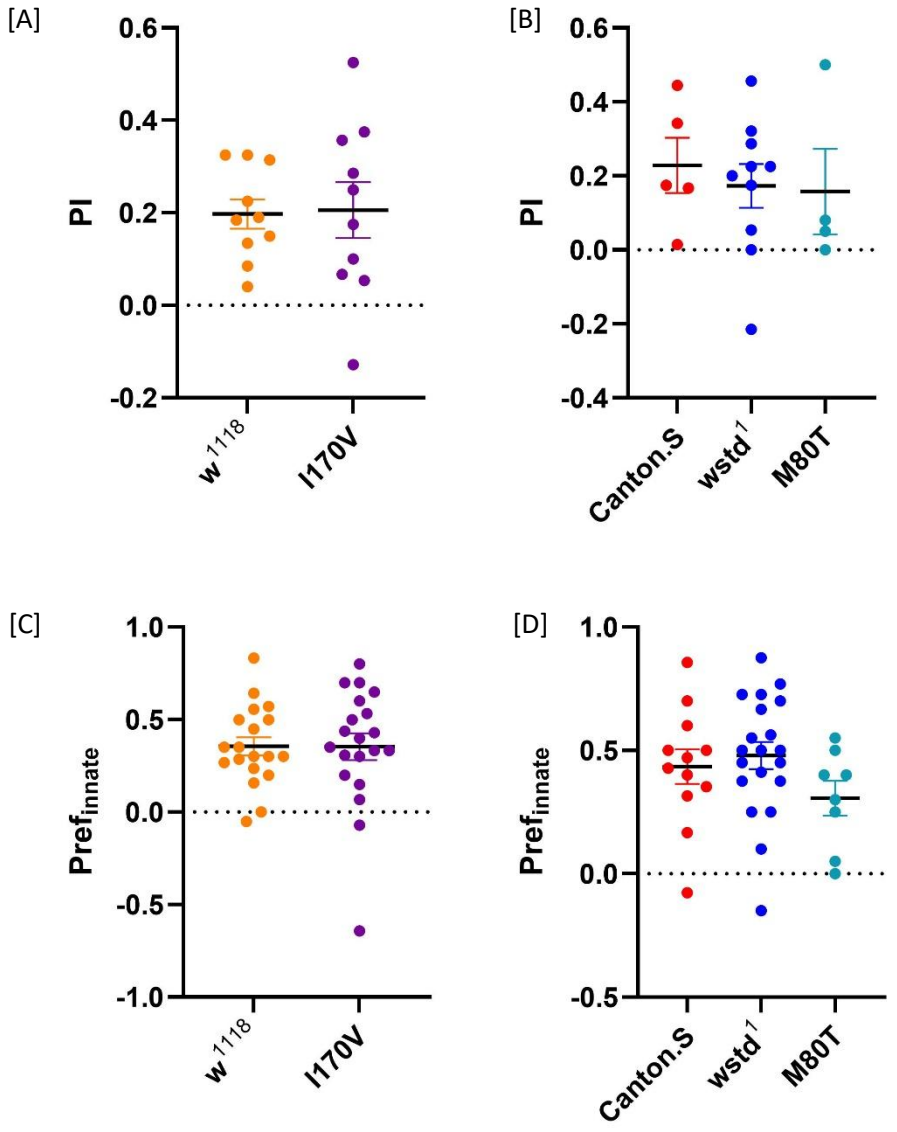

*Figure 6-19: Learning and memory data for sugar associated odour after training larvae raised at 25°C with a 12hr light dark cycle data expressed as mean±SEM [A] PI learnt association w^{1118}: 0.20±0.03 ***p<0.0005, I170V: 0.21±0.06 **p<0.01 [B] PI learnt association Canton.S: 0.23±0.07 *p<0.05, $wstd^{1}$: 0.17±0.06 *p<0.05, M80T: 0.16±0.1 ns. [C] $Pref_{innate}$ values w^{1118}: 0.36±0.05 ****p<0.0001, I170V: 0.35±0.07 ****p<0.0001 [D] Canton.S: 0.43±0.07 ****p<0.0001, wstd1: 0.48±0.05 ****p<0.0001, M80T: 0.31±0.07 **p<0.005. One-way ANOVA and student t test used to test for statistical significance between lines none was found, one sample t tests were used to test preference against hypothetical 0 value, significance is stated after mean values, N≥4.*

6.8: Conclusions and discussion

Behavioural readouts were found to be altered in all mutant lines. The behavioural data for longevity motor function and learning and memory for mutant lines in comparison to controls is summarised in Table 6.1

Table 6.1: Summarized significant results for behaviour in mutant lines in comparison to relevant controls

	wstd[1]	**M80T**	**I170V**	**Glo(KO)**
Longevity 25°C	Longevity was reduced ****p <0.0001	Longevity was reduced ****p <0.0001	Longevity was reduced ****p <0.0001	Longevity was reduced ****p <0.0001
Longevity 29°C	Longevity was reduced ****p <0.0001	Longevity was reduced ****p <0.0001	ns	N/A
Longevity H_2O_2	Longevity was reduced with H_2O_2 treatment compared to water ****p <0.0001	Longevity was increased with H_2O_2 treatment compared to water ***p<0.0005	Longevity was reduced with H_2O_2 treatment compared to water ****p <0.0001	Longevity was reduced with H_2O_2 treatment compared to water ****p <0.0001
Longevity glutathione	ns	ns	ns	Longevity was reduced with glutathione treatment compared to water ***p<0.001
Circadian rhythm	Poorer circadian control, less overall sleep	N/A	Poorer circadian control, more overall sleep	N/A
Larval crawling	Larvae treated ***p<0.001 and untreated *p<0.05 with H_2O_2 travelled further than untreated	Distance travelled was increased ****p <0.0001	N/A	N/A

	w^{1118} and turned less than $wstd^{1}$ untreated larvae *p<0.05			
Adult climbing	Climbing was reduced in 5 and 20 day old flies ****p <0.0001	Climbing was reduced in 5 day old females **p<0.005 and males ****p <0.0001 and in 20 day old flies ****p <0.0001	Climbing was increased in 5 day old females ***p<0.001, and males ****p<0.0001 and in 20 day old flies **p<0.005	N/A

The I170V line showed reduced longevity at 25 °C but not to the extent of the *Sugarkill* mutants, reinforcing the hypothesis that this mutation of TPI leads to a less extreme loss of function and the previously reported lifespan data for this line (Roland et al. 2014). Longevity was not significantly altered at 29 °C in comparison to controls, in contrast to the *Sugarkill* mutants that have been reported as temperature sensitive mutations (Palladino et al. 2002), this could suggest a better compensation and stress resistance in the I170V line, possibly due to the increased levels of TPI protein seen in Section 5.4. Reduced longevity with H_2O_2 was expected and shows that the I170V line is affected by increases in environmental redox stress (Gnerer et al. 2006; Hrizo et al. 2013; Stone et al. 2023). The circadian rhythm studies suggest that in the I170V line there is a poorer regulation of the day-night cycle, with more regular and more frequent sleeps, but shorter sleeps at night and reduced activity while awake. The I170V line appeared to sleep more overall compared to control lines, this could suggest a possible route of compensation, reducing overall energetic output. Males appeared to be more active in adult flies for I170V, both sexes however showed significantly increased climbing behaviour in comparison to controls. This corroborates the sex difference in this pathology, but does also suggests that both sexes see a similar dysfunction. The overall increase in climbing could suggest an overall increase in activity, however the climbing assay does not take into account flies that fly rather than crawl over the threshold, so it is possible we are seeing a reduction in flying activity rather than an overall increase in activity. Given flying is a highly energy taxing process this could in fact show the opposite with a reduction in overall activity seen by an increase in crawling over flying.

wstd^{1} and M80T as expected showed significantly reduced longevity at 25 °C (Celotto et al. 2006b; Celotto et al. 2006a; Gnerer et al. 2006; Seigle et al. 2008). Both lines also showed reduced longevity at 29 °C, the larger impact of this temperature change on control lines compared to *Sugarkill* mutants (wstd^{1} and M80T) support the previous suggestion that increased temperatures reduce TPI protein stability (disproportionately for mutant proteins) and increase the activity of molecular chaperones and enhance degradation of TPI via proteosomes (Olah et al. 2002; Hrizo and Palladino 2010). The increased impact of temperature on controls could suggest that in the *Sugarkill* mutants (wstd^{1} and M80T) this degradation pathway is closer to saturation, so the increased temperature has a smaller impact.

The M80T line shows an increased longevity with Glutathione treatment which could suggest that unlike all other lines M80T does see some benefit from the antioxidant treatment (Bonilla et al. 2006). However, this line also shows an increased longevity when treated with H_2O_2 which is unexpected. This possibly suggests that the presence of the H_2O_2 triggers alternative functional pathways with compensatory or protective mechanisms somehow improving disease phenotypes. It could be beneficial to repeat this study with altered dosages of H_2O_2 or alternative stressors, to see at what concentration this protective pathway is saturated and lifespans start to drop again or if the pathway is specific to H_2O_2.

A reduced lifespan would be expected with H_2O_2 treatment due to increased oxidative stress (Gnerer et al. 2006; Fukai and Ushio-Fukai 2011; Hrizo et al. 2013; Stone et al. 2023), that no change is seen in the wstd^{1} line could again suggest a plateau phenotype in the redox stress associated reduction in lifespan in this line.

The M80T line showed increased distance travelled by larvae. In adult fly climbing however a reduction in activity was found which suggests a glycolytic change in this line with higher energy at larval stage and lower energy in adult flies. The sex difference seen in climbing activity of 5 day old flies supports the hypothesis from the I170V line that TPI dysfunction may be sex linked.

The circadian data collected for the wstd^{1} line suggests that, similarly to I170V, there is less effective control of the day-night cycle. For wstd^{1} this is shown with longer and more frequent sleeps in the light and shorter sleeps in the dark with flies taking longer to get to sleep in the dark. The wstd^{1} line slept less overall compared to controls, in counter to I170V. This is shown by a reduction in activity while awake in the dark and shorter sleeps in the dark and second 12 hrs. Although in the 12 hr light-dark cycle wstd^{1} appears to compensate more effectively with increased sleep in the light, this is not unexpected as the

dysregulation of the circadian clock is generally worsened without light cues (Dubowy and Sehgal 2017; Breda et al. 2020; Johnson et al. 2023). The $wstd^1$ line was not included in the old age data set as the flies were too practically difficult to keep alive for the length of experiment, given the median lifespan at 25 °C is 30 days this is unexpected. This is particularly surprising in 24 hr dark and with socially isolated flies, as it has been widely reported that in constant darkness and socially isolated *Drosophila* live longer (Leech et al. 2017; Lin et al. 2022; Johnson et al. 2023).

$wstd^1$ larvae treated with H_2O_2 travelled further than w^{1118} larvae fed a standard diet, this could suggest that the $wstd^1$ dysfunction is similar to that of M80T but less extreme, so the effect is only observed with the increase in environmental redox stress. They also showed reduced turning activity with treatment possibly showing reduced control of motor activity. This data set did not manage to include the Canton.S line as a more comparable control, but the result is still relevant as w^{1118} can be used as a wild type phenotype in comparison to $wstd^1$.

Climbing activity was significantly reduced in $wstd^1$ flies of both sexes and ages. This was as significant as possible in all data sets, so it is possible the sex difference observed in the other mutant lines was present, but the data sets were too extreme to distinguish differences with this technique.

The reduced climbing ability in $wstd^1$ and M80T is in contrast to the I170V line, corroborating the hypothesis that dysfunction is distinct between the I170V and *Sugarkill* mutants.

The Glo(KO) line showed reduced longevity which was enhanced by treatment with H_2O_2, in contrast to previously published work which showed an increase in longevity in this line (Moraru et al. 2018). The increased lifespan found was explained by the presence of MGO which was suggested to promote a negative feedback loop minimising the production of DHAP from G3P. The methodology differed in that the previously published work was only done in female flies this could suggest a sex difference in this line. As the result found in this work was a reduced lifespan, an alternate pathway of MGO promoting damage via AGE production seems likely.

The lack of significant differences and broad data sets found in longevity experiments with glutathione treatment gave an unclear picture. Altered doses could be investigated, however the breadth of response could be explained simply as the glutathione is not reaching the required synapses in the required form to be consistently beneficial. The antioxidant properties of glutathione are well established, however they rely on both the ingested glutathione spreading through the system, and the glutathione being in or being converted to a

reduced state before antioxidant activity can occur (Chyan et al. 1994; Bonilla et al. 2006; Mason et al. 2013; Dias et al. 2016).

6.9: Future directions

Possible future experiments could use different doses of treatments or a fixed form of glutathione alongside other dietary antioxidants and redox stressors to better investigate whether use of antioxidants, or avoidance of redox stressors could provide a potential route for treatments or disease preventions. Including all lines in data sets, such as circadian rhythm would also be beneficial, as well as further investigating the sex differences in disease expression.

Chapter 7: Overall Discussion

7.1: Conclusions for individual mutant lines

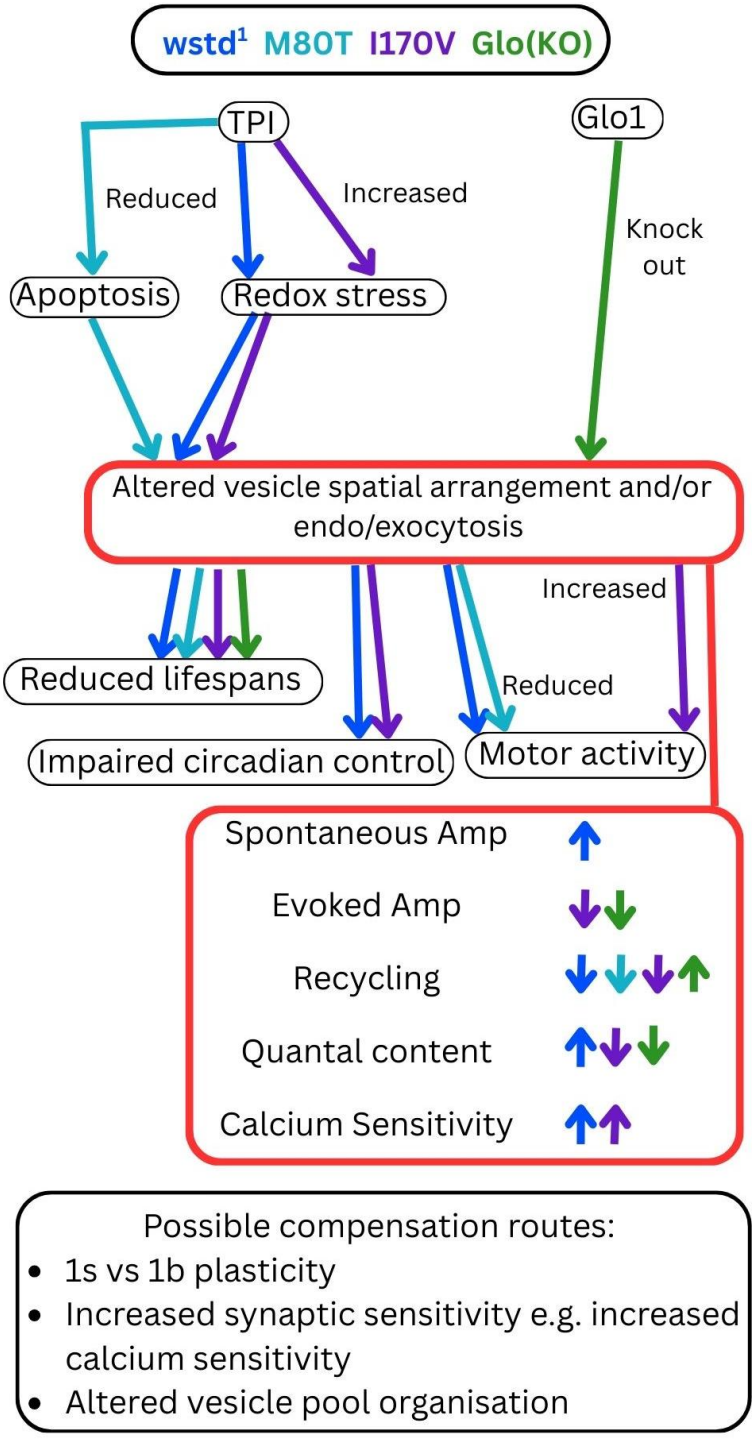

Figure 7-1: Summary of thesis. Main results for wstd[1] (blue), M80T (cyan), I170V (purple), and Glo(KO) (green) mutant lines. Reduction and increase of TPI expression in wstd[1], M80T, and I170V lines increases in significance with age in comparison to controls. Possible compensation routes suggested in black box. Only connections with supporting evidence from significant data sets presented in this thesis are shown.

The data collected on the TPI mutant I170V suggests that a reduced release of vesicles is present in these synapses, possibly due to an altered vesicle spatial arrangement or altered recycling mechanisms. Calcium dependency in this line was altered, maximal release occurring at lower calcium concentration in I170V than in the control w^{1118}; this could be due to a higher expression of TPI. By Western blot TPI expression was increased in this line suggesting a reduced clearance of TPI from synapses, possibly an indication of a stronger dimerization in this mutant TPI as previously suggested (Roland et al. 2014). Redox stress does seem to be increased in this line with levels of AGE seen to be increased compared to controls, corroborating the hypothesis that dysfunction stems from increased redox stress via AGE formation (Gnerer et al. 2006; Hrizo et al. 2013; Stone et al. 2023). Overall behaviour was also altered in this line with reduced lifespans, poorer circadian rhythm control, reduced crawling in male I170V larvae, and increased climbing in adult I170V flies. The apparent sex difference in crawling and climbing activity suggests, like in Glo(KO) which showed a sex difference in longevity, that this dysfunction is sex linked, an effect previously unreported in the literature.

Data collected for the TPI mutant $wstd^{1}$ suggests that vesicles are larger or contain more glutamate by sEJP amplitude measurements. Vesicles in this line may also have a higher release probability or a larger ready releasable pool than in controls as the quantal content from sEJC/eEJC was seen to increase with no change in sEJC amplitudes. However as individual eEJC amplitudes were also unchanged, this puts the increased quantal content into question as the quantal content derivation was from a smaller data set than the eEJC or sEJC single amplitude data sets. Calcium dependence was altered as in I170V, lower calcium concentrations were required for maximal eEJC response. However the effect was smaller in this mutant, which could be explained by the higher release probability in this line suggested by the sEJC, sEJP, and eEJC measurements. Depletion and recovery plots also suggest that recycling of vesicles is impaired in this line. Reduced TPI expression in larvae and adult flies supports the previous suggestion that mutant TPI is more readily cleared away from synapses than wild type TPI (Seigle et al. 2008; Hrizo and Palladino 2010; Roland et al. 2019). Redox stress was found to be increased in this line by quantification of AGE. Overall behaviour was also found to be altered with dramatically reduced lifespans, poorer circadian rhythm control, and reduced climbing ability as expected from previously published work (Gnerer et al. 2006; Seigle et al. 2008; Hrizo and Palladino 2010). Unlike other lines this line did not show sex differences in behaviour, however effects were generally higher significance, so it is possible a sex difference was present but unable to be

identified by the techniques used here, and an alternative, more sensitive test is required if detailed sex differences were relevant. Although as the comparisons to controls in this line were highly significant in both sexes, the sex-independent mechanism of disease is more interesting in this case than any possible sex differences.

The data presented for the M80T line suggests a reduced vesicle release, from the potentiation at the start of the 60 Hz train. This effect was not seen in single eEJC amplitudes or other trains however, so was not as extreme a phenotype as in the Glo(KO) line. Vesicle organisation or recycling are likely to also be altered in this line based on the depletion and recovery data. Similar to wstd[1], TPI expression was dramatically reduced, an effect that increased with age. This corroborates the previous suggestion of increased TPI clearance in these *Sugarkill* lines (Seigle et al. 2008; Hrizo and Palladino 2010). No markers for redox stress were found to be increased in this line but cell death was seen to be increased in adult 20 day old fly brains. An increase in active zone (BRP) area was found in this line, which could connect to altered vesicle release mechanisms as BRP has been shown to facilitate vesicle release for olfactory memory in *Drosophila* (Knapek et al. 2011). Alterations in overall animal behaviour were also found in this line with dramatically reduced lifespans, increased crawling activity in larvae and reduced climbing activity in adult flies, an effect which is also increased with age of flies, as expected from literature data on *Sugarkill* mutants (Gnerer et al. 2006; Seigle et al. 2008; Hrizo and Palladino 2010). Sex differences in climbing activity are seen in young flies supporting the data from the Glo(KO) and I170V lines that this mechanism is somehow sex linked. The increased lifespans seen in this line with treatments of glutathione and H_2O_2 were not seen in any other mutant or control line. For glutathione treatment this could indicate an antioxidant effect. As no change in redox stress markers were found in this line it is possible redox stress is only marginally increased so the antioxidant is able to make a significant difference that is not observed in other mutants. The increased lifespan seen with H_2O_2 treatment was unexpected and the route of this mechanism is unclear, it is possible this increase is due to a compensation mechanism triggered by the increased redox stress, one way to check this would be to quantify redox states of key markers such as MGO and levels of redox stress in synapses both pre and post exposure in this line.

The data for the glyoxalase mutant Glo(KO) suggests that the vesicle organisation in this line is altered and that fewer vesicles are released per single stimulation. This suggests that the spatial arrangement and so release of vesicles is reduced in this line compared to controls. The reduced longevity found in mixed gender vials of this line, counter to previously reported findings

of increased longevity in female flies (Moraru et al. 2018), implies that the dysfunction in this line is sex linked. However this difference could also be due to a change in availability of mates which has been previously suggested to affect longevity (Fowler and Partridge 1989; Markow 2011).

7.2: Overall discussion and future work

The work presented here gives a detailed picture of the complicated pathology of four Drosophila mutant models of neurodegenerative disease. Specifically investigating the connection between the glycolysis cascade, redox stress, and synaptic function, and how specifically TPI dysfunction impacts on pathology.

The data for mutant lines expressing dysfunctional TPI enzyme strongly suggests that pathology is directly connected to impaired vesicle dynamics. All three TPI mutant lines showed reduced vesicle recycling, which is counter to the Glo(KO) line, that appeared to show an increased rate of vesicle recycling. Alternately, the faster recovery in Glo(KO) could be explained by an altered vesicle pool organisation, with pools sitting further from release sites so the rate limiting factor in release would be the vesicles moving to the cell membrane. This could also explain the potentiation seen in this line as the bulk of the required vesicles would take longer to reach release sites giving a delayed maximal response. These two possibilities could be further investigated by application of a longer train stimulation at 60 Hz to ensure a steady state of release is reached, as depletion in the Glo(KO) line was not found to plateau at the ends of trains it can not be assumed that the response was limited to vesicle recycling as it can in other lines.

Altered vesicle organisation is implied in this work for all mutant lines by at least one measure, because of this the first experiments I would set up if I were continuing this work would be a complete electron microscopy study to quantify vesicle pool organisation, and FM1 live imaging to quantify vesicle recycling during train stimulation and recoveries (Ramaswami et al. 1994; Robinson et al. 2017).

Another experiment that would further help to identify the exact causes of augmented synaptic transmission would be electrophysiological experiments with precisely controlled stimulation. This would allow separation of the two excitatory motor neurons that are present in *Drosophila* NMJs: 1s which has less spontaneous activity and larger quantal sizes and; 1b which has more spontaneous activity and smaller quantal sizes. These two motor neurons have been shown to compensate for each other (Wang et al. 2021), this form of

compensation could explain some of the phenotypes we see in the mutant lines described here. For example the reduced quantal contents and increased frequency of sEJP events in the I170V line could imply that the 1s neuron is disproportionately impacted by dysfunction, and the 1b neuron activity is increased to compensate. A similar explanation could also fit the data for the Glo(KO) line. The wstd^{1} line in counter, shows increased quantal content and larger vesicles, that this line is also unable to maintain firing or recover as controls following high frequency stimulation, could imply a reduced number of available vesicles. This all could be explained by a reduction in the 1b line and compensation by the 1s. Separating and individually investigating these pathways therefore would be invaluable to define the differences in pathology and compensation mechanisms in the different TPI and Glo mutant lines.

As shown previously in the *Sugarkill* TPI mutants (wstd^{1} and M80T) TPI expression is reduced (Seigle et al. 2008), an effect that in the M80T line is shown to increase with age by the Western blot data presented here. This degradation has been suggested to be due to increased proteosome activity via molecular chaperones that recognise the mutant TPI as a misfolded protein, this is a strong possibility in the *Sugarkill* lines as they have been reported to show reduced TPI enzyme stability (Seigle et al. 2008; Hrizo and Palladino 2010). That this effect is reversed in the I170V line – which has been reported to express a more stable TPI enzyme - (Roland et al. 2014) strongly suggests that part of the mechanism for dysfunction in the *Sugarkill* (wstd^{1} and M80T) mutants is an altered cell clearance mechanism, which could also explain the different pathology seen in the I170V line. In *Human* TPI deficiency one cause of pathology has been suggested to be due to impaired dimerization in the TPI protein, and subsequent clearance of the monomer (Olah et al. 2002). As all three mutant TPI proteins are reported to be capable of dimerization (Celotto et al. 2006b; Seigle et al. 2008; Roland et al. 2014), this may not be the case in the *Drosophila* mutants described here. Although the two *Sugarkill* mutations have been shown to lead to an enzyme of reduced stability (Olah et al. 2002; Hrizo and Palladino 2010) which could lead to a similar pathology, the I170V mutation has been shown to increase enzyme stability (Roland et al. 2014). The increase in TPI expression observed in the I170V line could suggest a reduced clearance, possibly due to the more stable dimerization (Roland et al. 2014). The physical impact of having more TPI protein present in synapses is unknown, but could have a compensatory or a pathological effect.

Although dimerization of TPI in some mutants like I170V has been reported to not be impaired by the mutation (Roland et al. 2014), in the *Sugarkill* mutants (wstd^{1} and M80T) this is just an indirect suggestion based on catalytic viability. The previous suggestion that ATP levels are unaffected in TPI mutants (Celotto

et al. 2006b; Gnerer et al. 2006; Hrizo et al. 2013) does not fit with the reported significant reduction in TPI expression and correlated reduction in physical activity. Both of these effects appear to be increased over age and, given the lack of energetic deficit has only been reported in young flies, checking ATP levels in all lines at various age points would be prudent to confirm no deficit is found in any of the mutants throughout lifespans. The altered circadian rhythm shown here for wstd^{1}, namely the overall reduction in sleep and activity, also suggests an altered energetic availability in these flies. There is an altered circadian rhythm seen in I170V as well with increased levels of overall sleep, which could suggest reduced energetic availability, however there is not a change in physical activity. The catalytic efficiency in the I170V mutant TPI is reduced compared to controls, so having more enzyme present could compensate for this allowing for the maintained activity levels. However the physical placement of this enzyme could also impact on the spatial organisation of boutons, as TPI has been associated with vesicle dynamics (Roland et al. 2016; Stone et al. 2023) this could be the cause of the perceived change in vesicle organisation in this line.

Mitochondrial dysfunction has been suggested as a cause of pathology in *Drosophila* following redox stress and hyperoxia, and has been described as having a more significant impact on neurodegenerative disorders than redox stress alone (Walker and Benzer 2004; McBean et al. 2016). Both inhibition of cytochrome c oxidase, and physical changes in mitochondria cristae termed 'swirls' were described, leading to apoptotic cell death predominantly in flight muscles. Flying is an energy taxing process, and flies have developed a mitochondrial system to manage this. The number of mitochondria, mitochondrial positioning in the abdomen, and mitochondrial efficiency are all optimised in *Drosophila*. The increase in efficiency is tightly related to the ease of Ca movement – relaxation requiring the movement of Ca ions against the gradient back into the muscle's sarcoplasmic reticulum (Mesquita et al. 2021). If this pathway is impacted by TPI mediated increases in redox stress, this could explain the decreased activity seen in *Sugarkill* mutant (wstd^{1} and M80T) flies, and possibly the increased climbing in I170V flies. Celotto et al have previously reported that no change in mitochondria was seen in the *Sugarkill* mutants, however this was only checked at 5 days old so could still be relevant for dysfunction in aged flies (Celotto et al. 2006b). The I170V pathology seems to be less extreme than in the *Sugarkill* mutants, which could be that a route to pathology via mitochondrial dysfunction is present in both lines, but the rate of disease progression is different. Assuming flight muscles are the first to be impacted by a redox stress dysfunction due to the energetic requirements of flying, then initially climbing activity is likely to increase, as is observed in I170V.

This would continue until the dysfunction became large enough to impact all motor activity, as is seen in the *Sugarkill* lines.

Imaging mitochondria to check lines for an increased presence of swirls at various age points in these mutants could confirm this hypothesis. Similarly checking cytochrome c oxidase activity would also help to confirm this hypothesis.

As discussed in chapter 1 inhibition of cytochrome c oxidase has been shown via gases such as NO and CO in an oxygen dependent manner (Cooper and Brown 2008). Hyperoxic conditions (100% O_2) have been shown to increase degradation of muscle, and induce mitochondrial dysfunction in *Drosophila* (Walker and Benzer 2004), although *Drosophila* have also been reported to be generally resistant to hypoxia (Romero et al. 2007). In *Drosophila* larvae oxygen is circulated by a tracheal system that branches out into tissue (Ghabrial et al. 2003). This system is not presently fully understood, with various cells, proteins, and co-factors being reported as having a role in oxygen supply control (Jarecki et al. 1999; Centanin et al. 2008; Grifoni et al. 2015; Shin et al. 2024). This all suggests that oxygen availability is likely to impact on synaptic activity, TPI dysfunction also being strongly linked to oxygen and reactive oxygen species (ROS) (Gnerer et al. 2006; Hrizo et al. 2013; Enriquez-Flores et al. 2023; Stone et al. 2023), makes the system of oxygen supply and connected dysfunctions highly relevant in these pathways. Therefore, as the fileted electrophysiology method presented here is run in atmospheric conditions (O_2 ~20%), this could impact on electrophysiological recordings and synaptic health, so running experiments at physiological oxygen concentrations would be a beneficial future study to more accurately record *in vivo* synaptic activity in these lines.

Altered cytochrome c oxidase in mitochondria has also been linked to altered behaviour including altered dietary preferences, as previously mentioned (Mesquita et al. 2021). This could impact on food based treatments, with H_2O_2 and glutathione treatments being added on the surface of food rather than mixed homogenously, so it could be possible some lines are avoiding the treatments more than others. Innate preferences for AM however were not found to be significantly different. Running these innate preference experiments with all treatments would give an indication if this effect was pronounced enough to significantly impact the amount of treatment individuals are exposed to. If this was found to be significant this could lead to a better understanding of how dietary treatments for TPI related disorders may be organised and how effective they are likely to be.

Bruchpilot (BRP) is also connected to memory formation, via facilitation of vesicle release in olfactory memory (Knapek et al. 2011). BRP expression was

not found to be significantly altered, however as this data was only collected for larvae it could be worth checking BRP expression in adult flies to see if a difference is found which could link into the observed alterations in vesicle dynamics.

Treatments with glutathione and H_2O_2 showed some unexpected results, particularly with the M80T line exhibiting increased lifespans with treatments of either factor. Neither of these compounds are perfect for redox stress or antioxidant treatment physiologically. Glutathione, as previously mentioned, to act as an antioxidant needs to first reach the required synapse and to be reduced before it can be functional. This, in the glycolysis cascade in *Drosophila*, relies on the glyoxalse 1 enzyme and the protective path discussed previously, shown in green in Figure 1-1. In the TPI mutant lines this pathway is thought to be maximally activated by the increase in DHAP from the dysfunctional TPI enzyme. Glo1 enzyme activity is known to be impaired when cellular levels of glutathione are compromised (Nigro et al. 2017), therefore increasing cellular glutathione will increase Glo1 function and should improve pathology in these lines. This benefit however is dependent on the state of catalysis. If the available Glo1 enzyme is functioning to capacity no additional benefit would be seen with glutathione treatment. Therefore, a prudent further experiment would be to quantify the saturation of this pathway, confirming whether this pathway is indeed maximally activated in the *Sugarkill* TPI mutant lines.

Using other redox stressors and antioxidants would also be beneficial to better understand the different pathologies stemming from the various TPI mutations. However, it may be more useful for application of this research to take these broader physiology treatment options into a mammalian model, that would better mimic *Human* digestion and pharmacodynamics.

The Glo(KO), I170V, and M80T lines all showed sex differences in disease expression, dysfunction seemingly impacting disproportionately on males. Electrophysiological data however did not show this difference. However, all electrophysiological data shown here was collected on larvae, and the sex differences seen in behaviour were more common in flies than larvae, possibly as dysfunction becomes more pronounced with age. Collection of a small electrophysiology data set in adult flies could show if synaptic dysfunction is sex linked, or the sex differences seen in behaviour read-outs stem from mechanisms downstream of synaptic function.

Investigating *Drosophila* lines that over express TPI or Glo1 enzymes would be beneficial to further probe the varying mechanisms of dysfunction. The Glo overexpressing line was investigated throughout this project but genetic expression was not successful with no significant increase in protein expression

by Western blot (data in Appendix). These data sets would still be useful additions to better understand this pathway, however genetic confirmation by PCR and subsequent genetic clean up would be required before the lines could be used effectively.

It is important to note that dementia and other neurodegenerative disorders rarely appear alone but more often than not exist as comorbidities, so models based on an individual protein modification are only one piece of the puzzle. This should also be considered when moving into mammalian models as various mechanisms discussed here are also implicated in other disease phenotypes such as in vascular damage (Nigro et al. 2017). Although it is clear that the synaptic dysfunctions described here would be prudent mechanisms to consider in human cases of neurodegeneration, particularly given the conservation of the pathways investigated here in human central nervous systems (Bradley and Steinert 2015; Robinson et al. 2017). Another important aspect to consider when applying this understanding of the impact of dysfunctional TPI to Alzheimer's disease or any late onset neurodegeneration, is the stage of disease progression. For example, if species known to increase post translational modifications via redox stress pathways such as Aβ(Ill-Raga et al. 2010) are present, then targeting functionality of TPI may not be particularly useful as TPI is a known target of such modifications. However targeting post translational modifications could be beneficial and has been suggested for a possible treatment route. For example, targeting TPI deamidation, a common post translational modification in TPI pathology, has been reported (Enriquez-Flores et al. 2020). Treatments to compensate for the reduced enzyme activity such as the removal of excess DHAP could also be beneficial, although any effects observed would only be temporary, and require repetitive treatments.

For early onset diseases like TPI deficiency, targeting TPI activity could be hugely beneficial, either directly in activity of the enzyme itself or indirectly via removal of excess DHAP. Identifying lifestyle factors that could boost and support the possible pharmacological effects would also be highly beneficial, rather than focusing solely on pharmacology. This is particularly relevant in early onset illnesses where the huge quantity and variety of phenotypes leads patients to have many overlapping prescriptions, a situation that often leads to a reduced overall quality of life.

Chapter 8: References

Acuna, C., Guo, Q., Burre, J., Sharma, M., Sun, J. and Sudhof, T. 2014. Microsecond Dissection of Neurotransmitter Release: SNARE-Complex Assembly Dictates Speed and Ca2+ Sensitivity. Neuron 82(5), pp. 1088–1100.

Aigaki, T., Seong, K. and Matsuo, T. 2002. Longevity determination genes in Drosophila melanogaster. Mech Ageing Dev. 123(12), pp. 1531–1541.

Akbergenova, Y. and Bykhovskaia, M. 2007. Synapsin maintains the reserve vesicle pool and spatial segregation of the recycling pool in Drosophila presynaptic boutons. Brain research 1178, pp. 52–64.

Akiyama, H. et al. 2000. Inflammation and Alzheimer's disease. Neurobiology of ageing 21(3), pp. 383–421.

Alderton, W., Cooper, C. and Knowles, R. 2001. Nitric oxide synthases: structure, function and inhibition. Biochem. J. 357, pp. 593–615.

Benzer, S. 1967. Behavioural mutants of Drosophila isolated by countercurrent distribution. Genetics 58, pp. 1112–1119.

Bonilla, E., Medina-Leendertz, S., Villalobos, V., Molero, L. and Bohorquez, A. 2006. Paraquat-induced Oxidative Stress in Drosophila melanogaster: Effects of Melatonin, Glutathione, Serotonin, Minocycline, Lipoic Acid and Ascorbic Acid. Neurochemical Research, pp. 1425–1432.

Bourgognon, J. et al. 2021. Inhibition of neuroinflammatory nitric oxide signaling suppresses glycation and prevents neuronal dysfunction in mouse prion disease. Proceedings of the National Academy of Sciences of the United States of America 118(10).

Bradley, S. and Steinert, J. 2015. Nitric oxide-mediated posttranslational modifications: Impacts at the synapse. Oxidative Medicine and Cellular longevity 2016, pp. 1–9.

Breda, C., Rosato, E. and Kyriacou, C. 2020. Norpa Signalling and the Seasonal Circadian Locomotor Phenotype in Drosophila. Biology 9(6).

Bredt, D., Glatt, C., Hwang, P., Fotuhi, M., Dawson, T. and Snyder, S. 1991. Nitric oxide synthase protein and mRNA are discretely localized in neuronal populations of the mammalian CNS together with NADPH diaphorase. Neuron 7(4), pp. 615–624.

Brent, J., Werner, K. and McCabe, B. 2009. Drosophila larval NMJ dissection. J Vis Exp 4(24).

Bruns, D., Riedel, D., Klingauf, J., Jahn, R. 2000. Quantal release of serotonin. Neuron 28, pp. 205-220.

Bykhovskaia, M. and Vasin, A. 2017. Electrophysiological Analysis of Synaptic Transmission in Drosophila. Wiley Interdiscip Rev Dev Biol 6(5).

Care Policy and Evaluation Centre. 2019. What are the costs of dementia care in the UK? Available at: https://www.alzheimers.org.uk/about-us/policy-and-influencing/dementia-scale-impact-numbers [Accessed: 14 March 2024].

Castillo, J., Katz, B. 1954. Quantal components of the end-plate potential. J. Physiol. 124, pp. 560-573.

Celotto, A. et al. 2006a. Mitochondrial encephalomyopathy in Drosophila. J Neurosci. 26(3), pp. 810–820.

Celotto, A., Frank, A., Seigle, J. and Palladino, M. 2006b. Drosophila model of human inherited Triosephosphate Isomerase deficiency glycolytic ezymopathy. Genetics 174, pp. 1237–1246.

Centanin, L., Dekanty, A., Romero, N., Irisarri, M., Gorr, T. and Wappner, P. 2008. Cell Autonomy of HIF Effects in Drosophila: Tracheal Cells Sense Hypoxia and Induce Terminal Branch Sprouting. Developmental Cell 14(4), pp. 547–558.

Cho, R., Buhl, L., Volfson, D., Tran, A., Li, F., Akbergenova, Y. and Littleton, J. 2015. Phosphorylation of Complexin by PKA Regulates Activity-dependent Spontaneous Neurotransmitter Release and Structural Synaptic Plasticity. Neuron 88(4), pp. 749–761.

Chyan, M., Elia, A., Principato, G., Giovannini, E., Rosi, G. and Norton, S. 1994. S-Fluorenylmethoxycarbonyl Glutathione and Diesters: Inhibition of Mammalian Glyoxalase II. Enzyme and Protein 48(3), pp. 164–173.

Cooper, C. and Brown, G. 2008. The inhibition of mitochondrial cytochrome oxidase by the gases carbon monoxide, nitric oxide, hydrogen cyanide and hydrogen sulfide: chemical mechanism and physiological significance. J Bioenerg Biomembr 40(5), pp. 533–539.

Cortizo, F. et al. 2022. The activity of glyoxylase 1 is regulated by glucose-responsive phosphorylation on Tyr136. Molecular Metabolism 55.

Cruz, P., Cossins, J., Beeson, D. and Vincent, A. 2020. The Neuromuscular Junction in Health and Disease: Molecular Mechanisms Governing Synaptic Formation and Homeostasis. Front. Mol. Neurosci.

Cuddy, L., Gordon, A., Black, S., Jaworski, E., Ferguson, S. and Rylett, R. 2012. Peroxynitrite Donor SIN-1 Alters High-Affinity Choline Transporter Activity by Modifying Its Intracellular Trafficking. Journal of Neuroscience 32(16), pp. 5573–5584.

Dahmann, C. ed. 2016. Drosophila - Methods and Protocols. 2nd ed.

Danysz, W. and Parsons, C. 2012. Alzheimer's disease, β-amyloid, glutamate, NMDA receptors and memantine – searching for the connections. Br J Pharmacol 167(2), pp. 324–352.

Dias, C., Lourenco, C., Ferreiro, E., Barbosa, R., Laranjinha, J. and Ledo, A. 2016. Age-dependent changes in the glutamate-nitric oxide pathway in the hippocampus of the triple transgenic model of Alzheimer's disease: implications for neurometabolic regulation. Neurobiology of ageing 46, pp. 84–95.

Driscoll, M., Hyland, C. and Sitaraman, D. 2019. Measurement of Sleep and Arousal in Drosophila. Bio-protocol 9(12).

Dubowy, C. and Sehgal, A. 2017. Circadian Rhythms and Sleep in Drosophila melanogaster. Genetics 205(4), pp. 1373–1397.

Enriquez-Flores, S. et al. 2020. Deamidated Human Triosephosphate Isomerase is a Promising Druggable Target. Biomolecules 10(7).

Enriquez-Flores, S., De la Mora, I., Garcia-Torres, I., Flores-Lopez, L., Martinez-Perez, Y. and Lopez-Velazquez, G. 2023. Human Triosephosphate Isomerase Is a Potential Target in Cancer Due to Commonly Occurring Post-Translational Modifications. Molecules 28(16).

Erxleben, C., Kriebel, M. 1988. Characteristics of spontaneous miniature and subminiature end-plate currents at the mouse neuromuscular junction. Journal of Physiology 400, pp. 645-658.

Feng, Y., Ueda, A. and Wu, C. 2004. A modified minimal hemolymph-like solution, HL3.1, for physiological recordings at the neuromuscular junctions of normal and mutant Drosophila larvae. Journal of Neurogenetics 18(2), pp. 377–402.

Ferguson, M., Mockett, R., Shen, Y., Orr, W. and Sohal, R. 2005. Age-associated decline in mitochondrial respiration and electron transport in Drosophila melanogaster. Biochem J. 390(2), pp. 501-511.

Fernandez-Funez, P., Mena, L. and Rincon-Limas, D. 2015. Modeling the complex pathology of Alzheimer's disease in Drosophila. Exp Neurol. 274(0), pp. 58–71.

Fowler, K. and Partridge, L. 1989. A cost of mating in female fruitflies. Nature 338, pp. 760–761.

Friebe, A. and Koesling, D. 2003. Regulation of Nitric Oxide-Sensitive Guanylyl Cyclase. Circulation research 93, pp. 96–105.

Fukai, T. and Ushio-Fukai, M. 2011. Superoxide dismutases: role in redox signaling, vascular function, and diseases. Antioxid Redox Signal. 15(6), pp. 1583–1606.

Ganetzky, B. 2015. Triosephosphate Isomerase Deficiency. Available at: https://rarediseases.org/rare-diseases/triosephosphate-isomerase-deficiency/ [Accessed: 14 March 2024].

GARD. 2023. Triosephosphate isomerase deficiency. Available at: https://rarediseases.info.nih.gov/diseases/5287/triosephosphate-isomerase-deficiency [Accessed: 26 June 2023].

Ghabrial, A., Luschnig, S., Metzstein, M. and Krasnow, M. 2003. Branching Morphogenesis of the Drosophila Tracheal System. Annual review of cell and developmental biology 19, pp. 623–647.

Gill, V., Kumar, V., Singh, K., Kumar, A. and Kim, J. 2019. Advanced Glycation End Products (AGEs) May Be a Striking Link Between Modern Diet and Health. Biomolecules 9(12).

Gnerer, J., Kreber, R. and Ganetzky, B. 2006. wasted away, a Drosophila mutation in triosephosphate isomerase, causes paralysis, neurodegeneration, and early death. PNAS 103(41), pp. 14987–14993.

Goedert, M. and Spillantini, M. 2006. A Century of Alzheimer's Disease. Science 314(5800), pp. 777–781.

Greenspan, R. 2004. Fly Pushing - The Theory and Practice of Drosophila Genetics. 2nd ed. Inglis, J. ed.

Grifoni, D., Sollazzo, M., Fontana, E., Froldi, F. and Pession, A. 2015. Multiple strategies of oxygen supply in Drosophila malignancies identify tracheogenesis as a novel cancer hallmark. Nature Scientific reports 5(9061).

Grzelczak, M.P., Hill, A.P., Belic, D., Bradley, D.F., Kunstmann-Olsen, C. and Brust, M. 2016. Design of artificial membrane transporters from gold nanoparticles with controllable hydrophobicity. Faraday Discussions 191, pp. 495–510. doi: 10.1039/c6fd00037a.

Guix, F. et al. 2009. Amyloid-dependent triosephosphate isomerase nitrotyrosination induces glycation and tau fibrillation. Brain 132(5), pp. 1335–1345.

Guo, Y. et al. 2024. Plasma proteomic profiles predict future dementia in healthy adults. Nature Aging 4, pp. 247–260.

Hambsch, B. et al. 2010. Methylglyoxal-mediated anxiolysis involves increased protein modification and elevated expression of glyoxalase 1 in the brain. Journal of Neurochemistry 113(5), pp. 1240–1251.

Harris, C., Nelson, B., Farber, D., Bickel, S., Huxol, H., Asamoah, A. and Morton, R. 2020. Child Neurology: Triosephosphate isomerase deficiency. Neurology 95(24).

Hartline, R. 2023. LibreTexts Biology 1.19: Cytochrome c Oxidase. In: Microbiology Laboratory Manual . West Hills College Lemoore.

Hay, B. and Guo, M. 2006. Caspase-dependent cell death in Drosophila. Annu Rev Cell Dev Biol. 22, pp. 623–650.

He, Q., Wu, B., Price., Zhao, Z. 2017. Circadian Rhythm Neuropeptides in Drosophila: Signals for Normal Circadian Function and Circadian Neurodegenerative Disease. Int J Mol Sci. 18(4).

Hime, G. 2013. Animals in research: Drosophila (the fruit fly). The Conversation. Available at: https://theconversation.com/animals-in-research-drosophila-the-fruit-fly-13571 [Accessed: 20 October 2023].

Hodgkin, A. and Huxley, A. 1939. Action Potentials Recorded from Inside a Nerve Fibre. Nature 144(3651), pp. 710–711.

Hrizo, S. et al. 2021. Identification of protein quality control regulators using a Drosophila model of TPI deficiency. Neurobiol Dis. 152.

Hrizo, S., Fisher, I., Long, D., Hutton, J., Liu, Z. and Palladino, M. 2013. Early mitochondrial dysfunction leads to altered redox chemistry underlying pathogenesis of TPI deficiency. Neurobiology of Disease 54, pp. 289–296.

Hrizo, S. and Palladino, M. 2010. Hsp70- and Hsp90-mediated proteasomal degradation underlies TPIsugarkill pathogenesis in Drosophila. Neurobiol Dis. 40(3), pp. 676–683.

Ill-Raga, G. et al. 2010. Amyloid-β peptide fibrils induce nitro-oxidative stress in neuronal cells. J Alzheimers Dis. 22(2), pp. 641–652.

Institute, Q.B. 2017. Action potentials and synapses. Available at: https://qbi.uq.edu.au/brain-basics/brain/brain-physiology/action-potentials-and-synapses [Accessed: 24 February 2021].

InterPro, E.C.D. 2023. Triosephosphate isomerase, active site - Classification of protein families. Available at: http://www.ebi.ac.uk/interpro/entry/InterPro/IPR020861/http://www.ebi.ac.uk/interpro/entry/InterPro/IPR020861/ [Accessed: 1 August 2023].

Jackson, M. 2011. Inferring Structures of Kinetic Intermediates in Ca2+-Triggered Exocytosis. In: Current Topics in Membranes. pp. 185–208.

Jan, L. and Jan, Y. 1982. Antibodies to horseradish peroxidase as specific neuronal markers in Drosophila and in grasshopper embryos. Proc. Natl. Acad. Sci. USA Neurobiology 79, pp. 2700–2704.

Jan, L., Jan, Y. 1976. Properties of the larval neuromuscular junction in Drosophila melanogaster. J Physiol. 262(1), pp. 189-214.

Jan, Y., Jan, L., Dennis, M. 1977. Two mutations of synaptic transmission in *Drosophila*. Proc. R. Soc. Lond. B. 198, pp. 87-108.

Jarecki, J., Johnson, E. and Krasnow, M. 1999. Oxygen regulation of airway branching in Drosophila is mediated by branchless FGF. Cell 99(2), pp. 211–220.

Johnson, J., Munneke, A., Richardson, H., Gendron, C. and Pletcher, S. 2023. Light modulates Drosophila lifespan via perceptual systems independent of circadian rhythms. Aging (Albany NY) 15(2), pp. 396–420.

Jove. 2009. Drosophila Larval NMJ Dissection. Available at: https://www.jove.com/v/1107/drosophila-larval-nmj-dissection [Accessed: 10 November 2020].

Jung, J., Yoon, T., Choi, E. and Lee, K. 2002. Interaction of Cofilin with Triose-phosphate Isomerase Contributes Glycolytic Fuel for Na,K-ATPase via Rho-mediated Signaling Pathway. Journal of Biological Chemistry, pp. 48931–48937.

Kadas, D., Klein, A., Krick, N., Worrell, J., Ryglewski, S., Duch, C. 2017. Dendritic and Axonal L-Type Calcium Channels Cooperate to Enhance Motoneuron Firing Output during Drosophila Larval Locomotion. J Neurosci. 37(45), pp. 10971-10982.

Kanao, T. et al. 2012. The Nitric Oxide-Cyclic GMP Pathway Regulates FoxO and Alters Dopaminergic Neuron Survival in Drosophila. PLoS ONE 7(2).

Karch, C., Cruchaga, C. and Goate, A. 2014. Alzheimer's disease genetics: from the bench to the clinic. Neuron 2(83), pp. 11–26.

Karunanithi, S., Marin, L., Wong, K. and Atwood, H. 2002. Quantal Size and Variation Determined by Vesicle Size in Normal and Mutant Drosophila Glutamatergic Synapses. J Neurosci. 22(23), pp. 10267–10276.

Kawasaki, F., Zou, B., Xu, X., Ordway, R. 2004. Active Zone Localization of Presynaptic Calcium Channels Encoded by the cacophony Locus of Drosophila. J. Neurosci. 24(1), pp. 282-285.

Kihara, T. and Shimohama, S. 2004. Alzheimer's disease and acetylcholine receptors. Acta Neurobiol Exp (Wars) 64(1), pp. 99–105.

Knapek, S., Sigrist, S. and Tanimoto, H. 2011. Bruchpilot, A Synaptic Active Zone Protein for Anesthesia-Resistant Memory. Journal of Neuroscience 31(9), pp. 3453–3458.

Koenig, J., Saito, K. and Ikeda, K. 1983. Reversible control of synaptic transmission in a single gene mutant of Drosophila melanogaster. The Journal of Cell Biology 96, pp. 1517–1522.

Koliada, A. et al. 2020. Mating status affects Drosophila lifespan, metabolism and antioxidant system. Comp Biochem Physiol A Mol Integr Physiol 246.

Konopka, R. and Benzer, S. 1971. Clock Mutants of Drosophila melanogaster. Proc. Nat. Acad. Sci. USA 68(9), pp. 2112–2116.

Kummer, M. et al. 2011. Nitration of Tyrosine 10 Critically Enhances Amyloid β Aggregation and Plaque Formation. Neuron 71(5), pp. 833–44.

Kuromi, H. and Kidokoro, Y. 1998. Two Distinct Pools of Synaptic Vesicles in Single Presynaptic Boutons in a Temperature-Sensitive Drosophila Mutant, shibire. Neuron 20, pp. 917–925.

Lee, B., Yang, C., Lee, S., Lee, S., Kim, Y. and Ho, W. 2022. Voltage-gated calcium channels contribute to spontaneous glutamate release directly via nanodomain coupling or indirectly via calmodulin. Progress in Neurobiology 208.

Lee, S. et al. 2016. The calcineurin inhibitor Sarah (Nebula) exacerbates Aβ42 phenotypes in a Drosophila model of Alzheimer's disease. Disease models and mechanisms 9, pp. 295–306.

Leech, T., Sait, S. and Bredtman, A. 2017. Sex-specific effects of social isolation on ageing in Drosophila melanogaster. J Insect Physiol. , pp. 12–17.

Lin, Y. et al. 2022. The deleterious effects of old social partners on Drosophila lifespan and stress resistance. NPJ Aging 8(1).

Littleton, J., Stern, M., Perin, M., Bellen, H. 1994. Calcium dependence of neurotransmitter release and rate of spontaneous vesicle fusions are altered in Drosophila synaptotagmin mutants. Proc Natl Acad Sci USA 91(23), pp. 10888-10892.

Liu, W., Zhuo, P., Li, L., Jin, H., Lin, B., Zhang, Y., Liang, S., Wu, J., Huang, J., Wang, Z., Lin, R., Chen, L., Tao, J. 2017. Activation of brain glucose metabolism ameliorating cognitive impairment in APP/PS1 transgenic mice by electroacupuncture. Free Radical Biology and Medicine 112, pp. 174-190.

Liu, Z., Cao, J., Ma, Q., Gao, X., Ren, J. and Xue, Y. 2011. GPS-YNO2: computational prediction of tyrosinenitration sites in proteins. Molecular BioSystems 7(4), pp. 1197–1204.

Lu, K., Yang, C., Sheu, J., Chung, C., Jayakumar, T., Chen, C. and Hsieh, C. 2023. Overexpressing glyoxalase 1 attenuates acute hyperglycemia-exacerbated neurological deficits of ischemic stroke in mice. Transl Res. 261, pp. 57–68.

Madabattula, S. et al. 2015. Quantitative Analysis of Climbing Defects in a Drosophila Model of Neurodegenerative Disorders. Journal of Visualized Experiments 100.

Mallozzi, C., D'Amore, C., Camerini, S., Macchia, G., Crescenzi, M., Petrucci, T. and Stasi, A. 2013. Phosphorylation and nitration of tyrosine residues affect functional properties of Synaptophysin and Dynamin I, two proteins involved in exo-endocytosis of synaptic vesicles. Biochimica et Biophysica Acta, pp. 110–121.

Markow, T. 2011. "Cost" of virginity in wild Drosophila melanogaster females. Ecol Evol. 1(4), pp. 596–600.

Marrus, S., Portman, S., Allen, M., Moffat, K. and DiAntonio, A. 2004. Differential Localization of Glutamate Receptor Subunits at the Drosophila Neuromuscular Junction. Journal of Neuroscience 24(6), pp. 1406–1415.

Martin, T. 2016. Chapter 3 - Control of Hormone Secretion. In: Endocrinology: Adult and Pediatric. 7th ed. pp. 30–40.

Mason, R. et al. 2013. Glutathione peroxidase activity is neuroprotective in models of Huntington's disease. Nat Genet. 45(10).

Mateo, A. and De Artinano, M. 2000. Nitric oxide reactivity and mechanisms involved in its biological effects. Pharmacological research 42(5).

McBean, G., Lopez, M. and Wallner, F. 2016. Redox-based therapeutics in neurodegenerative disease. Br J Pharmacol. 174(12), pp. 1750–1770.

McGuire, S., Roman, G. and Davis, R. 2004. Gene expression systems in Drosophila: a synthesis of time and space. Cell Press 20(8), pp. 384–391.

Mesquita, R. et al. 2021. Cytochrome c Oxidase at Full Thrust: Regulation and Biological Consequences to Flying Insects. Cells 10(2).

Miao, L. and Clair, D. 2009. Regulation of superoxide dismutase genes: implications in disease. Free Radic Biol Med. 47(4), pp. 344–356.

Michels, B. et al. 2017. Pavlovian Conditioning of Larval Drosophila: An Illustrated, Multilingual, Hands-On Manual for Odor-Taste Associative Learning in Maggots. Front Behav Neurosci. 11(45).

Miranda, H. et al. 2016. Glycation potentiates neurodegeneration in models of Huntington's disease. Sci Rep.

Miwa, S., St-Pierre, J., Partridge, L. and Brand, M. 2003. Superoxide and hydrogen peroxide production by Drosophila mitochondria. Free Radic Biol Med 35(8), pp. 938–948.

Moraru, A., Wiederstein, J., Pfaff, D., Fleming, T., Miller, A., Nawroth, P. and Teleman, A. 2018. Elevated Levels of the Reactive Metabolite Methylglyoxal Recapitulate Progression of Type 2 Diabetes. Cell metabolism 27, pp. 926–934.

Muller, U. 1994. Ca2+ /Calmodulin-dependent Nitric Oxide Synthase in Apismellifera and Drosophila melanogaster. European Journal of Neuroscience 6, pp. 1362–1370.

Muller, U. 1997. The nitric oxide system in insects. Progress in Neurobiology 51(3), pp. 363–381.

Myers, T. and Palladino, M. 2023. Newly discovered roles of triosephosphate isomerase including functions within the nucleus. Molecular Medicine 29(18).

Nagase, S., Takemura, K., Ueda, A., Hirayama, A., Aoyagi, K., Kondoh, M. and Koyama, A. 1997. A Novel Nonenzymatic Pathway for the Generation of Nitric Oxide by the Reaction of Hydrogen Peroxide and D- or L-Arginine. Biochemical and biophysical research communications 233(1), pp. 150–153.

Nakamura, T. and Lipton, S. 2008. Emerging Roles of S -Nitrosylation in Protein Misfolding and Neurodegenerative Diseases. Antioxidants and redox signalling 10(1), pp. 87–101.

Neher, E. and Sakmann, B. 1976. Single-channel currents recorded from membrane of denervated frog muscle fibres. Nature 260.

Nichols, C., Becnel, J. and Pandey, U. 2012. Methods to assay Drosophila behavior. J Vis Exp. 61, pp. 3791–3795.

Nigro, C. et al. 2017. Methylglyoxal-Glyoxalase 1 Balance: The Root of Vascular Damage. Int J Mol Sci. 18(1).

NIH Medline plus. 2014. Triosephosphate isomerase deficiency. Available at: https://medlineplus.gov/genetics/condition/triosephosphate-isomerase-deficiency/#frequency [Accessed: 26 June 2023].

Oakeshott. J, Gibson. J and Wilson. S. 1984. Selective effects of the genetic background ethanol on the alcohol dehydrogenasepolymorphism in Drosophila melanogaster. Heredity 53(1), pp. 51–67.

Office for Health Improvement and Disparities. 2022. Dementia: applying All Our Health. Available at: https://www.gov.uk/government/publications/dementia-applying-all-our-health/dementia-applying-all-our-health [Accessed: 14 March 2024].

Olah, J., Orosz, F., Keseru, G., Kovari, Z., Kovacs, J., Hollan, S. and Ovadi, J. 2002. Triosephosphate isomerase deficiency: a neurodegenerative misfolding disease. Biochem Soc Trans. 30(2), pp. 30–38.

Orosz, F., Judit, O. and Judit, O. 2006. Triosephosphate Isomerase Deficiency: Facts and Doubts. Life 58(12), pp. 703–715.

Orosz, F., Olah, J. and Ovadi, J. 2009. Triosephosphate isomerase deficiency: new insights into an enigmatic disease. Biochem Biophys Acta. 1792(12), pp. 1168–1174.

Pacher, P., Beckman, J. and Liaudet, L. 2007. Nitric Oxide and Peroxynitrite in Health and Disease. Physiol Rev. 87(1), pp. 315–424.

Palladino, M., Hadley, T. and Ganetzky, B. 2002. Temperature-sensitive paralytic mutants are enriched for those causing neurodegeneration in Drosophila. Genetics 161(3), pp. 1197–1208.

Piaceri, I., Nacmias, B. and Sorbi, S. 2013. Genetics of familial and sporadic Alzheimer's disease. Front Biosci (Elite Ed) 5(1), pp. 167–177.

Piccirillo, R., Demontis, F., Perrimon, N. and Goldberg, A. 2013. Mechanisms of muscle growth and atrophy in mammals and Drosophila. American association for anatomy 243(2), pp. 201–215.

Picón-Pagès, P., Garcia-Buendia, J. and Muñoz, F. 2019. Functions and dysfunctions of nitric oxide in brain. BBA mol basis of disease 1865, pp. 1949–1967.

Pini, L. et al. 2016. Brain atrophy in Alzheimer's Disease and aging. Ageing research reviews 30, pp. 25–48.

Poodry, C. and Edgar, L. 1979. Reversible alternations in the neuromuscular junctions of Drosophila melanogaster bearing a temperature-sensitive mutation, shibire. J Cell Biology 81, pp. 520–527.

Rabbani, N. 2022. Methylglyoxal and glyoxalase 1—a metabolic stress pathway-linking hyperglycemia to the unfolded protein response and vascular complications of diabetes. Clin Sci (Lond) 136(11), pp. 819–824.

Ramaswami, M., Krishnan, K.S. and Kelly, R.B. 1994. Intermediates in Synaptic Vesicle Recycling Revealed by Optical Imaging of Drosophila Neuromuscular Junctions. Neuron 13, pp. 363–375.

Ranganathan, S., Ciaccio, P., Walsh, E. and Tew, K. 1999. Genomic sequence of human glyoxalase-I: analysis of promoter activity and its regulation. Gene 240(1), pp. 149–155.

Reddy-Alla, S. et al. 2017. Stable Positioning of Unc13 Restricts Synaptic Vesicle Fusion to Defined Release Sites to Promote Synchronous Neurotransmission. Neuron 95(6), pp. 1350–1364.

Richmond, J. and Broadie, K. 2002. The synaptic vesicle cycle: exocytosis and endocytosis in Drosophila and C. elegans. Current Opinion in Neurobiology 12, pp. 499–507.

Robinson, N. and Robinson, A. 2004. Amide molecular clocks in drosophila proteins: potential regulators of aging and other processes. Mechanisms of Ageing and Development 125(4), pp. 259–267.

Robinson, S. et al. 2018. Nitric oxide-mediated posttranslational modifications control neurotransmitter release by modulating complexin farnesylation and enhancing its clamping ability. PLoS Biol. 16(4).

Robinson, S., Olmo, M., Martin, M., Smith, T., Morone, N. and Steinert, J. 2017. Endogenous Nitric Oxide Synthase Activity Regulates Synaptic Transmitter Release. Opera Med Physiol 3(2), pp. 31–38.

Roland, B. et al. 2014. Triosephosphate Isomerase I170V Alters Catalytic Site, Enhances Stability and Induces Pathology in a Drosophila Model of TPI Deficiency. Biochem Biophys Acta 1852(1), pp. 61–69.

Roland, B. et al. 2016. Structural and Genetic Studies Demonstrate Neurologic Dysfunction in Triosephosphate Isomerase Deficiency Is Associated with Impaired Synaptic Vesicle Dynamics. plos genetics 12(3).

Roland, B. et al. 2019. Missense variant in TPI1 (Arg189Gln) causes neurologic deficits through structural changes in the triosephosphate isomerase catalytic site and reduced enzyme levels in vivo. Biochem Biophys Acta Mol Basis Dis 1865(9), pp. 2257–2266.

Roland, B., Stuchul, K., Larsen, S., Amrich, C., VanDemark, A., Celotto, A. and Palladino, M. 2013. Evidence of a triosephosphate isomerase non-catalytic function crucial to behavior and longevity. J Cell Sci. 126(14), pp. 3151–3158.

Romero, N., Dekanty, A. and Wappner, P. 2007. Cellular and developmental adaptations to hypoxia: a Drosophila perspective. Methods Enzymol. 435, pp. 123–144.

Rosa, A. et al. 2020. Physical exercise in the prevention and treatment of Alzheimer's disease. J Sport Health Sci 9(5), pp. 394–404.

Scheckhuber, C. 2019. Studying the mechanisms and targets of glycation and advanced glycation end-products in simple eukaryotic model systems. International Journal of Biological Macromolecules 127, pp. 85–94.

Schneggenburger, R., Meyer, A. and Neher, E. 1999. Released Fraction and Total Size of a Pool of Immediately Available Transmitter Quanta at a Calyx Synapse. Neuron 23(2), pp. 399–409.

Schwarz, T. 2006. Transmitter Release at the Neuromuscular Junction. International Review of Neurobiology 75, pp. 105–144.

Schwarze, S., Weindruch, R. and Aiken, J. 1998. Oxidative stress and aging reduce COX I RNA and cytochrome oxidase activity in Drosophila. Free Radical Biology and Medicine 25(6), pp. 740–747.

Seigle, J., Celotto, A. and Palladino, M. 2008. Degradation of Functional Triose Phosphate Isomerase Protein Underlies sugarkill Pathology. Genetics 179, pp. 855–862.

Seneviratne, U., Nott, A., Bhat, V., Ravindra, K., Wishnok, J., Tsai, L. and Tannenbaum, S. 2016. S-nitrosation of proteins relevant to Alzheimer's disease during early stages of neurodegeneration. PNAS 113(15), pp. 4152–4157.

Shin, M. et al. 2024. Drosophila immune cells transport oxygen through PPO2 protein phase transition. Nature 631, pp. 350–359.

Sil, S., Ghosh, T., Ghosh, R. and Gupta, P. 2017. Nitric oxide synthase inhibitor, aminoguanidine reduces intracerebroventricular colchicine induced neurodegeneration, memory impairments and changes of systemic immune responses in rats. Journal of Neuroimmunology 303, pp. 51–61.

Silver, R. 2003. Estimation of nonuniform quantal parameters with multiple-probability fluctuation analysis: theory, application and limitations. Journal of Neuroscience Methods 130(2), pp. 127–141.

Sinenko, S., Starkova, T., Kuzmin, A. and Tomilin, A. 2021. Physiological Signaling Functions of Reactive Oxygen Species in Stem Cells: From Flies to Man. Front Cell Dev Biol. 9(714370).

Spiers, J., Breda, C., Robinson, S., Giorgini, F., Steinert, J. 2019. Drosophila Nrf2/Keap1 Mediated Redox Signalling Supports Synaptic Function and Longevity and Impacts on Circadian Activity. Front Mol Neurosci. 12(86).

Stampeli, R. and Huxley, A. 1949. Evidence for saltatory conduction in peripheral myelinated nerve fibres. The Journal of Physiology 108, pp. 315–339.

Stanley, E. 1997. The calcium channel and the organization of the presynaptic transmitter release face. Trends in Neurosciences 20(9), pp. 404-409.

Stone, Æ., Cujic, O., Rowlett, A., Aderhold, S., Savage, E., Graham, B. and Steinert, J. 2023. Triose-phosphate isomerase deficiency is associated with a dysregulation of synaptic vesicle recycling in Drosophila melanogaster. Front. Synaptic Neurosci. 15.

Sudhof, T. 2013. Neurotransmitter release: the last millisecond in the life of a synaptic vesicle. Neuron.

Tajes, M., Guivernau, B., Ramos-Fernandez, E., Bosch-Morato, M., Palomer, E., Guix, F. and Munoz, F. 2013. The pathophysiology of triose phosphate isomerase dysfunction in Alzheimer's disease. Histol Histopathol. 28(1), pp. 43–51.

The Plymouth Workshop Hanbook. 1994. Microelectrode Techniques. 2nd ed. Ogden, D. ed. The Company of Biologists Limited, Cambridge.

Torroja, L., Packard, M., Gorczyca, M., White, K., Budnik, V. 1999. The Drosophila beta-amyloid precursor protein homolog promotes synapse differentiation at the neuromuscular junction. J Neurosci. 19(18), pp. 7793-7803.

Tsakiri, E., Iliaki, K., Hohn, A., Grimm, S., Papassideri, I., Grune, T. and Trougakos, I. 2013. Diet-derived advanced glycation end products or lipofuscin disrupts proteostasis and reduces life span in Drosophila melanogaster. Free Radic Biol Med 65, p. 11551163.

Verstegen, A. et al. 2014. Phosphorylation of synapsin I by Cyclin-Dependent Kinase-5 sets the ratio between the Resting and Recycling pools of synaptic vessicles at hippocampal synapses. The Journal of Neuroscience 34(21), pp. 7266–7280.

Walker, D. and Benzer, S. 2004. Mitochondrial "swirls" induced by oxygen stress and in the Drosophila mutant hyperswirl. Proc Natl Acad Sci USA 101(28), pp. 10290–10295.

Wang, L., Hagemann, T., Kalwa, H., Michel, T., Messing, A. and Feany, M. 2015. Nitric oxide mediates glial-induced neurodegeneration in Alexander disease. nature communications 6(8966).

Wang, R. and Reddy, P. 2017. Role of glutamate and NMDA receptors in Alzheimer's disease. J Alzheimers Dis. 57(4), pp. 1041–1048.

Wang, Y., Lobb-Rabe, M., Ashley, J., Anand, V. and Carrillo, R. 2021. Structural and Functional Synaptic Plasticity Induced by Convergent Synapse Loss in the Drosophila Neuromuscular Circuit. J Neurosci. 41(7), pp. 1401–1417.

Wentzell, J., Bolkan, B., Carmine-Simmen, K., Swanson, T., Musashe, D. and Kretzschmar, D. 2012. Amyloid precursor proteins are protective in Drosophila models of progressive neurodegeneration. Neurobiol Dis. 46(1), pp. 78–87.

WHO. 2023. Dementia. Available at: https://www.who.int/news-room/fact-sheets/detail/dementia [Accessed: 10 August 2023].

Winding, M. et al. 2023. The connectome of an insect brain. Science 379(6636). Available at: https://www.science.org/doi/10.1126/science.add9330 [Accessed: 20 October 2023].

Wu, S., Cao, Z., Chang, K. and Juang, J. 2017. Intestinal microbial dysbiosis aggravates the progression of Alzheimer's disease in Drosophila. nature communications 8(1).

Zhang, P. et al. 2010. S-Nitrosylation of Cyclin-Dependent Kinase 5 (Cdk5) Regulates its Kinase Activity and Dendrite Growth During Neuronal Development. The Journal of Neuroscience 30(43), pp. 14366–14370.

Zhu, J. et al. 2021. Autophagy inhibition rescues structural and functional defects caused by the loss of mitochondrial chaperone Hsc70-5 in Drosophila. Autophagy 17(10), pp. 3160–3174.

Zucker, R., Kullmann, D. and Kaeser, P. 2014. Chapter 15 - Release of Neurotransmitters. In: From Molecules to Networks. 3rd ed. pp. 443–488.

Chapter 9: Appendices

9.1: Glo Overexpressor line

9.1.1: Results

The Glyoxalase overexpressing line was excluded from the main thesis as the overexpression could not be confirmed and the data showed many differences between the 'control' lines w^{1118}, Gal4, and UAS-Glo.

No differences were seen between amplitudes of spontaneous events, see Figure 9-1. Frequencies were seen to be altered, the frequency of sEJC events was increased in Glo(OE) compared to both Gal4 and UAS-Glo, and the frequency of sEJP events was increased in Glo(OE) compared to w^{1118}, see Figure 9-1 [B] and [D]

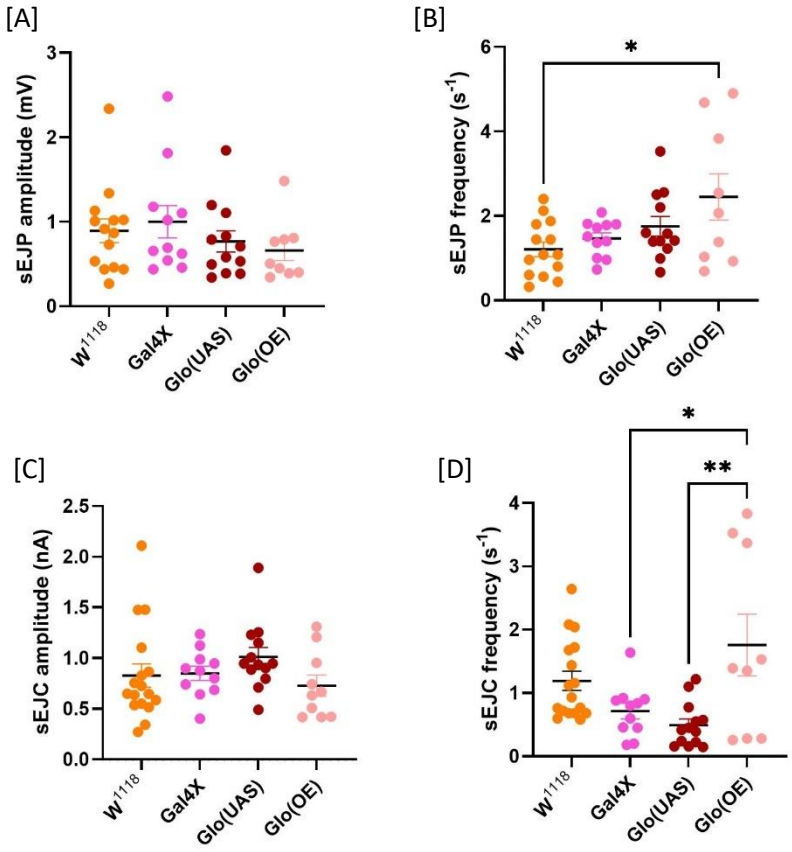

*Figure 9-1: sEJC/P data for Glo(OE), data expressed as mean±SEM [A] sEJC amplitudes; w^{1118}: 0.83±0.1 nA, Gal4: 0.85±0.07 nA, UAS-Glo : 1.0±0.09 nA, Glo(OE): 0.73±0.1 nA [B] sEJC frequency; w^{1118}: 1.2±0.2 s^{-1}, Gal4: 0.72±0.1 s^{-1}, UAS-Glo: 0.49±0.1 s^{-1}, Glo(OE): 1.8±0.5 s^{-1}, *p<0.05, **p<0.005 [C] sEJP amplitudes; w^{1118}: 0.89±0.1 mV, Gal4: 1.0±0.2 mV, UAS-Glo: 0.77±0.1 mV, Glo(OE): 0.66±0.1 mV [D] sEJP frequencies; w^{1118}: 1.2±0.2 s^{-1}, Gal4: 1.5±0.1 s^{-1}, UAS-Glo: 1.8±0.2 s^{-1}, Glo(OE): 2.5±0.5 s^{-1}, *p<0.05. One-way ANOVA was used to test significance.*

The frequency distributions of sEJC amplitudes was found to be shifted left significantly for Glo(OE) compared to UAS-Glo, see Figure 9-2.

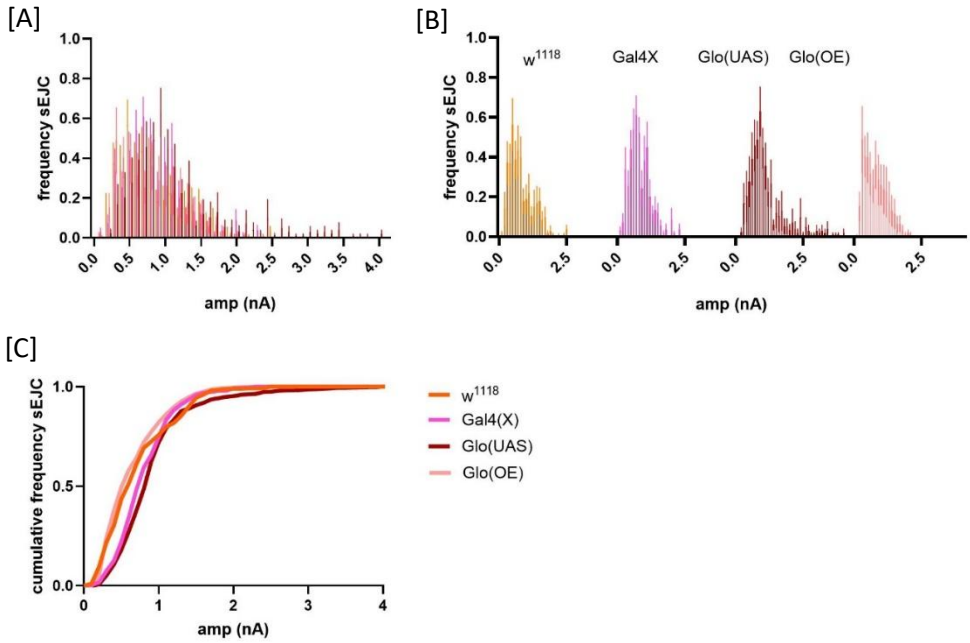

*Figure 9-2: TEVC data sEJC amplitude frequencies distributions for control lines w^{1118} (orange), Gal4 (pink), UAS-Glo (brown), Glo mutant line Glo(OE) (peach). [A] Normalised amplitude frequency distributions, data overlapped. [B] Normalised amplitude frequency distributions data separated out. [C] Normalised cumulative amplitude frequency found to be significantly different for Glo(OE) vs UAS-Glo, Students t-test, Kolmogorov-Smirnov test, ***p<0.001.*

Evoked excitatory junction current (eEJC) responses were found to have reduced amplitudes in Glo(OE) compared to w^{1118}. A similar reduction was found in the UAS-Glo line compared to w^{1118} and Gal4 see Figure 9-3 [A]. The decrease in amplitude of the Glo(OE) cross therefore may be an artifact from this parent line. Quantal content was found to be decreased in all lines compared to the w^{1118} control line, Gal4, UAS-Glo, and Glo(OE), see Figure 9-3 [B].

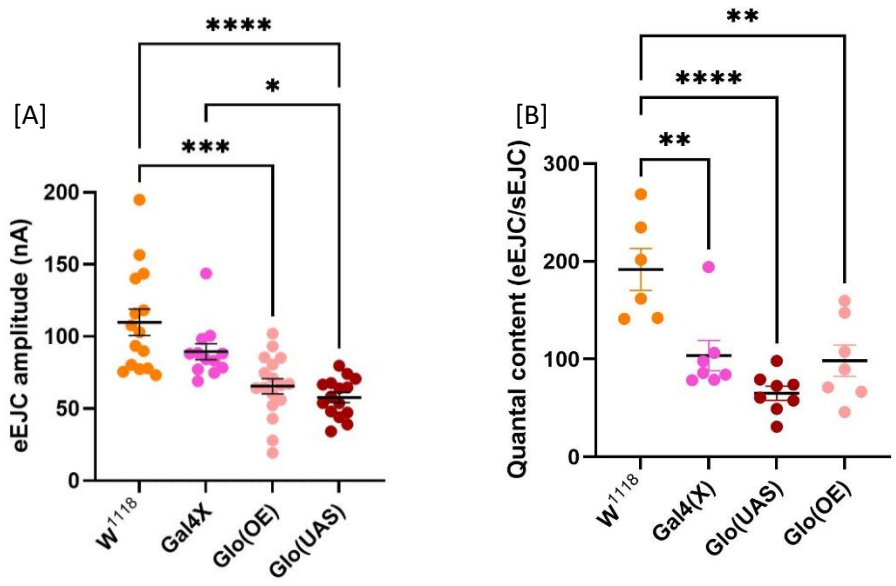

*Figure 9-3: eEJC data for GloOE [A] eEJC amplitudes, data expressed as mean±SEM, w^{1118}: 110±9 nA, Gal4: 90±6 nA, UAS-Glo: 58±3 nA, Glo(OE): 66±5 nA, *p<0.05, ***<0.005, ****p<0.0001 [B] Qunatal content eEJC amplitudes divided by sEJC amplitudes, data expressed as mean±SEM, w^{1118}: 190±20, Gal4: 104±20, UAS-Glo: 65±7, Glo(OE): 98±20. One-way ANOVA used to test significance.*

At 10 Hz there was little difference seen in kinetics between the lines, with tau values for trains and recoveries not showing any significant differences. Although the Glo(OE) cross and UAS-Glo line seemed to show significantly reduced levels of depletion with unaltered amplitudes at the end of the train relative to the start, Glo(OE) (97±6 %), UAS-Glo (120±7 %), compared to w^{1118} (70±3 %) and Gal4 (66±5 %). However as this effect is present in both Glo lines, this result in the Glo(OE) line is likely due to the genetics from the UAS-Glo background than the glyoxalase overexpression, see Figure 9-4 [A].

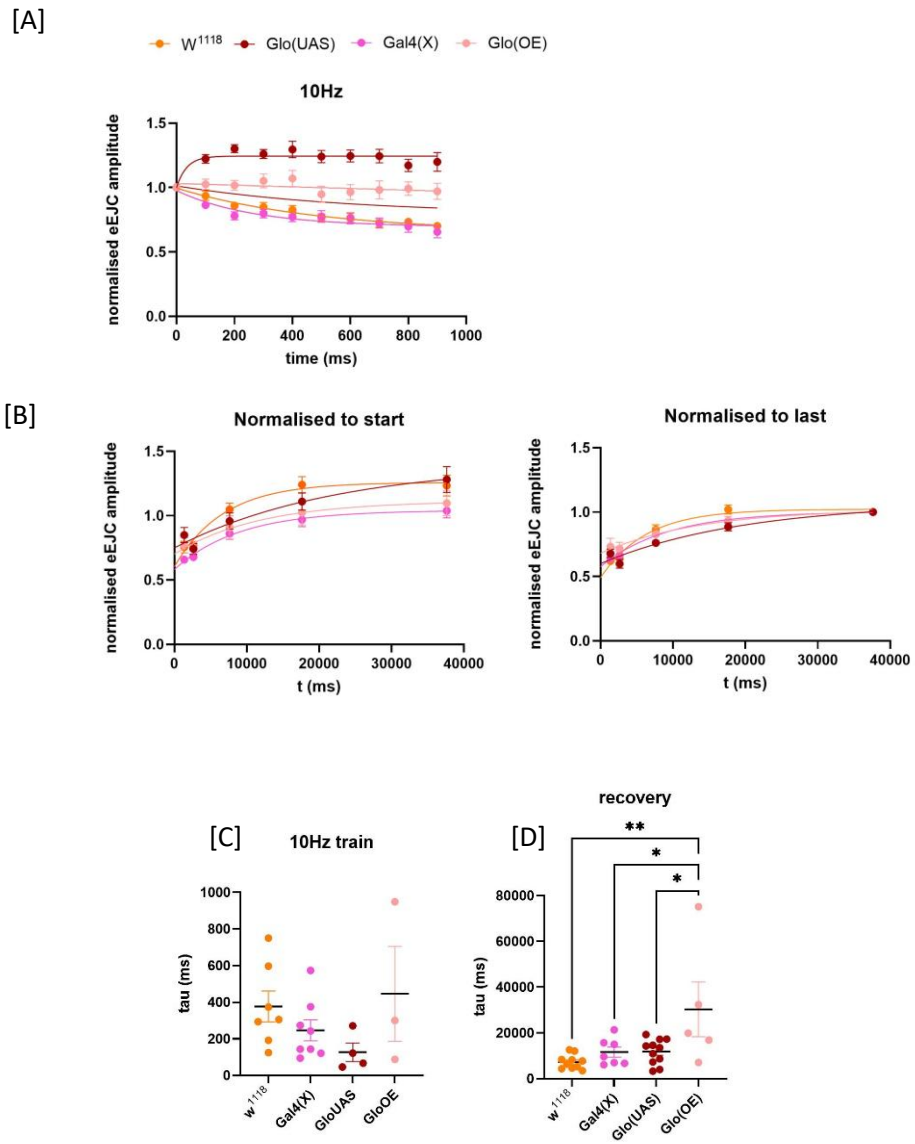

Figure 9-4: Normalised 10 Hz train stimulations [A] Train stimulation plateau values of; w^{1118}: 70±3 %, Gal4: 66±5 %, UAS-Glo: 120±7 %, Glo(OE): 97±6 %. [B] Recovery to first peak of train, and last peak of recovery. Degree of recovery normalised to the first amplitude in the preceding train; w^{1118}: 120±8 %, Gal4: 104±5 %, UAS-Glo: 130±10 %, Glo(OE): 110±10 % [C] Mean time constant values for train stimulation; w^{1118}: 380±80 ms, Gal4: 230±50 ms, GloUAS: 130±50 ms, Glo(OE): 320±200 ms, [D] Mean time constant values for recovery from train; w^{1118}: 7300±1000 ms, Gal4: 13000±2000 ms, GloUAS: 12000±2000 ms, Glo(OE): 9400±2000 ms. Nonliner fit was used to fit curves, one-way ANOVA used to test for significance between tau values, no significance was found.

As at 10 Hz, the Glo(OE) cross shows reduced levels of depletion at 60 Hz in comparison to w^{1118}, although depletion is seen here unlike at 10 Hz, Glo (OE) 89±10 %, compared to w^{1118} 56±4 %, and Gal4 35±10 %, although again this is mirrored by the UAS-Glo line, 120±10 %, so the Glo(OE) result should be taken with caution see Figure 9-5 [A]. The two Glo mutant lines also show a potentiation at the start of the train not seen in w^{1118} or Gal4, an effect which is greater in UAS-Glo than in Glo(OE). Comparisons of time constants from the 60 Hz train show increased time constants in the two Glo lines, this is only significant in UAS-Glo 470±90 ms vs 220±20 ms in w^{1118} and 220±30 ms in Gal4 see Figure 9-5 [C]. Time courses for recovery following the 60 Hz train were seen to be increased in Gal4 compared to w^{1118}, no differences were seen in the two Glo lines, see Figure 9-5 [C].

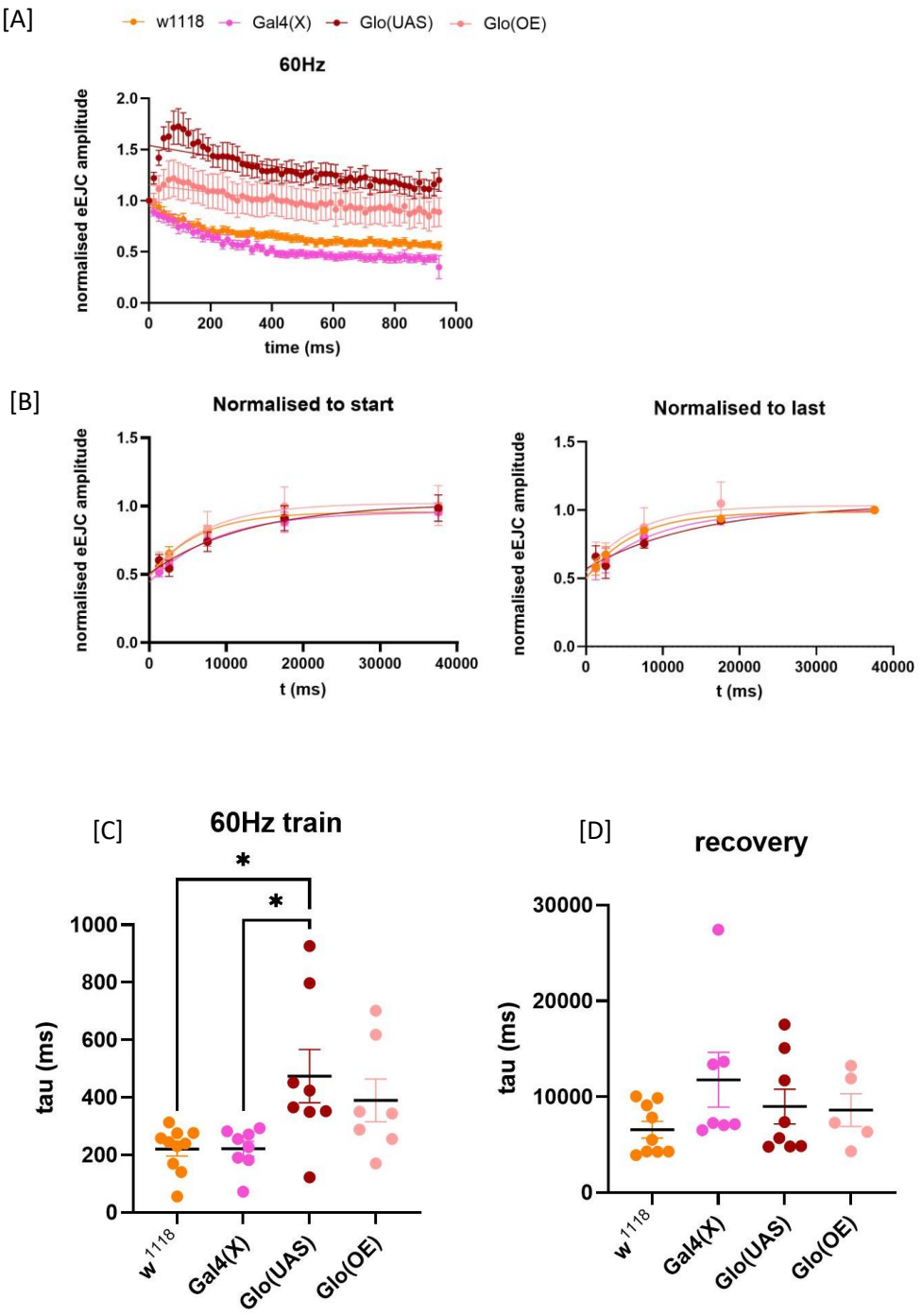

*Figure 9-5: Normalised 60 Hz train stimulations [A] Train stimulation plateau values of; w^{1118}: 56±4 %, Gal4: 35±10 %, UAS-Glo: 120±10 %, Glo(OE): 89±10 %. [B] Recovery to first peak of train, and last peak of recovery. Degree of recovery normalised to the first amplitude in the preceding train; w^{1118}: 97±4 %, Gal4: 96±7 %, UAS-Glo: 99±10 %, Glo(OE): 100±10 % [C] Mean time constant values for train stimulation; w^{1118}: 220±20 ms, Gal4: 220±30 ms, UAS-Glo: 470±90 ms, Glo(OE): 390±70 ms, *p<0.05 [D] Mean time constant values for recovery from train; w^{1118}: 6600±900 ms, Gal4: 14000±3000 ms, GloUAS: 9000±2000 ms, Glo(OE): 8600±2000 ms, *p<0.05. Nonliner fit was used to fit curves, one-way ANOVA used to test for significance between tau values.*

Longevity for Glo(OE) was found to be significantly increased compared to all control lines at 25 °C in a 12 hr light-dark cycle. With H_2O_2 treatment Glo(OE) lifespan is still significantly increased compared to w^{1118} and Gal4, although less than without treatment. With H_2O_2 treatment the significance is lost in comparison to UAS-Glo. Lifespan with H_2O_2 treatment is significantly reduced compared to without treatment in a similar manner to control lines. With glutathione treatment Glo(OE) is still significantly longer lived than all control lines, the glutathione treatment did not significantly alter the lifespan data compared to no treatment, see Figure 9-6 [F].

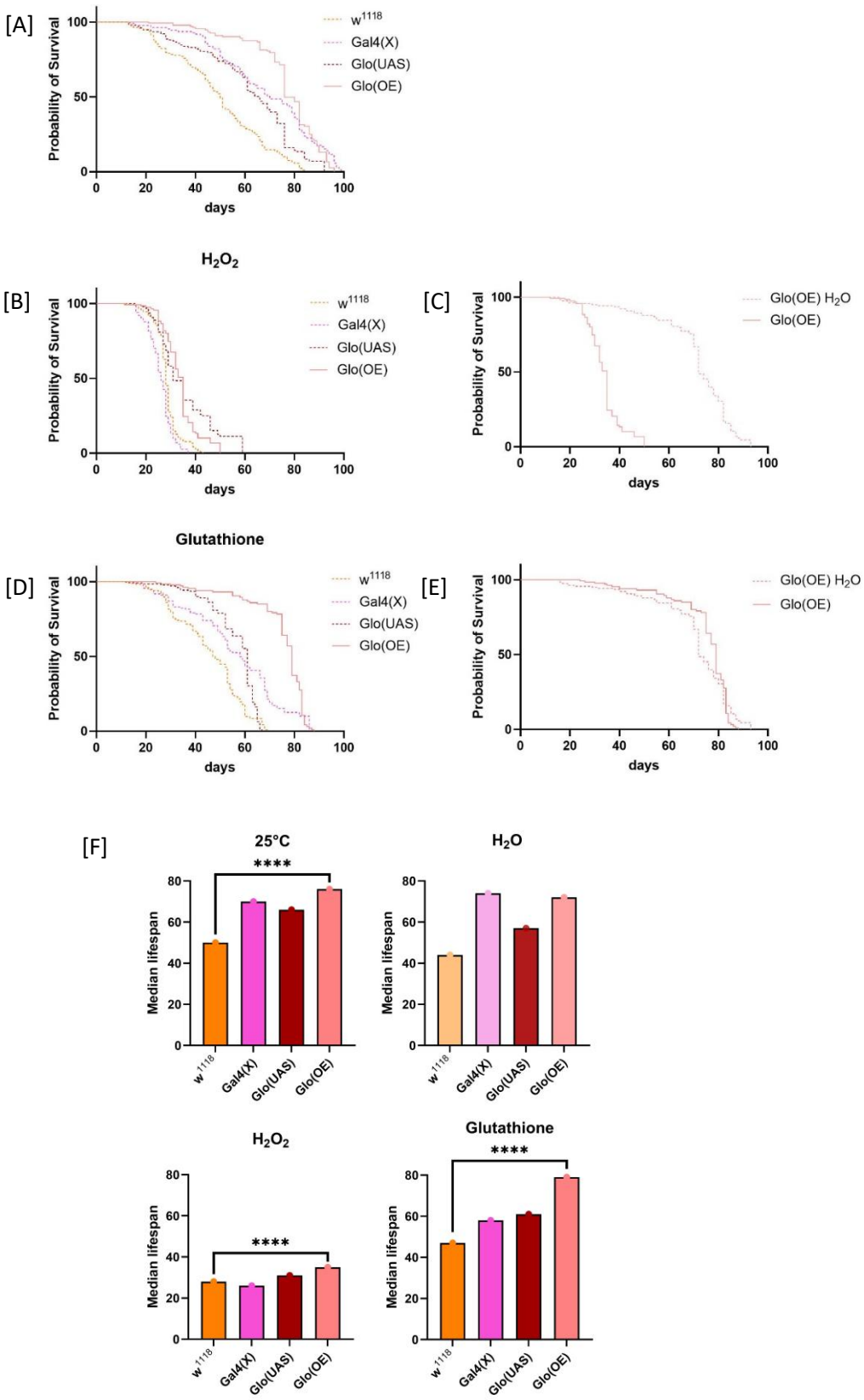

*Figure 9-6: Longevity data for Glo(OE) pairwise comparisons are made to Glo(OE) [A] 25 °C 12 hr light dark cycle median survival; w^{1118}: 50, ****p<0.0001, Gal4: 70, ns, ***p<0.001, UAS-Glo: 66, ****p<0.0001, Glo(OE): 76. [B] H_2O_2 treatment 25 °C 12 hr light dark cycle median survival; w^{1118}: 28, ****p<0.0001, Gal4: 26, ****p<0.0001, UAS-Glo: 31, ns, Glo(OE): 35 [C] H_2O_2 treatment 25 °C 12 hr light dark cycle median survival; Glo(OE) H_2O: 72, ****p<0.0001, Glo(OE): 35 [D] Glutathione treatment 25 °C 12 hr light dark cycle median survival; w^{1118}: 47, ****p<0.0001, Gal4: 58, ****p<0.0001, UAS-Glo: 61, ****p<0.0001, Glo(OE): 79 [E] Glo(OE) H_2O: 72, ns, **p<0.01, Glo(OE): 79. Kaplan-Meier survival analysis, log rank Mantel-Cox test and Gehan-Breslow-Wilcoxon tests respectively used for significance.*

A Western blot experiment was attempted to show the overexpression of Glo in the Glo(OE) cross, and wild type expression in the three control lines. No binding was seen for either of the two antibodies trialled, so this data was unfortunately not usable. Tubulin binding worked as normal, a cell line (Bv2) was used as a positive control for Glo expression. See Figure 9-7 for an example blot from the attempted optimisation. A Western blot for Glo expression with the synthetic antibody created by Teleman et al was reported for the Glo(KO) line compared to a control and showed significant Glo signal in controls vs no signal in the KO (Moraru et al. 2018).

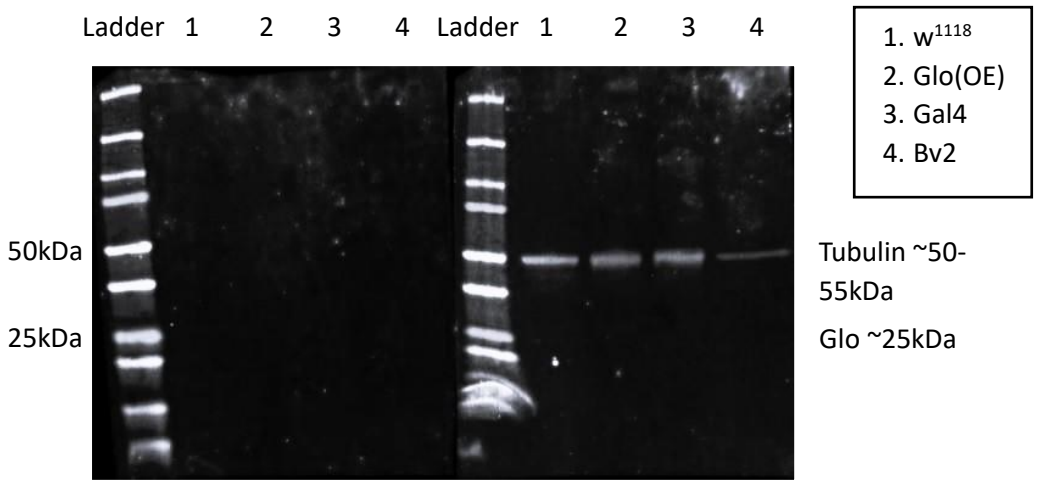

Figure 9-7: Example Western blot for detection of Glo1 expression. Left hand side blot was stained for Glo1 we trialled two antibodies: Glyoxalase I Antibody (D-5): sc-133214 from Santa Cruiz with m-IgG Fc BP-CFL 488 sc-533653 secondary, and a novel antibody synthesised by Teleman et al 2022 (Cortizo et al. 2022)

9.1.2: Discussion

Significant results for the Glo(OE) cross are summarised in Table 9.1 below.

Table 9.1: Summary of significant data for Glo(OE) and parents Gal4 and UAS-Glo. All comparisons shown are to the control line w^{1118}.

	Gal4	UAS-Glo	Glo(OE)
Spontaneous events	ns	ns	sEJC *p<0.05, **p<0.005 and sEJP *p<0.05 frequency increased
Evoked events	ns	eEJC amplitude decreased *p<0.05, ****p<0.0001	eEJC amplitude decreased ***p<0.0005
Quantal content	Quantal content decreased **p<0.005	Quantal content decreased ****p<0.0001	Quantal content decreased **p<0.005
Train stimulation	ns	No depletion seen, potentiation at start of trains, increased time constant *p<0.05	No depletion seen, potentiation at start of trains
Recovery from train	Increased time constants *p<0.05	ns	ns
Longevity	Increased longevity ****p<0.0001	Increased longevity ****p<0.0001	Increased longevity ****p<0.0001
Longevity H2O2	Reduced longevity ***p<0.0005	Increased longevity ****p<0.0001	Increased longevity ****p<0.0001
Longevity glutathione	Increased longevity ****p<0.00001	Increased longevity ****p<0.0001	Increased longevity ****p<0.0001

The Glyoxalase mutant Glo(OE) showed reduced eEJC amplitudes and reduced quantal content, this suggests smaller vesicles and fewer released per evoked event. Frequency of spontaneous events was found to be increased for sEJP and sEJCs, so release may be less controlled in this line. Similar to the Glo(KO)

line, no depletion was seen at 10 Hz, the following degree of recovery and corresponding time constant was found to be reduced compared to the parent line UAS-Glo. Again similarly to the Glo(KO) line 60 Hz train led to a potentiation followed by a slight depletion, time constants following this train for Glo(OE) were not significantly altered, the UAS-Glo parent line showed significantly increased time constants. This all suggests a difference in vesicle release that is maintained in the UAS-Glo parent and Glo(OE) offspring. The Gal4 line showed an increased time constant for the recovery following the 60 Hz train, this is unexpected and calls into question the 'wild type' genetics of the Gal4 line.

Longevity did show significant differences for both parent lines Gal4 and UAS-Glo, along with the Glo(OE) offspring. All three lines showed increased lifespans in comparison to w^{1118}, H_2O_2 treatment showed reduced lifespans for all lines, glutathione did not significantly alter longevity for w^{1118} or Glo(OE). Gal4 saw a significantly reduced lifespan with glutathione treatment compared to no treatment by Log-Rank Mantel-Cox test and Gehan-Breslow-Wilcoxon test, and UAS-Glo saw a significantly increased lifespan with glutathione treatment compared to no treatment by Gehan-Breslow-Wilcoxon test.